Boundary element methods for solving inverse boundary conditions identification problems

Thomas Tonny Mboya Onyango

Submitted in accordance with the requirements for the degree of Doctor of Philosophy

The University of Leeds

Department of Applied Mathematics

October 2008

Acknowledgements

The last three years have been both challenging and memorable. Let me start by recalling that when I arrived in Leeds, Professor Ingham was unwell, and Dr. Elliott took charge as my overall supervisor, assisted by Professor Lesnic and Dr. Mera. With zero computaional skills and no knowledge of the Boundary Elements Method, my world was turned upside down, things seemed stagnated and failure glaring. With patience, understanding and encouragement, the supervisory team rejuvenated my world and for this I remain forever grateful.

At the end of first year, Dr. Elliott retired and Dr. Mera moved to a financial career, thankfully Professor Ingham recovered and took over the mantle, forming a special complementing supervisory team with Professor Lesnic. On settling down we realised tremendous research work and with their skillfull and diligent supervision I was able to achieve several publications. Then on entering my third year Professor Ingham moved to the Centre for CFD, Professor Lesnic becoming my supervisor and Professor Ingham co-supervisor. I offer my heartfelt thanks to this team, especially to Professor Lesnic who travelled with me through all the stages, making input in almost all the difficult questions I had. To Dr. Wen, I appreciate your positive criticism of my work. The staff of the School of Mathematics, especially Jeanne, Debra, Pauline and Tim, I received special attension whenever I needed your help, I will never forget you. Friends like Dr. Johansson and Dr. Zeb, not forgetting my friend and colleague Dumitru, your support and useful comments and encouragements whilst in Leeds are highly appreciated. To Dr. Elliott, for the efforts you made in getting my kids the best schools in Leeds, not forgeting the adventures and the visits you paid us. You have a special spot in my family.

My mom Auma and dad Onyango, the parental care, love and humble beginning you gave me not to mention your constant prayers, place you limitless routed in my heart and of course special. Without forgetting my family, my daughter Akinyi, son Onyango Jnr. who had to do with minimal parental time during this demanding period, and particularly my wife Atieno for her undying love and trust, who had to do with losing her professional work for the sake of my advancement, the selflessness is remarkable, I will ever cherish you. Friends whom I have not mentioned here by name, please accept my sincere gratitude.

Finally, I want to thank the Catholic University of Eastern Africa, the Commonwealth Scholarship and Fellowship Commission and the University of Leeds for the financial support. I credit all these to the creator for the blessings and life.

Abstract

This thesis explores various features of the boundary element method (BEM) used in solving heat transfer boundary conditions identification problems. In particular, we present boundary integral equation (BIE) formulations and procedures of the numerical computation for the approximation of the boundary temperatures, heat fluxes and space, time or temperature dependent heat transfer coefficients.

There are many practical heat transfer situations where such problems occur, for example in high temperature regions or hostile environments, such as in combustion chambers, steel cooling processes, etc., in which the actual method of heat transfer on the surface is unknown. In such situations the boundary condition relating the heat flux to the difference between the boundary temperature and that of the surrounding fluid is represented by an unknown function which may depend on space, time, or temperature.

In these inverse heat conduction problems (IHCP), the BEM is formulated as a minimization of some functional that measures the discrepancy between the measured data, say the average temperature on a portion of the boundary or at an instant over the whole domain. The minimization provides solutions that are consistent with the data. This indicates that the BEM algorithms for the IHCP are robust, stable and predict reliable results.

When the input data is noisy, we have used the truncated singular value decomposition and the Tikhonov regularisation methods to stabilise the solution of the IHCP boundary conditions identification. Numerical approximations have been obtained and, where possible, the results obtained are compared to the analytical solutions.

Information

(i) T.T.M. Onyango, D.B. Ingham and D. Lesnic, Inverse reconstruction of spacewise dependent coefficients in the boundary conditions of one-dimensional transient heat conduction, *Applied Mathematics and Computation*, (accepted) (2008).

(ii) T.T.M. Onyango, D.B. Ingham, D. Lesnic and M. Slodička, Determination of a time-dependent heat transfer coefficient from non-standard boundary measurements, *Mathematics and Computers in Simulation*, (accepted) (2008).

(iii) T.T.M. Onyango, D.B. Ingham and D. Lesnic, Reconstruction of boundary condition laws in heat conduction using the boundary element method, *Computers and Mathematics with Applications*, (accepted), (2008).

(iv) T.T.M. Onyango, D.B. Ingham and D. Lesnic, Reconstruction of boundary condition laws in heat conduction, 6^{th} *International Conference on Inverse Problems in Engineering: Theory and Practice*, Dourdan (Paris), France, June 15-19, 2008, Ch. **68**, (8 pages).

(v) T.T.M. Onyango, D.B. Ingham and D. Lesnic, Restoring boundary conditions in heat conduction using the boundary element method, *Advances in Boundary Element Methods - Proceedings of the Sixth UK Conference on Boundary Integral Methods*, (ed. J. Trevelyan), Ch. **15**, 139–47, (2007).

(vi) T.T.M. Onyango, D.B. Ingham and D. Lesnic, Restoring boundary conditions in heat conduction, *Journal of Engineering Mathematics*, **62**, 85–101, (2008).

(vii) T.T.M. Onyango, D.B. Ingham and D. Lesnic, Reconstruction of heat transfer coefficients using the boundary element method, *Computers and Mathematics with Applications*, **56**, 114–26, (2008).

(viii) T.T.M. Onyango, D.B. Ingham and D. Lesnic, Reconstruction of boundary condition laws in two-dimensional steady inverse heat transfer problems, (in preparation) (2008).

Nomenclature

Roman Symbols

a_i	coefficient of the ith term in polynomials
$\mathbf{a}$	the vector containing the coefficients a_i
A_f	nonlinear operator associated with the unknown function f
b_0, b_1	known functions on the boundaries $x = 0$ and $x = 1$, respectively
B_0, B_1	known functions on the boundaries $x = 0$ and $x = 1$, respectively
C	matrix
$C^{2,1}$	space of functions twice continuously differentiable in the space variable and once continuously differentiable in the time variable
C^α	space of Hölder continuous functions with exponent $\alpha \in (0, 1)$
d	thickness of a transverse section of a conductor
e_0, e_1	average boundary temperature measurements
f_0, f_1, f	unknown boundary functions
F	fundamental solution for the heat equation
g	initial temperature
G	fundamental solution for Laplace's equation
h_0, h_1	known functions on the boundaries $x = 0$ and $x = 1$, respectively
$h(T)$	temperature dependent nonlinear function
H	Heaviside function
H^1, H^2	Sobolev spaces
i, j, k, l, m, n	indices
I	identity matrix
K	order of the polynomial function
L	operator
$L^2(\Omega)$	space of square integrable functions in Ω
$L^\infty(\Omega)$	space of uniformly bounded function in Ω
$\mathbf{n}$	outward unit normal vector to the boundary

N	number of boundary elements
N_0	number of space cells
P_K	space of polynomials of degree K
q	heat flux
Q	solution domain
r	radial distance
$\widetilde{R}$	regularization matrix
S	objective function least-squares residual (chapters 3 and 4)
S	arc-length along the boundary of the domain (chapter 5)
t, t'	time variables
t_f	final time of interest
t_j	endpoint of boundary element
$\widetilde{t}_j$	boundary element node
t^0	time at which measurements are made
T	temperature
T_{ext}	temperature outside the top surface on $y = d$ (chapter 5)
T_{0j}, T_{1j}	discretised boundary temperatures
T'_{0j}, T'_{1j}	discretised heat fluxes
T_k^0	discretised initial temperature
u_1, u_2	coefficients (chapter 5)
w_1, w_2	prescribed boundary functions (chapter 1)
w_{1i}, w_{2i}	discretised prescribed boundary functions (chapter 1)
x	the x-coordinate
x_k	endpoint of cell
$\widetilde{x}_k$	cell node
$\mathbf{Y}$	vector containing unregularized numerical approximations
$\mathbf{Y}_\lambda$	vector containing regularized numerical approximations
Y_i	components of the unknown vector $\mathbf{Y}$
$\mathbf{Z}$	vector containing known values on the right-hand side of a system of algebraic equations

Greek Symbols

$\chi, \bar{\chi}, \chi_0, \chi_1$	temperature measurements
γ	boundary corrosion parameter (chapter 5)
γ_0, γ_1	constants
κ	known quantity (chapter 5)
ϵ	random variable
η	coefficient function
λ	regularization parameter
ρ	percentage of noise
$\sigma, \widetilde{\sigma}$	heat transfer coefficients
σ_0, σ_1	heat tranfer coefficients on the boundaries $x = 0$ and $x = 1$, respectively
φ	temperature measurement
Ω	the space domain
$\partial\Omega_j$	boundary element
$\bar{\Omega}$	the union of Ω and $\partial\Omega$
τ	time variable

Abbreviations

(analytical)	analytical solution
(calculated)	calculated solution
(measured)	solution derived from direct problem
(true)	exact solution
(diag)	diagonal matrix components
BEM	boundary element method(s)
BIE	boundary integral equation(s)
Cond	condition number of a matrix
DHCP	direct heat conduction problem(s)
FDM	finite difference method
FEM	finite element method(s)
HTC	heat transfer coefficient

IHCP	inverse heat conduction problem(s)
LEM	linear energy dispersion model(s)
LOM	loss of matter model(s)
PDE	partial differential equation(s)
Sup	supremum
sv	singular values
SVD	singular value decomposition
TSVD	truncated SVD

Contents

List of Figures

List of Tables

Chapter 1

General introduction

1.1 Introduction

Physical problems in heat conduction can be formulated as a set of equations representing the heat equation, an initial condition and boundary conditions relating the heat flux to the difference between the temperatures of the solid and the surrounding fluid through a function f.

When the heat transfer is purely convective or solely radiative then one assumes that f is a linear function (Newton's law of cooling) or obeys a fourth-order power law (Stefan's law), respectively, see Carslaw and Jaeger [17]. However, there are many practical heat transfer situations, for example in high temperature hostile environments, such as combustion chambers, steel cooling processes, in which the heat transfer coefficient depends on the boundary temperature and the dependence has a complicated or unknown structure, see Rösch [76]. In processes such as fast cooling, there is limited opportunity to measure the temperature or the heat fluxes on the surface and in such a case one needs to set up an inverse problem to reconstruct the exact form of the function f, see Pilant and Rundell [68] who showed that by monitoring (recording and measuring) the transient temperature at one end of a rod the unknown function f depending on the temperature can be recovered uniquely. However, even if the solution exists and is unique it will not depend continously on the input data.

In this study, we investigate some direct heat conduction problems (DHCP) and the corresponding inverse heat conduction problems (IHCP) with both linear and nonlinear boundary conditions. Our aim is to use the boundary element method (BEM) to construct and solve numerically the missing terms involving boundary temperatures, heat fluxes and heat transfer

coefficients. To stabilise the solution of the IHCP we use the Tikhonov regularization method, see Tikhonov and Arsenin [83] and Morozov [61], or the truncated singular value decomposition (TSVD), see Xu [88]. Numerical results are then presented and discused.

1.1.1 Composition and structure of the thesis

This thesis aims at improving various features of the BEM for solving different types of steady and unsteady one-dimensional and two-dimensional direct and inverse heat conduction problems. This is because the BEM has been instrumental in solving many important steady and unsteady IHCPs. For example, inverse BEMs have been formulated to resolve unspecified boundary conditions in heat conduction, see Lesnic *et al.* [50], unknown initial temperature, see Lesnic *et al.* [53], Mera *et al.* [58], unknown thermophysical properties, see Lesnic *et al.* [51, 52, 55], Mera *et al.* [59], unknown heat sources, see Farcas *et al.* [25], Farcas and Lesnic [26], Rap *et al.* [70], and unknown heat transfer coefficients, see Maillet *et al.* [57], Chantasiriwan [18], Divo *et al.* [22]. In the thesis we examine the accuracy and stability of the BEM solutions to inverse problems which lack some information on the boundary of the physical domain. The Tikhonov regularisation and the TSVD methods are employed to stabilize the solutions of the inverse problems with the choice of the regularization parameter based on the L-curve method, see Hansen and O'Leary [36].

In chapter 1, the basic steps of developing the BEM technique, as used in one-dimensional time dependent DHCPs, are illustrated in detail. The accuracy of the numerical results obtained when solving the DHCP using the BEM is investigated for various numbers of boundary elements which discretise the boundary of the solution domain. The application of the BEM to solving IHCPs has been comprehensively described in Ingham and Yuan [40] for steady state and in Kurpisz and Nowak [49] for the unsteady-state (transient) heat conduction. Other applications of the BEM inverse analyses are described in Ingham and Wrobel [41]. The determination of the spacewise or time-dependent ambient temperature has been theoretically investigated by Kostin and Prilepko [47] and [48], respectively. In chapter 2, we investigate for the first time its numerical reconstruction using the BEM. The experimental difficulty of measuring both the temperature and heat flux at the same part of the boundary is overcome by setting up an IHCP which in the mathematical formulation allows for the convective boundary conditions to be prescribed over the whole boundary. Further in the chapter, the ambient temperature is allowed

to vary with space or time. Hence, a more realistic model can be proposed for the heat transfer in building enclosures, e.g. glazed surfaces, where the ambient temperature can vary from surface to surface in a building, as well as with time depending on the local air flow patterns, e.g. type of flows, operational state of equipment, external weather conditions, etc., see Trombe *et al.* [85].

We study the inverse problem of restoring the unknown function f in the boundary conditions (1.1.1) and (1.1.2) of the third kind (at the boundary of the heat conductor there is convective heat transfer (exchange) with the environment) for a one-dimensional heat conduction problem. Along with the temperature T in the domain, we seek the temperature f of the environment. In sections 2.2 and 2.4, respectively, we investigate two situations, namely:

(i) when the function $f(x,t)$, $x \in \{0,1\}$, $t \in (0,t_f]$ depends on x only, in which case we have to determine the constants f_0 and f_1 entering the boundary conditions (1.1.1) and (1.1.2), respectively, and

(ii) when the function $f(x,t)$, $x \in \{0,1\}$, $t \in (0,t_f]$ depends on t only, in which case we have to determine the same function $f(t)$ entering the boundary conditions (1.1.1) and (1.1.2). The boundary conditions (1.1.1) and (1.1.2) are given by

$$\frac{\partial T}{\partial n}(0,t) + \sigma_0(t)T(0,t) = h_0(t)f(0,t) + b_0(t), \qquad \text{for} \quad t \in (0,t_f], \tag{1.1.1}$$

$$\frac{\partial T}{\partial n}(1,t) + \sigma_1(t)T(1,t) = h_1(t)f(1,t) + b_1(t), \qquad \text{for} \quad t \in (0,t_f], \tag{1.1.2}$$

where n is the outer unit normal to the one-dimensional boundary $\{0,1\}$, $t_f > 0$ is an arbitrary final time of interest, and σ_i, h_i and b_i, $i = 0,1$, are given functions. In sections 2.3 and 2.5 we also study the inverse problem of restoring the heat transfer coefficient (HTC) function σ in the Robin boundary conditions (1.1.3) and (1.1.4) of the third kind, namely

$$\frac{\partial T}{\partial n}(0,t) + \sigma(0,t)T(0,t) = B_0(t) \qquad \text{for} \quad t \in (0,t_f], \tag{1.1.3}$$

$$\frac{\partial T}{\partial n}(1,t) + \sigma(1,t)T(1,t) = B_1(t) \qquad \text{for} \quad t \in (0,t_f], \tag{1.1.4}$$

where B_i, $i = 0,1$ are given functions. The heat conductor is exposed to a hostile environment such that no direct measurement of the HTC is practically possible. Along with σ we seek the temperature T in the domain. In sections 2.3 and 2.5, respectively, we investigate two situations, namely:

(iii) when the function $\sigma(x,t)$, $x \in \{0,1\}$, $t \in (0,t_f]$ depends on x only, in which case we have to determine the constants σ_0 and σ_1 entering the boundary conditions (1.1.3) and (1.1.4), respectively, and

(iv) when the function $\sigma(x,t)$, $x \in \{0,1\}$, $t \in (0,t_f]$ depends on t only, in which case we determine the same function $\sigma(t)$, which enters the boundary conditions (1.1.3) and (1.1.4).

In all the four cases, additional information, called "effect", is necessary to be measured in order to compensate for the unknown "causes" of the inverse problems. In what follows we distinguish between the paired situations (i) and (ii) defined as Problems I and III, respectively, and the situations (iii) and (iv) defining Problems II and IV, respectively.

Whilst in chapter 2, Problem IV, the retrieval of the time-dependent HTC, $\sigma(t)$, is sought from the additional boundary temperature measurement $T(0,t)$, in chapter 3, we consider the additional information given by some non-standard boundary measurements

$$0 < E(t) = T^2(0,t) + T^2(1,t), \quad \forall\, t \in [0,t_f]. \tag{1.1.5}$$

To stabilise the solution of this inverse problem we have used the Tikhonov regularization method.

In chapter 4, we investigate physical processes in high temperatures and hostile environments, such as fast cooling of molten steel, in which there is limited opportunity for the measurement of the temperature and heat flux on the surface and the heat transfer method is complex or unknown. We propose a model based on the one-dimensional heat equation involving the heat exchange between the ends of a rod and the surrounding environment. It is important to note that this IHCP is investigated in chapter 5 as a two-dimensional steady-state IHCP. In these hostile high temperature environments the HTC depends on the boundary temperature and the dependence has a complicated or unknown structure, see Rösch [76]. In such a case one has to set up an inverse problem to reconstruct the exact form of the function f on the boundary satisfying

$$\frac{\partial T}{\partial n}(x,t) = f(T(x,t)), \qquad t \in (0,t_f],\ x \in \{0,1\}\,. \tag{1.1.6}$$

In the first instance, we seek to obtain the function $f(T)$ as a polynomial function of degree K

$$f(T) = \sum_{k=0}^{K} a_k T^k, \tag{1.1.7}$$

with unknown coefficients $(a_k)_{k=\overline{0,K}}$.

In section 4.3 we develop the BEM to construct and solve numerically the missing terms involving the boundary temperature, the heat fluxes and the function f. In section 4.4, numerical solutions for various test examples of the DHCP with the term f being linear and quadratic are

obtained using the BEM. In sections 4.5 we study the IHCP and stabilised approximate values of the heat flux and the function f for different degrees K of the polynomial function (1.1.7) are presented and discussed.

The ability of the BEM to obtain accurate numerical results is tested by increasing the number of discretisations for the space and time domain, respectively, from $(N, N_0) = (10, 10)$ to $(80, 80)$, and the stability of the solution examined by adding from 0% to 5% additive and multiplicative noise in the input data. The Tikhonov regularization method has been used with great success to stabilize the numerical solutions.

In chapter 5 we investigate the application of the BEM to the solution of an inverse steady-state heat conduction problem in two dimensions, where the governing equation is the classical Laplace equation and the enforced boundary conditions are unknown nonlinear relations between the heat flux and the boundary temperature. Specifically, in a practical sense, the chapter attempts to localize and evaluate the corrosion damage in a non-intrusive framework for a two-dimensional steady IHCP. In section 5.2, the BEM is developed for the two-dimensional DHCP and IHCP. In section 5.3 the use of the BEM in the numerical examples for the nonlinear DHCP representing the physical phenomenon of predicting the corrosion damage is investigated. The temperature T satisfies the Laplace equation in the physical domain, and various boundary conditions are prescribed to describe the presence or absence of corrosion damage. In the chapter we investigate the absence of corrosion at the interface $y = d$ by assuming that the heat exchange between the metal and the fluid is described by the classical Newton cooling law, see Carslaw and Jaeger [17],

$$T_y(x, d) + \gamma(T(x, d) - T_{\text{ext}}) = 0, \tag{1.1.8}$$

where T_{ext} is the temperature outside the top surface on $y = d$. Therefore, the constant γ is the ratio between the thermal conductivities of the fluid and the metal, and can be assumed to be non-negative for physical reasons. To localise and evaluate the corrosion damage on the bounday $y = d$ in a non-intrusive framework, we assume a model for the fluid-metal interface, namely a non-linear boundary condition given by, see Jones [44],

$$T_y(x, d) + \gamma f(T(x, d)) = 0, \tag{1.1.9}$$

where f is an unknown function to be determined. We also use the linear energy dispersion (LED) model which assumes the complex situation characterizing the presence of corrosion, because the precipitate formed on the upper surface and producing a heating interaction between

the metal and the fluid is characterised by a nonlinear perturbation of the boundary condition given by

$$T_y(x,d) + \gamma T(x,d) + \kappa h(T(x,d)) = 0, \tag{1.1.10}$$

where the nonlinear term $h(T)$, which physically models the presence of the corrosion damage, is assumed unknown and to be determined. This approach is possible through applying a nontrivial heat flux $T_y(x,0)$ on a suitable portion of the boundary of the rectangular conductor, say $y = 0$, measuring the temperature $T(x,0)$ on the same boundary portion, whilst the heat fluxes T_x on the vertical boundaries are assumed to be zero. The results obtained when no regularisation is applied are, as expected, highly fluctuating. Therefore, the Tikhonov regularization method is employed when the input data is noisy.

Finally, in chapter 6 general conclusions and suggestions for future work are provided.

1.2 Stability analysis

According to Hadamard [33], a problem requires three sets of conditions to be well-posed, namely, (i) a solution satisfies the problem (existence of solution), (ii) there exists at most one solution of the problem (uniqueness of solution), and (iii) small changes in the input data result in small changes in the solution (continuous dependence of the solution upon the data). The third condition is the stability requirement. If any one is not met then the problem is not well-posed, and it is called an ill-posed problem.

In the thesis we simulate some practical problems which means that additional data has to come from measurements which inherently contain random noise. Therefore, if the problem under investigation is ill-posed, due to the ill-conditioned nature of the resulting system of algebraic equations, then the numerical solution may be unstable. On the other hand if the problem is well-posed then numerical solutions are stable. In order to illustrate the stability of the numerical solutions in direct heat conduction problems (DHCP) and the instability of the numerical solutions in the inverse heat conduction problems (IHCP), we introduce 1%, 3% and 5% noise in the input data and then monitor the amount of error occuring in the output data.

1.2.1 The Tikhonov regularization

Assume that we wish to obtain a regularized solution to the system of algebraic equations given by

$$X\mathbf{Y} = \mathbf{Z} \tag{1.2.1}$$

in the least-squares sense, but penalizing solutions of large norm. For this we minimize the Tikhonov functional

$$(X\mathbf{Y} - \mathbf{Z})^{tr}(\mathbf{XY} - \mathbf{Z}) + \lambda(\widetilde{R}\mathbf{Y})^{tr}(\widetilde{R}\mathbf{Y}), \tag{1.2.2}$$

which gives the approximate solution $\mathbf{Y}_\lambda$ depending on λ as

$$\mathbf{Y}_\lambda = (X^{tr}X + \lambda\widetilde{R}^{tr}\widetilde{R})^{-1}X^{tr}\mathbf{Z}. \tag{1.2.3}$$

When $\lambda = 0$, we obtain the ordinary least-squares method, but $\lambda > 0$ plays the role of a regularization parameter whose choice can be based on the discrepancy principle, see Morozov [60], the cross validation principle, see Golub *et al.* [32], or the L-curve method, see Hansen [35].

The regularization matrix $\widetilde{R}$ can be chosen as

$$\widetilde{R}^{tr}\widetilde{R} = \begin{pmatrix} 1 & 0 & 0 & 0 & \dots \\ 0 & 1 & 0 & 0 & \dots \\ 0 & 0 & 1 & 0 & \dots \\ 0 & 0 & 0 & 1 & \dots \\ \vdots & \vdots & \vdots & \vdots & \ddots \end{pmatrix} \text{(zeroth-order regularization)}, \tag{1.2.4}$$

or

$$\widetilde{R}^{tr}\widetilde{R} = \begin{pmatrix} 1 & -1 & 0 & 0 & \dots \\ -1 & 2 & -1 & 0 & \dots \\ 0 & -1 & 2 & -1 & \dots \\ 0 & 0 & -1 & 2 & \dots \\ \vdots & \vdots & \vdots & \vdots & \ddots \end{pmatrix} \text{(first-order regularization)}, \tag{1.2.5}$$

or

$$\widetilde{R}^{tr}\widetilde{R} = \begin{pmatrix} 1 & -2 & 1 & 0 & 0 & \dots \\ -2 & 5 & -4 & 1 & 0 & \dots \\ 1 & -4 & 6 & -4 & 1 & \dots \\ 0 & 1 & -4 & 6 & -4 & \dots \\ 0 & 0 & 1 & -4 & 6 & \dots \\ \vdots & \vdots & \vdots & \vdots & \vdots & \ddots \end{pmatrix} \text{(second-order regularization)}. \tag{1.2.6}$$

The challenge is to choose a good value of $\lambda > 0$ that keeps the regularized solution $\mathbf{Y}_\lambda$ sufficiently smooth without losing too much information on the solution $\mathbf{Y}_{true}$. Another method used to regularize a linear ill-conditioned system of equations is the truncated singular value decomposition (TSVD) which is briefly described in the next section.

1.2.2 Singular value decomposition (SVD)

SVD methods are based on the theorem of linear algebra, namely that any $M \times N$ matrix X whose number of rows M is greater than or equal to its number of columns N, can be written as the product of an $M \times N$ matrix Φ, an $N \times N$ diagonal matrix Λ with positive or zero elements (singular values), and transpose of an $N \times N$ orthogonal matrix Ψ, namely

$$X = \Phi \Lambda \Psi^{tr}. \tag{1.2.7}$$

The matrices Φ and Ψ are each orthogonal in the sense that their columns are orthonormal, such that

$$\Phi^{tr}\Phi = \Psi\Psi^{tr} = I. \tag{1.2.8}$$

Since Ψ is a square matrix, it is also row orthonormal, i.e. $\Psi^{tr} \cdot \Psi = I$. The advantage of SVD is that the decomposition in equation (1.2.7) is unique and can be done no matter if the matrix X is singular or not. The SVD is also a method of choice for solving linear least squares problems. If the matrix X is square, $N \times N$ say, then there exist Φ, Ψ and Λ which are all square matrices of the same size. The matrices Φ and Ψ are orthogonal, so their inverses are equal to their transposes and the matrix Λ is diagonal, and therefore its inverse is the diagonal matrix whose elements are the reciprocal of the elements sv_j. From equation (1.2.7) it now follows immediately that the inverse of X is given by

$$X^{-1} = \Psi[\mathrm{diag}(1/sv_j)]\Phi^{tr}, \tag{1.2.9}$$

where, $sv_1 > sv_2 > \ldots > sv_i > sv_{i+1} > sv_{i+2} > \ldots > sv_N \geq 0$.
The only thing that can go wrong is that the construction of one of the sv_j turns out to be zero, or so small to the extent that its value is dominated by rounding-off error. If this is the situation then the matrix X is even more singular.

Formally, the condition number of a matrix X is defined as the ratio of the largest sv_j to the smallest sv_j. A matrix is singular if its condition number is infinite, and it is ill-conditioned if its condition number is too large, i.e. its value is approaching the machine floating point precision,

namely 10^{-8} for single precision or 10^{-16} for double precision. When the $sv_j's$ are very small but nonzero then the solution vector has large components whose algebraic cancellation when multiplying with the matrix X may give a very poor approximation to the right-hand side vector $\mathbf{Z}$ in equation (1.2.1). The solution vector $\mathbf{Y}$, obtained by zeroing the small $sv_j's$ and then using equation (1.2.9), is better (in the sense of the residual $|X\mathbf{Y} - \mathbf{Z}|$ being smaller) than both the direct-method solution and the SVD solution, see Xu [88]. In throwing away a combination of equations that are corrupted with round-off errors we are in some sense reducing the components that makes the residual $|X\mathbf{Y} - \mathbf{Z}|$ larger. On the other hand, SVD cannot be applied blindly, one needs to exercise some discretion in deciding the threshold to the zeros of the small $sv_j's$, and/or must have knowledge of what size of computed residual $|X\mathbf{Y} - \mathbf{Z}|$ is acceptable.

1.2.3 Choice of the regularization parameter

A classical method already in use for the selection of the regularization parameter is the discrepancy principle, see Morozov [60]. However, this method depends on the knowledge of the amount of noise in the known vector $\mathbf{Z}$. Recently, Hansen [35] proposed that the regularization parameter be chosen by inspecting the plots of the smoothness in the solution versus the fit to the data. This is through plotting the norm of the regularized solution $\|\mathbf{Y}_\lambda\|$ versus the norm of the residual $\|X\mathbf{Y}_\lambda - \mathbf{Z}\|$ for various values of $\lambda > 0$. Usually, the figure turns out to be an L-shaped curve, with the corner point defining the maximum curvature. The horizontal portion of the curve which falls to the right hand side of the corner, corresponds to large values of λ, which results in an over-smoothed solution. In contrast, the vertical portion of the curve, which lies on the left hand side of the corner, corresponds to small values of λ, resulting in an under-regularized solution containing instabilities. Hence, the regularised solution $\mathbf{Y}_\lambda$ changes its nature at the corner of the curve, from being dominated by regularization to being dominated by the errors in the right hand side of the equation (1.2.3). Therefore, the value of λ at the L-corner of the curve povides an acceptable balance and simultaneously minimizes the solution norm and the norm of the residual vector. This may be viewed as providing the desired amount of regularization in the solution.

Similarly, the TSVD involves the determination of the proper value of the threshold truncation level, which can also be chosen on the basis of the above L-curve analysis. However, now the L-curve plot is between $\|\mathbf{Y}_j\|$ and the norm of the residual $\|X\mathbf{Y}_j - \mathbf{Z}\|$ for various truncation

levels j from 1 to N. The curve is also L-shaped in general and the optimal value of j exists near the corner, see Hansen [34, 35].

In this thesis we have extensively made use of the L-curve in determining the optimal value of the regularizing parameter λ. This is because the L-curve method does not depend on the prior knowledge of the level of noise in the right-hand side vector $\mathbf{Z}$, or on the properties of the matrix X . Therefore, it is widely applicable in most physical problems.

1.3 The boundary element method (BEM)

There are several advantages of using the BEM over the finite element (FEM) or the finite-difference (FDM) methods. First, the BEM only requires a boundary mesh to discretise the problem and as such, it reduces by one the dimensionality of the problem, it deals easily with both infinite and semi-infinite domains, it is very flexible and applicable to complex geometries without having to resort to intricate internal mesh generation of unnecesary internal information as required by the traditional FDM or FEM. Secondly, in this thesis the unknown ambient temperature, heat transfer coefficient, boundary temperature and heat flux are boundary quantites to be determined and the discretisation of the boundary only is the essence of the BEM. It is important to note that all these gains are possible only when the fundamental solution of the governing equation is available, a fact that forms the major drawback in the use of the BEM in general.

The mathematical background of the BEM is represented by the divergence and Green's theorems. Also the definition of the Kronecker symbol, the Heaviside function, the Dirac distribution, and the *erf*, *erfc* and *erfi* functions are introduced.

Divergence theorem gives

$$\int_{\partial\Omega} \mathbf{F}\cdot\mathbf{n}\,\mathrm{d}S = \int_{\Omega} \nabla\cdot\mathbf{F}\,\mathrm{d}\Omega, \tag{1.3.1}$$

where the vector field $\mathbf{F}$ is defined throughout the domain Ω enclosed by the boundary $\partial\Omega$, and $\mathbf{n}$ is the unit outward normal to $\partial\Omega$.

Green's theorems give

$$\int_{\Omega} \left(U\nabla^2 V + \nabla U\cdot\nabla V\right)\mathrm{d}\Omega = \int_{\partial\Omega} U\frac{\partial V}{\partial n}\mathrm{d}S, \tag{1.3.2}$$

$$\int_{\Omega} \left(U\nabla^2 V - V\nabla^2 U\right)\mathrm{d}\Omega = \int_{\partial\Omega} \left(U\frac{\partial V}{\partial n} - V\frac{\partial U}{\partial n}\right)\mathrm{d}S. \tag{1.3.3}$$

These identitities can be obtained by taking $\mathbf{F} = U\nabla V$ and applying the divergence theorem (1.3.1) to obtain equation (1.3.2), whilst equation (1.3.3) is obtained by applying equation (1.3.2) for U and V interchanged and then subtracting these two equations. The identities (1.3.1) and (1.3.2) form the basis upon which the mathematical formulation of the BEM is anchored.

The Kronecker delta symbol is given by

$$\delta_{ij} = \begin{cases} 1 & \text{if} \quad i = j, \\ 0 & \text{if} \quad i \neq j. \end{cases} \tag{1.3.4}$$

The Heaviside function is given by

$$H(t) = \begin{cases} 1 & \text{if} \quad t > 0, \\ 0 & \text{if} \quad t \leq 0. \end{cases} \tag{1.3.5}$$

The generalized Dirac delta distribution fuction is given by

$$\delta(x,\xi) = \delta(x-\xi) = \begin{cases} 0 & \text{if} \quad x \neq \xi, \\ \infty & \text{if} \quad x = \xi. \end{cases} \tag{1.3.6}$$

The fundamental properties of the Dirac delta distribution are given by

$$\delta(x) = H'(x), \quad \int_\Omega f(\xi)\delta(x,\xi)\mathrm{d}\xi = f(x), \quad x \in \Omega. \tag{1.3.7}$$

The *erf*, *erfc* and *erfi* functions are given by

$$erf(x) = \frac{2}{\sqrt{\pi}}\int_0^x \exp(-\sigma^2)\mathrm{d}\sigma, \quad erfc(x) = 1 - erf(x), \tag{1.3.8}$$

$$erfi(x) = -i\, erf(ix) = \frac{2}{\sqrt{\pi}}\int_0^x \exp(\sigma^2)\mathrm{d}\sigma, \quad i = \sqrt{-1}. \tag{1.3.9}$$

1.3.1 Fundamental solution for the one-dimensional heat equation

One-dimensional transient heat equation is mathematically modelled by a parabolic partial differential equation of the form

$$LT(\underline{p}) = 0, \qquad \underline{p} = (x,t) \in (0,1) \times (0,t_f] =: Q, \tag{1.3.10}$$

where L is the partial differential heat operator $\frac{\partial^2}{\partial x^2} - \frac{\partial}{\partial t}$ and T is the temperature. The function $G(\underline{p};\underline{p}')$ is a fundamental solution for the heat equation (1.3.10) if

$$L^*G(\underline{p};\underline{p}') = -\delta(\underline{p};\underline{p}'), \tag{1.3.11}$$

where $L^* = \frac{\partial^2}{\partial x^2} + \frac{\partial}{\partial t}$ is the adjoint of L, $\underline{p} = (x,t)$ is a field point, $\underline{p}' = (\xi,\tau)$ is a source point and δ is the Dirac delta distribution function defined in (1.3.6). Thus, the fundamental solution of the heat conduction equation (1.3.10) satisfies the equation

$$\frac{\partial G}{\partial \tau}(x,t;\xi,\tau) + \frac{\partial^2 G}{\partial \xi^2}(x,t;\xi,\tau) = -\delta(x,t;\xi,\tau). \tag{1.3.12}$$

If we look for a solution of equation (1.3.12) that depends only on the distance $r = |x-\xi|$ and time period $t' = |t-\tau|$, then the following expression is obtained, see e.g. Garroni and Menaldi [31],

$$G(x,t;\xi,\tau) = \frac{H(t-\tau)}{2\sqrt{\pi(t-\tau)}} exp\left(-\frac{(x-\xi)^2}{4(t-\tau)}\right), \tag{1.3.13}$$

where H is the Heaviside function given in (1.3.5), which is introduced to emphasise the fact that the fundamental solution is zero when $t \leq \tau$.

1.3.2 Boundary integral equation (BIE)

The governing partial differential equation (1.3.10) transforms into an integral equation by means of the fundamental solution (1.3.13) and Green's second formula given in (1.3.3). For an arbitrary function V, the following equation holds:

$$\int_Q \left[T(\underline{p}')L^*V(\underline{p}') - V(\underline{p}')LT(\underline{p}')\right] \mathrm{d}Q = \int_{\partial Q} \left[T(\underline{p}')\frac{\partial V}{\partial n}(\underline{p}') - V(\underline{p}')\frac{\partial T}{\partial n}(\underline{p}')\right] \mathrm{d}S. \tag{1.3.14}$$

Next, taking $V = G(\underline{p};\underline{p}')$ we obtain that for every $\underline{p} \in Q$

$$\begin{aligned} &\int_Q \left[T(\underline{p}')L^*G(\underline{p};\underline{p}') - G(\underline{p};\underline{p}')LT(\underline{p}')\right] \mathrm{d}Q \\ &= \int_{\partial Q} \left[T(\underline{p}')\frac{\partial G}{\partial n(\underline{p}')}(\underline{p};\underline{p}') - G(\underline{p};\underline{p}')\frac{\partial T}{\partial n}(\underline{p}')\right] \mathrm{d}S. \end{aligned} \tag{1.3.15}$$

If equations (1.3.10) and (1.3.11) are used in (1.3.15) then we obtain

$$-\int_Q T(\underline{p}')\delta(\underline{p},\underline{p}')\mathrm{d}Q = \int_{\partial Q} \left[T(\underline{p}')\frac{\partial G}{\partial n(\underline{p}')}(\underline{p};\underline{p}') - G(\underline{p};\underline{p}')\frac{\partial T}{\partial n}(\underline{p}')\right] \mathrm{d}S. \tag{1.3.16}$$

Using the property (1.3.7) of the Dirac delta function, we obtain

$$T(\underline{p}) = \int_{\partial Q} \left[G(\underline{p};\underline{p}')\frac{\partial T}{\partial n}(\underline{p}') - T(\underline{p}')\frac{\partial G}{\partial n}(\underline{p};\underline{p}')\right] \mathrm{d}S, \qquad \underline{p} \in Q. \tag{1.3.17}$$

On letting x tend to a boundary point, i.e. 0 or 1, then one obtains the boundary integral equation, see e.g. Brebbia *et al.* [11], Chen and Zhou [19], Wrobel [87],

$$\frac{1}{2}T(\underline{p}) = \int_{\partial Q} \left[G(\underline{p};\underline{p}')\frac{\partial T}{\partial n}(\underline{p}') - T(\underline{p}')\frac{\partial G}{\partial n}(\underline{p};\underline{p}')\right] \mathrm{d}S, \quad \underline{p} \in \{0,1\} \times (0,t_f] \tag{1.3.18}$$

or, combining (1.3.17) and (1.3.18), we obtain

$$\eta(x)T(\underline{p}) = \int_{\partial Q} \left[G(\underline{p};\underline{p}')\frac{\partial T}{\partial n}(\underline{p}') - T(\underline{p}')\frac{\partial G}{\partial n}(\underline{p};\underline{p}') \right] \mathrm{d}S, \tag{1.3.19}$$

for any $\underline{p} = (x,t) \in \overline{Q}$, where $\eta(x) = 1$ if $x \in (0,1)$ and $\eta(x) = \frac{1}{2}$ if $x \in \{0,1\}$.

The boundary integral equation (BIE) (1.3.19) can then be transformed into the form

$$\begin{aligned} \eta(x)T(\underline{p}) = &\int_{S_1} \left[G(\underline{p};\underline{p}')\frac{\partial T}{\partial n}(\underline{p}') - T(\underline{p}')\frac{\partial G}{\partial n(\underline{p}')}(\underline{p};\underline{p}') \right] \mathrm{d}S_1 \\ &+ \int_{S_2} T(\underline{p}')G(\underline{p};\underline{p}')\mathrm{d}S_2, \qquad \underline{p} = (x,t) \in \overline{Q}, \end{aligned} \tag{1.3.20}$$

where $S_1 = \{0,1\} \times (0,t_f]$ and $S_2 = [0,1] \times \{0\}$. The integral over $S_3 = [0,1] \times \{t_f\}$ vanishes due to the Heaviside function in expression (1.3.13), and $\mathbf{n}(0) = -\mathbf{i}$ and $\mathbf{n}(1) = \mathbf{i}$ for the boundaries $x = 0$ and $x = 1$, respectively. Note that the last domain integral in (1.3.20) includes the specified initial condition at $t = 0$.

We also note that the BIE (1.3.18) provides a linear relation between the boundary values of the solution T and those of its normal derivative $\frac{\partial T}{\partial n}$. Hence given T at each point on part of the boundary and $\frac{\partial T}{\partial n}$ on the remainder, we obtain a linear BIE, or a pair of such equations for the complementary boundary values. By solving these equations and then substituting their solutions, together with the boundary data, into equation (1.3.17), we obtain the solution at any point $\underline{p}$ in the domain Q.

1.3.3 Numerical discretisation

In practice the integral equation (1.3.20) may rarely be solved analytically and thus some form of numerical approximation is necessary. Therefore, the boundary S_1 is discretised into a series of boundary elements, namely,

$$S_{11} = \{0\} \times (0,t_f] = \cup_{j=1}^{N} \{0\} \times (t_{j-1},t_j], \tag{1.3.21}$$

$$S_{12} = \{1\} \times (0,t_f] = \cup_{j=1}^{N} \{1\} \times (t_{j-1},t_j]. \tag{1.3.22}$$

Also the boundary S_2 is discretised into a series of cells, namely,

$$S_2 = [0,1] \times \{0\} = \cup_{k=1}^{N_0} [x_{k-1},x_k] \times \{0\}. \tag{1.3.23}$$

Over each time boundary element $(t_{j-1}, t_j]$, the boundary temperature T and the heat flux $\frac{\partial T}{\partial n}$ are assumed to be constant and take their values at the mid-point $\widetilde{t}_j = \frac{t_{j-1}+t_j}{2}$, i.e.

$$T(0,t) = T(0,\widetilde{t}_j) = T_{0j} \qquad \text{for} \quad t \in (t_{j-1}, t_j], \tag{1.3.24}$$

$$T(1,t) = T(1,\widetilde{t}_j) = T_{1j} \qquad \text{for} \quad t \in (t_{j-1}, t_j], \tag{1.3.25}$$

$$\frac{\partial T}{\partial n}(0,t) = \frac{\partial T}{\partial n}(0,\widetilde{t}_j) = T'_{0j} \qquad \text{for} \quad t \in (t_{j-1}, t_j], \tag{1.3.26}$$

$$\frac{\partial T}{\partial n}(1,t) = \frac{\partial T}{\partial n}(1,\widetilde{t}_j) = T'_{1j} \qquad \text{for} \quad t \in (t_{j-1}, t_j]. \tag{1.3.27}$$

Also over each space cell $[x_{k-1}, x_k)$, the initial temperature T is assumed constant and takes its values at the mid point $\widetilde{x}_k = \frac{x_{k-1}+x_k}{2}$, i.e.

$$T(x,0) = T(\widetilde{x}_k, 0) = T^0_k \qquad \text{for} \quad x \in [x_{k-1}, x_k). \tag{1.3.28}$$

Then using the approximations (1.3.24)–(1.3.28), the integral equation (1.3.20) can be discretised as

$$\begin{aligned}\eta(x)T(x,t) = &\sum_{j=1}^{N}\left[T'_{0j}\int_{t_{j-1}}^{t_j} G(x,t;0,\tau)\mathrm{d}\tau + T'_{1j}\int_{t_{j-1}}^{t_j} G(x,t;1,\tau)\mathrm{d}\tau\right] \\ &-\sum_{j=1}^{N}\left[T_{0j}\int_{t_{j-1}}^{t_j}\frac{\partial G}{\partial n_0}(x,t;0,\tau) + T_{1j}\int_{t_{j-1}}^{t_j}\frac{\partial G}{\partial n_1}(x,t;1,\tau)\right] \\ &+\sum_{k=1}^{N_0} T^0_k\int_{x_{k-1}}^{x_k} G(x,t;\xi,0)\mathrm{d}\xi \qquad \text{for} \quad (x,t) \in [0,1]\times(0,1],\end{aligned} \tag{1.3.29}$$

where n_0 and n_1 represent the outward normals at the boundaries $x = 0$ and $x = 1$, respectively. Equation (1.3.29) can be rewritten as

$$\begin{aligned}\eta(x)T(x,t) = &\sum_{j=1}^{N}\left[T'_{0j}C^0_j(x,t) + T'_{1j}(x,t)C^1_j(x,t) - T_{0j}D^0_j(x,t) - T_{1j}D^1_j(x,t)\right] \\ &+\sum_{k=1}^{N_0} T^0_k E_k(x,t), \quad \text{for} \quad (x,t) \in [0,1]\times(0,1],\end{aligned} \tag{1.3.30}$$

where the coefficients are given by

$$C^\xi_j(x,t) = \int_{t_{j-1}}^{t_j} G(x,t;\xi,\tau)\mathrm{d}\tau = \int_{t_{j-1}}^{t_j}\frac{H(t-\tau)}{2\sqrt{\pi(t-\tau)}}\exp\left(-\frac{(x-\xi)^2}{4(t-\tau)}\right)\mathrm{d}\tau, \tag{1.3.31}$$

$$D^\xi_j(x,t) = \int_{t_{j-1}}^{t_j}\frac{\partial}{\partial\eta_\xi}G(x,t;\xi,\tau)\mathrm{d}\tau = \int_{t_{j-1}}^{t_j}\frac{H(t-\tau)}{4\sqrt{\pi(t-\tau)^3}}|x-\xi|\exp\left(-\frac{(x-\xi)^2}{4(t-\tau)}\right)\mathrm{d}\tau, \tag{1.3.32}$$

$$E_k(x,t) = \int_{x_{k-1}}^{x_k} G(x,t;y,0)\mathrm{d}y = \int_{x_{k-1}}^{x_k}\frac{1}{2\sqrt{\pi t}}\exp\left(-\frac{(x-y)^2}{4t}\right)\mathrm{d}y, \tag{1.3.33}$$

where $\xi \in \{0,1\}$.

The integrals (1.3.31)–(1.3.33) can be evaluated analytically and their expressions are given by

$$C_j^{\xi}(x,j) = \begin{cases} 0, & t \le t_{j-1} \\ [(t-t_{j-1})/\pi]^{1/2}, & t_{j-1} < t \le t_j; r = 0 \\ r[\exp(-z^2)/z - \pi^{1/2} erfc(z)]/(2\pi^{1/2}), & t_{j-1} < t \le t_j; r \ne 0 \\ \left[(t-t_{j-1})^{1/2} - (t-t_j)^{1/2}\right]/\pi^{1/2}, & t_j < t; r = 0 \\ r[\exp(-z^2)/z - \exp(-z_1^2)/z_1 + \\ \pi^{1/2}\{erfc(z) - erf(z_1)\}]/(2\pi^{1/2}), & t_j < t; r \ne 0 \end{cases} \tag{1.3.34}$$

$$D_j^{\xi}(x,t) = \begin{cases} 0, & t \le t_{j-1} \\ 0, & t_{j-1} < t \le t_j; \quad r = 0 \\ -erfc(z)/2, & t_{j-1} < t \le t_j; \quad r \ne 0 \\ [erf(z) - erf(z_1)]/2, & t_j < t \end{cases} \tag{1.3.35}$$

$$E_k(x,t) = \frac{1}{2}\left[erf\left(\frac{x - x_{k-1}}{2t^{1/2}}\right) - erf\left(\frac{x - x_k}{2t^{1/2}}\right)\right], \tag{1.3.36}$$

where the functions erf and $erfc$ are defined in (1.3.8) and

$$r = |x - \xi|, \quad z = r\frac{(t-t_{j-1})^{-1/2}}{2}, \quad z_1 = r\frac{(t-t_j)^{-1/2}}{2}. \tag{1.3.37}$$

If (1.3.37) is applied at every node on the boundary S_1 then the following set of linear algebraic equations is obtained:

$$\sum_{j=1}^{N}\left[C_{ij}^{0\xi}T'_{0j} + C_{ij}^{1\xi}T'_{1j} - D_{ij}^{0\xi}T_{0j} - D_{ij}^{1\xi}T_{1j}\right] + \sum_{k=1}^{N_0} E_{ik}(\xi)T_k^0 = 0, \quad i = \overline{1,N}, \quad \xi \in \{0,1\}, \tag{1.3.38}$$

where the matrices $C^{0\xi}$,$C^{1\xi}$, $D^{0\xi}$ and $D^{1\xi}$ are defined by

$$C_{ij}^{0\xi} = C_j^{\xi}(0,\widetilde{t}_i), \quad C_{ij}^{1\xi} = C_j^{\xi}(1,\widetilde{t}_i), \tag{1.3.39}$$

$$D_{ij}^{0\xi} = D_j^{\xi}(0,\widetilde{t}_i) + 0.5\delta_{ij}(1-\xi), \quad D_{ij}^{1\xi} = D_j^{\xi}(1,\widetilde{t}_i) + 0.5\delta_{ij}\xi, \tag{1.3.40}$$

$$E_{ik}(\xi) = E_k(\xi,\widetilde{t}_i), \tag{1.3.41}$$

for $\xi \in \{0,1\}$, $i,j = \overline{1,N}$, and $k = \overline{1,N_0}$.

1.4 Boundary element method for solving one-dimensional direct heat conduction problems (DHCP)

1.4.1 Mathematical formulation of a one-dimensional DHCP

Consider the DHCP given by

$$\frac{\partial T}{\partial t}(x,t) = \frac{\partial^2 T}{\partial x^2}(x,t), \qquad \text{for} \quad (x,t) \in (0,1) \times (0,t_f] =: Q, \tag{1.4.1}$$

$$\alpha_0 T(0,t) + \beta_0 \frac{\partial T}{\partial n}(0,t) = w_0(t) \qquad \text{for} \quad t \in (0,t_f], \tag{1.4.2}$$

$$\alpha_1 T(1,t) + \beta_1 \frac{\partial T}{\partial n}(1,t) = w_1(t), \qquad \text{for} \quad t \in (0,t_f], \tag{1.4.3}$$

$$T(x,0) = g(x), \qquad \text{for} \quad x \in [0,1], \tag{1.4.4}$$

where the thermal diffusivity has been taken to be 1 for simplicity, $w_0(t), w_1(t)$ and $g(x)$ are prescribed functions, $\alpha_0, \alpha_1, \beta_0, \beta_1$ are known constants and it is also assumed that there is no heat generation throughout the solution domain.

When $\alpha_0 = \alpha_1 = 1$ and $\beta_0 = \beta_1 = 0$, we have Dirichlet boundary conditions in equations (1.4.2) and (1.4.3), namely

$$T(0,t) = w_0(t) \qquad \text{for} \quad t \in (0,t_f], \tag{1.4.5}$$

$$T(1,t) = w_1(t) \qquad \text{for} \quad t \in (0,t_f], \tag{1.4.6}$$

whilst if $\alpha_0 = \alpha_1 = 0$ and $\beta_0 = \beta_1 = 1$, then Neumann boundary conditions are obtained as

$$\frac{\partial T}{\partial n}(0,t) = w_0(t) \qquad \text{for} \quad t \in (0,t_f], \tag{1.4.7}$$

$$\frac{\partial T}{\partial n}(1,t) = w_1(t) \qquad \text{for} \quad \in (0,t_f]. \tag{1.4.8}$$

Otherwise, when $\alpha_0, \alpha_1, \beta_0$ and β_1 are non-zero then the boundary conditions (1.4.2) and (1.4.3) are of Robin type which is a generalization of the Dirichlet and Neumann boundary conditions. Physically, they represent convective boundary conditions. We have the following existence, uniqueness and stability theorem, see Friedman ([30], pp.182, 188) of the DHCP (1.4.1)–(1.4.4).

Theorem 1.4.1 *Suppose* $g \in C^1([0,1])$, $w_0, w_1 \in C([0,t_f])$. *Then there exists a unique solution* $T \in C^{2,1}(Q) \cap C(\overline{Q})$ *of the problem* (1.4.1)–(1.4.4). *Moreover, the function* $\frac{\partial T}{\partial x}$ *is uniformly continuous on* $[0,1] \times [\xi, t_f]$ *for any* $\xi \in (0,t_f)$, *and the function* $\frac{\partial T}{\partial n}$ *is bounded on* $[0,t_f]$.

1.4.2 The BEM

On applying the boundary conditions (1.4.2) and (1.4.3) at the nodes $(0, \widetilde{t}_i)$ and $(1, \widetilde{t}_i)$, respectively, for $i = \overline{1, N}$, the following equations are obtained:

$$\alpha_0 T_{0i} + \beta_0 T'_{0i} = w_0(\widetilde{t}_i) = w_{0i}, \quad i = \overline{1, N}, \tag{1.4.9}$$

$$\alpha_1 T_{1i} + \beta_1 T'_{1i} = w_1(\widetilde{t}_i) = w_{1i}, \quad i = \overline{1, N}. \tag{1.4.10}$$

Also, on applying the initial condition (1.4.4) at the cell nodes $(\widetilde{x}_k, 0)$, for $k = \overline{1, N_0}$, the values of T^0_k are determined, namely

$$T^0_k = T(\widetilde{x}_k, 0) = g(\widetilde{x}_k) = g_k, \quad k = \overline{1, N_0}. \tag{1.4.11}$$

Recasting together equations (1.3.38), (1.4.9)–(1.4.11) results in a system of equations which in a generic form can be written as

$$X\mathbf{Y} = \mathbf{Z} \tag{1.4.12}$$

where X is a known $4N \times 4N$ square matrix, which includes the matrices C^0, C^1, D^0, D^1 and E given by the expressions (1.3.39)–(1.3.41), $\mathbf{Y}$ is a vector of $4N$ unknowns which contains T_{0i}, T_{1i}, T'_{0i} and T'_{1i} recast as

$Y_i = T_{0i}$ for $i = \overline{1, N}$, $Y_i = T_{1(i-N)}$ for $i = \overline{N+1, 2N}$, $Y_i = T'_{0(i-2N)}$ for $i = \overline{2N+1, 3N}$, $Y_i = T'_{1(i-3N)}$ for $i = \overline{3N+1, 4N}$,

and $\mathbf{Z}$ is a vector with $4N$ known elements defined by

$Z_i = -\sum_{k=1}^{N_0} E_{ik}(0) g_k$ for $i = \overline{1, N}$, $Z_i = -\sum_{k=1}^{N_0} E_{(i-N)k}(1) g_k$ for $i = \overline{N+1, 2N}$, $Z_i = w_{0(i-2N)}$ for $i = \overline{2N+1, 3N}$, $Z_i = w_{1(i-3N)}$ for $i = \overline{3N+1, 4N}$.

Often in practical computations the simple conditions (1.4.9) and (1.4.10) permit elimination of $2N$ unknowns, and this reduces the problem to solving a system of $2N$ equations with $2N$ unknowns.

The system of linear algebraic equations (1.4.12) can be solved using a Gaussian elimination procedure giving rise to the values of T_{0i}, T_{1i}, T'_{0i} and T'_{1i} for $i = \overline{1, N}$ which represent the boundary solution. These values are then introduced in the integral equation (1.3.30) and the solution $T(x, t)$ at any point (x, t) in the domain Q is explicitly obtained.

1.4.3 Numerical Examples, Results and Discussion

In the previous section we examined the development of the BEM and the discretisation process necessary for the computation of the approximate solutions of a one-dimensional transient DHCP. In this section we illustrate how these basic ideas of the BEM can be used to solve a simple problem of transient heat conduction, for example in a DHCP associated with the cooling of a room resulting from the heat exchange between the two surfaces of a large glass window. This problem can be more clearly appreciated when a simple one-dimensional model consisting of a finite length slab is used to represent the medium, the relationship between the temperature and the heat flux at the boundary is specified and in the bounded region heat is neither generated nor lost.

In order to illustrate the method, we consider the partial differential equation (1.4.1) in the region $Q = (0,1) \times (0, t_f = 1]$, subject to boundary and initial conditions derived from equations (1.4.2)–(1.4.4) with $\alpha_0 = \alpha_1 = \beta_0 = \beta_1 = 1$, namely

$$T(0,t) + \frac{\partial T}{\partial n}(0,t) = w_0(t) = 2t, \quad t \in (0,1], \tag{1.4.13}$$

$$T(1,t) + \frac{\partial T}{\partial n}(1,t) = w_1(t) = 2t + 3, \quad t \in (0,1], \tag{1.4.14}$$

$$T(x,0) = g(x) = x^2, \quad x \in [0,1]. \tag{1.4.15}$$

Then the DHCP given by equations (1.4.1) and (1.4.13)–(1.4.15) has the analytical solution $T(x,t) = x^2 + 2t$. It is important to investigate the suitability of the BEM to obtain convergent approximations of the boundary temperature, heat flux and temperature in the domain. These can be reliably achieved by varying the number of time elements N when the number of space cells N_0 is maintained fixed, then repeating the procedure for different numbers of space cells N_0 when the number of time elements N is kept fixed.

Although not illustrated, it was observed that on increasing the number of space cells N_0 when the number of time elements N is kept constant results in the numerical solutions of the boundary temperatures and heat fluxes converging monotonically to their analytical values, such that there is a close agreement between the numerical approximation when $(N_0, N) = (160, 20)$ and the analytical solutions. Alternatively, keeping the number of space cells N_0 constant at 20 and subsequently increasing to 160, the number of time elements N we came to the same conclusion. Figures 1.1 and 1.2 illustrate convergent results which agree very well with the analytical solution for $(N_0, N) = (160, 160)$. In addition, it is concluded that $(N_0, N) = (40, 40)$

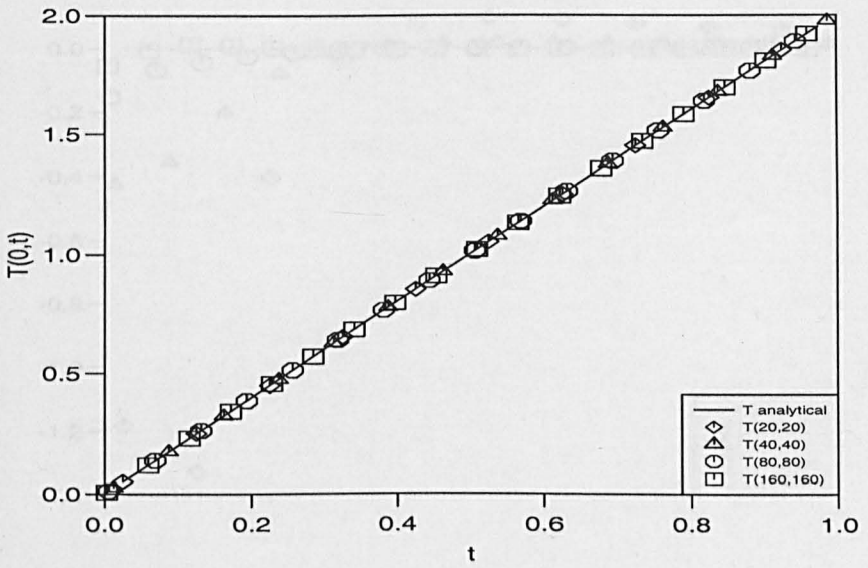

(a)

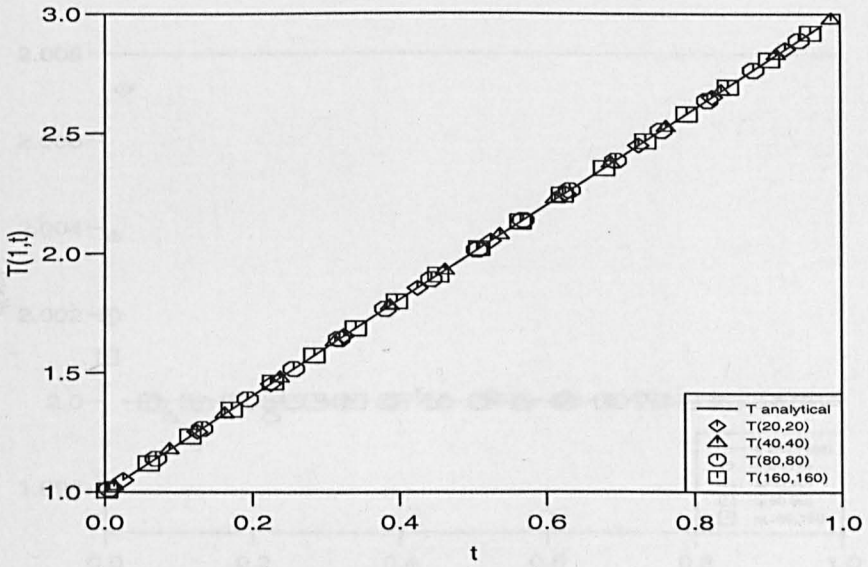

(b)

Figure 1.1: The analytical and numerical boundary temperatures (a) $T(0,t)$ and (b) $T(1,t)$, as functions of time t, for various (N_0, N).

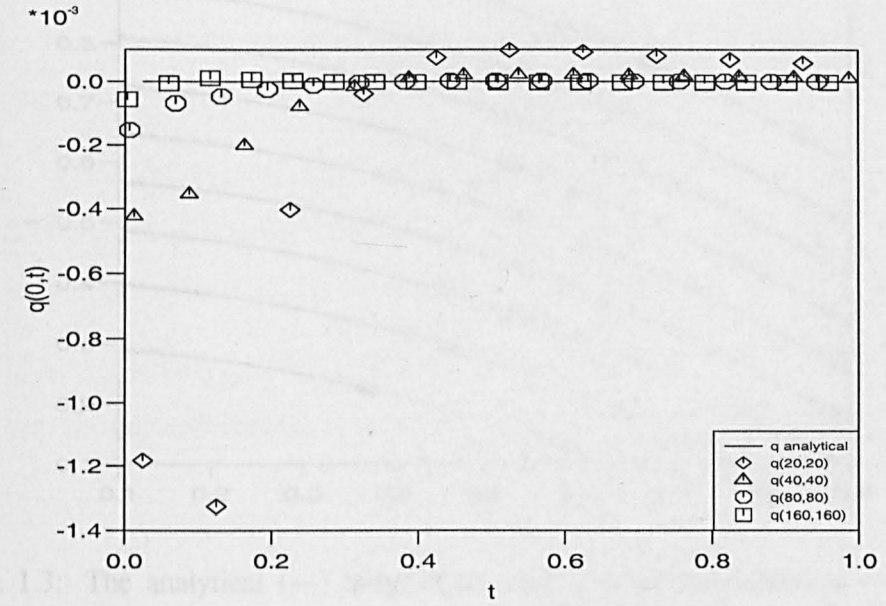

(a)

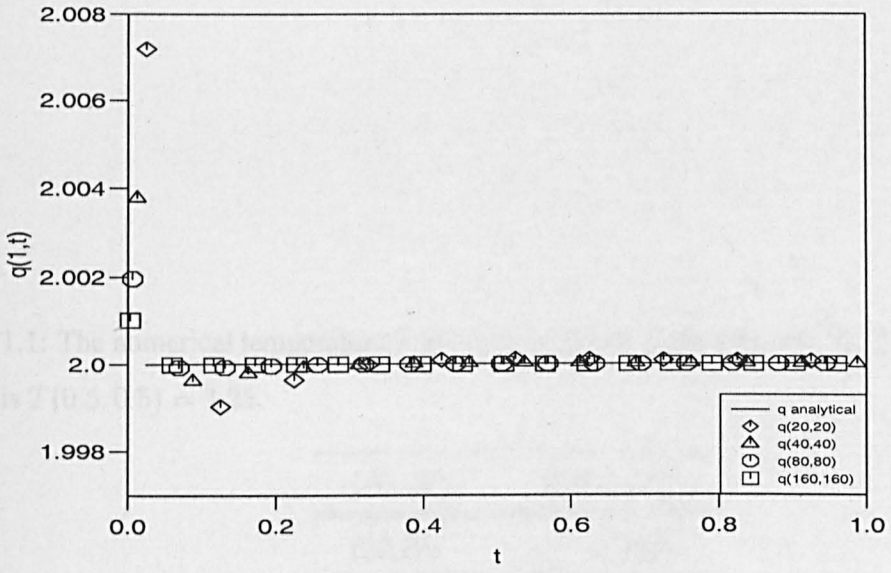

(b)

Figure 1.2: The analytical and numerical heat fluxes (a) $q(0,t)$ and (b) $q(1,t)$, as functions of time t, for various (N_0, N).

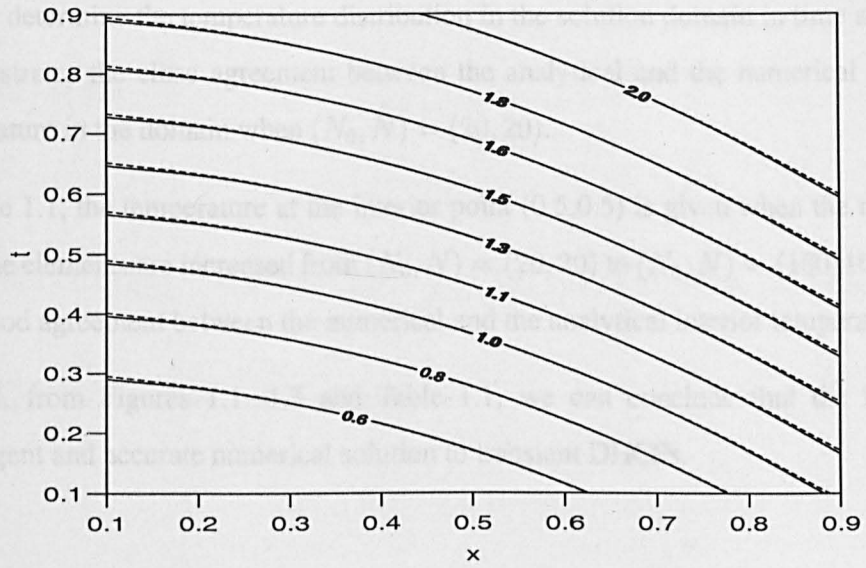

Figure 1.3: The analytical (—) temperature contours and the numerical (−−) temperature contours in the domain $(x,t) \in (0.1, 0.9)^2$, for $(N_0, N) = (20, 20)$.

Table 1.1: The numerical temperature T at $(x,t) = (0.5, 0.5)$ for various (N_0, N). The analytical value is $T(0.5, 0.5) = 1.25$.

(N_0, N)	$T(0.5, 0.5)$
(20,20)	1.2506
(40,40)	1.2501
(80,80)	1.2500
(160,160)	1.2500

produces a sufficiently fine mesh which provides an accurate approximation of the temperature T and the heat flux $\frac{\partial T}{\partial n}$ at the boundary without necesarily increasing the computation time by introducing more space cells and time steps. The boundary temperature and heat flux are then used to determine the temperature distribution in the solution domain in time and space. Figure 1.3 illustrates the close agreement between the analytical and the numerical solutions for the temperature in the domain when $(N_0, N) = (20, 20)$.

In Table 1.1, the temperature at the interior point (0.5,0.5) is given when the numbers of space and time elements are increased from $(N_0, N) = (20, 20)$ to $(N_0, N) = (160, 160)$. These results give good agreement between the numerical and the analytical interior temperatures.

Overall, from Figures 1.1−1.3 and Table 1.1, we can conclude that the BEM provides a convergent and accurate numerical solution to transient DHCPs.

Chapter 2

Restoring boundary conditions and heat transfer coefficients

2.1 Introduction

Non-intrusive experimental techniques to determine the boundary conditions or the convective heat transfer coefficients currently in use, both in industry and academia, rely on analytical solutions for the surface temperature. For instance, techniques based on characteristic colour changes of liquid crystal films at a given temperature, see Hippensteele *et al.* [38], or on laser induced fluorescence, see Bizzak and Chyu [10], both rely on the analytical temperature solution for a semi-infinite medium to determine the heat transfer coefficient at a point once the temperature history is obtained from the experiment. However, in many practical situations the analytical model is not the most appropriate and rather a numerical model should be employed.

2.2 Restoring spacewise dependent ambient temperatures – Problem 2.I

In this section we investigate an inverse problem in which the spacewise dependent temperature of the environment is unknown.

2.2.1 Mathematical formulation of Problem 2.I

The inverse heat conduction problem (IHCP) under investigation (Problem 2.I) in this section replaces the boundary conditions (1.4.2) and (1.4.3) by

$$\frac{\partial T}{\partial n}(0,t) + \sigma_0 T(0,t) = h_0(t) f_0 + b_0(t) =: B_0(t) \qquad \text{for} \quad t \in (0, t_f], \tag{2.2.1}$$

$$\frac{\partial T}{\partial n}(1,t) + \sigma_1 T(1,t) = h_1(t) f_1 + b_1(t) =: B_1(t) \qquad \text{for} \quad t \in (0, t_f], \tag{2.2.2}$$

where σ_0, σ_1 are specified constants, h_0, h_1, b_0 and b_1 are specified functions of time, but the constants f_0 and f_1 are unknown. Therefore, additional information is necessary to compensate for the number of unknowns, and in the first instance we assume that two measurements of the boundary temperature at the same fixed time $t = \widetilde{t}_{i_0}$, where $i_0 \in \{1, .., N\}$, are available, namely

$$T(0, \widetilde{t}_{i_0}) = \chi_0, \qquad T(1, \widetilde{t}_{i_0}) = \chi_1. \tag{2.2.3}$$

Alternatively, instead of (2.2.3) we can measure the average boundary temperatures as

$$e_0 = \frac{1}{t_f} \int_0^{t_f} T(0,t)\mathrm{d}t, \qquad e_1 = \frac{1}{t_f} \int_0^{t_f} T(1,t)\mathrm{d}t. \tag{2.2.4}$$

Conditions (2.2.3) and (2.2.4) are called terminal and integral boundary observations, respectivley. Then we have the following uniqueness theorem, see Kostin and Prilepko [47].

Theorem 2.2.1 *Suppose* $g \in C^1([0,1])$, $h_i, b_i \in C([0,t_f])$, $\sigma_i \geq 0$, *and the functions* $h_i > 0$ *are monotone nondecreasing,* $i = 0, 1$, *on* $(0, t_f]$. *Then a solution* $(T \in C^{2,1}(Q), f_0, f_1)$ *to the inverse problem* (1.4.1), (1.4.4), (2.2.1)-(2.2.3), *or* (1.4.1),(1.4.4), (2.2.1), (2.2.2), (2.2.4) *is unique.*

Remarks

(i) For the uniqueness of the problem (1.4.1), (1.4.4), (2.2.1), (2.2.2) and (2.2.4) it is sufficient to require that $\int_0^{t_f} h_i(t)\mathrm{d}t > 0$, $i = 0, 1$.

(ii) In higher dimensions, the inverse Problem 2.I can be recast as a Fredholm integral equation of the first kind which is a classical example of an ill-posed problem, see e.g. Tikhonov and Arsenin [83].

(iii) A function T satisfying (1.4.1), (1.4.4), (2.2.1) and (2.2.2) has the representation, see Ozisik ([66], Chapter 2),

$$T(x,t) = \sum_{m=1}^{\infty} e^{-\beta_m^2 t} K(\beta_m, x) \left[\int_0^1 K(\beta_m, x') \left(g(x') - z_1 x' - z_2 \right) \mathrm{d}x' + \int_0^t e^{\beta_m^2 t'} A(\beta_m, t') \mathrm{d}t' \right] + z_1 x + z_2, \tag{2.2.5}$$

where

$$z_1 = \frac{\sigma_1 g'(0) + \sigma_0 g'(1) + \sigma_1 \sigma_0 \left(g(1) - g(0) \right)}{\sigma_0 + \sigma_1 + \sigma_0 \sigma_1},$$
$$z_2 = \frac{g'(1) + \sigma_1 g(1) - (1+\sigma_1) g'(0) + \sigma_0 (1+\sigma_1) g(0)}{\sigma_0 + \sigma_1 + \sigma_0 \sigma_1},$$

$$\begin{aligned} A(\beta_m, t) =& K(\beta_m, 0) \left(B_0(t) + z_1 - \sigma_0 z_2 \right) + K(\beta_m, 1) \left(B_1(t) - \sigma_1 z_2 - (1+\sigma_1) z_1 \right) \\ =& K(\beta_m, 0) \left(h_0(t) f_0 + b_0(t) + g'(1) - \sigma_0 g(0) \right) \\ &+ K(\beta_m, 1) \left(h_1(t) f_1 + b_1(t) - g'(1) - \sigma_1 g(1) \right), \end{aligned} \tag{2.2.6}$$

and the kernel $K(\beta_m, x)$ is given by

$$K(\beta_m, x) = \frac{\sqrt{2} \left(\beta_m \cos(\beta_m x) + \sigma_1 \sin(\beta_m x) \right)}{\sqrt{(\beta_m^2 + \sigma_1^2) \left(1 + \frac{\sigma_2}{\beta_m^2 + \sigma_2^2} \right) + \sigma_1}}, \tag{2.2.7}$$

where β_m are the positive roots of the transcedental equation

$$tan(\beta) = \frac{\beta (\sigma_1 + \sigma_2)}{\beta^2 - \sigma_1 \sigma_2}. \tag{2.2.8}$$

The expression (2.2.5) involves a complicated series expansion and in higher dimensions there is little hope it can be usable in practice. Therefore, numerical methods able to discretise any multi-dimensional problem analogous to the one above appear more useful.

2.2.2 The BEM

Now instead of (1.4.9) and (1.4.10) we have the discretised version of (2.2.1) and (2.2.2), namely,

$$T'_{0i} = h_{0i} f_0 + b_{0i} - \sigma_0 T_{0i}, \qquad i = \overline{1, N}, \tag{2.2.9}$$

$$T'_{1i} = h_{1i} f_1 + b_{1i} - \sigma_1 T_{1i}, \qquad i = \overline{1, N}, \tag{2.2.10}$$

where $h_{0i} = h_0(\widetilde{t}_i)$, $h_{1i} = h_1(\widetilde{t}_i)$, $b_{0i} = b_0(\widetilde{t}_i)$ and $b_{1i} = b_1(\widetilde{t}_i)$. Also, instead of (2.2.3) and (2.2.4) we write

$$T_{0i_0} = \chi_0, \qquad T_{1i_0} = \chi_1, \tag{2.2.11}$$

and

$$e_0 = \frac{t_f}{N}\sum_{i=1}^{N} T_{0i}, \qquad e_1 = \frac{t_f}{N}\sum_{i=1}^{N} T_{1i}, \tag{2.2.12}$$

respectively.

The IHCP given by equations (1.4.1), (1.4.4), (2.2.1), (2.2.2), and (2.2.3) or (2.2.4) reduces to its discretised version given by equations (1.3.38), (1.4.11), (2.2.9), (2.2.10), and (2.2.11) or (2.2.12). Then the resulting system of equations (1.4.12) becomes of the form

$$X\mathbf{Y} = \mathbf{Z} \tag{2.2.13}$$

where X is a known $(4N+2) \times (4N+2)$ square matrix which contains the influence matrices C^0, C^1, D^0, D^1 and E given by expressions (1.3.34)-(1.3.36), $\mathbf{Y}$ is a vector of $4N+2$ unknowns, namely T_{0j}, T_{1j}, T'_{0j}, T'_{1j}, f_0 and f_1, recast as follows:

$Y_j = T_{0j}$ for $j = \overline{1,N}$, $Y_j = T_{1(j-N)}$ for $j = \overline{N+1,2N}$,

$Y_j = T'_{0(j-2N)}$ for $j = \overline{2N+1,3N}$, $Y_j = T'_{1(j-3N)}$ for $j = \overline{3N+1,4N}$,

$Y_{4N+1} = f_0$ and $Y_{4N+2} = f_1$,

and $\mathbf{Z}$ is a vector of $4N+2$ known elements defined by

$Z_j = -\sum_{k=1}^{N_0} E_{jk}(0) g_k$ for $j = \overline{1,N}$,

$Z_j = -\sum_{k=1}^{N_0} E_{(j-N)k}(1) g_k$ for $j = \overline{N+1,2N}$,

$Z_j = b_{0(j-2N)}$ for $j = \overline{2N+1,3N}$, $Z_j = b_{1(j-3N)}$ for $j = \overline{3N+1,4N}$,

$Z_{4N+1} = \chi_0$ and $Z_{4N+2} = \chi_1$ for (2.2.11),

or,

$Z_{4N+1} = e_0$ and $Z_{4N+2} = e_1$ for (2.2.2).

For simplicity, with the assistance of equations (2.2.9) and (2.2.10), we can choose to eliminate T'_{0j} and T'_{1j}, so as to reduce the system of equations to have $2N+2$ unknowns in $2N+2$ equations. This transforms the system considerably, reducing it so that the solution for only f_0, f_1, T_{0j} and T_{1j} is required. After that, the heat flux and the temperature T inside the solution domain may be obtained by direct substitution.

The system of linear algebraic equations (2.2.13) can be solved using the Gaussian elimination method. In the event that this method fails to give satisfactory results, due to the ill-conditioning

of the matrix X, one of the options is to use the regularization methods described in chapter 1 to obtain a stable solution to an ill-posed problem.

2.2.3 Numerical Examples, Results and Discussion

Example 2.1

In this example, we solve the IHCP given by the heat equation (1.4.1) in the domain $Q = (0,1) \times (0, t_f = 1]$, subject to the initial condition (1.4.4) of the form

$$T(x,0) = g(x) = x^2, \qquad x \in [0,1]. \tag{2.2.14}$$

The boundary conditions (2.2.1) and (2.2.2), with $\sigma_0 = \sigma_1 = 1$, $h_0(t) = h_1(t) = t$, $b_0(t) = 0$, $b_1(t) = 3$, are given by

$$\frac{\partial T}{\partial n}(0,t) + T(0,t) = f_0 t, \qquad t \in (0,1], \tag{2.2.15}$$

$$\frac{\partial T}{\partial n}(1,t) + T(1,t) = f_1 t + 3, \qquad t \in (0,1], \tag{2.2.16}$$

and the additional measurements (2.2.3) are given by

$$T(0,\widetilde{t}_{i_0}) = 2\widetilde{t}_{i_0} = \chi_0, \qquad T(1,\widetilde{t}_{i_0}) = 1 + 2\widetilde{t}_{i_0} = \chi_1. \tag{2.2.17}$$

It can easily be seen that the conditions of Theorem 2.2.1 are satisfied and therefore the solution to the inverse problem (1.4.1),(2.2.14)-(2.2.17) is unique. Further, the analytical solution (T, f_0, f_1) to be determined is given by $T(x,t) = x^2 + 2t$, $f_0 = f_1 = 2$. Noise is included in the measurements (2.2.17) by replacing χ_i with $\chi_i(1+\rho)$ for $i = 0, 1$, where ρ is the percentage of noise.

In Table 2.1, we find that increasing the number of time elements N from 20 to 160, when $i_0 = 1$, results in the condition number of the matrix X increasing significantly. The condition number of the matrix X in (2.2.13) has been calculated using the NAG routine F07AGF.

The ill-conditioning produces inaccuracies in the values of f_0 and f_1, especially when the number N of the time elements increases. The error in f_0 is far less than that in f_1, a fact that is attributed to the smaller value of the the additional measurement χ_0 in comparison to χ_1. However, for a fixed number of time elements N, the accuracy in the numerical approximations improve when increasing the number of space cells N_0. This is because: (i) the number of space cells increases

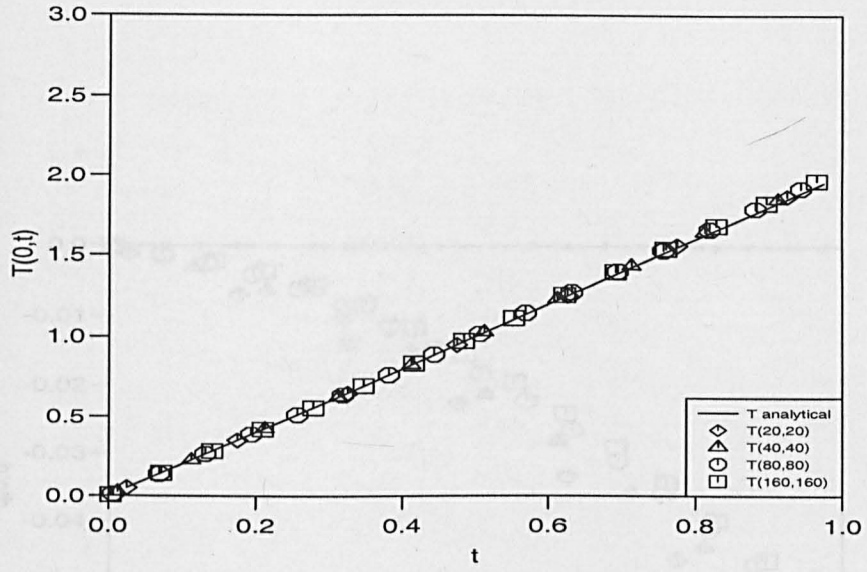

(a)

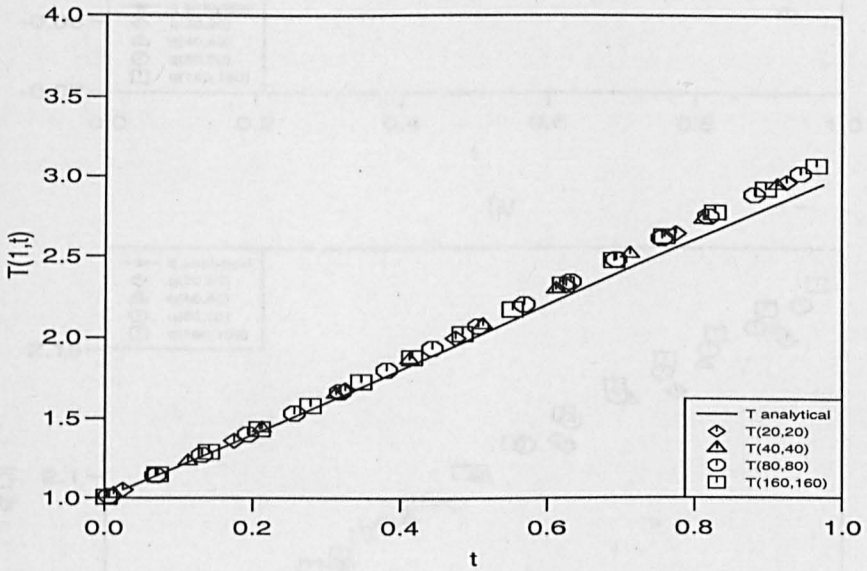

(b)

Figure 2.1: The analytical and numerical boundary temperatures (a) $T(0,t)$, and (b) $T(1,t)$, as functions of time t, for the IHCP given by Example 2.1, when $i_0 = 1$ for various (N_0, N) (no noise).

the accuracy of the approximation (1.3.19), and (ii) the boundary values χ_0 and χ_1 are measured at the same point from the initial condition. Thus the ill-conditioning of the system of equations remains unchanged. The best results are obtained when $N = 20$ and $N_0 = 160$.

Figures 2.1(a), (b) and Figures 2.2(a), (b) show the boundary temperature $T(0,t)$, $T(1,t)$ and the heat fluxes $q_0(t) = -T_x(0,t)$, $q_1(t) = T_x(1,t)$, respectively, for various values of (N_0, N). It is observed that reasonable numerical approximations to the exact solutions are obtained.

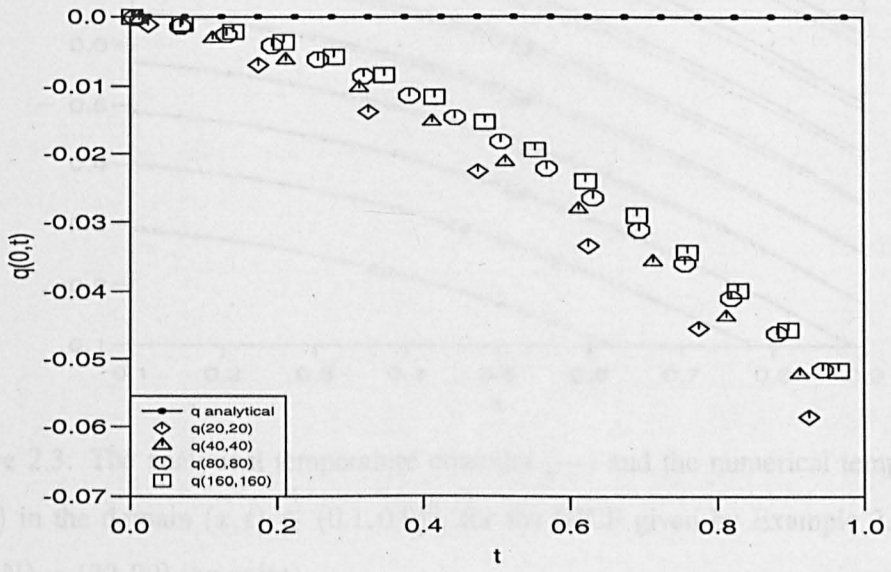

(a)

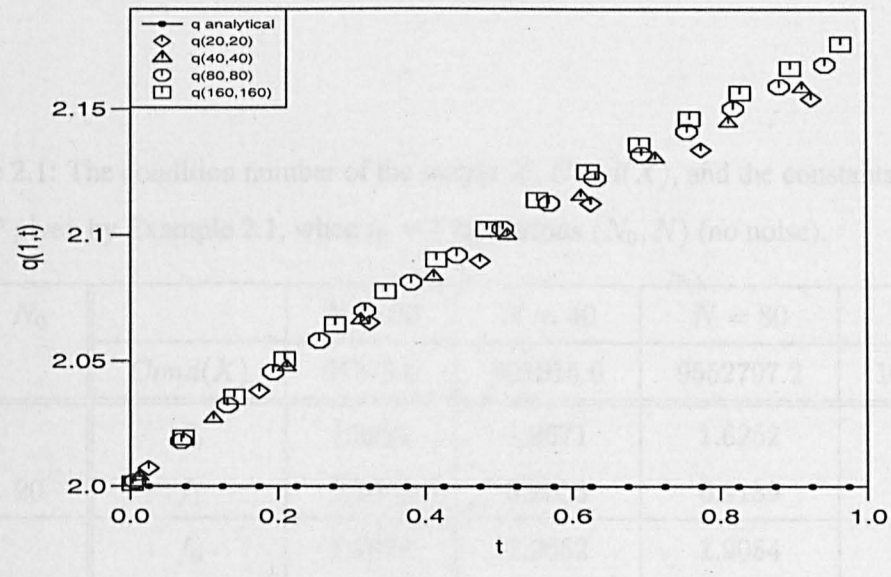

(b)

Figure 2.2: The analytical and numerical heat fluxes (a) $q(0,t)$, and (b) $q(1,t)$, as functions of time t, for the IHCP given by Example 2.1, when $i_0 = 1$ for various (N_0, N) (no noise).

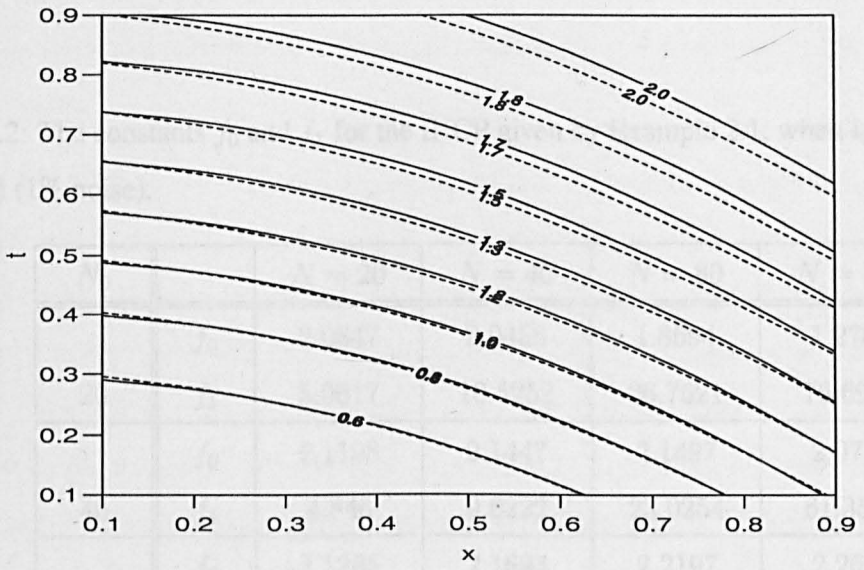

Figure 2.3: The analytical temperature contours (—) and the numerical temperature contours (−−) in the domain $(x,t) \in (0.1,0.9)^2$, for the IHCP given by Example 2.1, when $i_0 = 1$, $(N_0, N) = (20, 20)$ (no noise).

Table 2.1: The condition number of the matrix X, $Cond(X)$, and the constants f_0 and f_1 for the IHCP given by Example 2.1, when $i_0 = 1$ for various (N_0, N) (no noise).

N_0		$N = 20$	$N = 40$	$N = 80$	$N = 160$
	$Cond(X)$	87275.6	891615.6	9552797.2	105070529.1
20	f_0	1.9527	1.8671	1.6252	0.9415
	f_1	2.2876	3.2053	6.9189	22.4320
40	f_0	1.9876	1.9662	1.9054	1.7342
	f_1	2.0723	2.3023	3.2452	7.0871
80	f_0	1.9964	1.9909	1.9755	1.9323
	f_1	2.0186	2.0770	2.3142	3.2769
160	f_0	1.9986	1.9971	1.9930	1.9819
	f_1	2.0051	2.0206	2.0817	2.3259

Table 2.2: The constants f_0 and f_1 for the IHCP given by Example 2.1, when $i_0 = 1$ for various (N_0, N) (1% noise).

N_0		$N = 20$	$N = 40$	$N = 80$	$N = 160$
	f_0	2.0847	2.0456	1.8694	1.2786
20	f_1	5.0617	10.5252	26.7621	76.6997
	f_0	2.1198	2.1447	2.1497	2.0713
40	f_1	4.846	9.6222	23.0254	61.3548
	f_0	2.1285	2.1694	2.2197	2.2694
80	f_1	4.7927	9.3968	22.0944	57.5445
	f_0	2.1307	2.1756	2.2372	2.3189
160	f_1	4.7793	9.3405	21.8618	56.5935

Table 2.3: The condition number of the matrix X, $Cond(X)$, and the constants f_0 and f_1 for the IHCP given by Example 2.1, when $i_0 = N$ and $N_0 \in \{20, 40, 80, 160\}$ for various N (1% noise).

	$N = 20$	$N = 40$	$N = 80$	$N = 160$
$Cond(X)$	705.4	2576.7	9910.3	3911.7
f_0	2.0268	2.0266	2.0666	2.0265
f_1	2.0593	2.0588	2.0585	2.0584

Figure 2.3 shows the temperature contours when the measurement (2.2.17) is taken at $i_0 = 1$ in the absence of noise. We observe some inaccuracies in the temperature, especially with increasing time, and particularly towards the boundary $x = 1$ where the maximum of $T(x,t) = x^2 + 2t$ occurs.

In Table 2.2, when $i_0 = 1$ and noise is introduced into the system, as expected, the approximated values of the constants f_0 and f_1 blow up, as a result of the noise introduced. However, they improve slightly with an increase in the value of N_0, when N is fixed. On the other hand, the inaccuracy in the numerical approximations of f_0 and f_1 decreases with increasing N, for a fixed N_0. These inaccurate results which are full of significant jumps in the values of f_0 and f_1 demonstrate the instability of the numerical solution of the system of equations (2.2.13) for the IHCP given by Example 2.1. Finally, we note that using Tikhonov's regularization method of zeroth and first-order when taking $10^{-12} < \lambda < 10^{-1}$ did not improve the results for predicting f_0 and f_1. Similarly, when the last two smallest singular values were set to zero, the use of the truncated SVD also did not improve the numerical results. In Figure 2.4, the last two singular values are close to zero when $i_0 = 1$ and thus they increase the condition number significantly, whereas when $i_0 = N$, the system has a normalised singular value reducing from 1 to approximately 0.1, which is not very low and hence the system becomes well-conditioned.

In Table 2.3, when $i_0 = N$, the condition numbers of the system remain low, and the approximate values of f_0 and f_1 are stable and accurate, being the same for all values of N_0 or almost the same for all values of N when 1% noise is introduced (2.2.17).

In the next test example, we examine an analytical solution which yields symmetry in the boundary conditions at $x = 0$ and $x = 1$. We maintain the number of time steps and space cells fixed at $(40, 40)$, but we vary the value of i_0 at which the measurements (2.2.11) are taken.

Example 2.2

In this example we solve the IHCP given by equation (1.4.1) in the domain $Q = (0,1) \times (0, t_f = 1]$, subject to the initial condition (1.4.4) of the form

$$T(x,0) = g(x) = \left(x - \frac{1}{2}\right)^2, \qquad x \in [0,1]. \tag{2.2.18}$$

The boundary conditions (2.2.1) and (2.2.2) with $\sigma_0 = \sigma_1 = 1$, $h_0(t) = h_1(t) = t$, $b_0(t) =$

Table 2.4: The condition number of the matrix X, $Cond(X)$, and the constants f_0 and f_1 for the IHCP given by Example 2.2, when $i_0 = N$, for various (N_0, N) (no noise).

N_0		$N = 20$	$N = 40$	$N = 80$	$N = 160$
	$Cond(X)$	536.0	1916.2	7286.6	28593.3
	f_0	2.0000	2.0000	2.0000	2.0000
20	f_1	2.0000	2.0000	2.0000	2.0000
	f_0	2.0000	2.0000	2.0000	2.0000
40	f_1	2.0000	2.0000	2.0000	2.0000
	f_0	1.9999	1.9999	1.9999	1.9999
80	f_1	1.9999	1.9999	1.9999	1.9999
	f_0	1.9999	1.9999	1.9999	1.9999
160	f_1	1.9999	1.9999	1.9999	1.9999

$b_1(t) = \frac{5}{4}$ are given by

$$\frac{\partial T}{\partial n}(0,t) + T(0,t) = f_0 t + \frac{5}{4}, \qquad t \in (0,1], \tag{2.2.19}$$

$$\frac{\partial T}{\partial n}(1,t) + T(1,t) = f_1 t + \frac{5}{4}, \qquad t \in (0,1], \tag{2.2.20}$$

and the additional measurements (2.2.3) are given by

$$T(0,\tilde{t}_{i_0}) = \frac{1}{4} + 2\tilde{t}_{i_0} = \chi_0, \qquad T(1,\tilde{t}_{i_0}) = \frac{1}{4} + 2\tilde{t}_{i_0} = \chi_1. \tag{2.2.21}$$

The analytical solution $(T(x,t), f_0, f_1)$ to be determined is given by $T(x,t) = \left(x - \frac{1}{2}\right)^2 + 2t$, $f_0 = f_1 = 2$.

From Table 2.4, we observe that when the measurements (2.2.21) are taken at $i_0 = N$, a small condition number of the matrix X is obtained, producing a very accurate approximation of the constants f_0 and f_1 when no noise is introduced in the measurements (2.2.21).

Numerical approximations obtained when 1% noisy temperature measurements (2.2.21) are taken at various values of $i_0 \in \{1, ..., N\}$ are shown in Table 2.5, and Figures 2.5 and 2.6. In Figure 2.5 and Table 2.5 we observe that the condition numbers when $i_0 = 1$ and $i_0 = N = 40$ are very large and small, respectively. This shows that the system is well-conditioned when $i_0 = N = 40$ and gradually becomes ill-conditioned when reducing i_0 to 1, such that the approximate values of the constants f_0 and f_1 in both Examples 2.1 and 2.2, when i_0 approaches

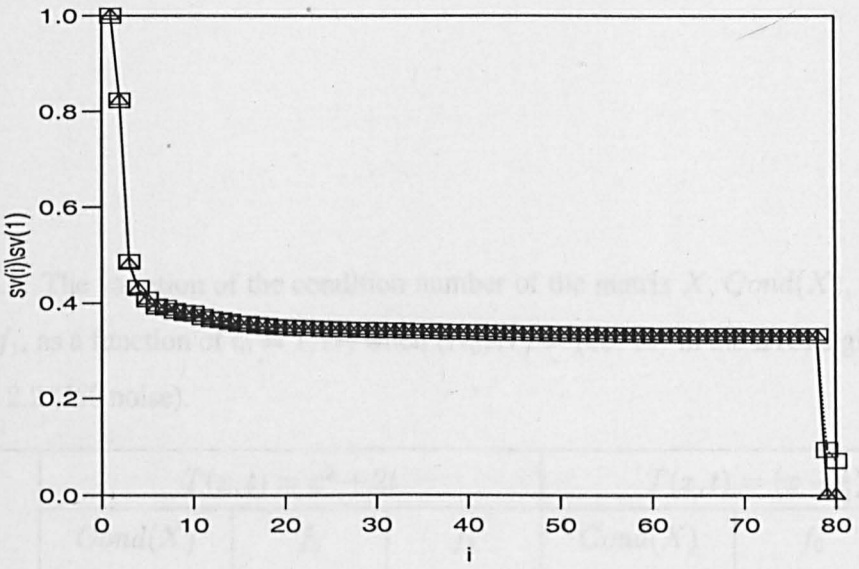

Figure 2.4: The normalised singular values $\frac{sv(i)}{sv(1)}$ for the IHCPs given by Example 2.1, when $(N_0, N) = (40, 40)$, as a function of i, when $i_0 = 1(\triangle)$ and $i_0 = N(\square)$.

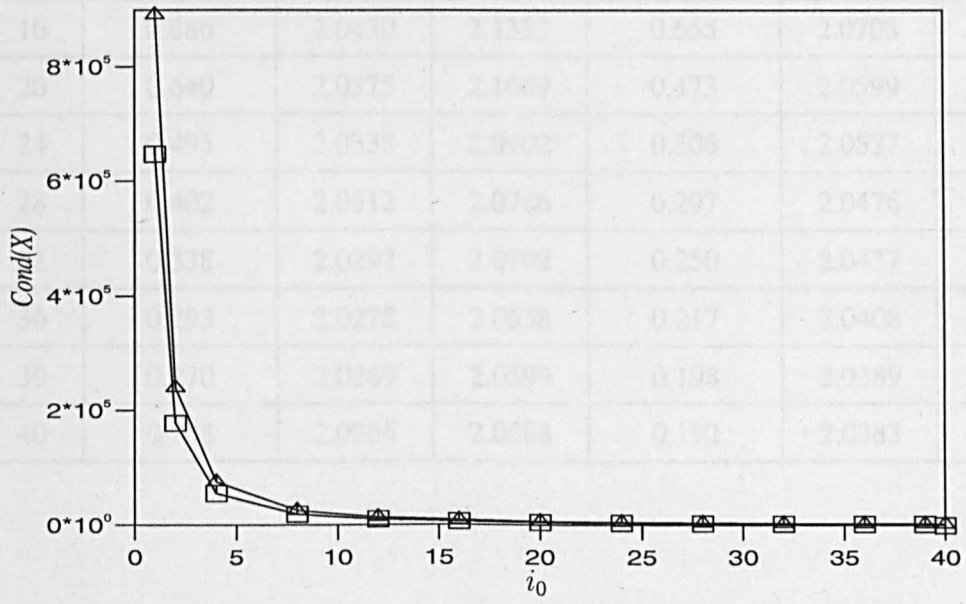

Figure 2.5: The condition numbers $(\triangle)$ and $(\square)$ of the matrix X for the IHCPs given by Examples 2.1 and 2.2, respectively, as a function of i_0, when $(N_0, N) = (40, 40)$.

Table 2.5: The variation of the condition number of the matrix X, $Cond(X)$, and the constants f_0 and f_1, as a function of $i_0 = \overline{1, N}$, when $(N_0, N) = (40, 40)$ in the IHCPs given by Examples 2.1 and 2.2 (1% noise).

i_0	$T(x,t) = x^2 + 2t$			$T(x,t) = (x - \frac{1}{2})^2 + 2t$		
	$Cond(X)$ $(\times 10^4)$	f_0	f_1	$Cond(X)$ $(\times 10^4)$	f_0	f_1
1	89.176	2.1447	9.6222	64.639	4.0981	4.0981
2	24.064	2.1371	4.1400	17.723	2.6495	2.6495
4	7.472	2.0990	2.7171	5.506	2.2566	2.2566
8	2.530	2.0672	2.2874	1.866	2.1264	2.1264
12	1.364	2.0517	2.1804	1.007	2.0890	2.0890
16	0.886	2.0430	2.1332	0.655	2.0708	2.0708
20	0.640	2.0375	2.1069	0.473	2.0599	2.0599
24	0.495	2.0338	2.0902	0.366	2.0527	2.0527
28	0.402	2.0312	2.0786	0.297	2.0476	2.0476
32	0.338	2.0292	2.0702	0.250	2.0437	2.0437
36	0.293	2.0278	2.0638	0.217	2.0408	2.0408
39	0.270	2.0269	2.0599	0.198	2.0389	2.0389
40	0.258	2.0266	2.0588	0.192	2.0383	2.0383

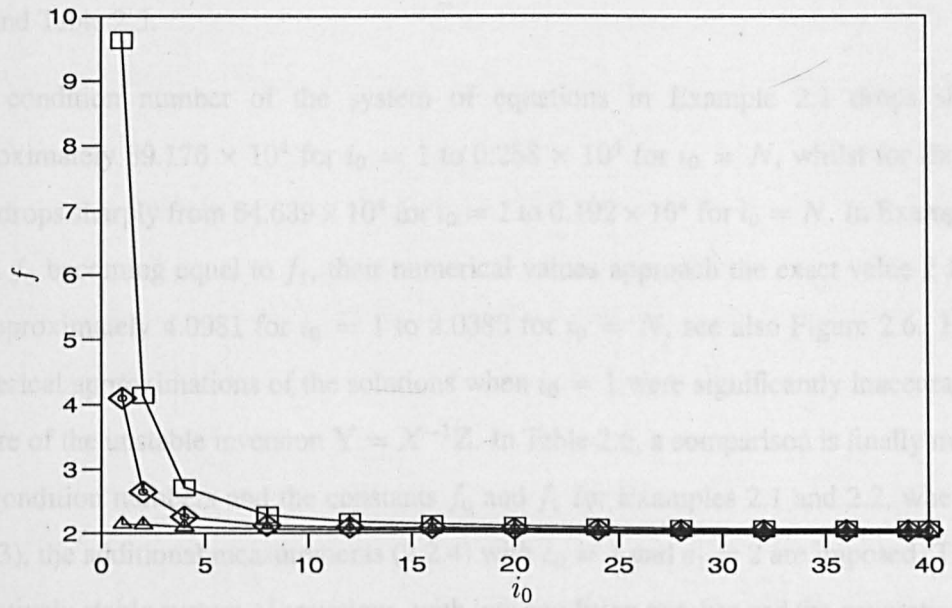

Figure 2.6: The constants f_0 ((△) and (○)) and f_1 ((□) and (◇)) for the IHCPs given by Examples 2.1 and 2.2, respectively, as a function of i_0 when $(N_0, N) = (40, 40)$ and 1% noise.

Table 2.6: The condition numbers, and the values of the constants f_0 and f_1 when the additional measurements (2.2.4) instead of (2.2.3) are imposed, for various (N_0, N) in the IHCPs given by Examples 2.1 and 2.2.

N_0, N	$Cond(X)$ $(\times 10^4)$	ρ	$T(x,t) = x^2 + 2t$ 0.00	$T(x,t) = x^2 + 2t$ 0.01	$T(x,t) = (x - \frac{1}{2})^2 + 2t$ 0.00	$T(x,t) = (x - \frac{1}{2})^2 + 2t$ 0.01
20,20	13.30	f_0	1.9998	2.0288	1.9998	2.0522
		f_1	2.0002	2.0964	1.9998	2.0522
40, 40	26.98	f_0	1.9998	2.0292	1.9999	2.0531
		f_1	2.0000	2.0963	1.9999	2.0531
80, 80	54.83	f_0	1.9999	2.0293	1.9999	2.0531
		f_1	2.0000	2.0963	1.9999	2.0531
160, 160	111.30	f_0	1.9999	2.0293	1.9999	2.0531
		f_1	1.9999	2.0963	1.9999	2.0531

N become more accurate, but becomes significantly inaccurate when i_0 approaches 1, see Figure 2.6 and Table 2.5.

The condition number of the system of equations in Example 2.1 drops sharply from approximately 89.176×10^4 for $i_0 = 1$ to 0.258×10^4 for $i_0 = N$, whilst for Example 2.2 it also drops sharply from 64.639×10^4 for $i_0 = 1$ to 0.192×10^4 for $i_0 = N$. In Example 2.2, apart from f_0 becoming equal to f_1, their numerical values approach the exact value 2 from a value of approximately 4.0981 for $i_0 = 1$ to 2.0383 for $i_0 = N$, see also Figure 2.6. However, the numerical approximations of the solutions when $i_0 = 1$ were significantly inaccurate due to the failure of the unstable inversion $\mathbf{Y} = X^{-1}\mathbf{Z}$. In Table 2.6, a comparison is finally made between the condition numbers and the constants f_0 and f_1 for Examples 2.1 and 2.2, when, instead of (2.2.3), the additional measurements (2.2.4) with $e_0 = 1$ and $e_1 = 2$ are imposed. This results in a relatively stable system of equations, with low condition number and the generation of accurate and stable approximations of the constants f_0 and f_1.

2.3 Reconstruction of spacewise dependent heat transfer coefficient – Problem 2.II

So far, the IHCPs considered in section 2.2 have been linear inverse problems. In this section, we investigate some nonlinear IHCPs involving the determination of a spacewise dependent heat transfer coefficient.

2.3.1 Mathematical formulation of Problem 2.II

The formulation of Problem 2.II reads as follows. Find the temperature $T(x,t)$ and the heat transfer constants σ_0 and σ_1 satisfying (1.4.1) subject to the initial condition (1.4.4), the Robin boundary condition

$$\frac{\partial T}{\partial n}(i,t) + \sigma_i T(i,t) = B_i(t), \qquad t \in (0,t_f], \qquad i = 0,1, \tag{2.3.1}$$

and the additional measurements (2.2.3) or (2.2.4), where B_i, $i = 0,1$, are given functions.

For this inverse problem the following existence and uniqueness result holds, see Kostin and Prilepko [47].

Theorem 2.3.1 *Suppose that* $g = 0$, $\chi_i > 0$ *for condition* (2.2.3) *or* $e_i > 0$ *for condition* (2.2.4), *and the functions* $B_i \in C([0, t_f])$, $B_i \geq 0$ *and are monotonically nondecreasing,* $i = 0, 1$. *Then there exists a unique solution* $(T(x,t) \in C^{2,1}(Q), \sigma_0 \geq 0, \sigma_1 \geq 0)$ *of the inverse Problem 2.II.*

2.3.2 The BEM

The numerical BEM discretisation of Problem 2.II consists of the equations (1.3.38), (1.4.11), (2.2.11) or (2.2.12) and

$$T'_{0i} + \sigma_0 T_{0i} = B_{0i}, \qquad T'_{1i} + \sigma_1 T_{1i} = B_{1i}, \qquad i = \overline{1, N}, \tag{2.3.2}$$

where $B_{0i} = B_0(\widetilde{t}_i)$, $B_{1i} = B_1(\widetilde{t}_i)$, $i = \overline{1, N}$. From (2.3.2) we can eliminate the normal derivative resulting in a system of $(2N + 2)$ nonlinear equations with $(2N + 2)$ unknowns T_{0i}, T_{1i} for $i = \overline{1, N}$, σ_0 and σ_1, which is solved using the NAG routine C05NCF. The non-negativity constraints $\sigma_0, \sigma_1 \geq 0$ are dealt with by choosing a non-negative initial guess, such as $\sigma_0 = \sigma_1 = 0.5$, and if in the iterative process they turn out to be negative at some stage of the iteration process then they are replaced by zero. Alternatively, one may use the more sophisticated NAG routine E04UCF to solve the nonlinear system of equations using the nonlinear least-squares method subject to the non-negativity constraints on the variables σ_0 and σ_1.

2.3.3 Numerical Examples, Results and Discussion

Example 2.3

In this example, we solve the IHCP given by the heat equation (1.4.1) in the domain $Q = (0, 1) \times (0, t_f = 1]$, subject to the initial condition (1.4.15), the boundary conditions (2.3.1) with $B_0(t) = 2t$, $B_1(t) = 2t + 3$, i.e.

$$\frac{\partial T}{\partial n}(0,t) + \sigma_0 T(0,t) = 2t, \qquad t \in (0, 1], \tag{2.3.3}$$

$$\frac{\partial T}{\partial n}(1,t) + \sigma_1 T(1,t) = 2t + 3, \qquad t \in (0, 1], \tag{2.3.4}$$

and the additional measurements (2.2.17).

First we show that this IHCP has a unique solution $(T(x,t) \in C^{2,1}(Q), \sigma_0 \geq 0, \sigma_1 \geq 0)$.

All the conditions of Theorem 2.3.1 are satisfied, except for the initial condition (1.4.15) which is not homogeneous. Given $\widetilde{\sigma}_0$, $\widetilde{\sigma}_1$ are arbitrary constants, we consider a solution $T(x, t; \widetilde{\sigma}_0, \widetilde{\sigma}_1)$

to the direct problem

$$\frac{\partial T}{\partial t}(x,t) = \frac{\partial^2 T}{\partial x^2}, \qquad (x,t) \in (0,1) \times (0,1] = Q, \tag{2.3.5}$$

$$T(x,0) = x^2, \qquad x \in [0,1], \tag{2.3.6}$$

$$\frac{\partial T}{\partial n}(0,t) + \widetilde{\sigma}_0 T(0,t) = 2t, \qquad t \in (0,1], \tag{2.3.7}$$

$$\frac{\partial T}{\partial n}(1,t) + \widetilde{\sigma}_1 T(1,t) = 2t+3, \qquad t \in (0,1]. \tag{2.3.8}$$

Since $g(x) = x^2 \in C^1([0,1])$, $B_0(t) = 2t \in C([0,1])$, $B_1(t) = 2t+3 \in C([0,1])$, this solution is unique and it has the desired differential properties in $C^{2,1}(Q) \cap C(\overline{Q})$, see Theorem 1.4.1.

We now introduce the nonlinear equations

$$\frac{2\widetilde{t_{i_0}} - \frac{\partial T}{\partial n}(0, \widetilde{t_{i_0}}; \widetilde{\sigma_0}, \widetilde{\sigma_1})}{2\widetilde{t_{i_0}}} = \widetilde{\sigma_0}, \qquad \frac{2\widetilde{t_{i_0}} + 3 - \frac{\partial T}{\partial n}(1, \widetilde{t_{i_0}}; \widetilde{\sigma_0}, \widetilde{\sigma_1})}{2\widetilde{t_{i_0}} + 1} = \widetilde{\sigma_1}. \tag{2.3.9}$$

It is easy to check that $\widetilde{\sigma_0} = \widetilde{\sigma_1} = 1$ is a positive solution to the system of nonlinear equations (2.3.9), since from (2.3.5)-(2.3.8), when $\widetilde{\sigma_0} = \widetilde{\sigma_1} = 1$ it immediately follows that $T(x,t;1,1) = x^2 + 2t$. Then based on Proposition 4 of Kostin and Prilepko [47], it follows that Problem 2.II given by Example 2.3 has a unique solution $(T(x,t) \in C^{2,1}(Q), \sigma_0 \geq 0, \sigma_1 \geq 0)$. It is easy to check that this solution is given by $T(x,t) = x^2 + 2t$, $\sigma_0 = \sigma_1 = 1$.

Figures 2.7(a) and (b) show the temperatures $T(0,t)$ and $T(1,t)$, respectively, when (N_0, N) are increased from (20,20) to (160,160), with no noise and the extra measurements (2.2.17) are taken at $i_0 = 1$. The results indicate only a slight improvement with increasing (N_0, N) such that there is close agreement with the exact solution.

Figures 2.8(a) and (b) show the heat fluxes $q(0,t)$ and $q(1,t)$, respectively. As expected, the errors in the heat fluxes become more visible in comparison with those in the boundary temperature, anyhow they decrease as N_0 and N increase. Figure 2.9 illustrates the numerical approximation and the analytical temperature contours $T(x,t)$ in the solution domain, when $(N_0, N) = (20, 20)$, with no noise and $i_0 = 1$. We observe that the BEM provides a very good numerical approximation to the exact $T(x,t)$, when the number of cells is only $(N_0, N) = (20, 20)$, and these results further improve with increasing N_0, N. This leads to the conclusion that the BEM provides a very good and convergent approximation for the nonlinear IHCP when no noise is introduced into the equations (2.2.3).

Table 2.7 shows the values of the constants σ_0 and σ_1 obtained using the BEM, when (N_0, N) is increased from (20,20) to (160,160) for various amounts of noise. We notice that when no noise

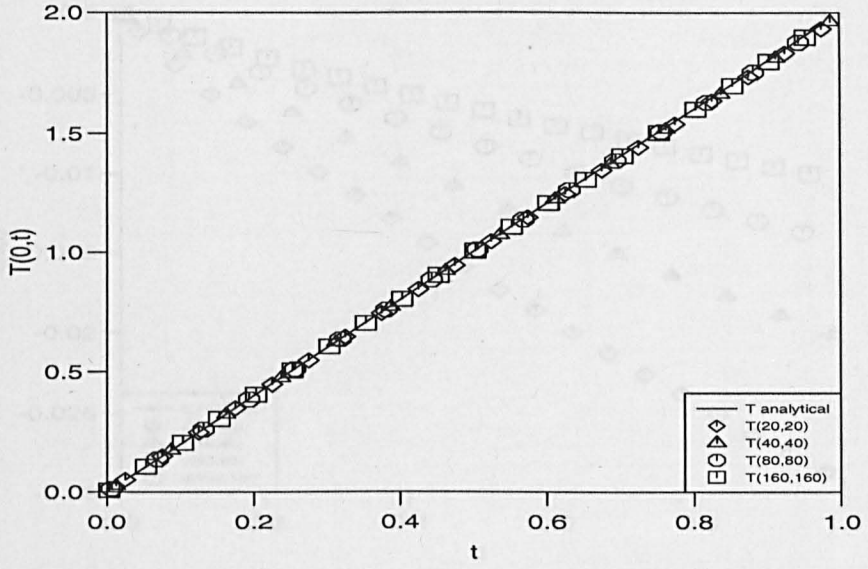

(a)

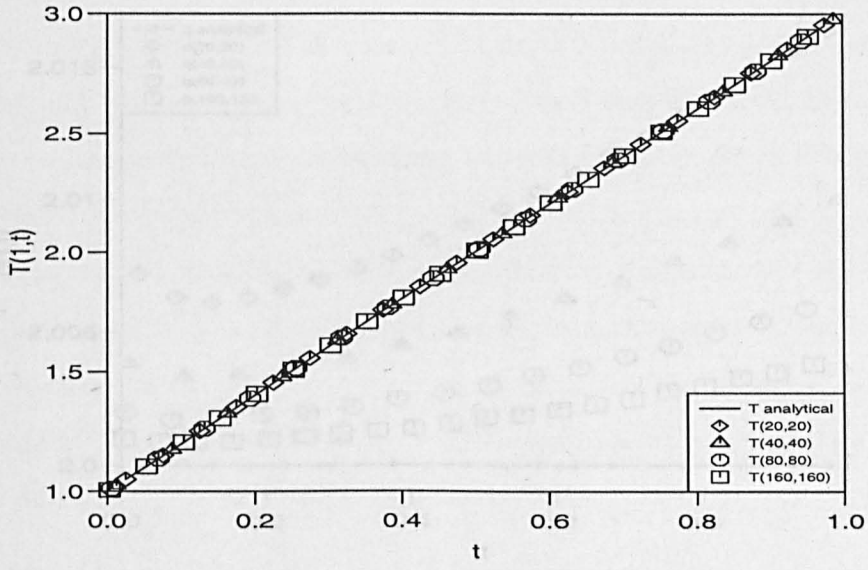

(b)

Figure 2.7: The analytical and numerical boundary temperatures (a) $T(0,t)$, and (b) $T(1,t)$, as functions of time t, for the nonlinear IHCP given by Example 2.3, when $i_0 = 1$ for various (N_0, N) (no noise).

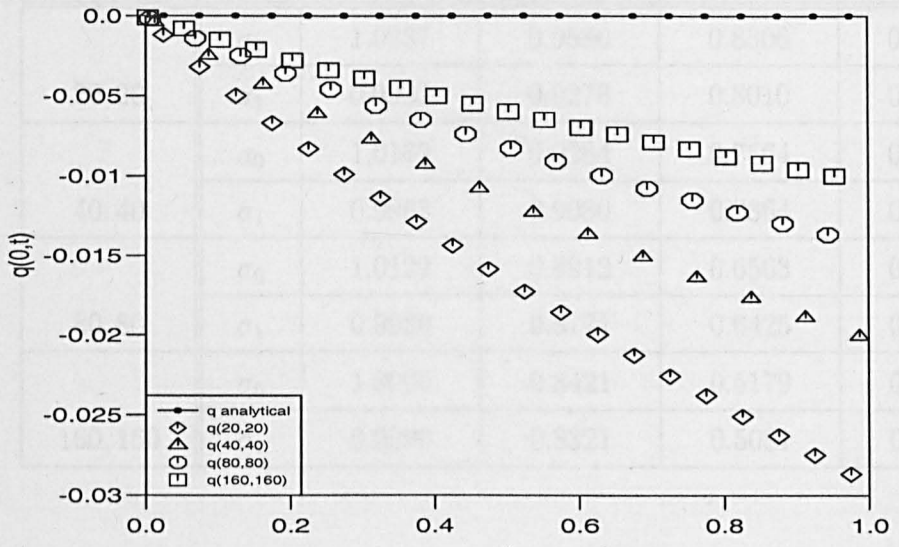

(a)

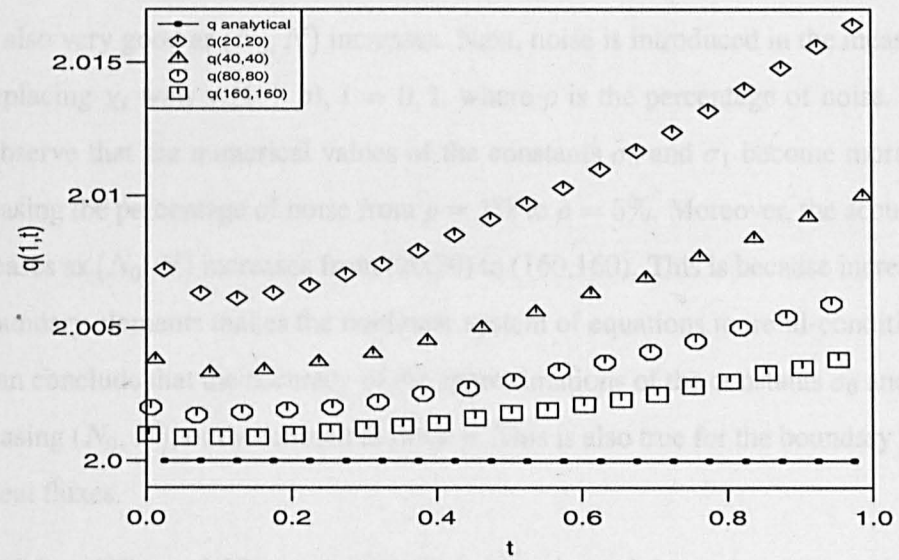

(b)

Figure 2.8: The analytical and numerical heat fluxes (a) $q(0,t)$, and (b) $q(1,t)$, as functions of time t, for the nonlinear IHCP given by Example 2.3, when $i_0 = 1$ for various (N_0, N) (no noise).

Table 2.7: The constants σ_0 and σ_1 for the nonlinear IHCP given by Example 2.3, when $i_0 = 1$ for various (N_0, N).

N_0, N		$\rho = 0.00$	$\rho = 0.01$	$\rho = 0.03$	$\rho = 0.05$
20, 20	σ_0	1.0237	0.9580	0.8306	0.7081
	σ_1	0.9932	0.9278	0.8010	0.6790
40, 40	σ_0	1.0169	0.9284	0.7564	0.5910
	σ_1	0.9963	0.9080	0.7364	0.5740
80, 80	σ_0	1.0122	0.8912	0.6563	0.4302
	σ_1	0.9980	0.8771	0.6425	0.4167
160, 160	σ_0	1.0090	0.8421	0.5179	0.2061
	σ_1	0.9990	0.8321	0.5081	0.1965

is introduced in the equations (2.2.3), as expected, the numerical values of σ_0 and σ_1 are close to the analytical values of $\sigma_0 = \sigma_1 = 1$. Also it is observed that the accuracy in obtaining σ_0 and σ_1 is also very good as (N_0, N) increases. Next, noise is introduced in the measurements (2.2.3) by replacing χ_i with $\chi_i(1 + \rho)$, $i = 0, 1$, where ρ is the percentage of noise. From Table 2.7, we observe that the numerical values of the constants σ_0 and σ_1 become more inaccurate with increasing the percentage of noise from $\rho = 1\%$ to $\rho = 5\%$. Moreover, the accuracy of σ_0 and σ_1 decreases as (N_0, N) increases from (20,20) to (160,160). This is because increasing the number of boundary elements makes the nonlinear system of equations more ill-conditioned. Therefore, we can conclude that the accuracy of the approximations of the constants σ_0 and σ_1 reduces with increasing (N_0, N), or the amount of noise ρ. This is also true for the boundary temperatures and the heat fluxes.

Table 2.8 and Figure 2.10 compare the approximations of the constants σ_0 and σ_1 for $(N_0, N) = (40, 40)$ and the measurement (2.2.3) is imposed at $i_0 = 1, ..., N = 40$, perturbed by $\rho = 0$ or $\rho = 1\%$ noise. It can be observed that the accuracy of σ_0 and σ_1 degrades when the measurements (2.2.17) are taken near the initial time $t = 0$, however, it keeps improving as i_0 increases.

In Table 2.9 we compare the approximations of the constants σ_0 and σ_1, when $(N_0, N) = (40, 40)$, and $\rho \in \{0, 1, 3, 5\}$ %. We observe that each level of noise produces a greater deviation in the approximate values of both σ_0 and σ_1 when $i_0 = 1$ compared to when $i_0 = 40$ and the deviation increases with increasing the amount of noise.

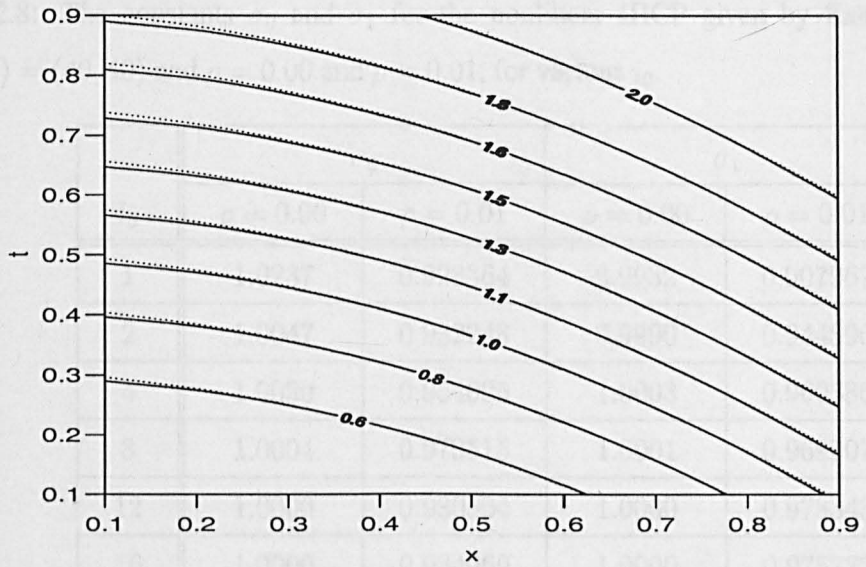

Figure 2.9: The analytical (—) and the numerical (...) temperature contours in the domain $(x,t) \in (0.1, 0.9)^2$ for the nonlinear IHCP given by Example 2.3, when $i_0 = 1$ and $(N_0, N) = (20, 20)$ (no noise).

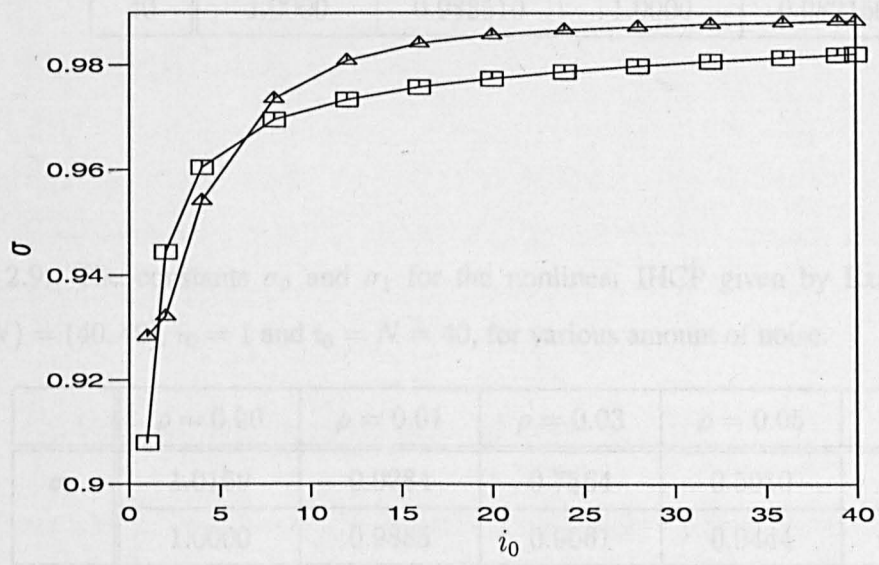

Figure 2.10: The constants σ_0 ($\triangle$) and σ_1 ($\square$) for the nonlinear IHCP given by Example 2.3, as a function of $i_0 = 1, ...N = 40$ when $(N_0, N) = (40, 40)$ (1% noise).

Table 2.8: The constants σ_0 and σ_1 for the nonlinear IHCP given by Example 2.3, when $(N_0, N) = (40, 40)$ and $\rho = 0.00$ and $\rho = 0.01$, for various i_0.

	σ_0		σ_1	
i_0	$\rho = 0.00$	$\rho = 0.01$	$\rho = 0.00$	$\rho = 0.01$
1	1.0237	0.928364	0.9932	0.907967
2	1.0047	0.932248	0.9990	0.944396
4	1.0030	0.954096	1.0003	0.960386
8	1.0004	0.973515	1.0001	0.969507
12	1.0000	0.980804	1.0000	0.973343
16	1.0000	0.984069	1.0000	0.975732
20	1.0000	0.985777	1.0000	0.977457
24	1.0000	0.986787	1.0000	0.978793
28	1.0000	0.987446	1.0000	0.979869
32	1.0000	0.987907	1.0000	0.980759
36	1.0000	0.988248	1.0000	0.981508
39	1.0000	0.988450	1.0000	0.981998
40	1.0000	0.988510	1.0000	0.982150

Table 2.9: The constants σ_0 and σ_1 for the nonlinear IHCP given by Example 2.3, when $(N_0, N) = (40, 40)$, $i_0 = 1$ and $i_0 = N = 40$, for various amount of noise.

	$\rho = 0.00$	$\rho = 0.01$	$\rho = 0.03$	$\rho = 0.05$	
σ_0	1.0169	0.9284	0.7564	0.5910	$i_0 = 1$
	1.0000	0.9885	0.9661	0.9444	$i_0 = 40$
σ_1	0.9963	0.9080	0.7364	0.5714	$i_0 = 1$
	1.0000	0.9821	0.9474	0.9139	$i_0 = 40$

Table 2.10: The constants σ_0 and σ_1 when the additional measurement (2.2.4) instead of (2.2.3) is imposed, for various (N_0, N) in the nonlinear IHCP given by Example 2.3.

	σ_0		σ_1	
N, N_0	$\rho = 0.00$	$\rho = 0.01$	$\rho = 0.00$	$\rho = 0.01$
20, 20	1.00028	0.98775	0.99993	0.97772
40, 40	1.00007	0.98754	0.99998	0.97775
80, 80	1.00002	0.98749	1.00005	0.97777
160, 160	1.00000	0.98748	1.00000	0.97777

Table 2.10 gives a comparison between the constants σ_0 and σ_1, when, instead of (2.2.3), the additional measurement (2.2.4) with $e_0 = 1$ and $e_1 = 2$ is imposed. As in Examples 2.1 and 2.2, see Table 2.6, this also results in a relatively stable system of equations, generating accurate and stable approximations for the constants σ_0 and σ_1. The noise introduced in (2.2.4) produces no unstable effects on the resulting output, as opposed to when the measurement (2.2.3) was used at small i_0, near the initial zero time.

2.4 Restoring timewise dependent ambient temperatures – Problem 2.III

The inverse problem in which the spacewise dependent temperature of the environment is unknown has been investigated in section 2.2. In this section we study the inverse problem of restoring the time-dependent ambient temperature.

2.4.1 Mathematical formulation of Problem 2.III

In Problem 2.III, we consider an IHCP in which we replace the boundary conditions (2.2.1) and (2.2.2) by

$$\frac{\partial T}{\partial n}(0,t) + \sigma_0(t)T(0,t) = h_0(t)f(t) + b_0(t), \quad \text{for} \quad t \in (0, t_f], \tag{2.4.1}$$

$$\frac{\partial T}{\partial n}(1,t) + \sigma_1(t)T(1,t) = h_1(t)f(t) + b_1(t), \quad \text{for} \quad t \in (0, t_f], \tag{2.4.2}$$

where $\sigma_i(t)$, $h_i(t)$, $b_i(t)$ are given functions of time, $i = 0, 1$, but the function $f(t)$ is unknown. The additional information necessary is given by the boundary temperature measurement

$$T(x,t) = \overline{\chi}(t), \quad \text{for} \qquad t \in [0, t_f], \tag{2.4.3}$$

where $x = 0$ or $x = 1$.

Alternatively, instead of (2.4.3) we can measure the boundary observation

$$\gamma_0 T(0,t) + \gamma_1 T(1,t) = \overline{\chi}(t), \quad \text{for} \qquad t \in [0, t_f], \tag{2.4.4}$$

where γ_0 and γ_1 are given constants. Conditions (2.4.3) and (2.4.4) are called a point and a boundary integral boundary observation, respectively.

We denote the solution of the direct problem (1.4.1), (1.4.4), and (2.4.1) and (2.4.2) with $f = 0$, i.e.

$$\frac{\partial T^0}{\partial n}(0,t) + \sigma_0(t) T^0(0,t) = b_0(t), \quad \text{for} \qquad t \in (0, t_f], \tag{2.4.5}$$

$$\frac{\partial T^0}{\partial n}(1,t) + \sigma_1(t) T^0(1,t) = b_1(t), \quad \text{for} \qquad t \in (0, t_f], \tag{2.4.6}$$

by $T^0(x,t)$, and introduduce the function $\chi(t) = \overline{\chi}(t) - T^0(x,t)$, where $x = 0$ or $x = 1$ for condition (2.4.3), and $\chi(t) = \overline{\chi}(t) - \gamma_0 T^0(0,t) - \gamma_1 T^0(1,t)$ for condition (2.4.4). Also we introduce the condition

$$\chi \in C^{1/2}([0, t_f]), \quad F(t) := \frac{\mathrm{d}}{\mathrm{d}t} \int_0^t \frac{\chi(\tau)}{\sqrt{t-\tau}} \mathrm{d}\tau \in C([0, t_f]), \tag{2.4.7}$$

where C^α is the space of Holder continuous functions with exponent $\alpha \in (0,1)$. Then we have the following existence, uniqueness and stability theorem, see Kostin and Prilepko [48].

Theorem 2.4.1 *Suppose* $g \in C^1([0,1])$, σ_i, $h_i, b_i \in C([0, t_f])$, $i = 0, 1$ *and* $h_0(t) \neq 0$ *or* $h_1(t) \neq 0$ *for condition* (2.4.3), *or* $\gamma_0 h_0(t) + \gamma_1 h_1(t) \neq 0$ *for condition* (2.4.4), *for all* $t \in [0, t_f]$. *Further, suppose that condition* (2.4.7) *is satisfied. Then there exists a unique solution* $(T \in C^{2,1}(Q), f \in C([0,T]))$ *of the inverse problem* (1.4.1), (1.4.4), (2.4.1)–(2.4.3), *or* (1.4.1), (1.4.4), (2.4.1), (2.4.2), (2.4.4). *Furthermore, the stability conditions*

$$||f|| + ||T - T^0|| \leq C||F||, \tag{2.4.8}$$

$$||f|| + ||T|| \leq C \left(||g|| + ||b_0|| + ||b_1|| + ||\frac{\mathrm{d}}{\mathrm{d}t} \int_0^t \frac{\overline{\chi}(\tau)}{\sqrt{t-\tau}} \mathrm{d}\tau|| \right) \tag{2.4.9}$$

for some positive constant C, are valid, where the norms are in the space of continuous functions.

From Theorem 2.4.1, it follows that under its hypotheses the inverse Problem 2.III is well-posed.

2.4.2 The BEM

Now instead of (1.4.9) and (1.4.10) we have the discretised version of (2.4.1) and (2.4.2), namely,

$$T'_{0i} + \sigma_{0i} T_{0i} = h_{0i} f_i + b_{0i}, \qquad i = \overline{1,N}, \tag{2.4.10}$$

$$T'_{1i} + \sigma_{1i} T_{1i} = h_{1i} f_i + b_{1i}, \qquad i = \overline{1,N}, \tag{2.4.11}$$

where $\sigma_{0i} = \sigma_0(\widetilde{t}_i)$, $\sigma_{1i} = \sigma_1(\widetilde{t}_i)$ and $f_i = f(\widetilde{t}_i)$. Also, instead of (2.4.3) and (2.4.4) we write their discretised versions, namely,

$$T_{0i} = \overline{\chi}_i \quad \text{or} \quad T_{1i} = \overline{\chi}_i, \qquad i = \overline{1,N}, \tag{2.4.12}$$

$$\gamma_0 T_{0i} + \gamma_1 T_{1i} = \overline{\chi}_i, \qquad i = \overline{1,N}, \tag{2.4.13}$$

respectively, where $\overline{\chi}_i = \overline{\chi}_i(\widetilde{t}_i)$. The IHCP given by equations (1.4.1), (1.4.4), (2.4.1), (2.4.2), and (2.4.3) or (2.4.4) reduces to its discretised version given by equations (1.3.38), (1.4.11), (2.4.10), (2.4.11), and (2.4.12) or (2.4.13). It should be noted that from (2.4.10) or (2.4.11) we can eliminate f_i, i.e.

$$f_i = \frac{T'_{0i} + \sigma_{0i} T_{0i} - b_{0i}}{h_{0i}} \quad \text{or} \quad \frac{T'_{1i} + \sigma_{1i} T_{1i} - b_{1i}}{h_{1i}} = f_i, \qquad i = \overline{1,N}, \tag{2.4.14}$$

depending on which data $h_0(t)$ or $h_1(t)$ is non-zero on the interval $[0, t_f]$. Based on the above elimination process, the whole inverse problem can be reduced to a $3N \times 3N$ system of equations of the type (2.2.13), where the unknown vector $\mathbf{Y}$ contains the components of $(T'_{0i})_{i=\overline{1,N}}$, $(T'_{1i})_{i=\overline{1,N}}$ and $(T_{0i})_{i=\overline{1,N}}$ or $(T_{1i})_{i=\overline{1,N}}$, depending whether they are known or unknown with respect to condition (2.4.3). Once $\mathbf{Y}$ is found, $(f_i)_{i=\overline{1,N}}$ can be obtained from (2.4.14).

2.4.3 Numerical Examples, Results and Discussion

Example 2.4

In this example, we solve the IHCP given by the heat equation (1.4.1) in the domain $Q = (0,1) \times (0, t_f = 1]$, subject to the initial condition (2.2.14), the boundary conditions (2.4.1) and (2.4.2) with $\sigma_0 = \sigma_1 = 1$, $h_0 = h_1 = 2$, $b_0 = 0$ and $b_1 = 3$, i.e.

$$\frac{\partial T}{\partial n}(0,t) + T(0,t) = 2f(t), \qquad t \in (0,1], \tag{2.4.15}$$

$$\frac{\partial T}{\partial n}(1,t) + T(1,t) = 2f(t) + 3, \qquad t \in (0,1], \tag{2.4.16}$$

and the additional measurement (2.4.3) at $x = 0$, i.e.

$$T(0,t) = \overline{\chi}(t) = 2t, \quad t \in [0,1]. \tag{2.4.17}$$

To check that the hypotheses of Theorem 2.4.1 are satified, and thus conclude the unique solvability of the inverse problem given by the equations (1.4.1), (2.2.14), (2.4.15)-(2.4.17), we need first to compute the solution $T^0(x,t)$ of the direct problem (1.4.1), (2.2.14), (2.4.5) and (2.4.6), i.e.

$$\frac{\partial T^0}{\partial t}(x,t) = \frac{\partial^2 T^0}{\partial x^2}(x,t), \qquad (x,t) \in (0,1) \times (0,1], \tag{2.4.18}$$

$$T^0(x,0) = x^2, \qquad x \in [0,1], \tag{2.4.19}$$

$$\frac{\partial T^0}{\partial n}(0,t) + T^0(0,t) = 0, \qquad t \in (0,1], \tag{2.4.20}$$

$$\frac{\partial T^0}{\partial n}(1,t) + T^0(1,t) = 3, \qquad t \in (0,1]. \tag{2.4.21}$$

The analytical solution of the problem (2.4.18)– (2.4.21) is given by, see Carlsaw and Jaeger ([17], pp.118, 126),

$$\begin{aligned} T^0(x,t) =& x + 1 + 2\sum_{n=1}^{\infty} \frac{e^{-\alpha_n^2 t}\left(\alpha_n cos(\alpha_n x) + sin(\alpha_n x)\right)}{\alpha_n^2 + 3} \int_0^1 (x^2 - x - 1) \\ & \times \left(\alpha_n cos(\alpha_n x) + sin(\alpha_n x)\right) \mathrm{d}x, \end{aligned} \tag{2.4.22}$$

where α_n are the positive real roots of the transcedental equation

$$tan(\alpha) = \frac{2\alpha}{\alpha^2 - 1}. \tag{2.4.23}$$

Remarking that from (2.4.23) we have

$$sin(\alpha) = \frac{2\alpha}{\alpha^2 + 1}, \qquad cos(\alpha) = \frac{\alpha^2 - 1}{\alpha^2 + 1}, \tag{2.4.24}$$

and performing the integration in (2.4.22) we obtain

$$T^0(x,t) = x + 1 - 8\sum_{n=1}^{\infty} \frac{1}{\alpha_n^3(\alpha_n^2 + 3)} \left(\alpha_n cos(\alpha_n x) + sin(\alpha_n x)\right) e^{-\alpha_n^2 t}. \tag{2.4.25}$$

From (2.4.18) and (2.4.25) we obtain the important identity

$$\frac{x + 1 - x^2}{8} = \sum_{n=1}^{\infty} \frac{\alpha_n \cos(\alpha_n x) + \sin(\alpha_n x)}{\alpha_n^3(\alpha_n^2 + 3)}, \qquad x \in [0,1]. \tag{2.4.26}$$

Differentiating twice with respect to x and setting $x = 0$, we obtain the identity $\frac{1}{4} = \sum_{n=1}^{\infty} \frac{1}{\alpha_n^2 + 3}$. Using (2.4.17) and (2.4.25) we have

$$\chi(t) = \overline{\chi}(t) - T^0(0,t) = 2t - 1 + 8\sum_{n=1}^{\infty} \frac{1}{\alpha_n^2(\alpha_n^2 + 3)} e^{-\alpha_n^2 t}. \tag{2.4.27}$$

Clearly, $\chi \in C^{\frac{1}{2}}([0,1])$ and $\chi(0) = 0$ since from (2.4.19) we have $T^0(0,0) = 0$ and from (2.4.17) we have $\overline{\chi}(0) = 0$. Consider now the function F defined in (2.4.7), namely,

$$\begin{aligned} F(t) &= \frac{\mathrm{d}}{\mathrm{d}t}\int_0^t \frac{1}{\sqrt{t-\tau}}\left(2\tau - 1 + 8\sum_{n=1}^{\infty}\frac{1}{\alpha_n^2(\alpha_n^2+3)}e^{-\alpha_n^2\tau}\right)\mathrm{d}\tau \\ &= 4\sqrt{t} - \frac{1}{\sqrt{t}} + 8\sum_{n=1}^{\infty}\frac{1}{\alpha_n^2(\alpha_n^2+3)}\frac{\mathrm{d}}{\mathrm{d}t}\int_0^t \frac{e^{-\alpha_n^2\tau}}{\sqrt{t-\tau}}\mathrm{d}\tau \\ &= 4\sqrt{t} - \frac{1}{\sqrt{t}} + \frac{8}{\sqrt{t}}\sum_{n=1}^{\infty}\frac{1}{\alpha_n^2(\alpha_n^2+3)} - 8\sqrt{\pi}\sum_{n=1}^{\infty}\frac{erfi(\sqrt{t}\alpha_n)}{\alpha_n(\alpha_n^2+3)}e^{-\alpha_n^2 t}, \end{aligned} \tag{2.4.28}$$

where the function $erfi$ is defined in equation (1.3.9).

Since $\chi(0) = 0$, from (2.4.28), we have that $-1 + 8\sum_{n=1}^{\infty}\frac{1}{\alpha_n^2(\alpha_n^2+3)} = 0$, so that $F(t) = 4\sqrt{t} - 8\sqrt{\pi}\sum_{n=1}^{\infty}\frac{erfi(\sqrt{t}\alpha_n)}{\alpha_n(\alpha_n^2+3)}e^{-\alpha_n^2 t} \in C([0,1])$.

The series is uniformly convergent on $[0,1]$ since

$$\begin{aligned} 8\sqrt{\pi}\sum_{n=1}^{\infty}\frac{erfi(\sqrt{t}\alpha_n)}{\alpha_n(\alpha_n^2+3)}e^{-\alpha_n^2 t} &= 16\sum_{n=1}^{\infty}\frac{1}{\alpha_n(\alpha_n^2+3)}\int_0^{\alpha_n\sqrt{t}} e^{\sigma^2-\alpha_n^2 t}\mathrm{d}\sigma \\ &\le 16\sum_{n=1}^{\infty}\frac{1}{\alpha_n(\alpha_n^2+3)}\int_0^{\alpha_n\sqrt{t}}\mathrm{d}\sigma \\ &= 16\sqrt{t}\sum_{n=1}^{\infty}\frac{1}{\alpha_n^2+3} = 4\sqrt{t}. \end{aligned}$$

Therefore, the conditions of Theorem 2.4.1 are satisfied and hence the inverse problem (1.4.1), (2.2.14), (2.4.15)–(2.4.17), is well-posed. It is easy to verify that its unique solution is given by $f(t) = t, T(x,t) = x^2 + 2t$.

In order to test the stability of the numerical inversion, both additive and multiplicative noise are introduced in the measurement data (2.4.17).

The additive noise is introduced as

$$T_{0i}^{\epsilon} = 2\widetilde{t}_i + \epsilon, \quad i = \overline{1,N}, \tag{2.4.29}$$

where ϵ are Gaussian random variables with zero mean and standard deviation 2ρ, where ρ is the percentage of noise, generated using the NAG routine G05DDF.

The multiplicative noise is introduced as

$$T_{0i}^{\epsilon} = 2\widetilde{t}_i(1+\rho\epsilon), \quad i = \overline{1,N}, \tag{2.4.30}$$

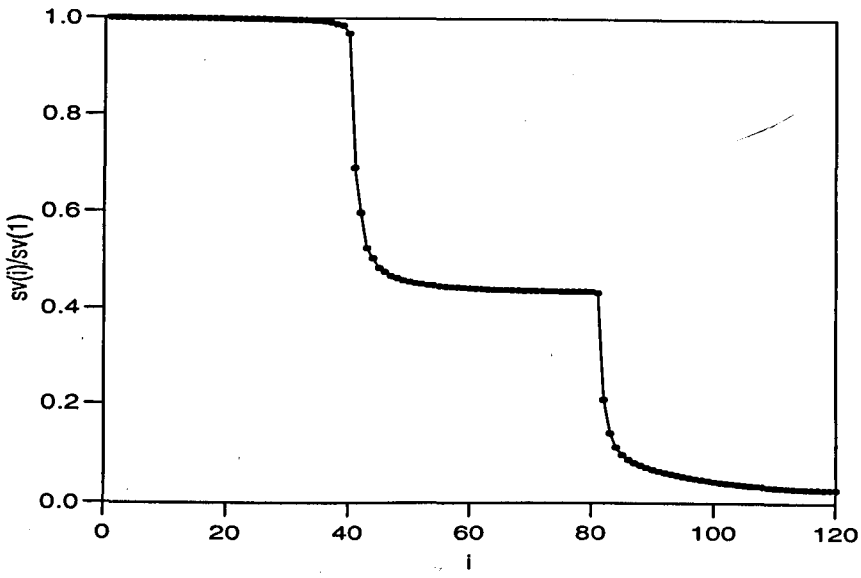

Figure 2.11: The normalised singular values $\frac{sv(i)}{sv(1)}$ of the system of equations, as a function of $i = \overline{1, 3N}$, for the IHCP given by Example 2.4, when $(N_0, N) = (40, 40)$.

where ϵ are random variables taken from a uniform distribution in [-1,1], generated using the NAG routine G05DAF.

Figure 2.11 shows the normalised singular values of the system of $3N$ equations with $3N$ unknowns $T_{1,i}$, $T'_{0,i}$ and $T'_{1,i}$, $i = \overline{1, N}$, when $(N_0, N) = (40, 40)$. From this figure it can be seen that the normalised singular values reduces from 1 to approximately 0.02, which gives the condition number equal to approximately $50 = \frac{sv(1)}{sv(120)}$. Thus, the system of equations is quite well-conditioned, as expected from the stability analysis given in Theorem 2.4.1. Figure 2.12(a) shows the analytical and the noisy values of $T(0,t)$ as functions of time t. We observe that the noisy $T(0,t)$ is more pronouced around $t_f = 1$ and approximately evenly distributed on either side of the analytical curve in the other portions of the figure.

Figures 2.12(b), 2.13(a) and (b), and 2.16(a) show the numerical solutions for $T(1,t)$, $q(0,t)$, $q(1,t)$ and $f(t)$, respectively, when $\rho = 5\%$ additive noise is introduced into the data (2.4.29). For no noise, the numerical results are in excellent agreement with the exact solutions $T(1,t) = 1 + 2t$, $q(0,t) = 0$, $q(1,t) = 2$ and $f(t) = t$. However, when noise is introduced, the numerical solutions, shown by $(- \triangle -)$, have a more prononounced disagreement with the exact solutions near $t = 1$. This is because they are obtained from the input values $T(0,t)$ which also had larger errors near $t = 1$, as shown in Figure 2.12(a). Furthermore, as is expected, the heat flux prediction is less accurate than the boundary temperature prediction.

Although not illustrated, it is reported that some regularised features of the heat flux have been

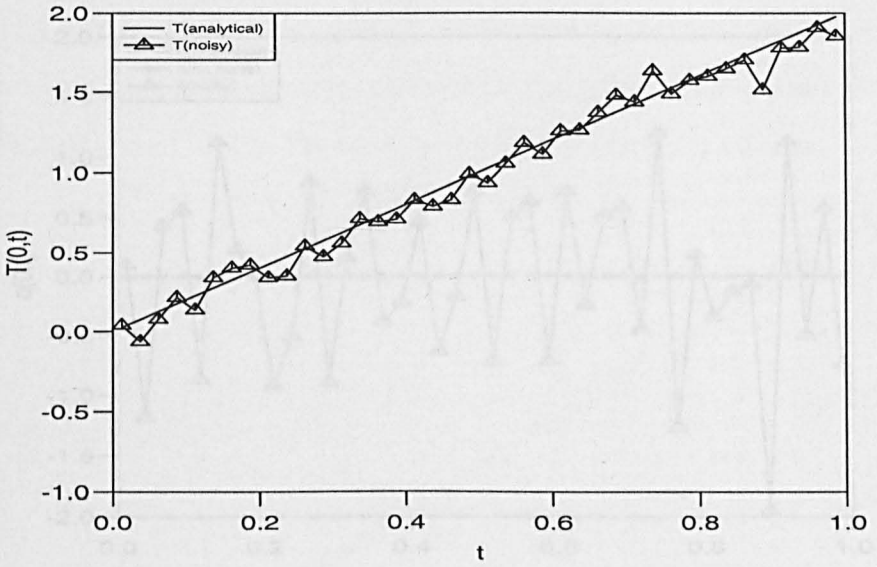

(a)

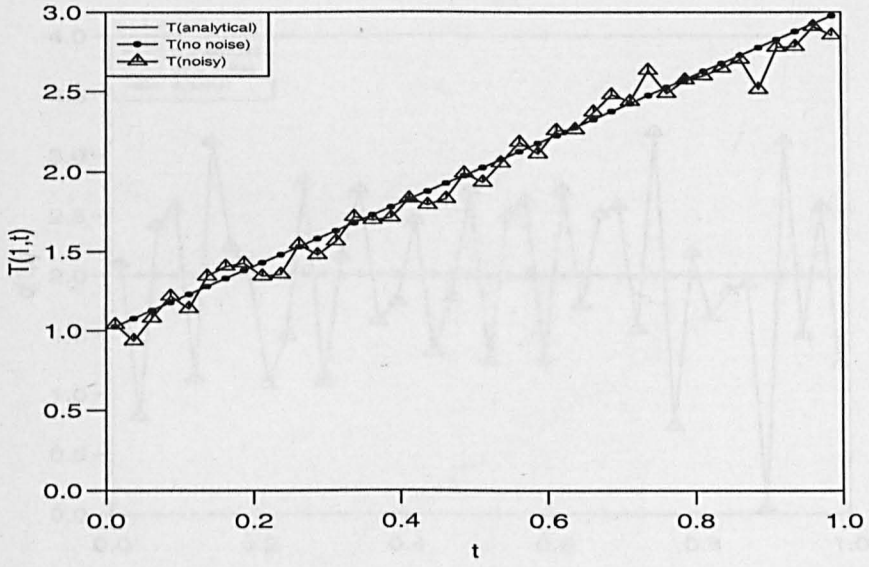

(b)

Figure 2.12: The analytical and numerical boundary temperatures (a) $T(0,t)$, and (b) $T(1,t)$, as functions of time t, for the IHCP given by Example 2.4, when $(N_0, N) = (40, 40)$, (5% additive noise).

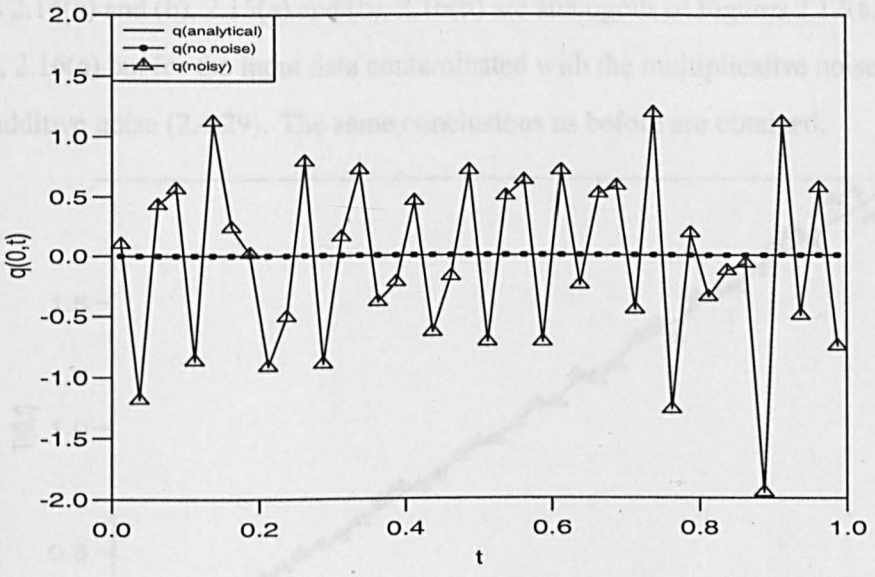

(a)

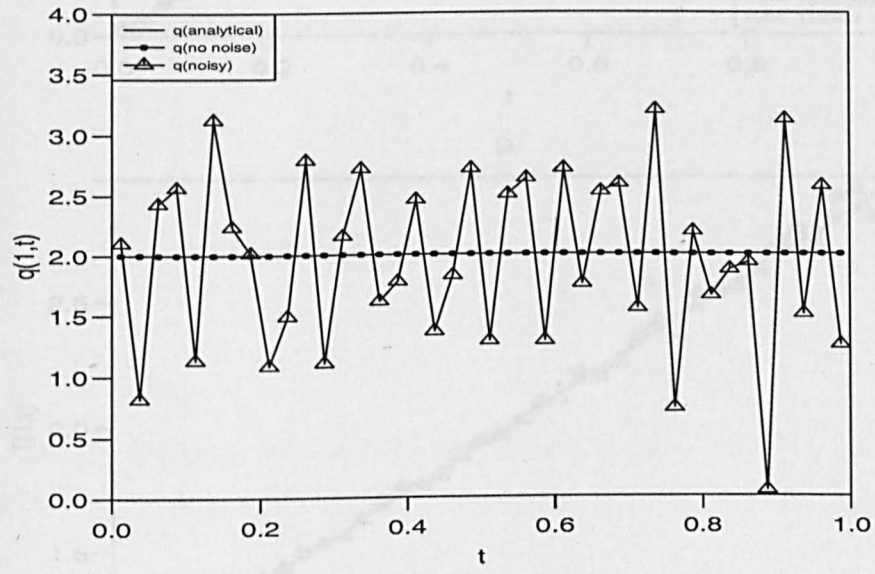

(b)

Figure 2.13: The analytical and numerical heat fluxes (a) $q(0,t)$, and (b) $q(1,t)$, as functions of time t, for the IHCP given by Example 2.4, when $(N_0, N) = (40, 40)$, (5% additive noise).

further obtained if one uses the TSVD, described in Section 2.2, for solving the direct ill-posed problem of retrieving higher-order (Neumann) derivatives from noisy lower order (Dirichlet) data $T(0,t)$ and $T(1,t)$ shown by $(-\ \triangle\ -)$ in Figures 2.12(a) and (b), respectively, as described in Lesnic *et al.* [54].

Figures 2.14(a) and (b), 2.15(a) and (b), 2.16(b) are analogous of Figures 2.12(a) and (b), 2.13(a) and (b), 2.16(a) but for the input data contaminated with the multiplicative noise (2.4.30) instead of the additive noise (2.4.29). The same conclusions as before are obtained.

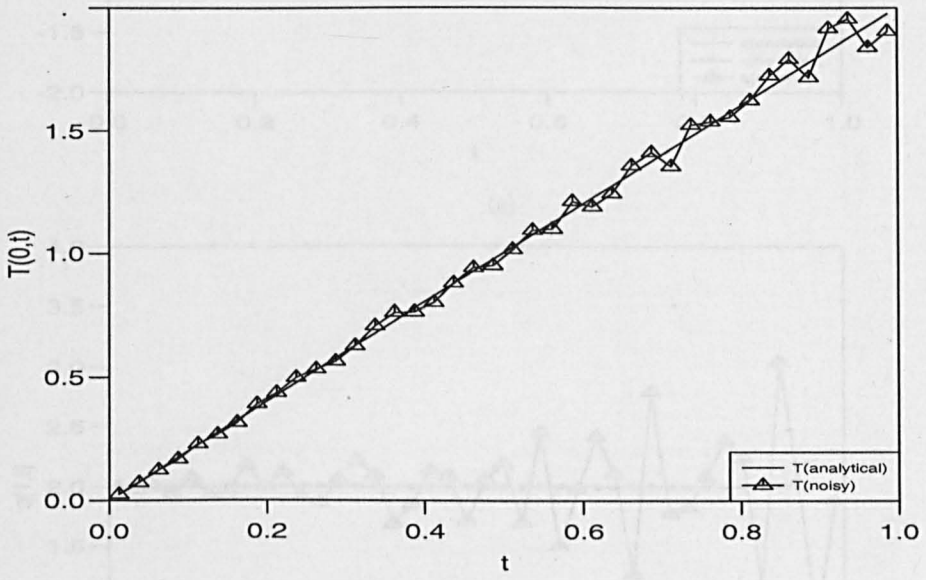

(a)

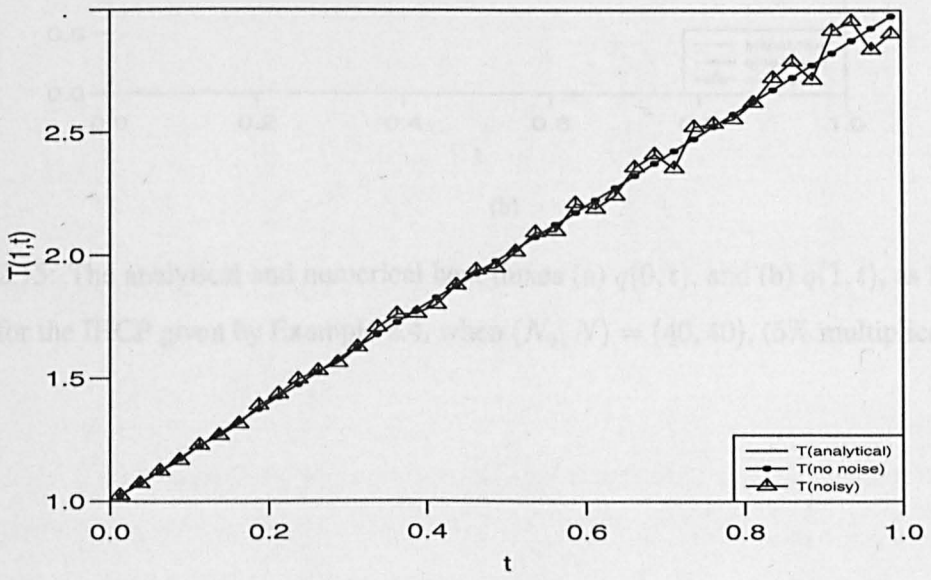

(b)

Figure 2.14: The analytical and numerical temperatures (a) $T(0,t)$, and (b) $T(1,t)$, as functions of time t, for the IHCP given by Example 2.4, when $(N_0, N) = (40, 40)$ (5% multiplicative noise).

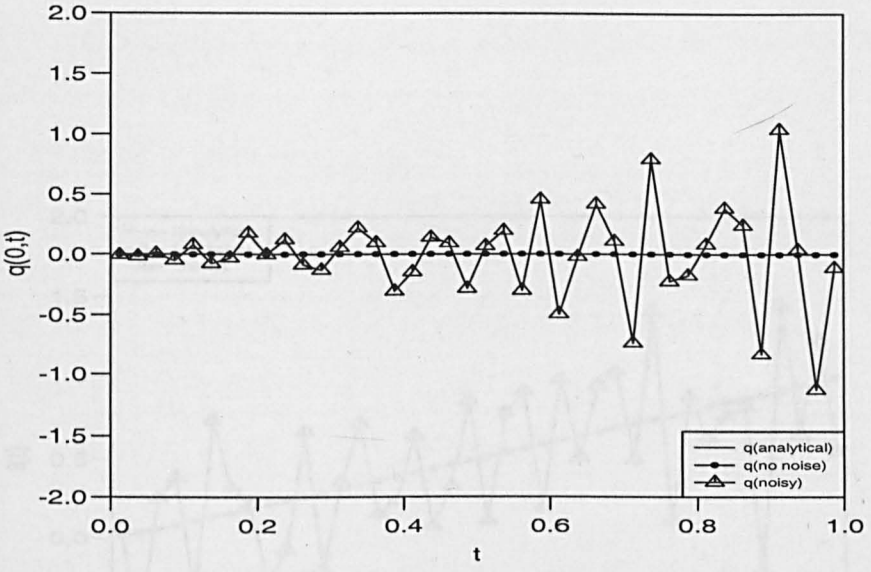

(a)

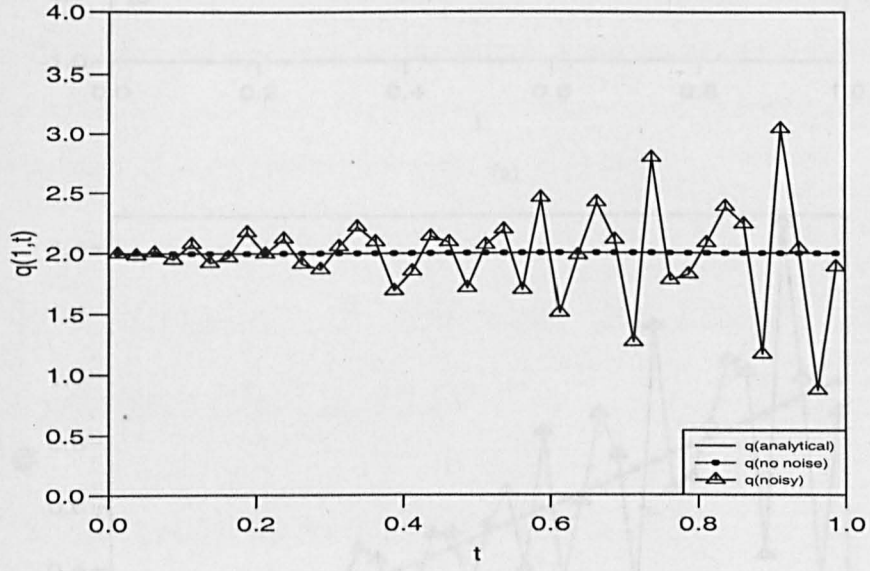

(b)

Figure 2.15: The analytical and numerical heat fluxes (a) $q(0,t)$, and (b) $q(1,t)$, as functions of time t, for the IHCP given by Example 2.4, when $(N_0, N) = (40, 40)$, (5% multiplicative noise).

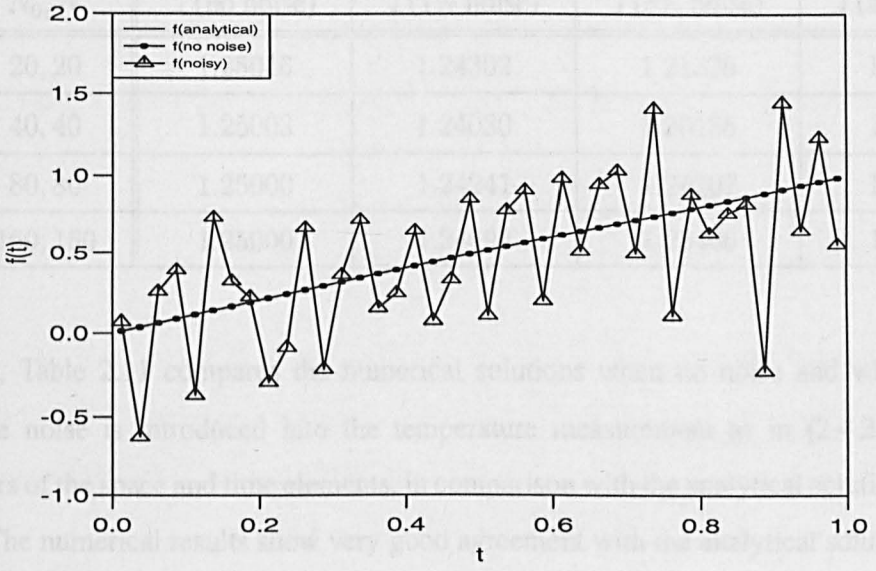

(a)

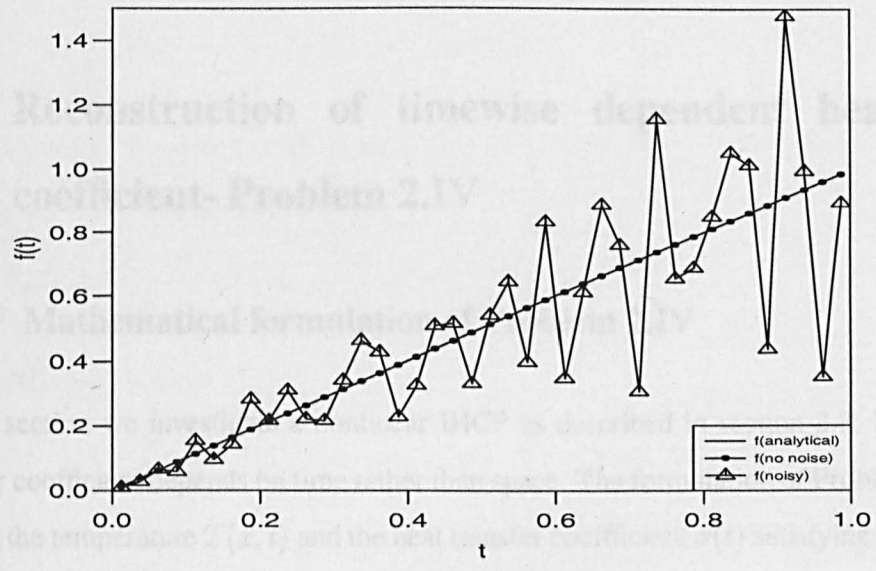

(b)

Figure 2.16: The analytical and numerical solutions for the function $f(t)$, as functions of time t, for the IHCP given by Example 2.4, when $(N_0, N) = (40, 40)$ and additional measurement has (a) 5% additive noise, and (b) 5% multiplicative noise.

Table 2.11: The analytical and the numerical solutions for the interior temperature $T(0.5, 0.5)$, when additive noise and no noise is introduced in the additional measurement (2.4.17) for various (N_0, N), for the IHCP given by Example 2.4.

N_0, N	T(no noise)	T(1% noise)	T(5% noise)	T(analytical)
20, 20	1.25046	1.24302	1.21326	1.25000
40, 40	1.25003	1.24030	1.20135	1.25000
80, 80	1.25000	1.24241	1.21207	1.25000
160, 160	1.25000	1.24693	1.23466	1.25000

Finally, Table 2.11 compares the numerical solutions when no noise and when 1% and 5% additive noise is introduced into the temperature measurement as in (2.4.29), for different numbers of the space and time elements, in comparison with the analytical solution $T(0.5, 0.5) = 1.25$. The numerical results show very good agreement with the analytical solution for errorless data and the stability of the numerical solution for noisy data.

2.5 Reconstruction of timewise dependent heat transfer coefficient- Problem 2.IV

2.5.1 Mathematical formulation of Problem 2.IV

In this section we investigate a nonlinear IHCP as described in section 2.3, but now the heat transfer coefficient depends on time rather than space. The formulation of Problem 2.IV requires finding the temperature $T(x, t)$ and the heat transfer coeffficient $\sigma(t)$ satisfying (1.4.1) subject to the initial condition (1.4.4), the Robin boundary condition

$$\frac{\partial T}{\partial n}(i, t) + \sigma(t)T(i, t) = B_i(t), \qquad t \in (0, t_f], \quad i = 0, 1, \tag{2.5.1}$$

and the additional measurements (2.4.3) or (2.4.4), where B_i, $i = 0, 1$, are given functions.

For this inverse problem the following uniqueness result holds, see Kostin and Prilepko [48].

Theorem 2.5.1 *Suppose* $g \in C^1([0,1])$, $B_i \in C([0,t_f])$, $i = 0,1$, *and* $|\overline{x}(t)| > 0$ *for all* $t \in [0,t_f]$. *Then a solution* $(T \in C^{2,1}(Q), \sigma \in C([0,t_f]))$ *of the inverse Problem 2.IV is unique.*

2.5.2 The BEM

The numerical BEM discretisation of Problem 2.IV consists of equations (1.3.38), (1.4.11), (2.4.12) or (2.4.13) and

$$T'_{0i} + \sigma_i T_{0i} = B_{0i}, \qquad T'_{1i} + \sigma_i T_{1i} = B_{1i}, \qquad i = \overline{1,N}, \tag{2.5.2}$$

where $\sigma_i = \sigma(\widetilde{t}_i)$, $i = \overline{1,N}$. From (2.5.2) we can eliminate the normal derivative and this results in a system of $3N$ nonlinear equations with $3N$ unknowns T_{0i}, T_{1i} and σ_i for $i = \overline{1,N}$, which is solved using the NAG routine C05NCF.

2.5.3 Numerical Examples, Results and Discussion

Example 2.5

In this example, we solve the IHCP given by the heat equation (1.4.1) in the domain $Q = (0,1) \times (0, t_f = 1]$, subject to the initial condition

$$T(x,0) = g(x) = x^2 + 1, \qquad x \in [0,1], \tag{2.5.3}$$

the boundary conditions (2.5.1) given by

$$\frac{\partial T}{\partial n}(0,t) + \sigma(t)T(0,t) = t(2t+1) = B_0(t), \qquad t \in (0,1], \tag{2.5.4}$$

$$\frac{\partial T}{\partial n}(1,t) + \sigma(t)T(1,t) = 2 + 2t(t+1) = B_1(t), \qquad t \in (0,1], \tag{2.5.5}$$

and the additional measurement (2.4.3) given by

$$T(0,t) = 2t + 1 = \overline{\chi}(t), \quad t \in [0,1]. \tag{2.5.6}$$

Since all the conditions of Theorem 2.5.1 are satisfied, it follows that the above inverse problem has at most one solution, namely

$$T(x,t) = x^2 + 2t + 1, \qquad \sigma(t) = t. \tag{2.5.7}$$

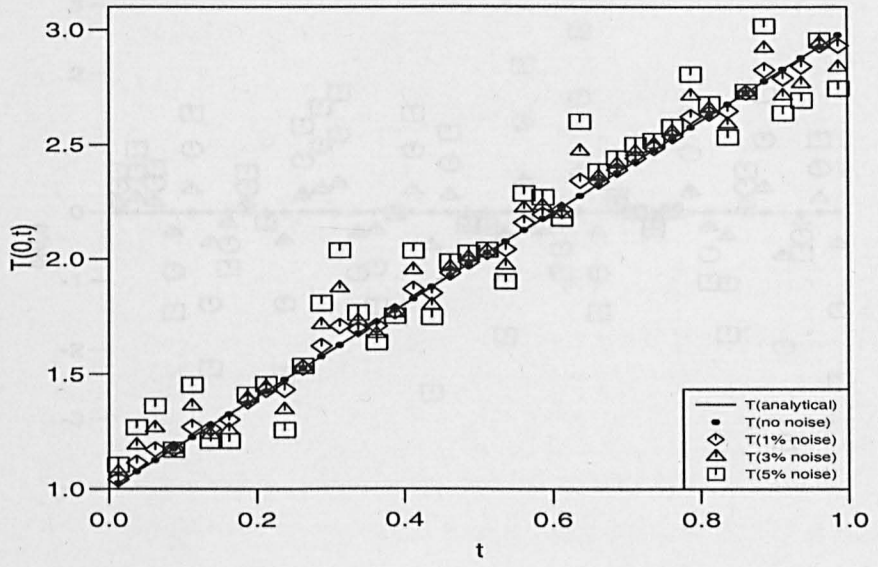

(a)

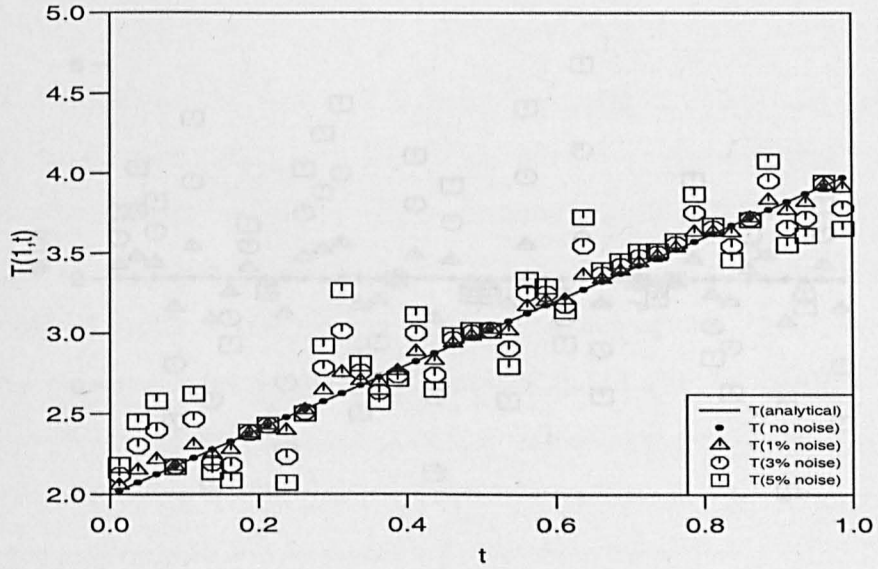

(b)

Figure 2.17: The analytical and numerical boundary temperatures (a) $T(0,t)$, and (b) $T(1,t)$, as functions of time t, for the nonlinear IHCP given by Example 2.5, for various amounts of noise and when $(N_0, N) = (40, 40)$.

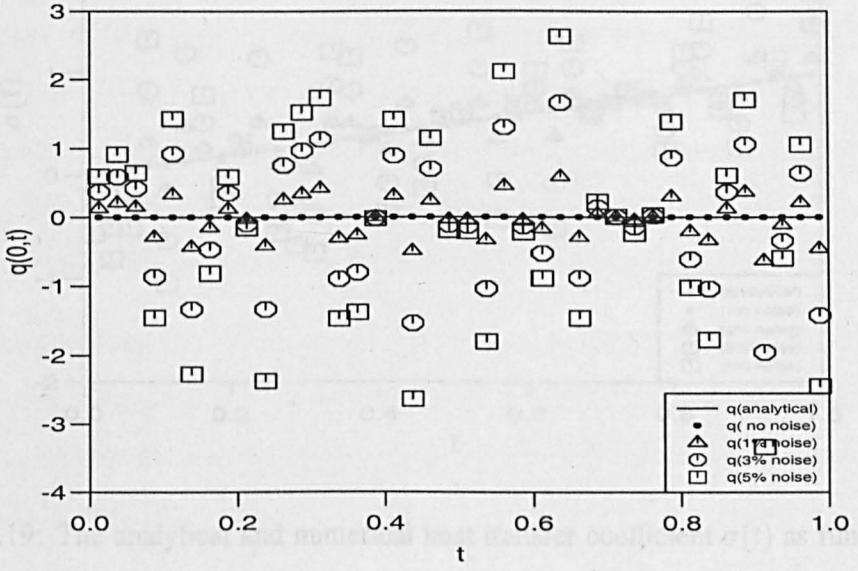

(a)

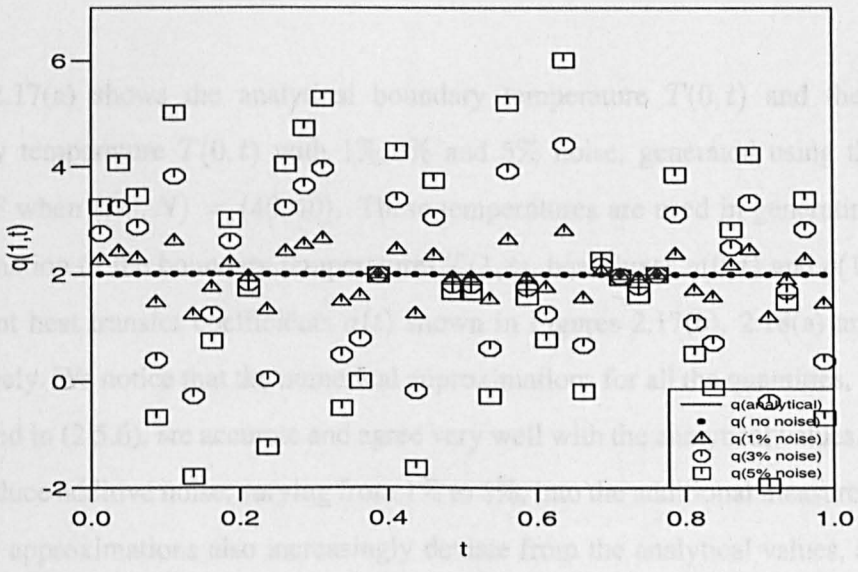

(b)

Figure 2.18: The analytical and numerical heat fluxes (a) $q(0,t)$, and (b) $q(1,t)$, as functions of time t, for the nonlinear IHCP given by Example 2.5, for various amounts of noise and when $(N_0, N) = (40, 40)$.

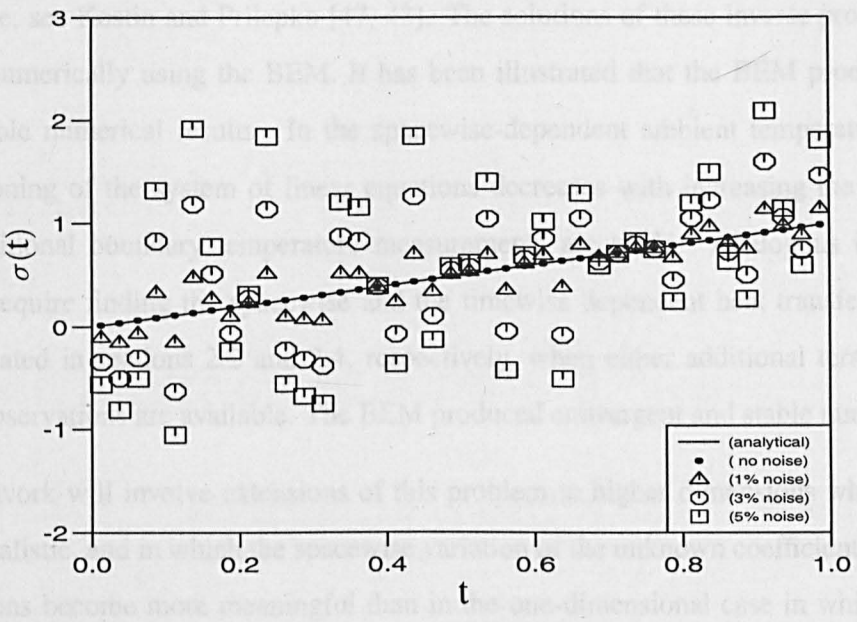

Figure 2.19: The analytical and numerical heat transfer coefficient $\sigma(t)$ as functions of time t, for the nonlinear IHCP given by Example 2.5, for various amounts of noise and when $(N_0, N) = (40, 40)$.

Figure 2.17(a) shows the analytical boundary temperature $T(0,t)$ and the noisy additive boundary temperature $T(0,t)$ with $1\%, 3\%$ and 5% noise, generated using the NAG routine G05DDF when $(N_0, N) = (40, 40)$. These temperatures are used in generating the numerical approximation of the boundary temperatures $T(1,t)$, heat fluxes $q(0,t)$ and $q(1,t)$ and the time dependent heat transfer coefficients $\sigma(t)$ shown in Figures 2.17(b), 2.18(a) and (b), and 2.19, respectively. We notice that the numerical approximations for all the quantities, when no noise is introduced in (2.5.6), are accurate and agree very well with the analytical values. However, when we introduce additive noise, varying from 1% to 5%, into the additional measurement (2.5.6), the resulting approximations also increasingly deviate from the analytical values, as the amount of noise increases.

2.6 Conclusions

In sections 2.1 and 2.3, inverse problems in heat conduction which require the determination of the spacewise and the timewise dependent ambient temperature appearing in the boundary conditions from additional terminal, integral or point observations have been investigated,

respectively. Under these additional measurements (observations), solvability results are available, see Kostin and Prilepko [47, 48]. The solutions of these inverse problems have been found numerically using the BEM. It has been illustrated that the BEM produced convergent and stable numerical results. In the spacewise-dependent ambient temperature case, the ill-conditioning of the system of linear equations decreases with increasing the instant at which the additional boundary temperature measurements are made. Analogous inverse problems which require finding the spacewise and the timewise dependent heat transfer coefficients are investigated in sections 2.2 and 2.4, respectively, when either additional terminal, integral or point observations are available. The BEM produced convergent and stable numerical results.

Future work will involve extensions of this problem to higher dimensions which is practically more realistic, and in which the spacewise variation of the unknown coefficients in the boundary conditions become more meaningful than in the one-dimensional case in which two constants only had to be retrieved.

Chapter 3

Determination of a time-dependent heat transfer coefficient from non-standard boundary measurements

3.1 Introduction

The heat transfer coefficient (HTC) characterises the contribution that an interface makes to the overall thermal resistance to the system and is defined in terms of the heat flux across the surface for a unit temperature gradient. It is well-known that the HTC is an important value in determining the heat transfer. Traditionally, partial boundary temperature and heat flux measurements are used as input to heat conduction models to extract the HTC values by solving a Cauchy ill-posed inverse heat conduction problem (IHCP) using, for example, Beck's function specification method, Tikhonov's regularization, Alifanov's iterative regularization or the mollification method, see Alifanov [4], Maillet *et al.* [57], Hinestroza and Murio [37], Orlande *et al.* [64], Chantasiriwan [18], Louahlia–Gualous *et al.* [56], Su and Hewitt [80], Osman and Beck [65], Divo *et al.* [22] and Chen and Wu [20]. However, in this chapter we do not measure Cauchy data which may experience some practical difficulties, but instead we measure some non-standard boundary transient quantity of the heat conducting system, whilst allowing for convectional boundary conditions to be prescribed over the whole boundary. Further, the HTC is allowed to vary with time. Hence, a more realistic model can be proposed for problems such as the forced-convection flow boiling over the outer surface of a heated tube, see Su and

Hewitt [80], quenching experiments, see Osman and Beck [65], or nucleate boiling on cylinders, see Louahlia–Gualous *et al.* [56].

3.2 Mathematical Formulation

The following initial boundary value problem for the one-dimensional parabolic heat equation is investigated. Given $t_f > 0$, an arbitrary fixed time of interest, find the pair $(T(x,t), \sigma(t))$, where T represents the temperature and σ is the time-dependent heat transfer coefficient, satisfying:

$$T_t(x,t) = T_{xx}(x,t), \qquad \forall\,(x,t) \in (0,1) \times (0,t_f), \tag{3.2.1}$$

$$T(x,0) = T_0(x), \qquad \forall\, x \in (0,1), \tag{3.2.2}$$

$$-T_x(0,t) + \sigma(t)T(0,t) = h_0(t), \qquad \forall\, t \in (0,t_f), \tag{3.2.3}$$

$$T_x(1,t) + \sigma(t)T(1,t) = h_1(t), \qquad \forall\, t \in (0,t_f), \tag{3.2.4}$$

where

(i) $\sigma(t) \geq 0, \quad \forall\, t \in [0,t_f],\ \sigma \in L_2((0,t_f))$;

(ii) $T \in C([0,t_f], L_2((0,1))) \cap L_2((0,t_f), H^1((0,1)))$;

(iii) $T_t \in L_2((0,t_f), L_2((0,1)))$;

(iv) $T_0 \in H^2((0,1))$, $h_i \in L_2((0,t_f))$, $i = 0,1$, are given functions.

In order to solve this inverse problem we consider some additional information given by the non-standard boundary measurement

$$0 < E(t) = T^2(0,t) + T^2(1,t), \quad \forall\, t \in [0,t_f], \tag{3.2.5}$$

where $E \in C([0,t_f])$ is a given function.

The cases when the additional information is given by the specification of the boundary temperature $T(0,t)$, or mass $M(t) = T(0,t) + T(1,t)$, have been investigated elsewhere, see Kostin and Prilepko [47], Onyango *et al.* [63] and Chapter 2. Note that by multiplying equation (3.2.1) with T and integrating over the space interval $(0,1)$ using the boundary conditions (3.2.3) and (3.2.4) result in

$$\frac{1}{2}\frac{d}{dt}\left(\int_0^1 T^2(x,t)dx\right) = T(1,t)h_1(t) + T(0,t)h_0(t) - \sigma(T)E(t), \quad \forall\, t \in [0,t_f]. \tag{3.2.6}$$

From this equation it can be remarked that the quantity $E(t)$ could be interpreted as the rate of change of energy divided by the heat transfer coefficient. Although this quantity does not have a

very clear physical meaning, we mention that equation (3.2.5) can be viewed as a non-local, non-standard boundary condition. Such non-standard formulations of IHCPs have been considered before, see e.g. Ames and Straughan [5] , Slodička and Van Keer [77, 78] and Dehghan [23].

3.2.1 Variational formulation

The variational formulation of the direct problem (3.2.1)–(3.2.4) for a given $\sigma \in L_2((0,t_f))$, $\sigma(t) \geq 0, \forall\, t \in [0,t_f]$, reads as follows.

Definition 3.2.1 *A function $T_\sigma \in L_2((0,t_f), H^1((0,1)))$ with $(T_\sigma)_t \in L_2((0,t_f), L_2((0,1)))$ is called a weak solution to the direct problem* (3.2.1)-(3.2.4) *if $T_\sigma(x,0) = T_0(x)$ and*

$$\int_0^1 \left[\frac{\partial T_\sigma}{\partial t}(x,t)\varphi(x,t) + \frac{\partial T_\sigma}{\partial x}(x,t)\frac{\partial \varphi}{\partial x}(x,t)\right] \mathrm{d}x = \varphi(1,t)\left(h_1(t) - \sigma(t)T_\sigma(1,t)\right)$$
$$+ \varphi(0,t)\left(h_0(t) - \sigma(t)T_\sigma(0,t)\right), \qquad \forall\, \varphi \in L_2\left((0,t_f), H^1((0,1))\right), \quad \forall\, t \in (0,t_f). \tag{3.2.7}$$

One can show that there is a unique weak solution to the direct problem (3.2.1)–(3.2.4), see e.g. Friedman [30].

3.2.2 Uniqueness

In this section, we prove the uniqueness of a weak solution (σ, T_σ) to the inverse problem (3.2.1)–(3.2.5). The proof is actually a simplification of that given in Slodička and Van Keer [78], and we include it for clarity and completeness of the explanation.

Theorem 3.2.1 *Let T_σ, $T_{\widetilde{\sigma}}$ be the unique weak solutions of the problem* (3.2.1)–(3.2.4). *Then if $0 < E(t) = T_\sigma^2(0,t) + T_\sigma^2(1,t) = T_{\widetilde{\sigma}}^2(0,t) + T_{\widetilde{\sigma}}^2(1,t)$, i.e. if $E_\sigma = E_{\widetilde{\sigma}}$, then $T_\sigma = T_{\widetilde{\sigma}}$ and $\sigma = \widetilde{\sigma}$.*

Proof:

We subtract (3.2.7) written for σ and $\widetilde{\sigma}$ to obtain

$$\begin{aligned}
&\int_0^1 \left[\frac{\partial}{\partial t}\left(T_{\widetilde{\sigma}} - T_\sigma\right)\varphi + \frac{\partial}{\partial x}\left(T_{\widetilde{\sigma}} - T_\sigma\right)\cdot\frac{\partial\varphi}{\partial x}\right]\mathrm{d}x \\
&= \sigma(t)\left[\varphi(1,t)\left(T_\sigma(1,t) - T_{\widetilde{\sigma}}(1,t)\right) + \varphi(0,t)\left(T_\sigma(0,t) - T_{\widetilde{\sigma}}(0,t)\right)\right] \\
&+ \left(\sigma(t) - \widetilde{\sigma}(t)\right)\left[\varphi(1,t)T_{\widetilde{\sigma}}(1,t) + \varphi(0,t)T_{\widetilde{\sigma}}(0,t)\right], \\
&\forall\,\varphi \in L_2\left((0,t_f), H^1((0,1))\right), \quad \forall\ t \in (0,t_f).
\end{aligned} \tag{3.2.8}$$

An equivalent form of this equation reads as

$$\begin{aligned}
&\int_0^1 \left[\frac{\partial}{\partial t}\left(T_{\widetilde{\sigma}} - T_\sigma\right)\varphi + \frac{\partial}{\partial x}\left(T_{\widetilde{\sigma}} - T_\sigma\right)\cdot\frac{\partial\varphi}{\partial x}\right]\mathrm{d}x \\
&= \widetilde{\sigma}(t)\left[\varphi(1,t)\left(T_\sigma(1,t) - T_{\widetilde{\sigma}}(1,t)\right) + \varphi(0,t)\left(T_\sigma(0,t) - T_{\widetilde{\sigma}}(0,t)\right)\right] \\
&+ \left(\sigma(t) - \widetilde{\sigma}(t)\right)\left[\varphi(1,t)T_\sigma(1,t) + \varphi(0,t)T_\sigma(0,t)\right] \\
&\forall\,\varphi \in L_2\left((0,t_f), H^1((0,1))\right), \quad \forall\, t \in (0,t_f).
\end{aligned} \tag{3.2.9}$$

Adding equation (3.2.8) and (3.2.9) results in

$$\begin{aligned}
&2\int_0^1 \left[\frac{\partial}{\partial t}\left(T_{\widetilde{\sigma}} - T_\sigma\right)\varphi + \frac{\partial}{\partial x}\left(T_{\widetilde{\sigma}} - T_\sigma\right)\cdot\frac{\partial\varphi}{\partial x}\right]\mathrm{d}x \\
&= \left(\sigma(t) + \widetilde{\sigma}(t)\right)\left[\varphi(1,t)\left(T_\sigma(1,t) - T_{\widetilde{\sigma}}(1,t)\right) + \varphi(0,t)\left(T_\sigma(0,t) - T_{\widetilde{\sigma}}(0,t)\right)\right] \\
&+ \left(\sigma(t) - \widetilde{\sigma}(t)\right)\left[\varphi(1,t)\left(T_\sigma(1,t) + T_{\widetilde{\sigma}}(1,t)\right) + \varphi(0,t)\left(T_\sigma(0,t) + T_{\widetilde{\sigma}}(0,t)\right)\right], \\
&\forall\,\varphi \in L_2\left((0,t_f), H^1((0,1))\right), \quad \forall\, t \in (0,t_f).
\end{aligned} \tag{3.2.10}$$

Choosing $\varphi(x,t) = T_{\widetilde{\sigma}}(x,t) - T_\sigma(x,t)$, we note that $\varphi(x,0) = 0$, and integrating the resulting identity (3.2.10) from 0 to t yields

$$\begin{aligned}
&\int_0^1 \left(T_{\widetilde{\sigma}} - T_\sigma\right)^2 \mathrm{d}x + 2\int_0^t\int_0^1 \left[\frac{\partial}{\partial x}\left(T_{\widetilde{\sigma}} - T_\sigma\right)\right]^2 \mathrm{d}x\mathrm{d}\tau \\
&= -\int_0^t \left(\sigma(\tau) + \widetilde{\sigma}(\tau)\right)\left[\left(T_{\widetilde{\sigma}}(1,\tau) - T_\sigma(1,\tau)\right)^2 + \left(T_{\widetilde{\sigma}}(0,\tau) - T_\sigma(0,\tau)\right)^2\right]\mathrm{d}\tau \\
&+ \int_0^t \left(\sigma(\tau) - \widetilde{\sigma}(\tau)\right)\left[T^2_{\widetilde{\sigma}}(1,\tau) - T^2_\sigma(1,\tau) + T^2_{\widetilde{\sigma}}(0,\tau) - T^2_{\widetilde{\sigma}}(0,\tau)\right]\mathrm{d}\tau.
\end{aligned} \tag{3.2.11}$$

Using that $E\sigma(t) = E_{\widetilde{\sigma}}(t)$, the last term vanishes and recalling that $\varphi(x,t) = T_{\widetilde{\sigma}}(x,t) - T_\sigma(x,t)$ we obtain

$$\begin{aligned}
&\int_0^1 \varphi^2(x,t)\mathrm{d}x + 2\int_0^t\int_0^1 \left[\frac{\partial\varphi}{\partial x}(x,\tau)\right]^2 \mathrm{d}x\mathrm{d}\tau \\
&+ \int_0^t \left(\sigma(\tau) + \widetilde{\sigma}(\tau)\right)\left[\varphi^2(1,\tau) + \varphi^2(0,\tau)\right]\mathrm{d}\tau = 0, \qquad \forall\, t \in (0,t_f).
\end{aligned} \tag{3.2.12}$$

It should be noted that this is also valid for $t = 0$ since $\varphi(x,0) = 0$. We also have $\sigma, \widetilde{\sigma} \geq 0$ and thus all the terms in (3.2.12) are non-negative. This yields $\varphi(x,t) \equiv 0$ in $C([0,t_f], L_2((0,1))) \cap L_2((0,t_f), H^1((0,1)))$. Hence $T_\sigma = T_{\widetilde{\sigma}}$ and then (3.2.10) becomes

$$2(\sigma(t) - \widetilde{\sigma}(t))(\varphi(1,t)T_\sigma(1,t) + \varphi(0,t)T_\sigma(0,t)) = 0, \quad \forall\, t \in (0,t_f). \tag{3.2.13}$$

Choosing $\varphi(x,t) = T_\sigma(x,t)$ we obtain

$$2(\sigma(t) - \widetilde{\sigma}(t))E(t) = 0, \qquad \forall\, t \in (0,t_f), \tag{3.2.14}$$

and since $E(t) > 0$ it follows that $\sigma = \widetilde{\sigma}$. This concludes the proof.

3.3 The BEM

Applying Green's formula, the heat equation (3.2.1) transforms into, see e.g. Brebbia *et al.* [11],

$$\begin{aligned}\eta(x)T(x,t) = &\int_0^t \left[G(x,t;\xi,\tau)\frac{\partial T}{\partial n}(\xi,\tau) - T(\xi,\tau)\frac{\partial G}{\partial n(\xi)}(x,t;\xi,\tau)\right]_{\xi\in\{0,1\}} \mathrm{d}\tau \\ &+ \int_0^1 G(x,t;y,0)T_0(y)\mathrm{d}y, \qquad (x,t) \in [0,1]\times(0,t_f],\end{aligned} \tag{3.3.1}$$

where the initial condition (3.2.2) has also been imposed.

Introducing the boundary conditions (3.2.3) and (3.2.4) into (3.3.1) results in

$$\begin{aligned}&\eta(x)T(x,t) = \int_0^1 G(x,t;y,0)T_0(y)\mathrm{d}y \\ &+ \int_0^t \left\{h_\xi(\tau)G(x,t;\xi,\tau) - T(\xi,\tau)\left[\sigma(\tau)G(x,t;\xi,\tau) + \frac{\partial G}{\partial n(\xi)}(x,t;\xi,\tau)\right]\right\}_{\xi\in\{0,1\}} \mathrm{d}\tau, \\ &(x,t) \in [0,1]\times(0,t_f].\end{aligned} \tag{3.3.2}$$

Applying this integral equation (3.3.2) at the boundary $(x,t) \in \{0,1\}\times(0,t_f]$, one obtains two nonlinear boundary integrals in the three unknowns $T(0,t)$, $T(1,t)$ and $\sigma(t)$. A further nonlinear equation is given by the measurement (3.2.5) which, when contaminated with noise, reads as

$$T^2(0,t) + T^2(1,t) = E(t)(1 + \rho\epsilon(t)), \quad \forall\, t \in (0,t_f], \tag{3.3.3}$$

where ρ is the percentage of noise and ϵ is a random variable taken from a uniform distribution in the interval [-1,1] using the NAG routine G05DAF.

Using a BEM with constant elements (N_0 uniform cells for discretising the space domain $(0,1)$ and N uniform constant boundary elements for discretising the time interval $(0,t_f]$, we obtain a nonlinear system of $3N$ equations with $3N$ unknowns, which is solved using the NAG routine E04FCF in a nonlinear least-squares minimization sense. The constraint (i) that σ is non-negative is not imposed in order to avoid a more sophisticated constrained minimization problem. However, if it happens that σ takes negative values, see later Figures 3.7 and 3.11, then these values are to be interpreted as zero values.

3.4 Numerical Results and Discussion

In order to illustrate the technique and discuss the numerical results obtained by the BEM, we take, for convenience, $t_f = 1$ with the input data $T_0(x) = x^2 + 1$, $h_0(t) = t(2t+1)$, $h_1(t) = 2+t(2t+2)$ and $E(t) = 8t^2 + 12t + 5$. Then the inverse problem (3.2.1)–(3.2.5) has the unique solution

$$\sigma(t) = t, \quad T(x,t) = x^2 + 2t + 1. \tag{3.4.1}$$

The numerical results for the boundary temperatures $T(0,t)$ and $T(1,t)$, see Figures 3.1(a) and 3.1(b), respectively, the heat fluxes $q(0,t)$ and $q(1,t)$, see Figures 3.2(a) and 3.2(b), respectively, and the heat transfer coefficient $\sigma(t)$, see Figure 3.3, obtained from the numerical inverse problem (3.2.1)-(3.2.5), when (N, N_0) is increased gradually from (10,10) to (80,80) and the amount of noise $\rho = 0.00$ are good approximations and match the corresponding analytical solution. These numerical results improve with increasing values of (N, N_0), confirming that the method is convergent. Further, the results obtained are sufficiently accurate when $(N, N_0) = (40, 40)$. Hence, there is no need to increase the number of boundary discretisations above (40,40).

When noise is gradually introduced into the additional condition (3.3.3) from $\rho = 0.00$ to $\rho = 0.05$, see Figure 3.4, and the value of $(N, N_0) = (40, 40)$, we observe that the computed boundary data for the temperatures $T(0,t)$ and $T(1,t)$, see Figures 3.5(a) and 3.5(b), respectively, remain stable with the increase in the amount of noise, i.e. the value of the numerical boundary temperature deviating from the analytical solution is proportional to the amount of noise given in (3.3.3). This indicates that the results do not require regularization. However, the numerical results for the heat fluxes $q(0,t)$ and $q(1,t)$, see Figures 3.6(a) and 3.6(b), respectively, and the heat transfer coefficient $\sigma(t)$, see Figure 3.7, obtained when the amount of noise is stepwise

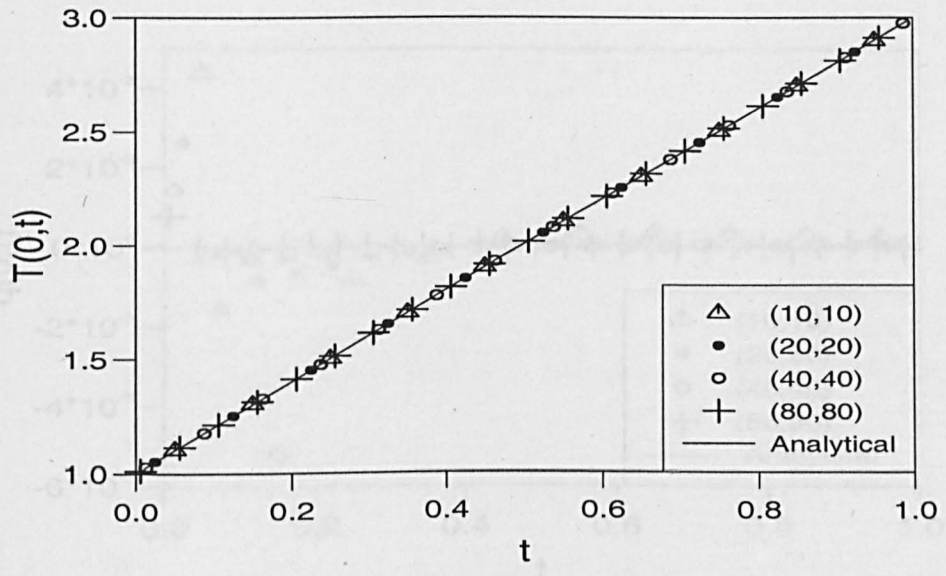

(a)

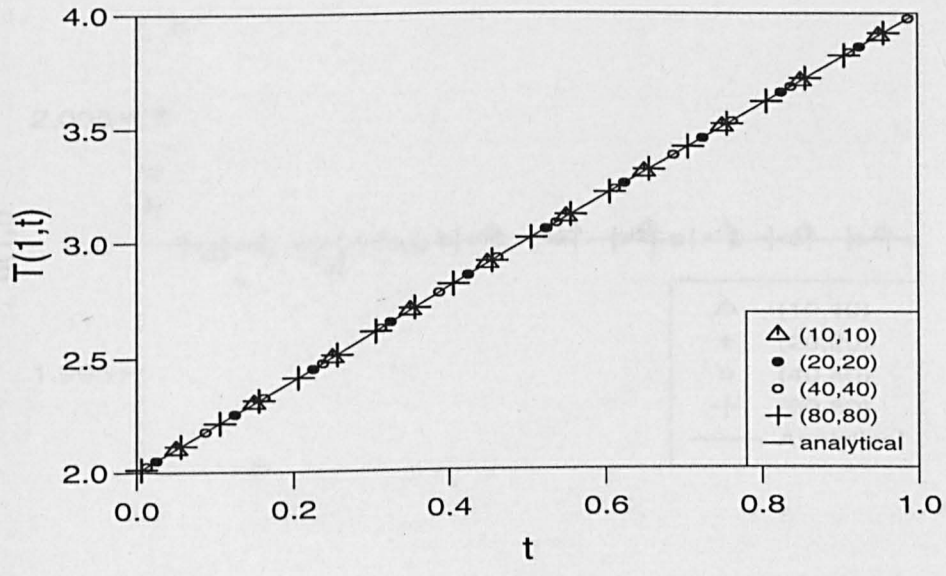

(b)

Figure 3.1: The (—) analytical and numerical boundary temperatures (a) $T(0,t)$ and (b) $T(1,t)$, as functions of time t, when (N, N_0) increases from (10,10) to (80,80), no noise.

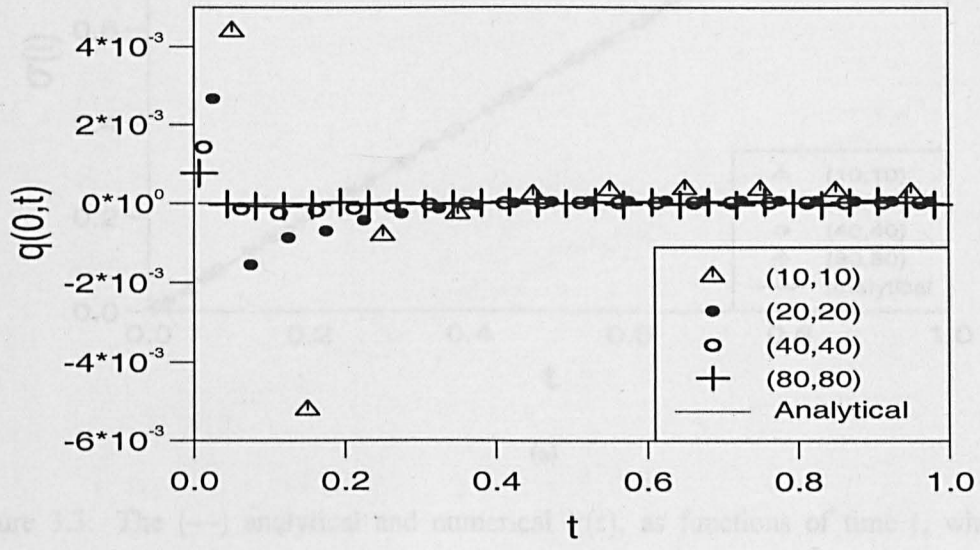

(a)

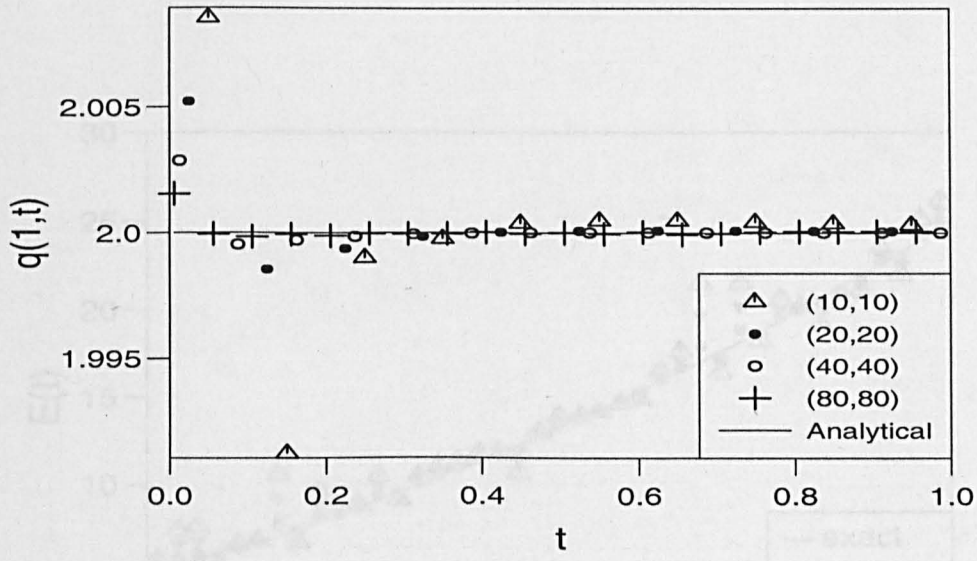

(b)

Figure 3.2: The (—) analytical and numerical heat fluxes (a) $q(0,t)$ and (a) $q(1,t)$, as functions of time t, when (N, N_0) increases from (10,10) to (80,80), no noise.

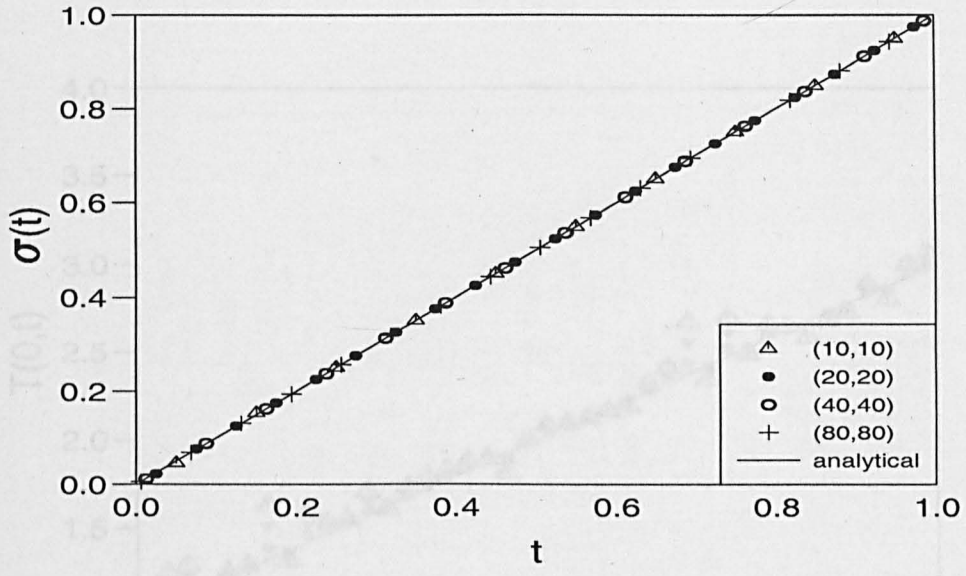

(a)

Figure 3.3: The (—) analytical and numerical $\sigma(t)$, as functions of time t, when (N, N_0) increases from (10,10) to (80,80), no noise.

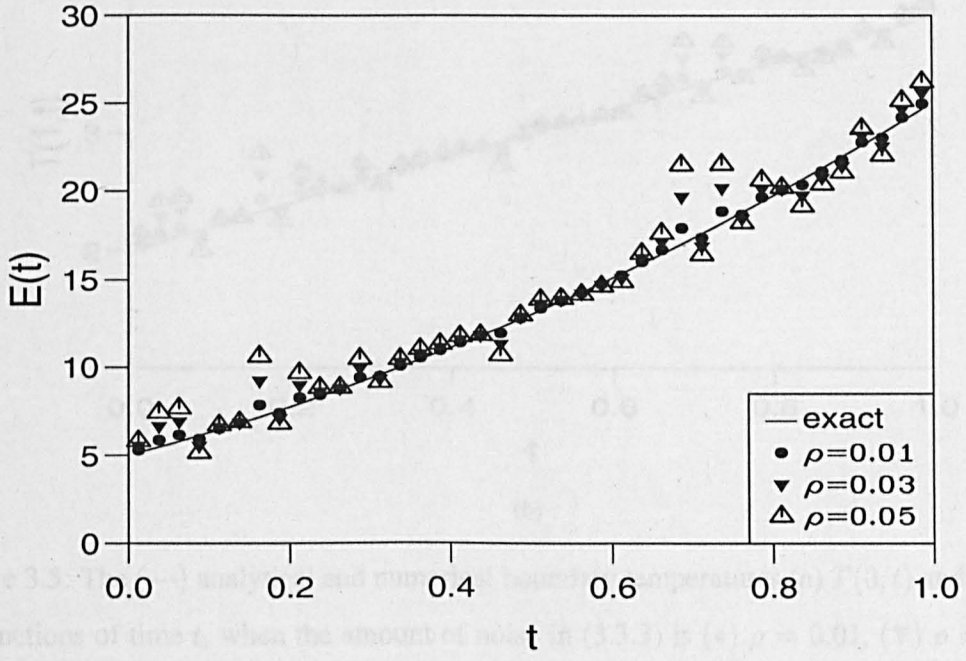

Figure 3.4: The (—) analytical and numerical measured function $E(t)$, as functions of time t, when the amount of noise in (3.3.3) is (•) $\rho = 0.01$, (▼) $\rho = 0.03$, and (△) $\rho = 0.05$.

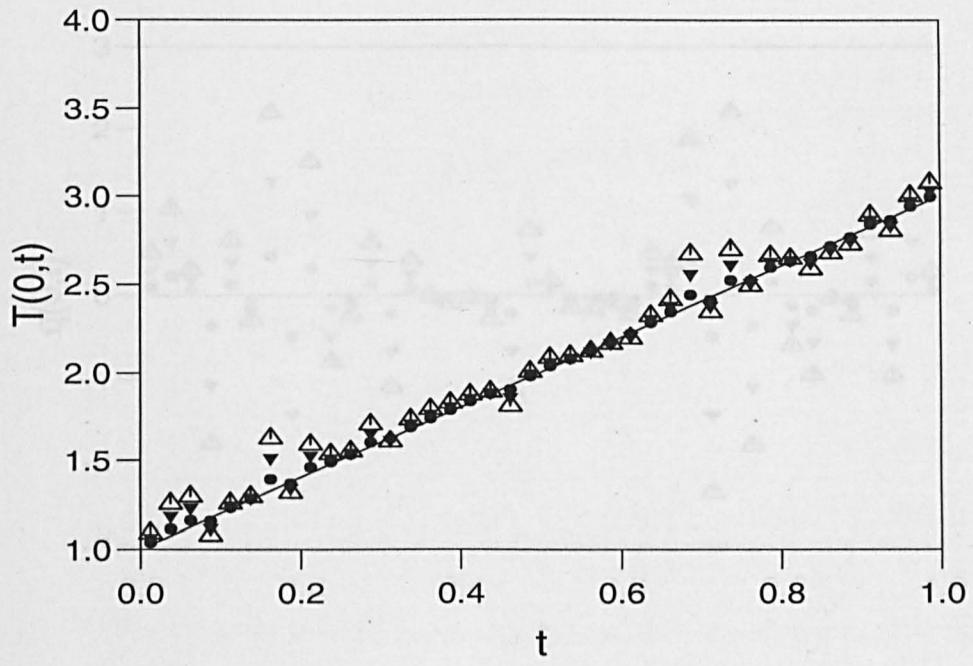

(a)

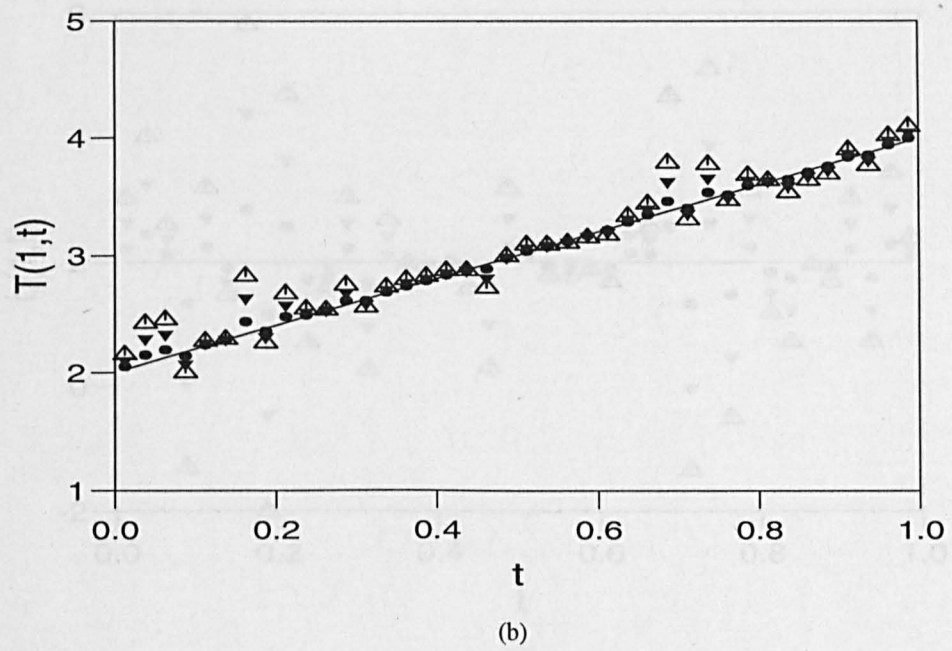

(b)

Figure 3.5: The (—) analytical and numerical boundary temperatures (a) $T(0,t)$ and (b) $T(1,t)$, as functions of time t, when the amount of noise in (3.3.3) is (•) $\rho = 0.01$, (▼) $\rho = 0.03$, and (△) $\rho = 0.05$.

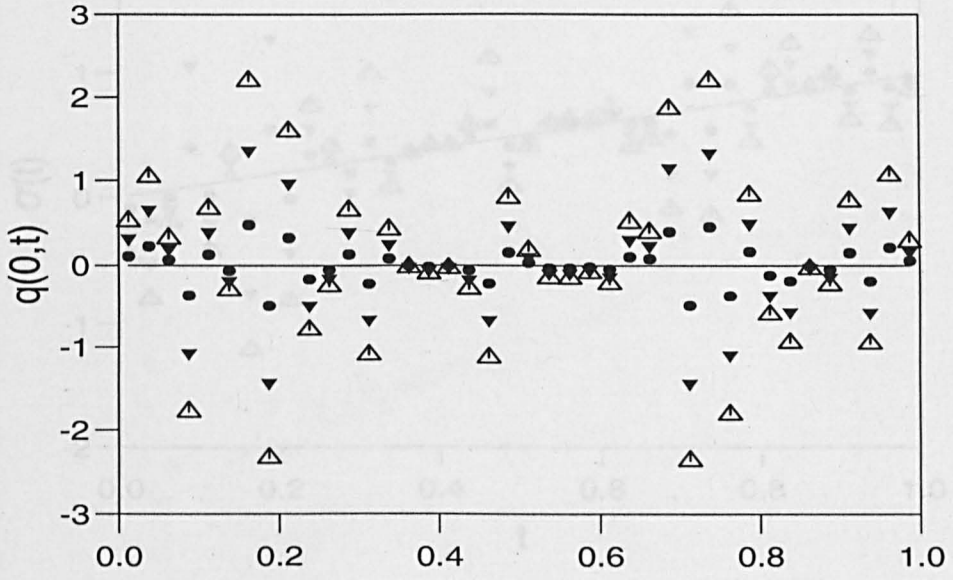

(a)

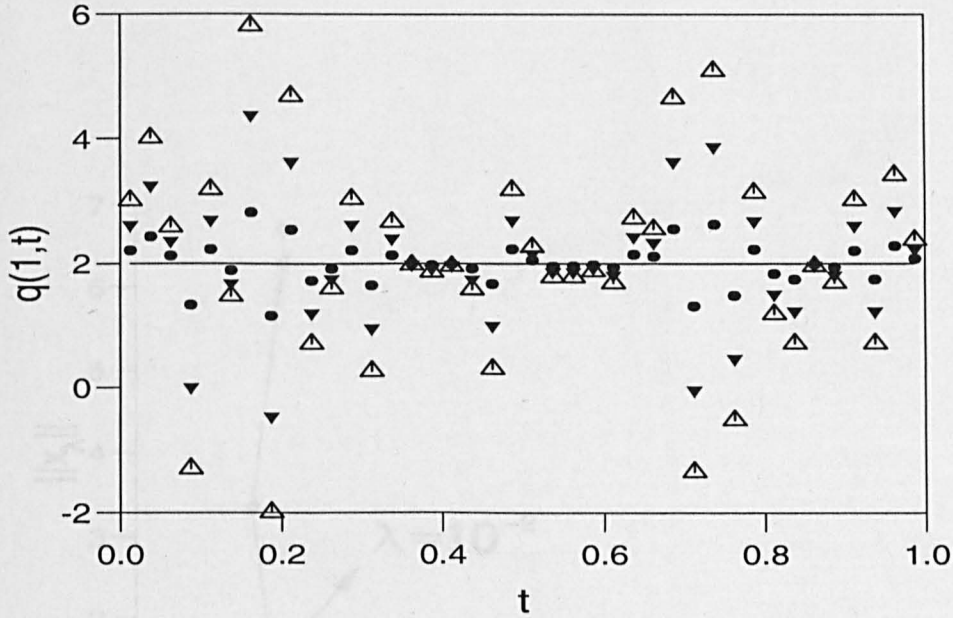

(b)

Figure 3.6: The (—) analytical and numerical heat fluxes (a) $q(0,t)$ and (b) $q(1,t)$, as functions of time t, when the amount of noise in (3.3.3) is (•) $\rho = 0.01$, (▼) $\rho = 0.03$, and (△) $\rho = 0.05$.

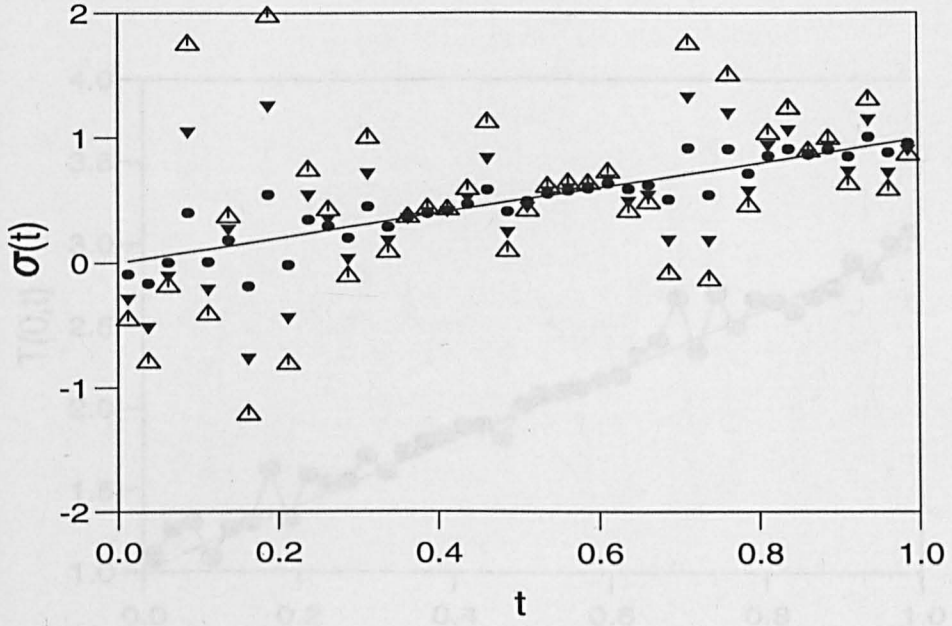

Figure 3.7: The (—) analytical and numerical $\sigma(t)$, as functions of time t, when the amount of noise in (3.3.3) is (•) $\rho = 0.01$, (▼) $\rho = 0.03$, and (△) $\rho = 0.05$.

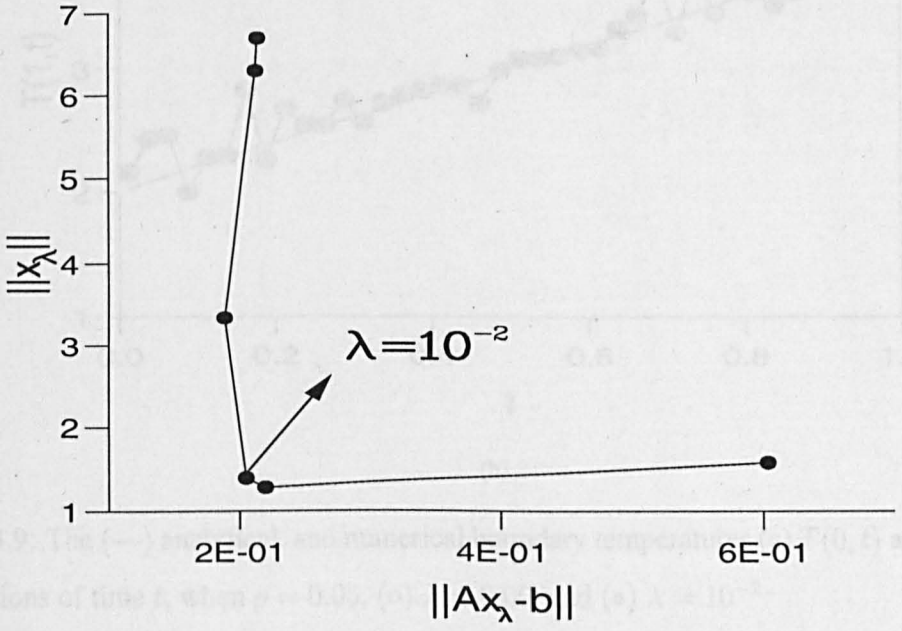

Figure 3.8: The L-curve for the amount of noise $\rho = 0.05$.

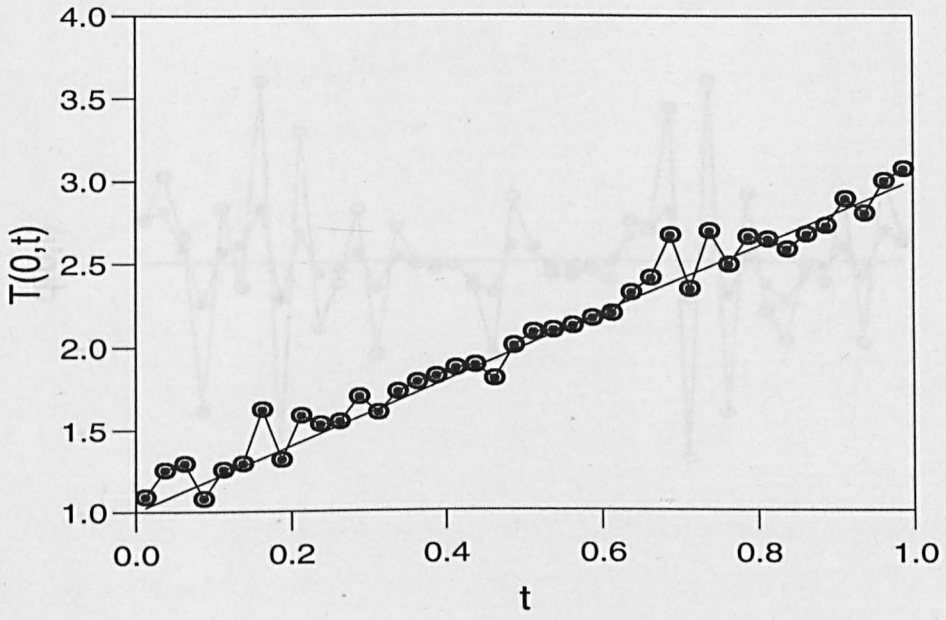

(a)

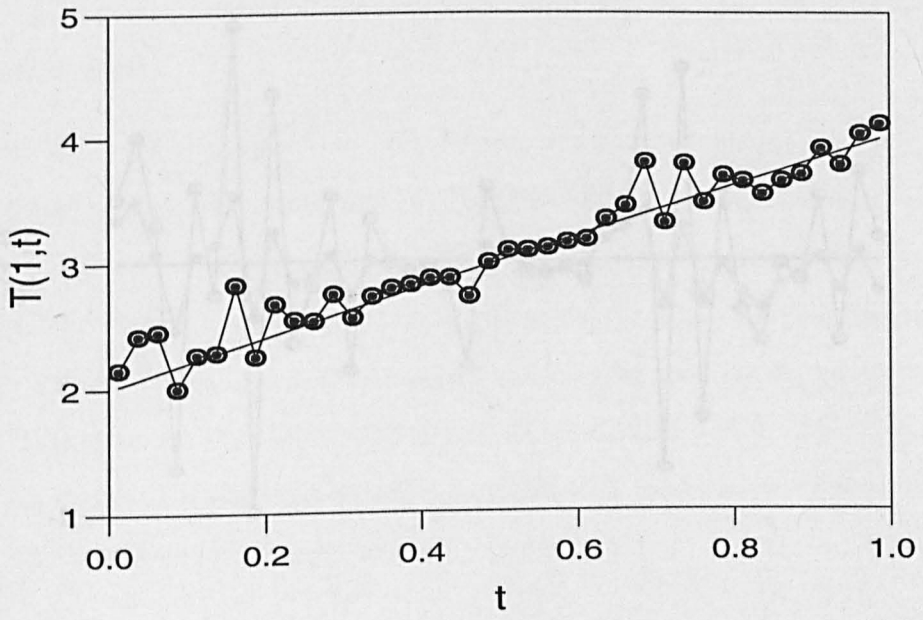

(b)

Figure 3.9: The (—) analytical, and numerical boundary temperatures (a) $T(0,t)$ and (b) $T(1,t)$, as functions of time t, when $\rho = 0.05$, ($\circ$) $\lambda = 0.00$, and ($\bullet$) $\lambda = 10^{-2}$.

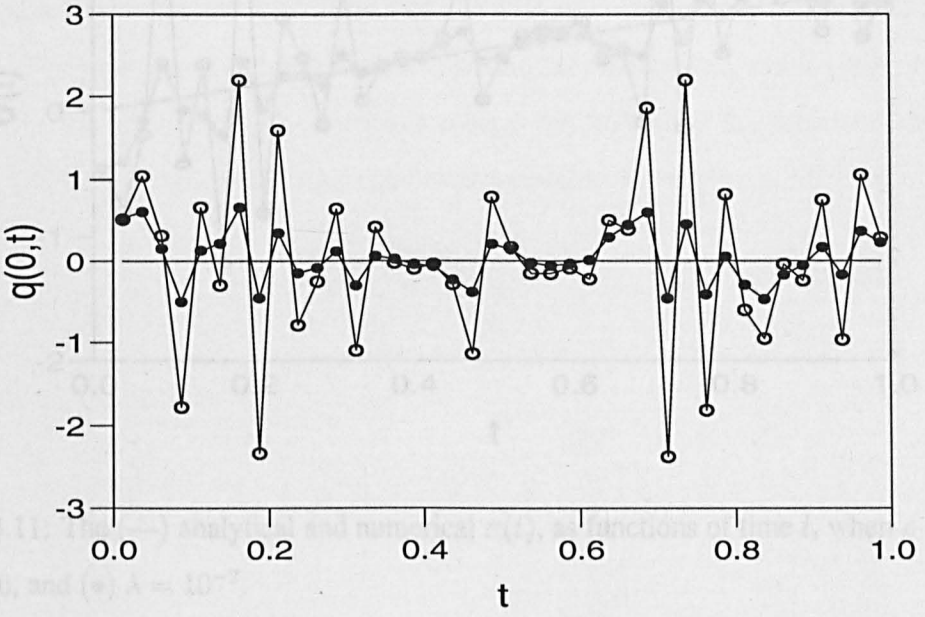

(a)

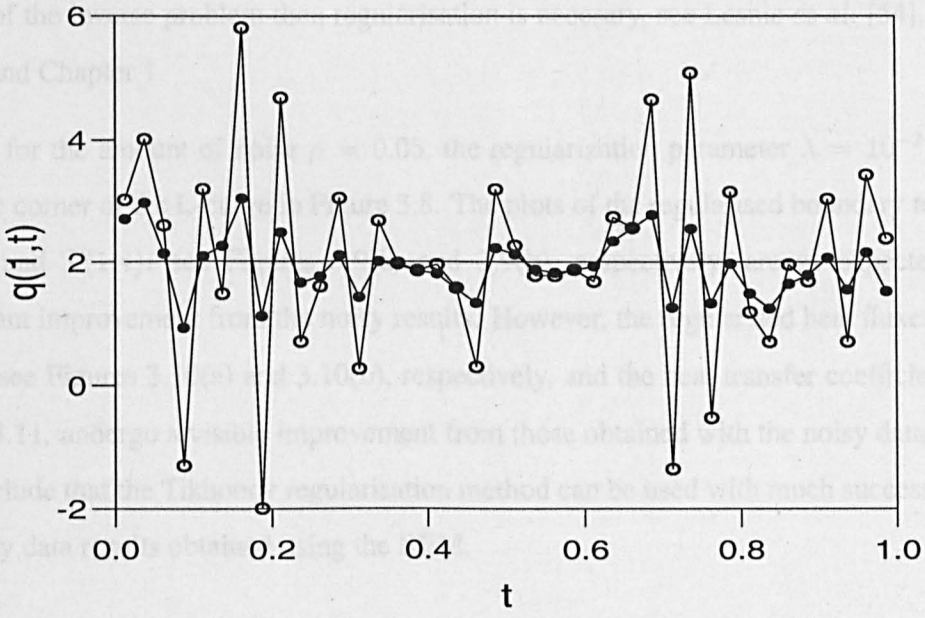

(b)

Figure 3.10: The (—) analytical, and numerical heat fluxes (a) $q(0,t)$ and (d) $q(1,t)$, as functions of time t, when $\rho = 0.05$, (○) $\lambda = 0.00$, and (●) $\lambda = 10^{-2}$.

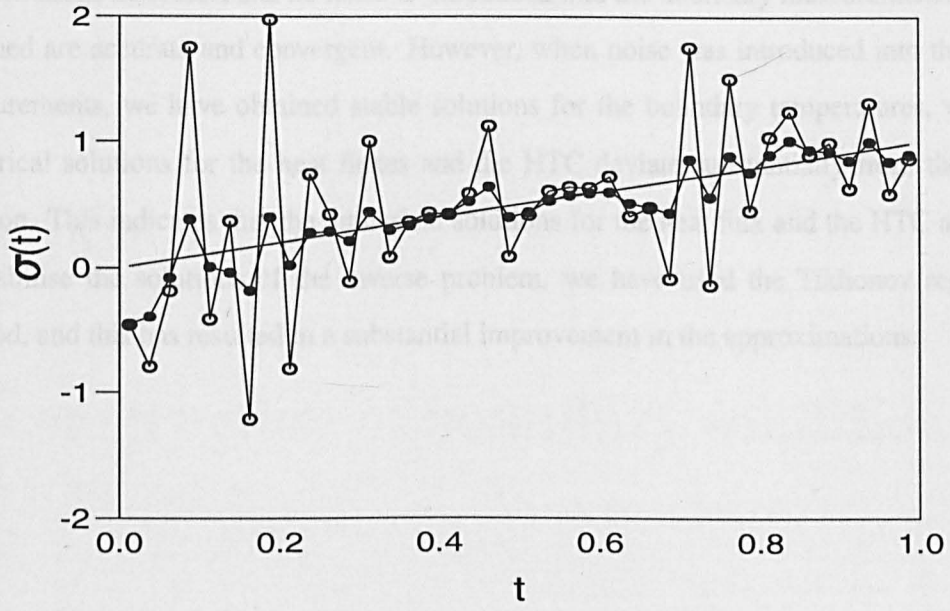

Figure 3.11: The (—) analytical and numerical $\sigma(t)$, as functions of time t, when $\rho = 0.05$, ($\circ$) $\lambda = 0.00$, and ($\bullet$) $\lambda = 10^{-2}$.

increased to $\rho = 0.05$, are divegent and unstable. This indicates that in order to improve the results of the inverse problem then regularisation is necesary, see Lesnic *et al.* [54], Bialecki *et al.* [9] and Chapter 1.

Finally, for the amount of noise $\rho = 0.05$, the regularization parameter $\lambda = 10^{-2}$ is obtained from the corner of the L-curve in Figure 3.8. The plots of the regularised boundary temperatures $T(0,t)$ and $T(1,t)$, see Figures 3.9(a) and 3.9(b), respectively, are as expected, with no significant improvement from the noisy results. However, the regularised heat fluxes $q(0,t)$ and $q(1,t)$, see Figures 3.10(a) and 3.10(b), respectively, and the heat transfer coefficient $\sigma(t)$, see Figure 3.11, undergo a visible improvement from those obtained with the noisy data. Therefore, we conclude that the Tikhonov regularisation method can be used with much success to improve the noisy data results obtained using the BEM.

3.5 Conclusions

In this chapter, we have investigated an IHCP with unknown linear boundary conditions. We have used the BEM to construct and solve numerically the missing terms involving the boundary temperatures, heat fluxes, and heat transfer coefficient. In the example, when the number of

discretisations increases, and no noise is introduced into the boundary measurements, the results obtained are accurate and convergent. However, when noise was introduced into the boundary measurements, we have obtained stable solutions for the boundary temperatures, whereas the numerical solutions for the heat fluxes and the HTC deviate substantially from the analytical solution. This indicates that the numerical solutions for the heat flux and the HTC are unstable. To stabilise the solutions of the inverse problem, we have used the Tikhonov regularization method, and this has resulted in a substantial improvement in the approximations.

Chapter 4

Reconstruction of boundary condition laws

4.1 Introduction

An interesting, mathematically challenging and well-investigated problem is the identification of coefficients that appear in partial differential equations, see e.g. Muzylev [62] and Pilant and Rundel [67]. However, the identification of nonlinear boundary conditions is less developed. In one-dimensional transient heat conduction these boundary conditions relate the heat flux at the ends of a rod to the boundary temperature through some unknown function f. For example, if the heat exchange between the rod and its environmental surroundings is solely by convection, then one commonly assumes that f is a linear function of the difference in the temperature between the ends of the rod and that of the surrounding fluid with the slope given by the heat transfer coefficient (Newton's law of cooling). Identifications of a time, space or both space and time dependent heat transfer coefficient in this case have been investigated in, for example, see Chantasiriwan [18], Divo *et al.* [22] and Huang *et al.* [39]. For the case of purely radiative transfer of energy, a fourth-order power law of the temperature for the function f is usual (Stefan's law), see Carslaw and Jaeger [17].

However, there are many practical heat transfer situations at high temperature, or in hostile environments, e.g. combustion chambers, cooling steel processes, gas turbines, etc. in which either the actual method of heat transfer is not known, or it cannot be assumed that the governing boundary laws have such a simple form. For example, in the cooling of hot steel or glass in fluids or gases, the heat transfer coefficient depends on the boundary temperature and this dependence has a complicated and unknown structure, see Rösch [76] and Wolf *et al.* [86]. From a technical

point of view, fast cooling and processes with limited opportunities to accurately measure surface temperatures and/or heat fluxes are of much interest. In such situations one can set up an inverse experiment that would allow the reconstruction (recovery) of the exact form of the function f. It is well-known that the identification of nonlinear boundary conditions is an ill-posed problem, see Rösch [72]. It has been shown elsewhere, see Pilant and Rundell [68], that by monitoring (recording, measuring) the transient temperature at one end of the rod one can recover uniquely the unknown function f. However, even if a solution exists and is unique, it will not depend continuously on the input data. Therefore, in order to stabilize the solution one can employ the Tikhonov regularization method, see Tikhonov and Arsenin [83] and Morozov [61]. It should be noted that for this approach one can also find error estimates of the regularised solutions for nonlinear problems, see Tautenhanh [82] and Tikhonov *et al.* [84].

In this chapter we investigate the application of the BEM with regularization for solving numerically the inverse problem of boundary condition law identification in heat conduction.

4.2 Mathematical formulation of the Inverse Problem

We consider the initial boundary value problem

$$\frac{\partial T}{\partial t}(x,t) = \frac{\partial^2 T}{\partial x^2}(x,t), \qquad (x,t) \in (0,1) \times (0,t_f], \tag{4.2.1}$$

$$T(x,0) = g(x), \qquad x \in (0,1), \tag{4.2.2}$$

$$\frac{\partial T}{\partial n}(0,t) = -\frac{\partial T}{\partial x}(0,t) = f(T(0,t)), \qquad t \in [0,t_f], \tag{4.2.3}$$

$$\frac{\partial T}{\partial n}(1,t) = \frac{\partial T}{\partial x}(1,t) = f(T(1,t)), \qquad t \in [0,t_f], \tag{4.2.4}$$

$$T(0,t) = h(t), \qquad t \in [0,t_f], \tag{4.2.5}$$

where T represents the unknown temperature in the one-dimensional rod (0,1), the function f represents the unknown law for the boundary condition, $t_f > 0$ is an arbitrary final time of interest, $\mathbf{n}$ is the outward unit normal, g is the given initial temperature, h is the additional measured boundary temperature, and, for simplicity, we have assumed that there are no heat sources. For certain conditions on f, the direct problem (4.2.1)–(4.2.4) is well-posed, see Rösch [75]. Moreover, the Fréchet differentiability of the solution T of the direct problem (4.2.1)–(4.2.4) with respect to f has been established in Rösch [74]. The compatibility

conditions associated with (4.2.2)–(4.2.5) require $-g'(0) = f(g(0))$, $g'(1) = f(g(1))$, $g(0) = h(0)$.

For the inverse problem (4.2.1)–(4.2.5) we assume that:

(i) $g \in C^{2+1/2}([0,1])$.

(ii) $h \in C^{1+1/2}([0,t_f])$ is strictly monotone and $h(0) = g(0)$.

(iii) $T(1,t;f) \in [h(0),h(t)]$ for all $t \in [0,t_f]$,

where $T(x,t;f)$ is the solution of the direct mixed problem (4.2.1), (4.2.2), (4.2.4) and (4.2.5) when f known. Solvability results for this latter direct problem are given in Friedman [30]. At this stage, it is worth mentioning that a related inverse problem replaces the boundary conditions (4.2.3) and (4.2.4) by

$$\frac{\partial T}{\partial n}(x,t) = f(T(x,t)) = \alpha(T(x,t))\,(T_{\text{ext}} - T(x,t))\,, \qquad x \in \{0,1\}\,, \tag{4.2.6}$$

where T_{ext} is the constant temperature of the surrounding fluid medium, and the heat exchange function $\alpha(T(x,t))$ is an unknown nonlinear function, which has to be identified by means of measurements of the temperature T. The measurements can be available in the whole time interval $(0,t_f]$ and the whole space domain $(0,1)$, or on a subdomain $(a,b) \subset (0,1)$, see Rösch and Tröltzsch [71] and Rösch [72], or on the boundary $\{0,1\}$, see Rösch [73, 74]. In these papers, stability estimates of the inverse problem are given. It should be noted that boundary conditions of the type (4.2.6) occur in many physical situations, e.g. in the cooling of hot steel in water, see Kaiser and Tröltzsch [46], in the concentration of gaseous diffusion with chemical reaction at the surface, or in the population density with a specific migration law at the boundary.

It is worth noting that for condition (iii), one cannot guarantee that the range of temperatures on the boundary $x = 1$ is contained in the range of temperature measured data (4.2.5) by giving conditions on the data g and h alone, since condition (iii) depends on the unknown function f. However, from the maximum principle for the heat equation, see Protter and Weinberger [69], there are easily obtainable conditions under which condition (iii) can be enforced. For example, if it is known *a priori* that $f \leq 0$, and if $g(0) = g(1)$, then it is easy to give conditions under which h will be a decreasing function of time t and

$$h(t) = T(0,t) \leq T(1,t) \leq T(1,0) = g(1) = g(0) = h(0) \tag{4.2.7}$$

for all $t \geq 0$. Also if $f(T) < 0$ for $T > 0$ with $f(0) = 0$, then $T(x,t) \to 0$ as $t \to \infty$ for all x, and thus both $T(0,t) = h(t)$ and $T(1,t)$ will be contained in the interval $(0, g(0))$ for all $t > 0$.

Under the assumptions (i)–(iii), we have the following local solvability result, see Pilant and Rundell [68].

Theorem 4.2.1 *Under the assumptions (i)–(iii), there exists a unique solution* $(T, f) \in C^{2,1}((0,1) \times [0,t^*]) \times C^{1/2}([0,t^*])$ *of the problem* (4.2.1)–(4.2.5) *for some* $t^* \in (0, t_f]$.

Several factors may allow us to extend this theorem to global solvability. If the admissible (allowable) class of functions f is restricted to uniformly Lipschitz functions C^{0+1}, this will be the case. Also if f is restricted to be non-positive, i.e. $f \leq 0$, with $f(0) = 0$, then there will be heat loss from the rod for all $t > 0$, and the maximum principle shows that $|T(x,t)|$ remains uniformly bounded by $||g||_\infty$. These two cases encompass many problems of physical interest.

4.2.1 Related problems

Several other inverse problems can be formulated. For example, the boundary conditions (4.2.3) and (4.2.4) can take the more general form

$$\frac{\partial T}{\partial n}(0,t) = -\frac{\partial T}{\partial x}(0,t) = \alpha_0(t) f(T(0,t)) + \beta_0(t), \qquad t \in [0,t_f], \tag{4.2.8}$$

$$\frac{\partial T}{\partial n}(1,t) = \frac{\partial T}{\partial x}(1,t) = \alpha_1(t) f(T(1,t)) + \beta_1(t), \qquad t \in [0,t_f], \tag{4.2.9}$$

where α_0, α_0, β_0 and β_1 are known functions of time, t.

We can also consider cases when T, or $\frac{\partial T}{\partial n}$, is prescribed at $x = 1$, e.g.

$$\frac{\partial T}{\partial n}(1,t) = \frac{\partial T}{\partial x}(1,t) = q_1(t), \qquad t \in [0,t_f], \tag{4.2.10}$$

instead of employing condition (4.2.4). In this case, the solution of the problem (4.2.1)–(4.2.3), (4.2.5) and (4.2.10) can be determined immediately. To see this, note that there exists a unique solution T of the problem (4.2.1), (4.2.2), (4.2.5) and (4.2.10), and (4.2.3) yields

$$-\frac{\partial T}{\partial x}(0,t) = f(h(t)), \qquad t \in [0,t_f]. \tag{4.2.11}$$

If h is strictly monotone, from (4.2.11) we obtain

$$f(\xi) = -\frac{\partial T}{\partial x}(0, h^{-1}(\xi)), \qquad \xi \in [h(0), h(t_f)]. \tag{4.2.12}$$

If instead of (4.2.4) we prescribe

$$\frac{\partial T}{\partial n}(0,t) = -\frac{\partial T}{\partial x}(0,t) = q_0(t), \qquad t \in [0,t_f], \tag{4.2.13}$$

then the Cauchy problem (4.2.1), (4.2.2), (4.2.5) and (4.2.13) will admit at most one solution pair (T, f), but existence can only be guaranteed by making extremely restrictive (and difficult to ensure) conditions on the data. Even if this can be done, continuous dependence of the solution on the data cannot be expected in any reasonable norm, see Cannon [14].

4.3 The BEM

Using the BEM, and applying the initial and boundary conditions (4.2.2)-(4.2.4), we obtain the integral representation,

$$\eta(x)T(x,t) = \int_0^t \left[G(x,t;\xi,\tau)f(T(\xi,\tau)) - T(\xi,\tau)\frac{\partial G}{\partial n(\xi)}(x,t;\xi,\tau)\right]_{\xi\in\{0,1\}} \mathrm{d}\tau + \int_0^1 g(y)G(x,t;y,0)\mathrm{d}y, \qquad (x,t) \in [0,1]\times(0,t_f]. \tag{4.3.1}$$

Applying (4.3.1) at the boundaries $x = 0$ and $x = 1$, and using (4.2.5), we obtain two nonlinear boundary integral equations in the unknowns f and $T(1,t)$, namely

$$\frac{1}{2}h(t) = \int_0^t \left[G(0,t;0,\tau)f(h(\tau)) + G(0,t;1,\tau)f(T(1,\tau)) - h(\tau)\frac{\partial G}{\partial n(0)}(0,t;0,\tau) - T(1,\tau)\frac{\partial G}{\partial n(1)}(0,t;1,\tau)\right]\mathrm{d}\tau + \int_0^1 g(y)G(0,t;y,0)\mathrm{d}y, \qquad t\in(0,t_f], \tag{4.3.2}$$

$$\frac{1}{2}T(1,t) = \int_0^t \left[G(1,t;0,\tau)f(h(\tau)) + G(1,t;1,\tau)f(T(1,\tau)) - h(\tau)\frac{\partial G}{\partial n(0)}(1,t;0,\tau) - T(1,\tau)\frac{\partial G}{\partial n(1)}(1,t;1,\tau)\right]\mathrm{d}\tau + \int_0^1 g(y)G(1,t;y,0)\mathrm{d}y, \qquad t\in(0,t_f], \tag{4.3.3}$$

where

$$\frac{\partial G}{\partial n(\xi)}(x,t;\xi,\tau) = \frac{(x-\xi)n(\xi)H(t-\tau)}{4\sqrt{\pi(t-\tau)^3}}\exp\left[-\frac{(x-\xi)^2}{4(t-\tau)}\right], \tag{4.3.4}$$

$n(0) = -1$ and $n(1) = 1$.

On discretizing the boundary integral equations (4.3.2) and (4.3.3), and using the piecewise constant boundary element approximations (1.3.23) and (1.3.28), result in a nonlinear system of $2N$ equations which, in a generic form, can be written as

$$A_f(\mathbf{T}_1) = \mathbf{b}, \tag{4.3.5}$$

where the vector $\mathbf{b}$ contains expressions of the known data g and h, and A_f is a nonlinear operator associated to the unknown function f.

4.4 Numerical Examples of DHCP, Results and Discussion

First we investigate the BEM for solving direct nonlinear heat conduction problems (DHCP) given by equations (4.2.1), (4.2.2), (4.2.8) and (4.2.9), when f is a given function of T. Applying (4.3.1) at the boundaries $x = 0$ and $x = 1$, we obtain two nonlinear boundary integral equations in the unknowns $T(0,t)$ and $T(1,t)$, namely

$$\begin{aligned}\frac{1}{2}T(x,t) = &\int_0^t [G(x,t;0,\tau)f(T(0,\tau)) + G(x,t;1,\tau)f(T(1,\tau))]\,\mathrm{d}\tau \\ &- \int_0^t \left[T(0,\tau)\frac{\partial G}{\partial n(0)}(x,t;0,\tau) + T(1,\tau)\frac{\partial G}{\partial n(1)}(x,t;1,\tau)\right]\mathrm{d}\tau \qquad (4.4.1) \\ &+ \int_0^1 g(y)G(x,t;y,0)\mathrm{d}y, \qquad t \in (0,t_f],\end{aligned}$$

for $x = 0$ and $x = 1$.

On discretizing equation (4.4.1), and using the piecewise constant BEM approximations (1.3.24) and (1.3.25), results in a nonlinear system of $2N$ equations which, in generic form, can be written as

$$A(\mathbf{T}_0, \mathbf{T}_1) = \mathbf{b}. \qquad (4.4.2)$$

We solve this system of nonlinear equations using the NAG routine C05NCF. The initial guess was taken as $(\mathbf{T}_0, \mathbf{T}_1) = (\mathbf{0}, \mathbf{0})$. Earlier chapter investigations on the effect of increasing the number of space cells N_0 indicated that $N_0 = 40$ produced good numerical approximations for linear DHCPs which agreed well with the analytical solutions. Therefore, in all the Examples 4.1–4.3 presented in this section the number of space cells is kept fixed at $N_0 = 40$, whilst the number of time boundary elements N is gradually varied from $N = 10, 20, 40, 80$ to 160.

4.4.1 Linear Direct Problem

Example 4.1

In order to illustrate the technique employed, in this example we solve a linear DHCP given by the heat equation (4.2.1) in the domain $Q = (0,1) \times (0, t_f = 1]$, subject to the initial condition (4.2.2) given as

$$T(x,0) = g(x) = \sin\left(\frac{\pi}{4}(x - \frac{1}{2})\right), \qquad x \in [0,1], \qquad (4.4.3)$$

and the boundary conditions (4.2.3) and (4.2.4) given as

$$\frac{\partial T}{\partial n}(0,t) = \frac{\pi}{4}\cot(\pi/8)T(0,t), \qquad t \in (0,1], \qquad (4.4.4)$$

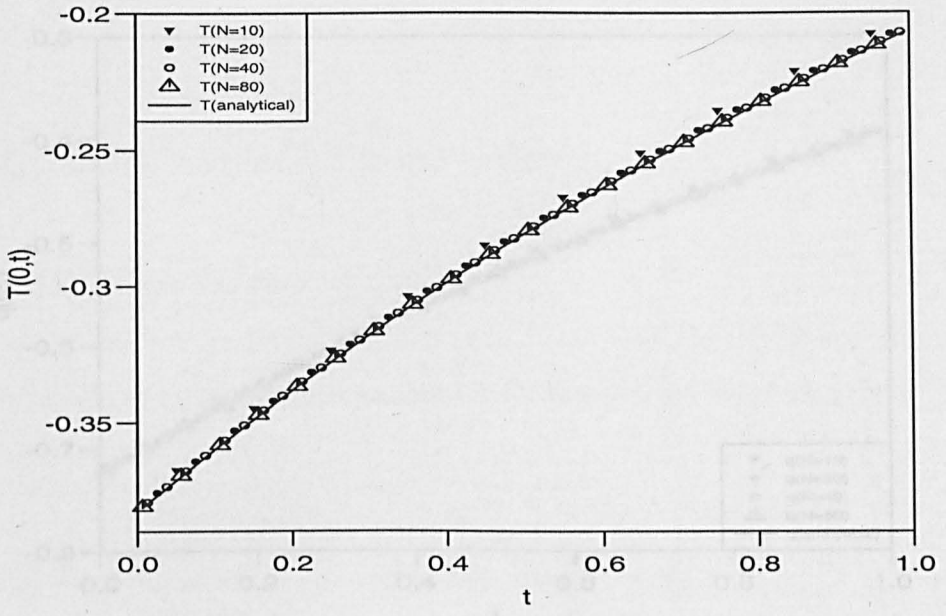

(a)

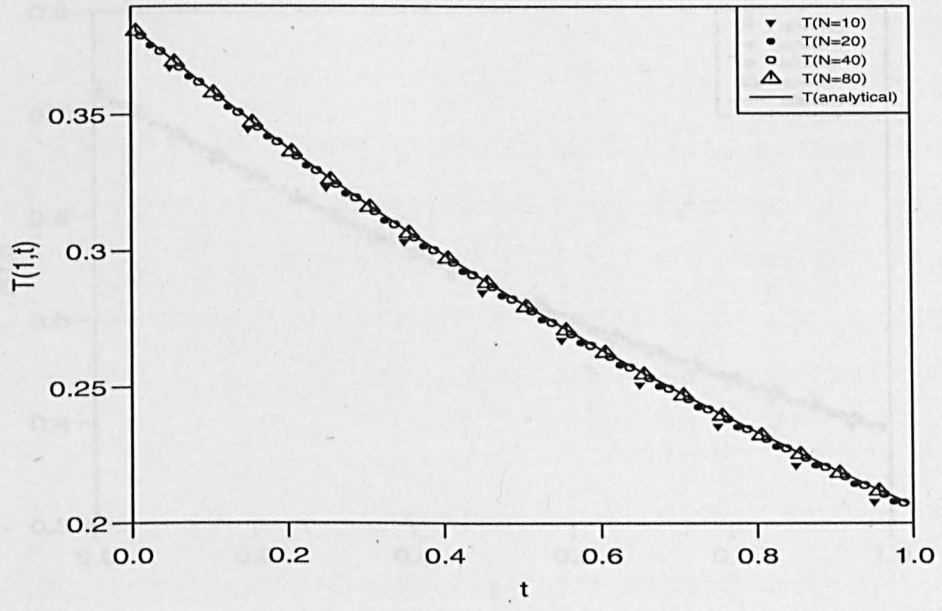

(b)

Figure 4.1: The analytical and numerical boundary temperatures (a) $T(0,t)$, and (b) $T(1,t)$, as functions of time t, for the linear DHCP given by Example 4.1, for various N.

$$\frac{\partial T}{\partial n}(1,t) = \frac{\pi}{4}\cot(\pi/8)T(1,t), \qquad t \in (0,1], \tag{4.4.5}$$

such that $f(T) = \frac{\pi}{4}\cot(\pi/8)T$ is a linear function of T.

This problem has the analytical solution

$$T(x,t) = \sin\left(\frac{\pi}{4}(x-\frac{1}{2})\right)\exp(-\frac{\pi^2}{16}t). \tag{4.4.6}$$

For this example, Figures 4.1(a) and (b) represent the boundary temperatures, and Figures 4.2(a)

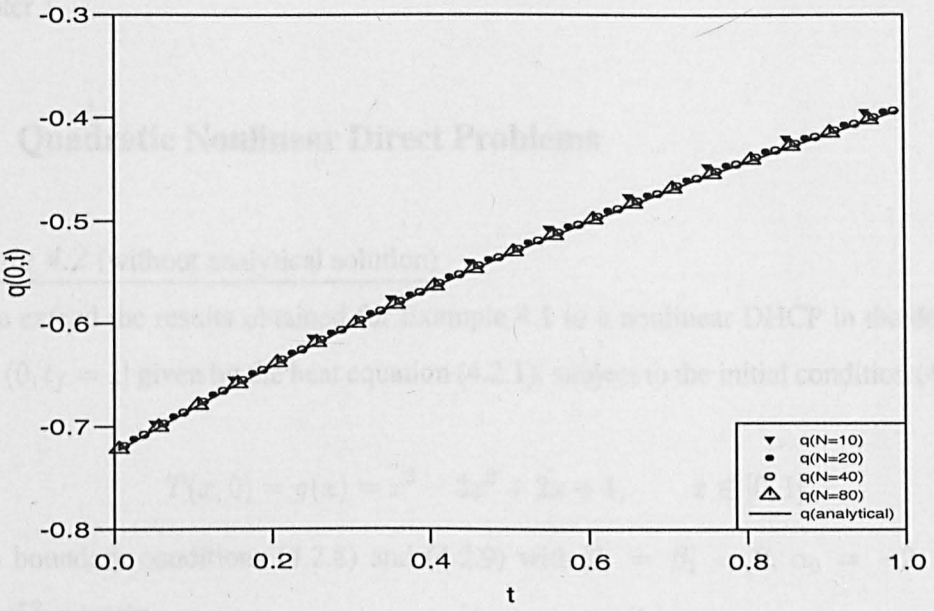

(a)

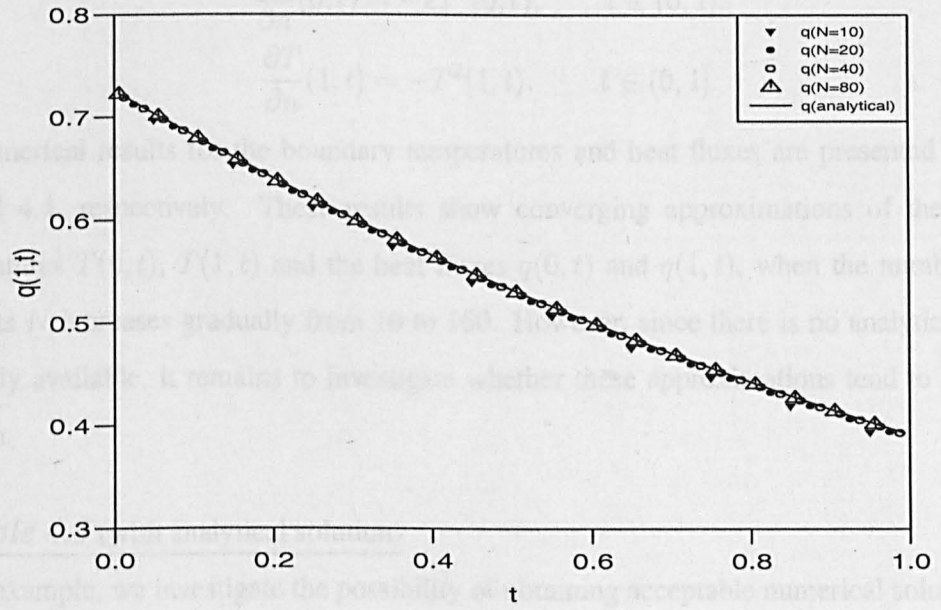

(b)

Figure 4.2: The analytical and numerical heat fluxes (a) $q(0,t)$, and (b) $q(1,t)$, as functions of time t, for the linear DHCP given by Example 4.1, for various N.

and (b) the heat fluxes, where (a) and (b) are on the boundaries $x = 0$ and $x = 1$, respectively. From these figures it can be seen that an increase in the number of time elements from 10 to 40 reveals rapid convergence to the analytical solution, such that when $(N, N_0) = (40, 40)$ we find numerical approximations of both boundary temperature and heat flux that compare well with the corresponding analytical solutions obtained from (4.4.6). Therefore, we conclude that the

BEM provides a reliable numerical approximation for linear DHCPs, as also has been obtained in Chapter 1.

4.4.2 Quadratic Nonlinear Direct Problems

Example 4.2 (without analytical solution)

Now we extend the results obtained for Example 4.1 to a nonlinear DHCP in the domain $Q = (0,1) \times (0, t_f = 1]$ given by the heat equation (4.2.1), subject to the initial condition (4.2.2) given as

$$T(x,0) = g(x) = x^3 - 3x^2 + 2x + 1, \qquad x \in [0,1], \tag{4.4.7}$$

and the boundary conditions (4.2.8) and (4.2.9) with $\beta_0 = \beta_1 = 0$, $\alpha_0 = -2$, $\alpha_1 = -1$, $f(T) = T^2$, namely

$$\frac{\partial T}{\partial n}(0,t) = -2T^2(0,t), \qquad t \in (0,1], \tag{4.4.8}$$

$$\frac{\partial T}{\partial n}(1,t) = -T^2(1,t), \qquad t \in (0,1]. \tag{4.4.9}$$

The numerical results for the boundary temperatures and heat fluxes are presented in Figures 4.3 and 4.4, respectively. These results show converging approximations of the boundary temperatures $T(0,t)$, $T(1,t)$ and the heat fluxes $q(0,t)$ and $q(1,t)$, when the number of time elements N increases gradually from 10 to 160. However, since there is no analytical solution explicitly available, it remains to investigate whether these approximations tend to the correct solution.

Example 4.3 (with analytical solution)

In this example, we investigate the possibility of obtaining acceptable numerical solutions using the BEM to a DHCP, similar to the problem tested in Example 4.2. We consider the nonlinear DHCP in the domain $Q = (0,1) \times (0, t_f = 1]$ given by the heat equation (4.2.1), subject to the initial condition (4.2.2) given as

$$T(x,0) = g(x) = x^2, \qquad x \in [0,1], \tag{4.4.10}$$

and the boundary conditions (4.2.8) and (4.2.9) with $\alpha_0 = \alpha_1 = -1$, $\beta_0(t) = 4t^2$, $\beta_1(t) = 2 + (1+2t)^2$, $f(T) = T^2$, namely

$$\frac{\partial T}{\partial n}(0,t) = -T^2(0,t) + 4t^2, \qquad t \in (0,1], \tag{4.4.11}$$

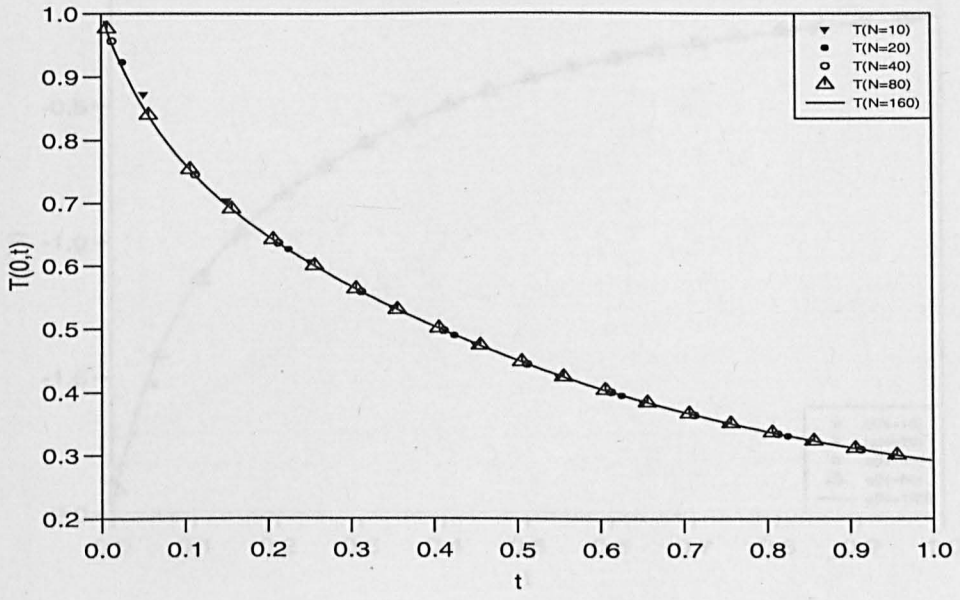

(a)

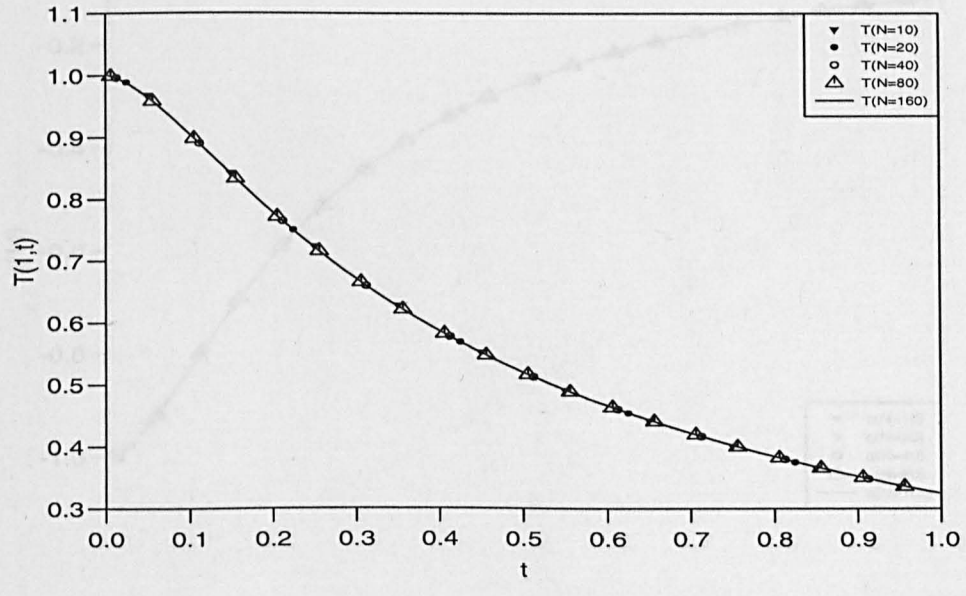

(b)

Figure 4.3: The numerical boundary temperatures (a) $T(0,t)$, and (b) $T(1,t)$, as functions of time t, for the nonlinear DHCP given by Example 4.2, for various N.

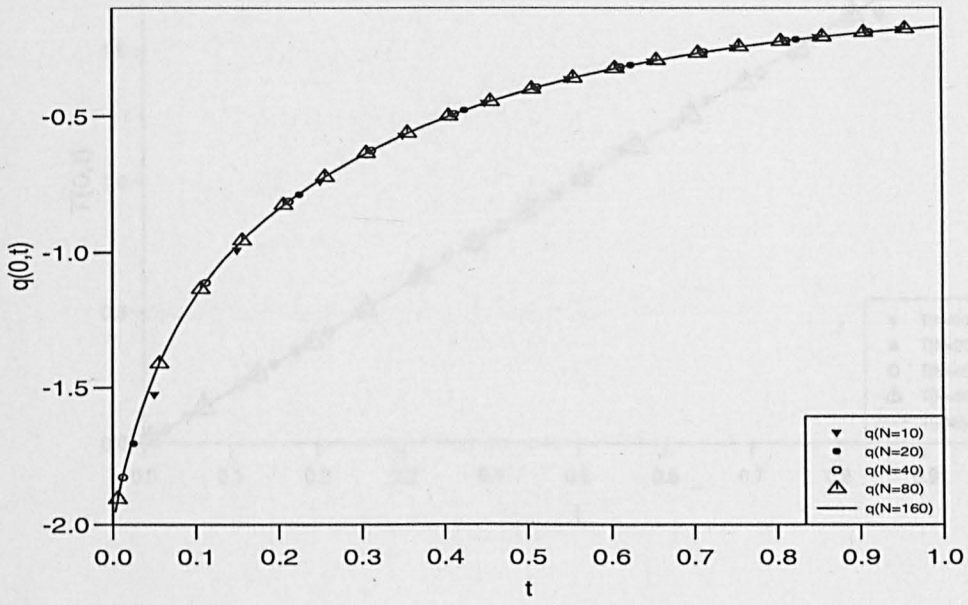

(a)

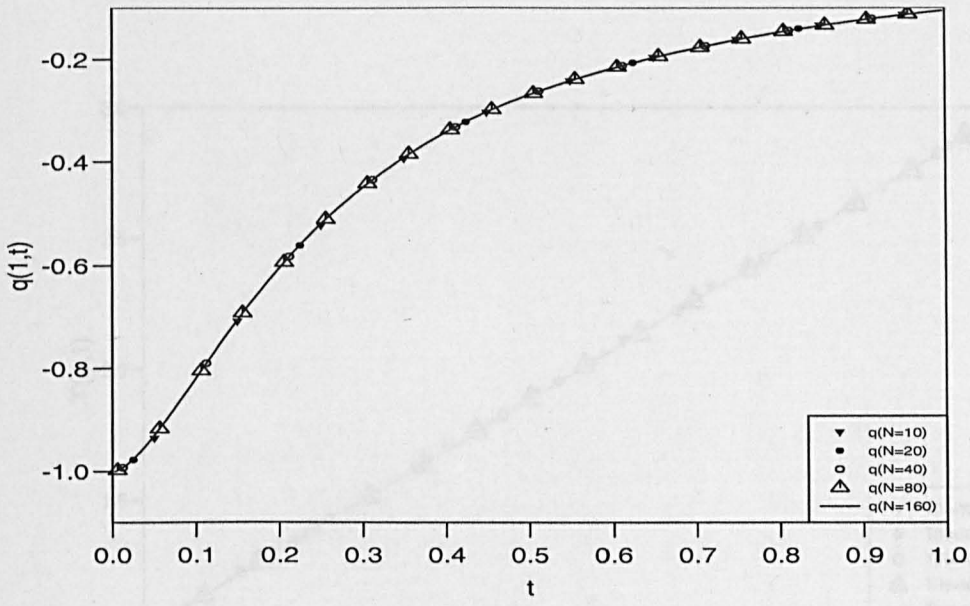

(b)

Figure 4.4: The numerical heat fluxes (a) $q(0,t)$, and (b) $q(1,t)$, as functions of time t, for the nonlinear DHCP given by Example 4.2, for various N.

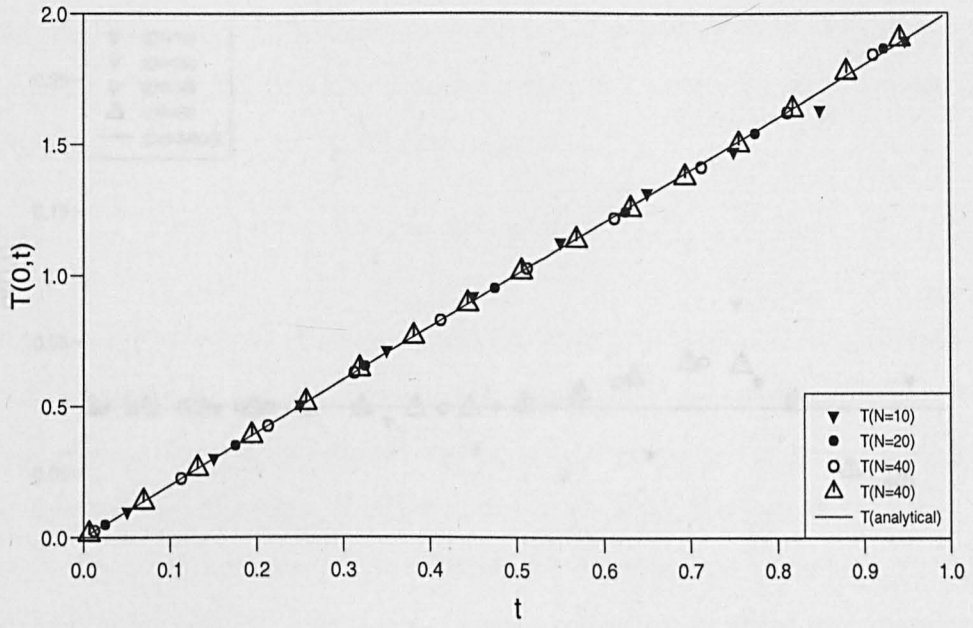

(a)

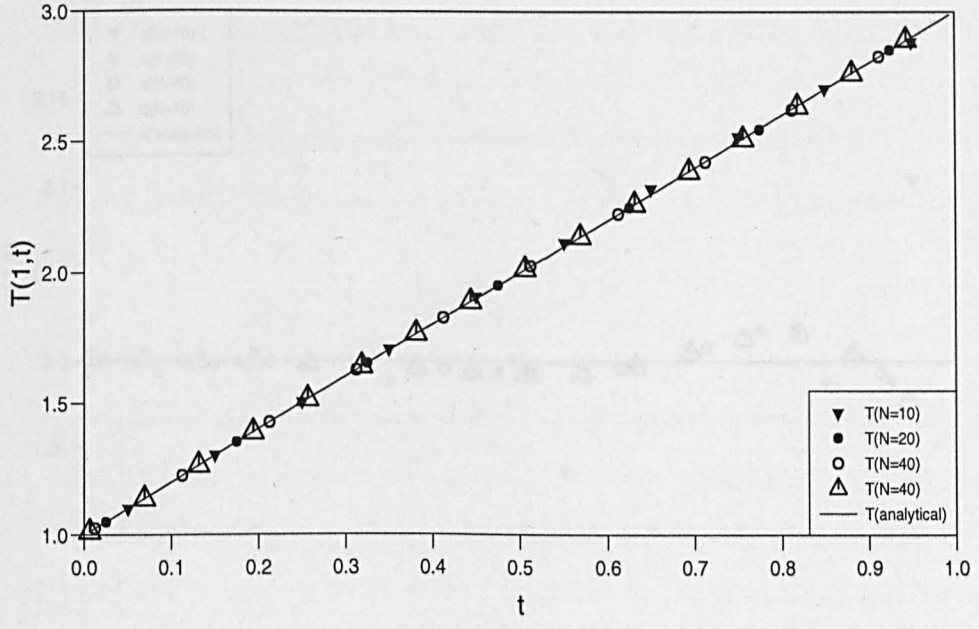

(b)

Figure 4.5: The analytical and numerical boundary temperatures (a) $T(0,t)$, and (b) $T(1,t)$, as functions of time t, for the nonlinear DHCP given by Example 4.3, for various N.

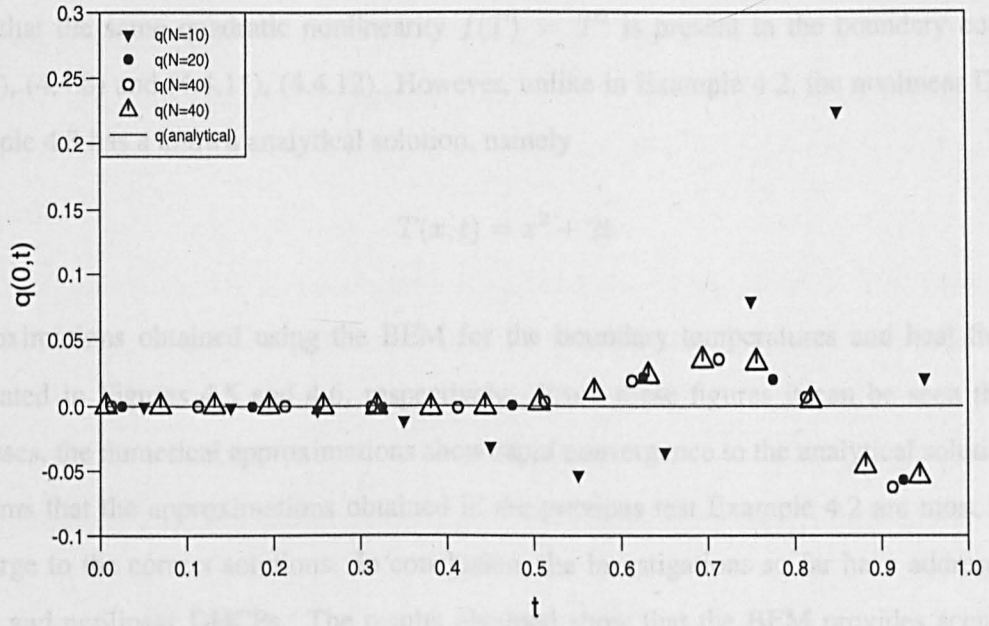

(a)

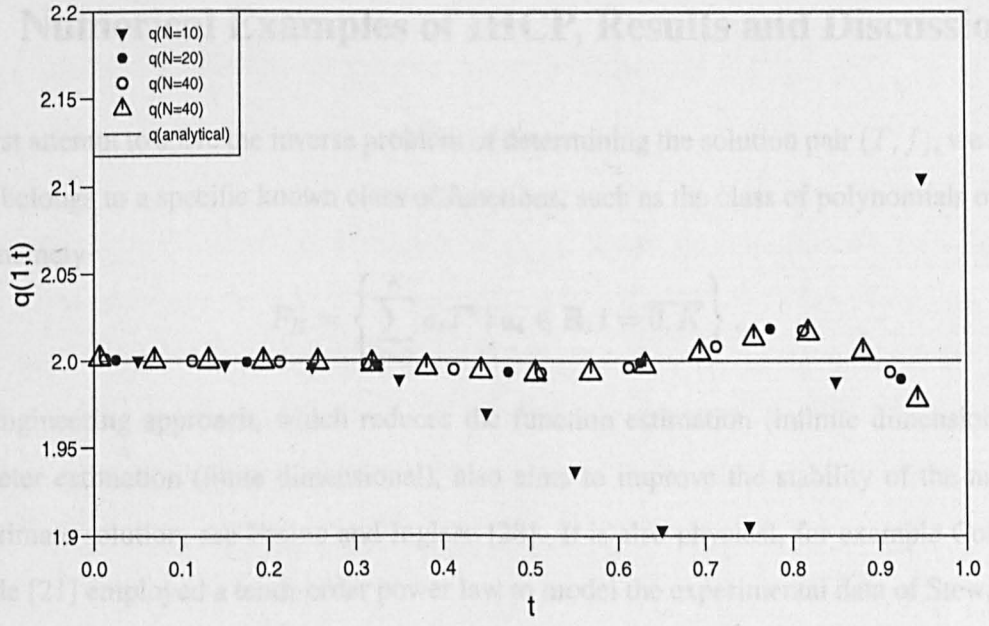

(b)

Figure 4.6: The analytical and numerical heat fluxes (a) $q(0,t)$, and (b) $q(1,t)$, as functions of time t, for the nonlinear DHCP given by Example 4.3, for various N.

$$\frac{\partial T}{\partial n}(1,t) = -T^2(1,t) + 2 + (1+2t)^2, \qquad t \in (0,1]. \tag{4.4.12}$$

Note that the same quadratic nonlinearity $f(T) = T^2$ is present in the boundary conditions (4.4.7), (4.4.8) and (4.4.11), (4.4.12). However, unlike in Example 4.2, the nonlinear DHCP in Example 4.3 has a known analytical solution, namely

$$T(x,t) = x^2 + 2t. \tag{4.4.13}$$

Approximations obtained using the BEM for the boundary temperatures and heat fluxes are illustrated in Figures 4.5 and 4.6, respectively. From these figures it can be seen that as N increases, the numerical approximations show rapid convergence to the analytical solution. This confirms that the approximations obtained in the previous test Example 4.2 are most likely to converge to the correct solutions. In conclusion, the investigations so far have addressed both linear and nonlinear DHCPs. The results obtained show that the BEM provides accurate and convergent numerical approximations. In the next subsection we apply the BEM to inverse boundary condition law identification problems.

4.5 Numerical Examples of IHCP, Results and Discussion

In a first attempt to solve the inverse problem of determining the solution pair (T, f), we suppose that f belongs to a specific known class of functions, such as the class of polynomials of degree $\leq K$, namely

$$P_K = \left\{ \sum_{i=0}^{K} a_i T^i \mid a_i \in \mathbb{R}, i = \overline{0,K} \right\}. \tag{4.5.1}$$

This engineering approach, which reduces the function estimation (infinite dimensional) to a parameter estimation (finite dimensional), also aims to improve the stability of the numerical approximate solution, see Fasino and Inglese [28]. It is also physical, for example Colaco and Orlande [21] employed a tenth-order power law to model the experimental data of Stewart *et al.* [79]. Piecewise polynomial approximations could also be adopted in a future work. Based on (4.3.5), equation (4.5.1) recasts as a nonlinear optimization problem consisting of minimizing the nonlinear least-squares functional

$$S(\mathbf{a}, \mathbf{T}_1) = ||A_f(\mathbf{T}_1) - \mathbf{b}||^2, \tag{4.5.2}$$

where $\mathbf{a} = (a_i)_{i=\overline{0,K}}$ and $f(T) = \sum_{i=0}^{K} a_i T^i$. Alternatively, in a sequential approach, one can first identify a linear boundary condition with a least-squares method at a given time step and then calculate the original nonlinear function at the next time step, see Beck *et al.* [7] and Beck and Murio [8]. If T is given everywhere in $(0,1) \times (0, t_f]$ then one can determine the unknown law directly as an optimal control problem where the nonlinear part plays the part of the control, see Rösch [72].

The minimization of (4.5.1) is performed using the NAG routine E04FCF. The initial guess is taken as $(\mathbf{a}, \mathbf{T}_1) = (\mathbf{0}, \mathbf{0})$. The unknown boundary condition law is sought in the form

$$f(T) = \sum_{k=0}^{K} a_k T^k. \tag{4.5.3}$$

The boundary temperature measurement (4.2.5) is contaminated with additive Gaussian noise as

$$h^{\epsilon}(t) = h(t) + \mu\epsilon \tag{4.5.4}$$

with mean zero and standard deviation $\mu = \rho||h||_{\infty}$ generated using the NAG routine G05DDF, where 100ρ represents the percentage of noise. The number of boundary elements and space cells is increased from $(N, N_0) = (10, 10)$ to (80,80).

4.5.1 Inverse Problem corresponding to Example 4.1

Example 4.4

In many physical situations, at both ends of a rod linear relations between heat fluxes and temperatures occur, i.e. the heat transfer models simply obey Newton's law of cooling. In some cases, this relation is not known in advance and it has to be verified using an inverse analysis. In this example, we investigate the IHCP which corresponds to the DHCP in Example 4.1. Therefore, we solve for T and f given by the heat equation (4.2.1), subject to the initial condition (4.4.3) and the boundary conditions (4.2.8) and (4.2.9) with $\beta_0 = \beta_1 = 0$, $\alpha_0 = \alpha_1 = \frac{\pi}{4}\cot(\pi/8)$, namely

$$\frac{\partial T}{\partial n}(0,t) = \frac{\pi}{4}\cot(\pi/8) f\left(T(0,t)\right), \qquad t \in (0,1], \tag{4.5.5}$$

$$\frac{\partial T}{\partial n}(1,t) = \frac{\pi}{4}\cot(\pi/8) f\left(T(1,t)\right), \qquad t \in (0,1], \tag{4.5.6}$$

and the additional boundary temperature measurement (4.2.5) given by

$$T(0,t) = h(t) = -\sin(\pi/8)\exp(-\frac{\pi^2}{16}t), \qquad t \in (0,1]. \tag{4.5.7}$$

Table 4.1: The coefficients a_k of the function $f(T) = \sum_{k=0}^{K} a_k T^k$ and the objective function S, for various values of (a) (N, N_0), when $K = 1$, (b) $K = \{1, ..., 4\}$, $(N, N_0) = (40, 40)$, no noise, and (c) $\rho = \{0.00, ..., 0.05\}$, when $(N, N_0) = (40, 40)$ and $K = 1$, for the IHCP given by Example 4.4.

(N_0, N)	$10, 10$	$20, 20$	$40, 40$	$80, 80$
$10^6 a_0$	18.3919	6.5265	2.0360	0.6029
a_1	1.0049	1.0015	1.0005	1.0002
S	4.6×10^{-5}	7.7×10^{-6}	1.3×10^{-6}	2.3×10^{-7}

(a)

K	1	2	3	4
a_0	0.0000	0.0087	0.0079	−0.0009
a_1	1.0005	0.9972	0.9978	1.0021
a_2	–	−0.0729	−0.0680	0.0755
a_3	–	–	0.0063	−0.0258
a_4	–	–	–	−0.5523
S	1.3×10^{-8}	2.5×10^{-7}	9.9×10^{-9}	9.7×10^{-9}

(b)

	$\rho = 0.00$	$\rho = 0.01$	$\rho = 0.03$	$\rho = 0.05$
$10^6 a_0$	2.0369	12.5205	33.5043	54.5045
a_1	1.0005	1.0010	1.0020	1.0030
S	1.0×10^{-6}	6.8×10^{-4}	6.2×10^{-3}	1.7×10^{-2}

(c)

The analytical solution of this IHCP is given by equation (4.4.6) for T and $f(T) = T$.

When the degree K of the function $f(T)$ in (4.5.2) is 1, and there is no noise in the data (4.5.3), i.e. $\rho = 0$, as the number of discretizations increases from $(N, N_0) = (10, 10)$ to (80,80), we find that the BEM provides accurate approximations of the temperature $T(1, t)$, in Figure 4.7, and the heat fluxes $q(0, t)$ and $q(1, t)$, in Figures 4.8(a) and (b), respectively. Further, the coefficients $a_0 \approx 0$ and $a_1 \approx 1$ of the function $f(T) = a_0 + a_1 T$ produce small values of the objective function (4.5.2), see Table 4.1(a). Since the function $f(T)$ is analytically linear, $K = 1$ gives a fair and accurate approximation, as is evident when the degree K of the function $f(T)$ increases gradually from 1 to 4, see Table 4.1(b), Figures 4.9 and 4.10, when $(N, N_0) = (40, 40)$ and there is no noise in the measurement (4.5.4). Also, good approximations are obtained if we take K to be 2, 3 and 4, but, as expected, a linear function is best approximated by a linear functional. This is partly because an increase in the order of the approximating functional increases the number of parameters, a fact that unnecessarily introduces instability into the problem.

When $K = 1$, $(N, N_0) = (40, 40)$ and noise is introduced in the measurement (4.5.7) as in (4.5.4), from $\rho = 0.00$ to 0.05, see Figure 4.11(a), the numerical results obtained for the coefficients a_k tabulated in Table 4.1(c), boundary temperature $T(1, t)$, see Figure 4.11(b), and the heat fluxes, see Figure 4.12, undergo an accuracy proportional to the amount of noise ρ

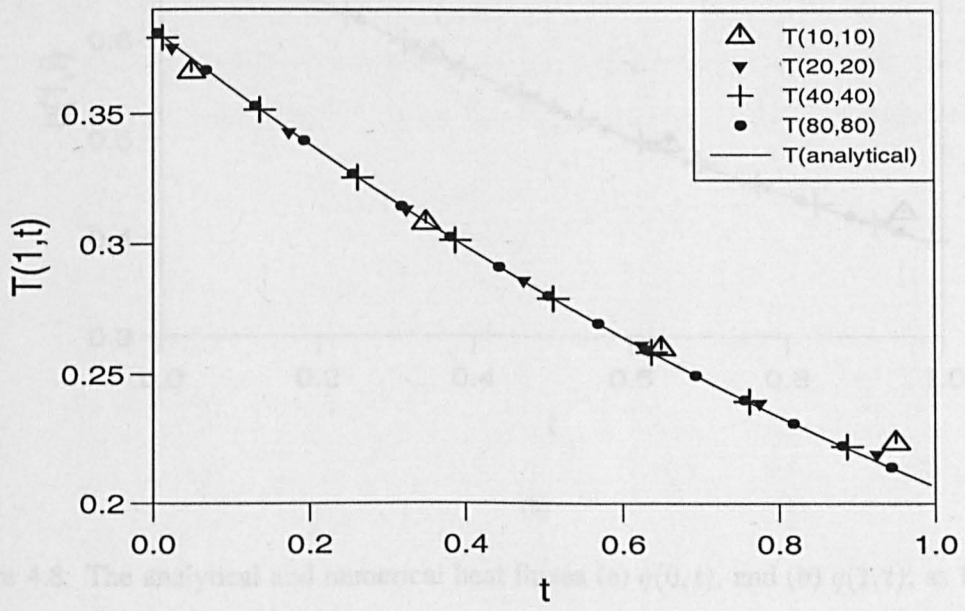

Figure 4.7: The analytical and numerical boundary temperatures $T(1, t)$, for the IHCP given by Example 4.4, as functions of time t, for various (N, N_0), $K = 1$ and no noise.

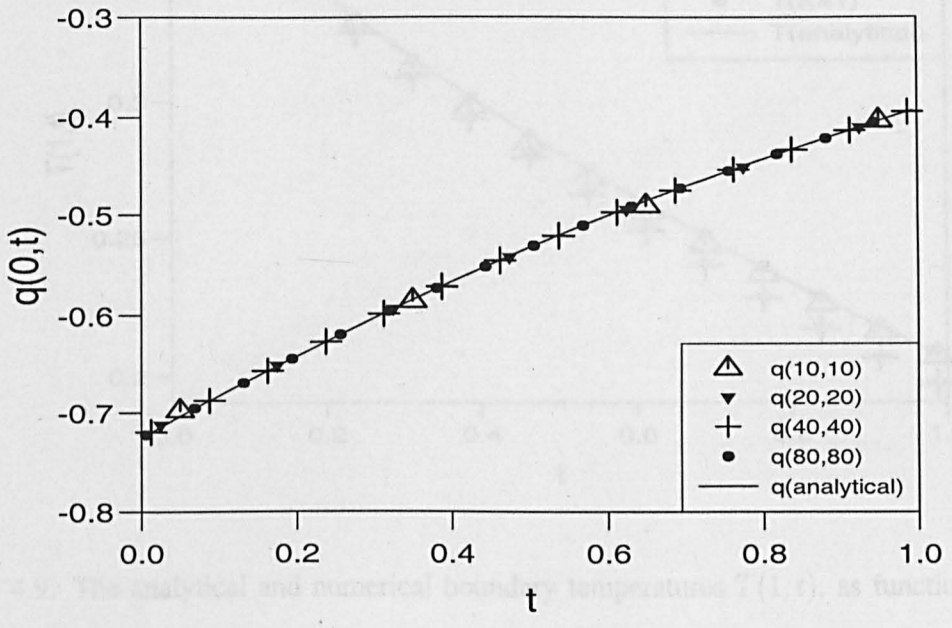

(a)

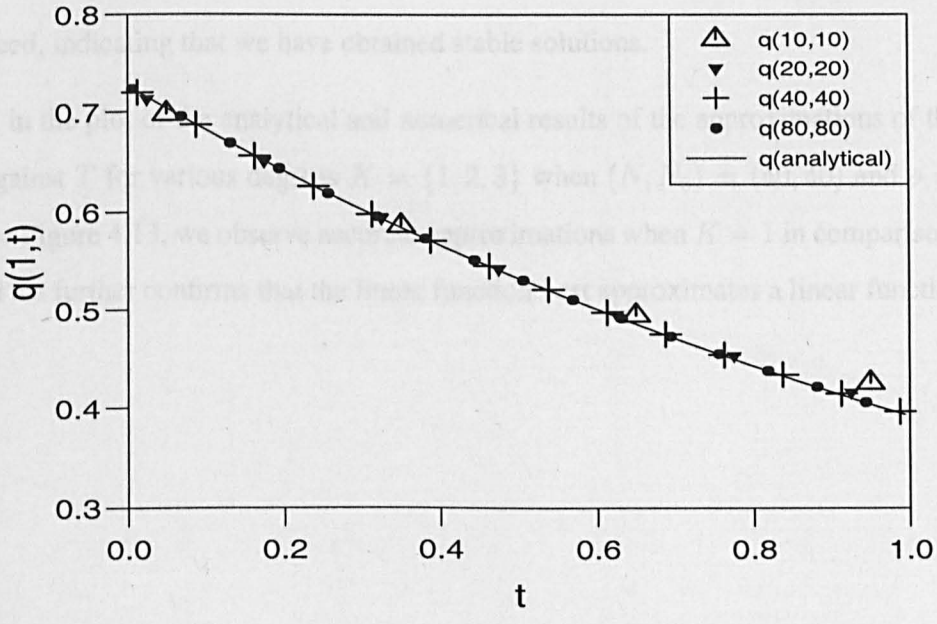

(b)

Figure 4.8: The analytical and numerical heat fluxes (a) $q(0,t)$, and (b) $q(1,t)$, as functions of time t, for the IHCP given by Example 4.4, for various (N, N_0), $K = 1$ and no noise.

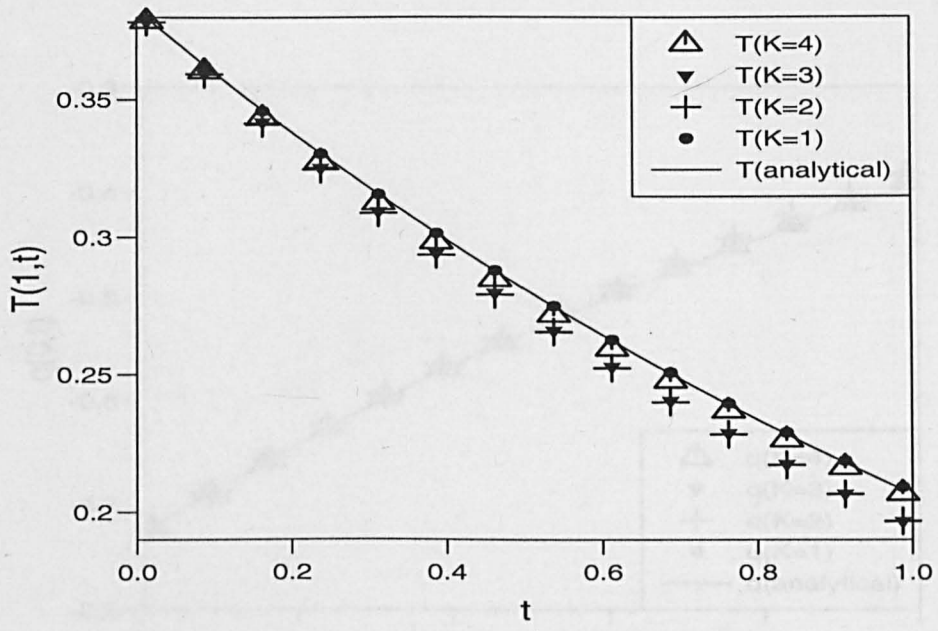

Figure 4.9: The analytical and numerical boundary temperatures $T(1,t)$, as functions of time t, for the IHCP given by Example 4.4, for various $K = \{1, ..., 4\}$, when (N, N_0)=(40, 40), no noise.

introduced, indicating that we have obtained stable solutions.

Finally, in the plot of the analytical and numerical results of the approximations of the function $f(T)$ against T for various degrees $K = \{1, 2, 3\}$ when $(N, N_0) = (40, 40)$ and $\rho = 0.00$ and 0.01, see Figure 4.13, we observe accurate approximations when $K = 1$ in comparison to $K = 2$ and 3. This further confirms that the linear function best approximates a linear functional.

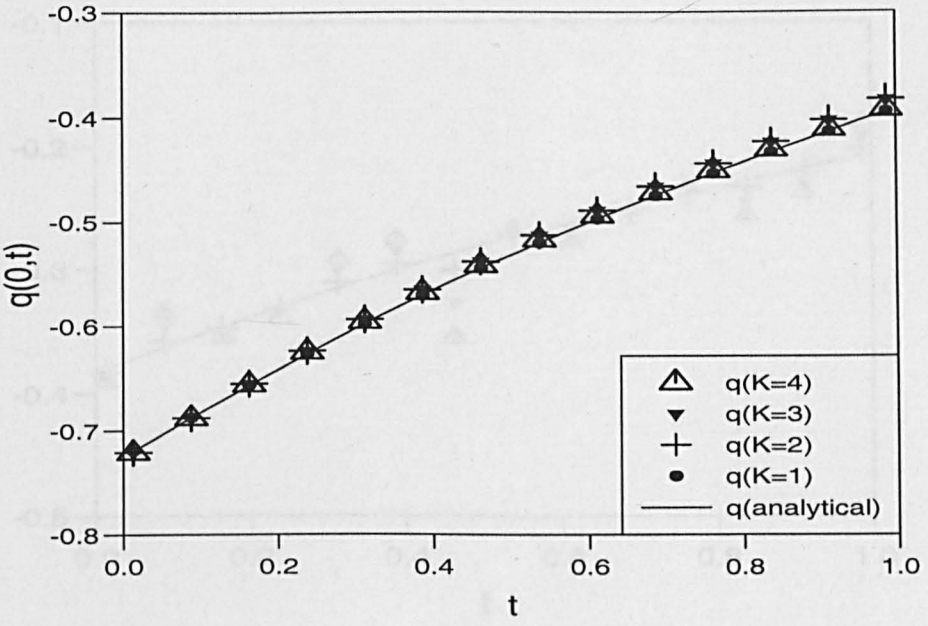

(a)

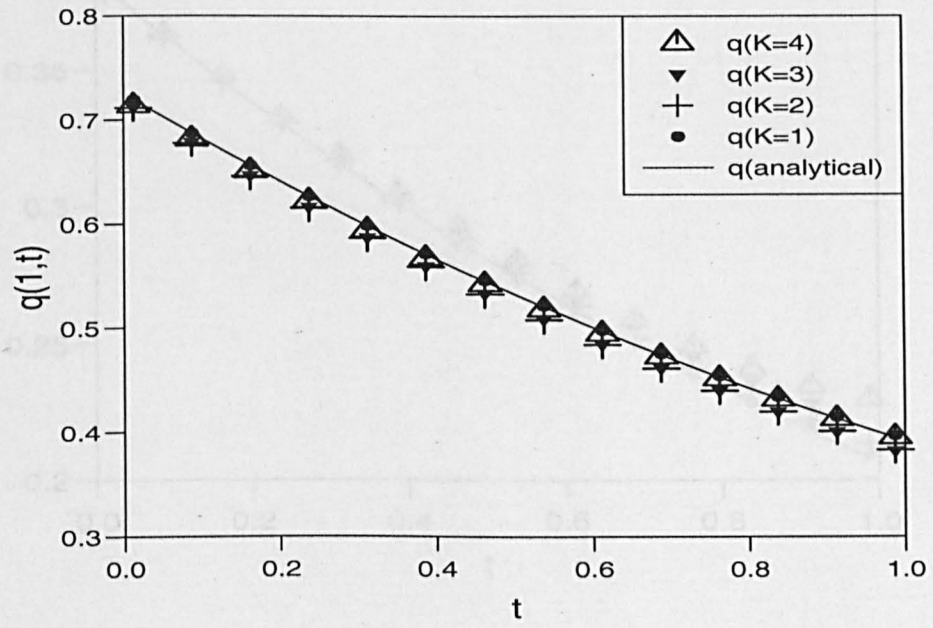

(b)

Figure 4.10: The analytical and numerical heat fluxes (a) $q(0,t)$ and (b) $q(1,t)$, as functions of time t, for the IHCP given by Example 4.4, for various degrees $K = \{1, ..., 4\}$ of the function $f(T)$, when $(N, N_0) = (40, 40)$, no noise.

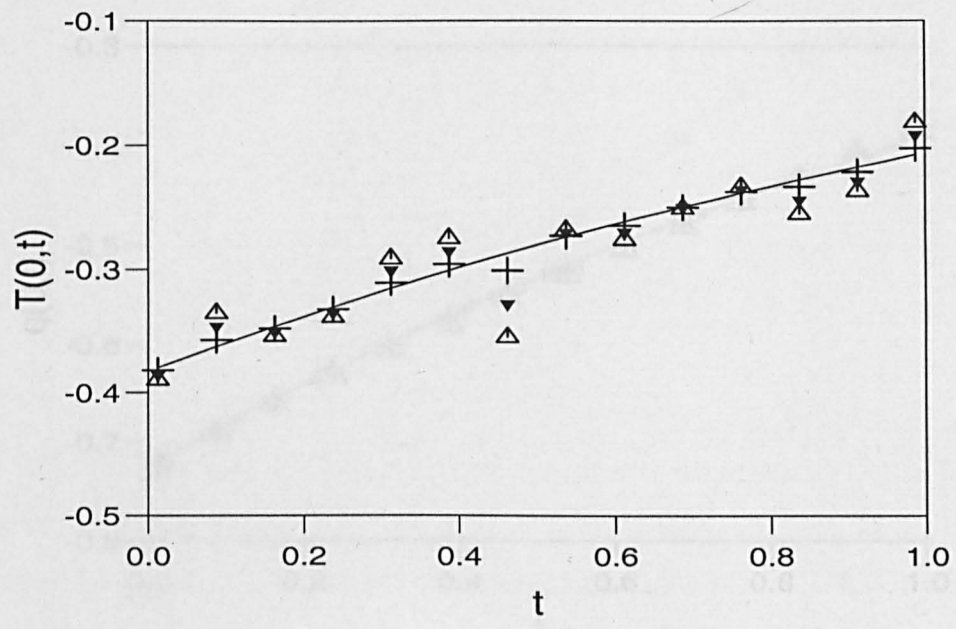

(a)

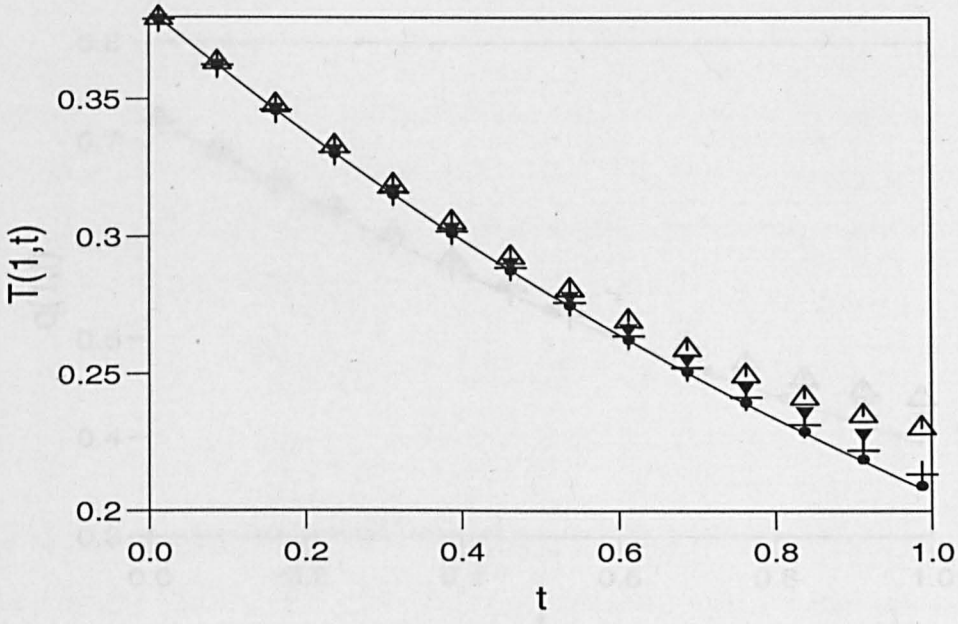

(b)

Figure 4.11: The (—) analytical and numerical boundary temperatures (a) $T(0,t)$, and (b) $T(1,t)$, as functions of time t, for various amounts of noise (•) $\rho = 0.00$, (+) $\rho = 0.01$, (▼) $\rho = 0.03$ and (△) $\rho = 0.05$, for the linear IHCP given by Example 4.4, for $(N, N_0) = (40, 40)$, $K = 1$.

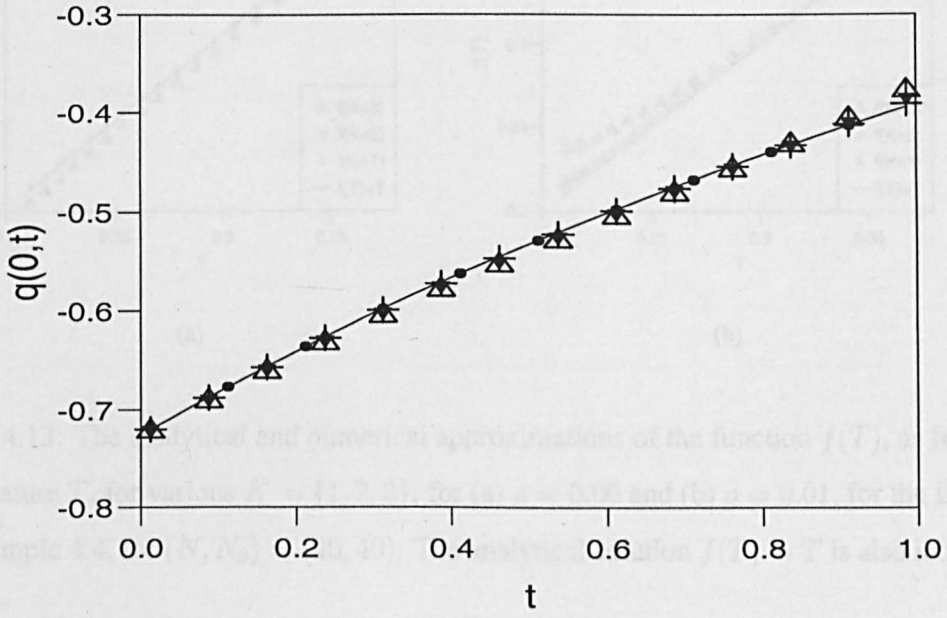

(a)

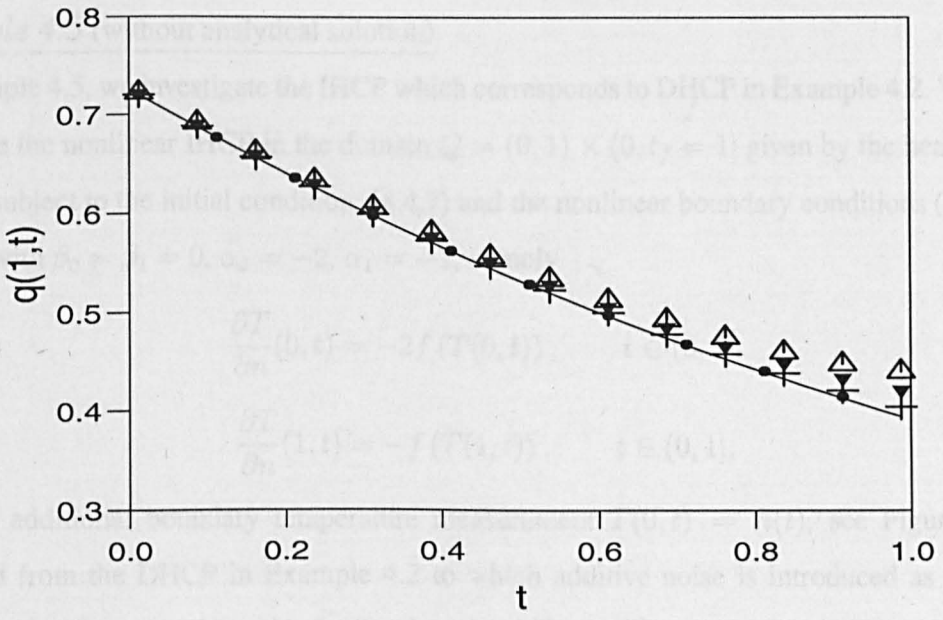

(b)

Figure 4.12: The (—) analytical and numerical heat fluxes (a) $q(0,t)$, and (b) $q(1,t)$, as functions of time t, for various amounts of noise (•) $\rho = 0.00$, (+) $\rho = 0.01$, (▼) $\rho = 0.03$ and (△) $\rho = 0.05$, for the IHCP given by Example 4.4, for $(N, N_0) = (40, 40)$, $K = 1$.

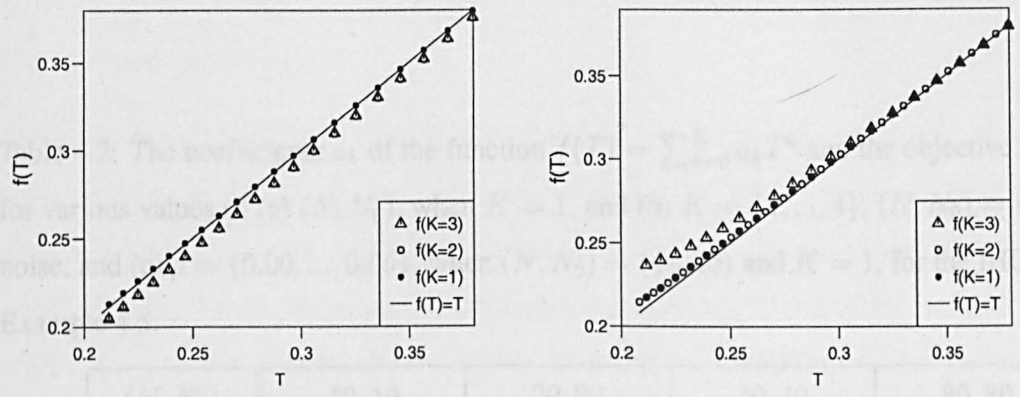

Figure 4.13: The analytical and numerical approximations of the function $f(T)$, as functions of temperature T, for various $K = \{1, 2, 3\}$, for (a) $\rho = 0.00$ and (b) $\rho = 0.01$, for the IHCP given by Example 4.4, for $(N, N_0) = (40, 40)$. The analytical solution $f(T) = T$ is also included.

4.5.2 Inverse Problem corresponding to Example 4.2

Example 4.5 (without analytical solution)

In Example 4.5, we investigate the IHCP which corresponds to DHCP in Example 4.2. Therefore, we solve the nonlinear IHCP in the domain $Q = (0, 1) \times (0, t_f = 1]$ given by the heat equation (4.2.1) subject to the initial condition, (4.4.7) and the nonlinear boundary conditions (4.2.8) and (4.2.9) with $\beta_0 = \beta_1 = 0$, $\alpha_0 = -2$, $\alpha_1 = -1$, namely

$$\frac{\partial T}{\partial n}(0,t) = -2f\left(T(0,t)\right), \qquad t \in (0,1], \tag{4.5.8}$$

$$\frac{\partial T}{\partial n}(1,t) = -f\left(T(1,t)\right), \qquad t \in (0,1], \tag{4.5.9}$$

and the additional boundary temperature measurement $T(0,t) = h(t)$, see Figure 4.18(a), obtained from the DHCP in Example 4.2 to which additive noise is introduced as in (4.5.4). The unknown function f is analytically given by $f(T) = T^2$, and the only non-zero coefficient is $a_2 = 1$. Remark that this problem does not have an analytical solution available for $T(x,t)$.

When there is no noise, initially the degree of the function f is taken to be $K = 2$, and the number of discretizations is increased from $(N, N_0) = (10, 10)$ to (80,80). The BEM accurately determines convergent approximations for the boundary temperature $T(1,t)$, see Figure 4.14, and the heat fluxes, see Figure 4.15. Also convergent and accurate approximations of the coefficients

Table 4.2: The coefficients a_k of the function $f(T) = \sum_{k=0}^{K} a_k T^k$ and the objective function S, for various values of (a) (N, N_0), when $K = 1$, and (b) $K = \{1, ..., 4\}$, $(N, N_0) = (40, 40)$, no noise, and (c) $\rho = \{0.00, ..., 0.05\}$, when $(N, N_0) = (40, 40)$ and $K = 1$, for the IHCP given by Example 4.5.

(N, N_0)	$10, 10$	$20, 20$	$40, 40$	$80, 80$
a_0	0.1866	0.0157	0.0142	0.0141
a_1	−10.6097	−0.0557	−0.0609	−0.0614
a_2	34.2754	1.0480	1.0503	1.0519
S	4.1×10^{-1}	2.6×10^{-1}	8.3×10^{-1}	2.0×10^{-1}

(a)

K	1	2	3	4
a_0	−0.2883	0.0142	0.0336	−0.3776
a_1	1.1287	−0.0609	−0.1778	3.0502
a_2	–	1.0503	1.2703	−7.7825
a_3	–	–	−0.1317	10.6225
a_4	–	–	–	−4.5680
S	5.0×10^{-3}	8.0×10^{-5}	8.1×10^{-5}	1.5×10^{-5}

(b)

	$\rho = 0.00$	$\rho = 0.01$	$\rho = 0.03$	$\rho = 0.05$
a_0	0.0142	−0.0240	−0.0908	−0.1489
a_1	−0.0609	0.1143	0.4261	0.7039
a_2	1.0503	0.8870	0.5678	0.2911
S	8.0×10^{-5}	3.0×10^{-3}	2.6×10^{-2}	7.2×10^{-2}

(c)

a_0, a_1 and a_2 of the function $f(T) = a_0 + a_1 T + a_0 T^2$ and a small value of the objective function S are obtained, see Table 4.2(a).

Since the function $f(T)$ is analytically quadratic, we expect $K = 2$ to give an accurate approximation, a fact that is evident when the degree K of the function $f(T)$ is increased gradually from 1 to 4, see Table 4.2(a), when the number of discretizations $(N, N_0) = (40, 40)$ and there is no noise. The results obtained for the approximations of the temperature $T(1,t)$, see Figure 4.16, the heat fluxes, see Figure 4.17, and the coefficients a_k of the function $f(T)$ in Table 4.2(b), when $K = 2$ best matches the analytical values. Although the values of the approximations of a_k, when $K = 3$ and 4 deviate significantly from their analytical values, we still obtain good approximations for the boundary temperature and heat fluxes. This can be explained by the fact that a higher-order function with a variety of coefficients can still be used to approximate, with a reasonable accuracy, a quadratic function. However, as expected, the approximations when $K = 1$ are poor because a linear function cannot well approximate a quadratic function. When $K = 2$, $(N, N_0) = (40, 40)$, and noise is introduced in (4.2.5) from $\rho = 0.00$ to 0.05, see Figure 4.18(a), the numerical results for the coefficients a_k tabulated in Table 4.2 (c), the temperature $T(1,t)$ in Figure 4.18(b) and the heat fluxes in Figure 4.19, undergo an accuracy proportional to the amount of noise ρ introduced. This indicates that we have obtained stable solutions.

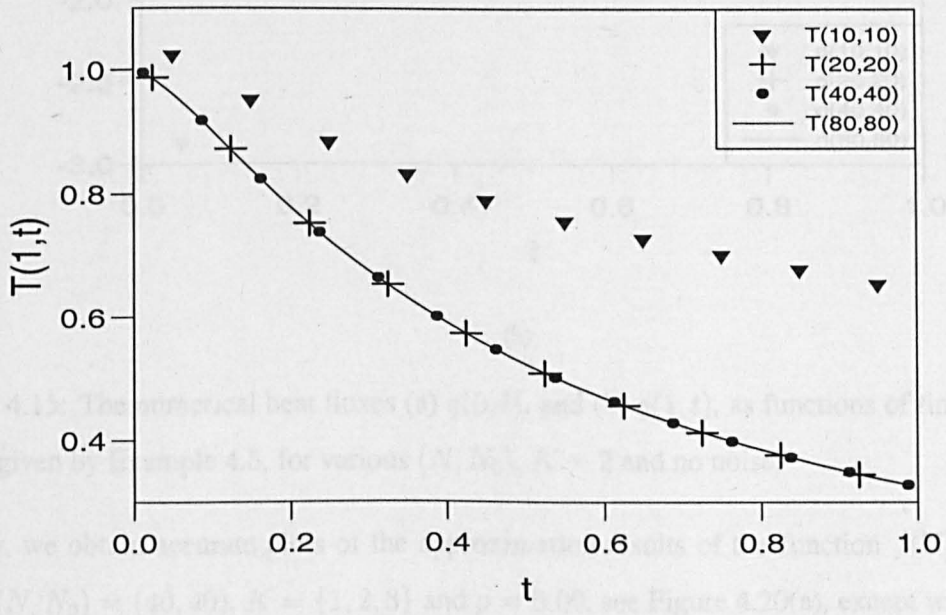

Figure 4.14: The numerical boundary temperature $T(1,t)$, as a function of time t, for the IHCP given by Example 4.5, for various (N, N_0), $K = 2$ and no noise.

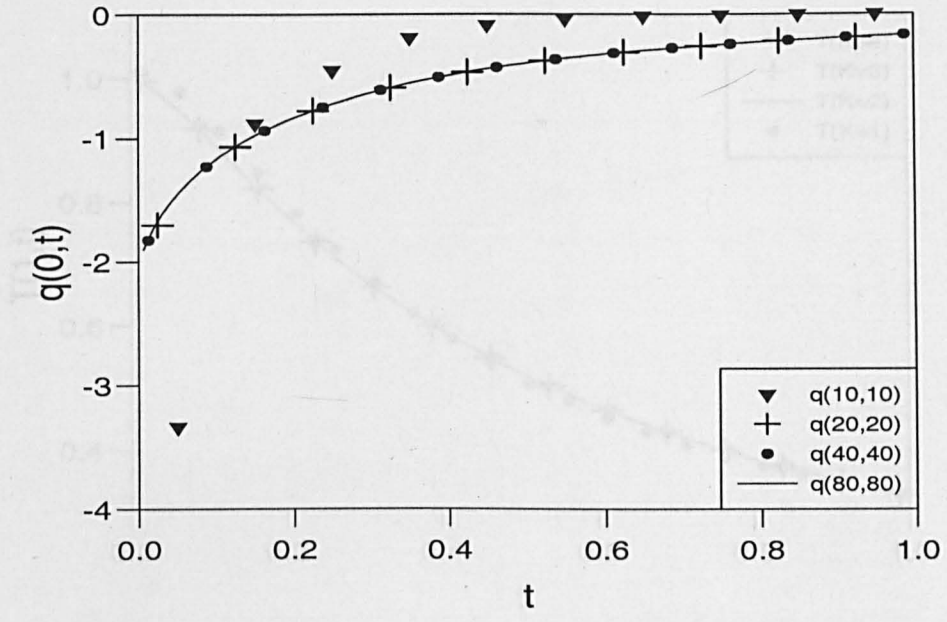

(a)

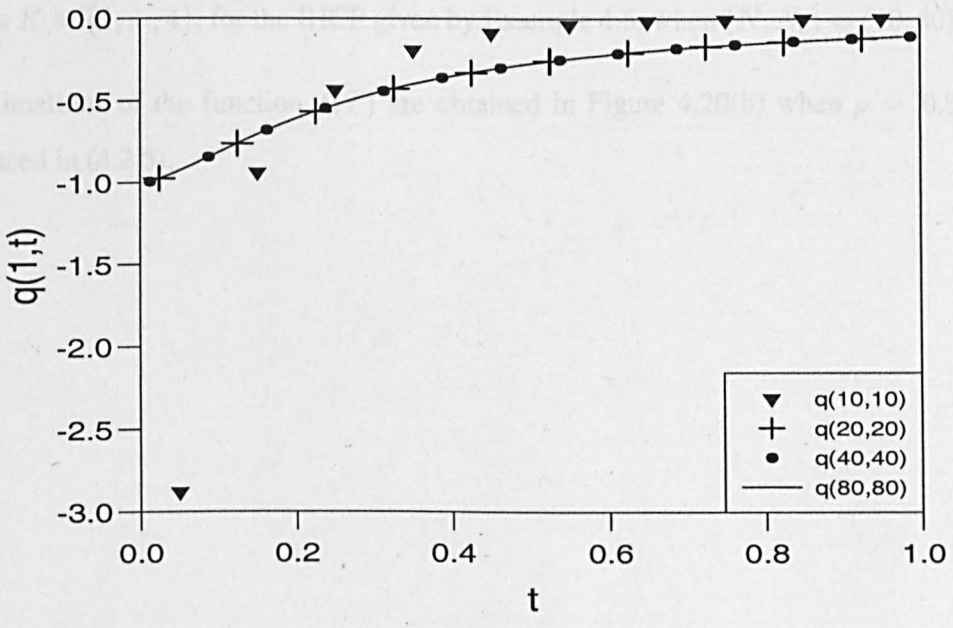

(b)

Figure 4.15: The numerical heat fluxes (a) $q(0,t)$, and (b) $q(1,t)$, as functions of time t, for the IHCP given by Example 4.5, for various (N, N_0), $K = 2$ and no noise.

Finally, we obtain accurate plots of the approximation results of the function $f(T)$ against T, when $(N, N_0) = (40, 40)$, $K = \{1, 2, 3\}$ and $\rho = 0.00$, see Figure 4.20(a), except when $K = 1$, confirming that when $K = 2$ any other higher order function can be used to obtain a best match between the analytical and numerical results for the quadratic function. Furthermore, stable

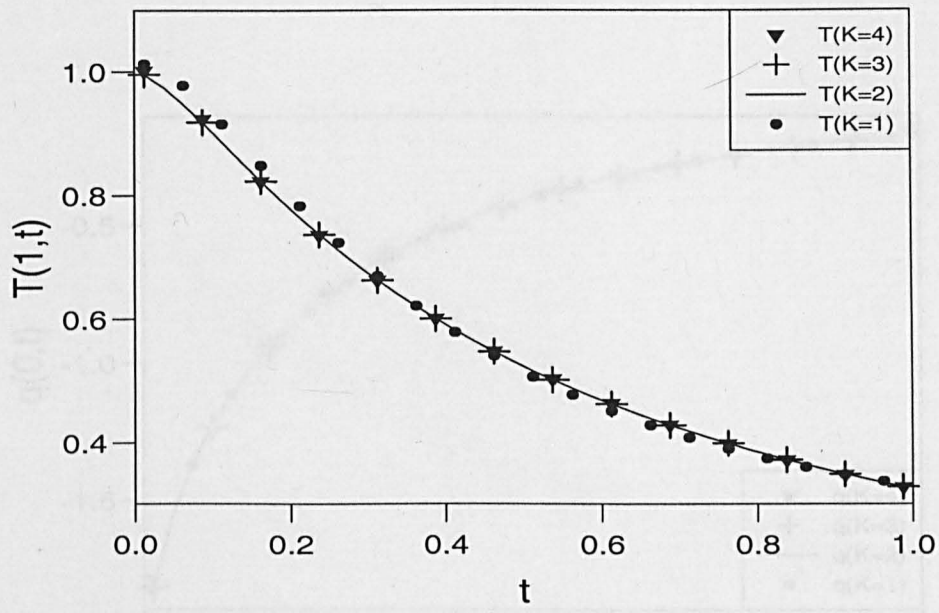

Figure 4.16: The numerical boundary temperature $T(1,t)$, as a function of time t, for various degrees $K = \{1, ..., 4\}$, for the IHCP given by Example 4.5, when $(N, N_0) = (40, 40)$, no noise.

approximations of the function $f(T)$ are obtained in Figure 4.20(b) when $\rho = 0.01$ noise is introduced in (4.2.5).

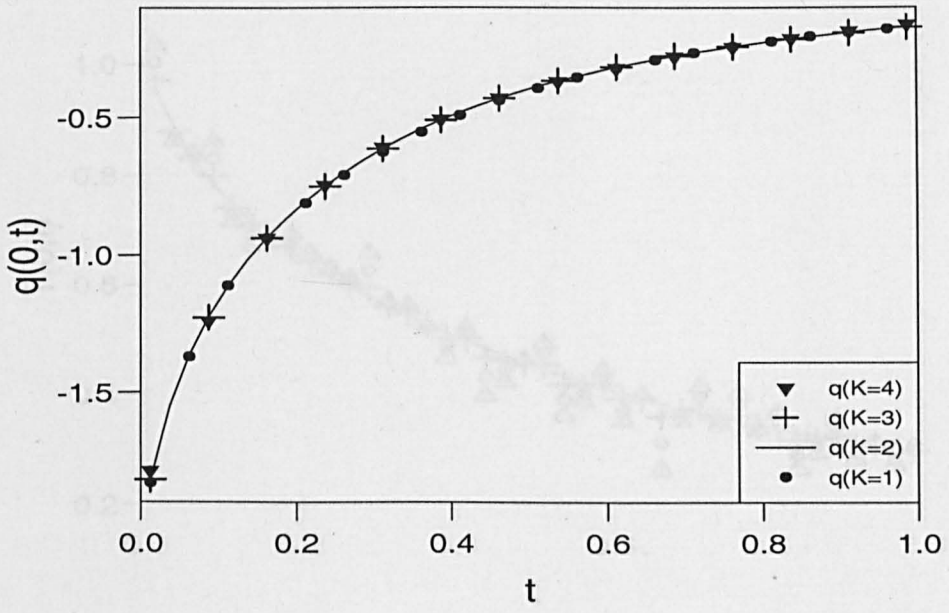

(a)

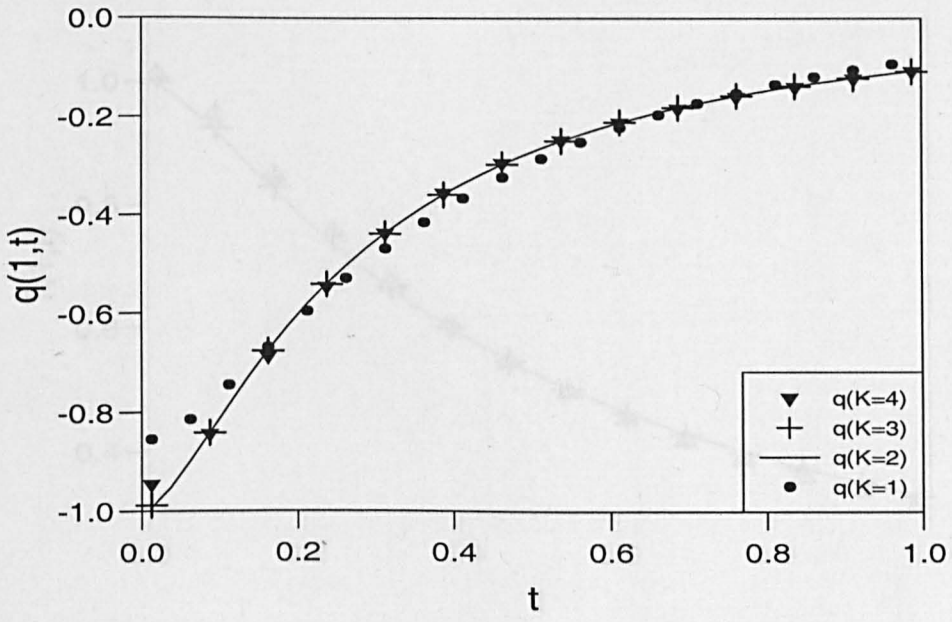

(b)

Figure 4.17: The numerical heat fluxes (a) $q(0,t)$, and (b) $q(1,t)$, as functions of time t, for various degrees $K = \{1, ..., 4\}$, of the function t, for the IHCP given by Example 4.5, when $(N, N_0) = (40, 40)$, no noise.

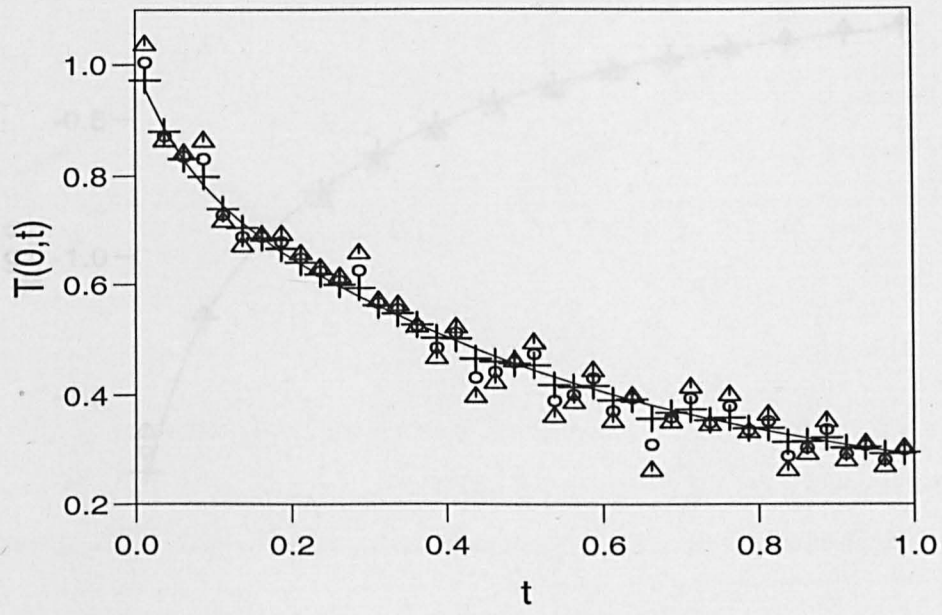

(a)

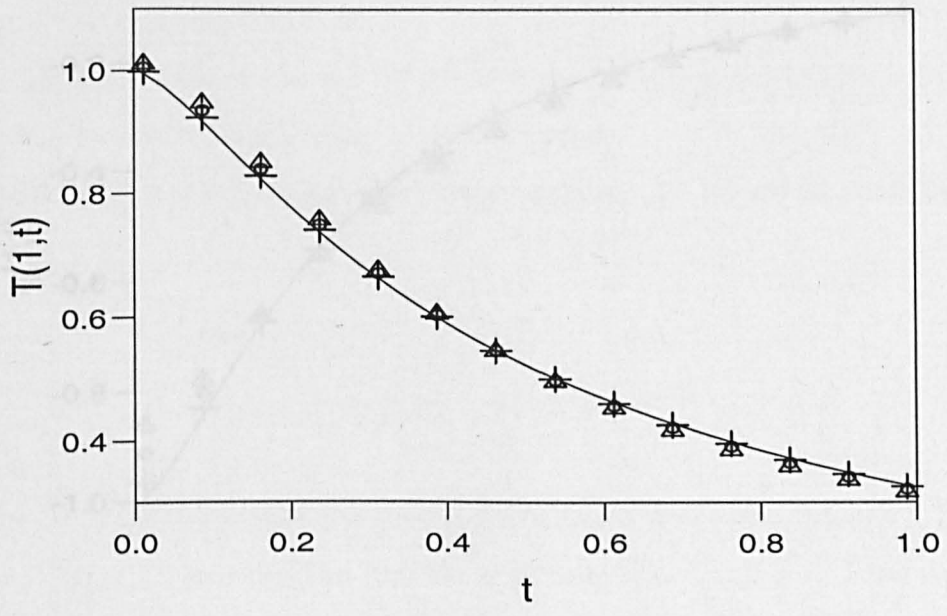

(b)

Figure 4.18: The measured and numerical boundary temperatures (a) $T(0,t)$, and (b) $T(1,t)$, as functions of time t, for various amounts of noise (—) $\rho = 0.00$, (+) $\rho = 0.01$, (∘) $\rho = 0.03$, (△) $\rho = 0.05$, for the nonlinear IHCP given by Example 4.5, when $(N, N_0) = (40, 40)$ and $K = 2$.

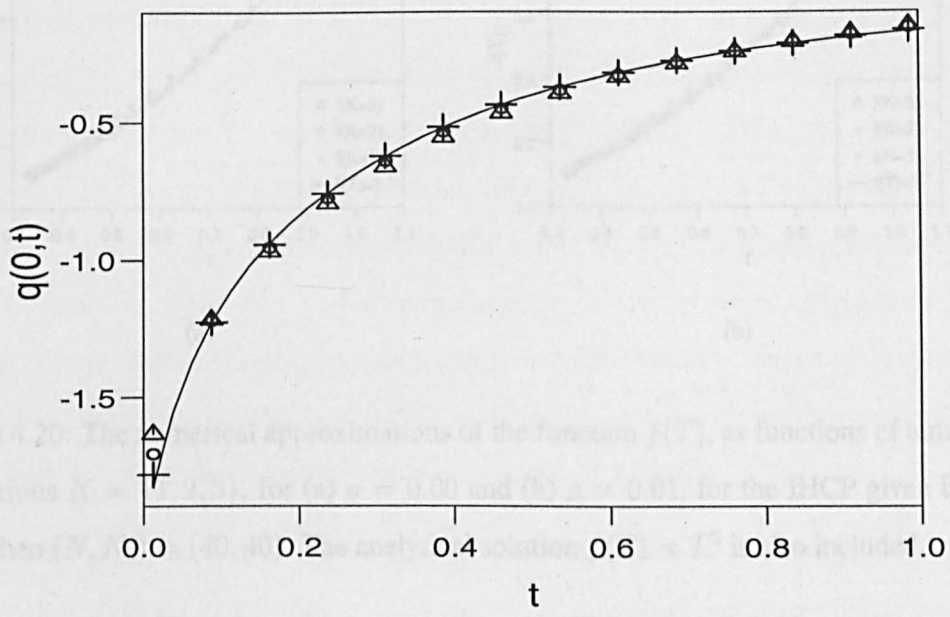

(a)

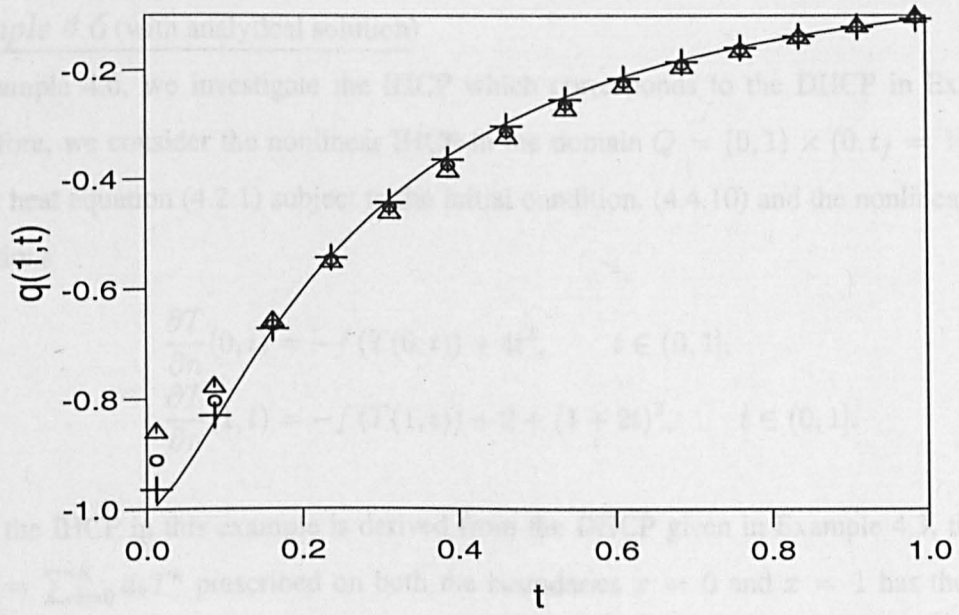

(b)

Figure 4.19: The numerical heat fluxes (a) $q(0,t)$, and (b) $q(1,t)$, as functions of time t, for various amounts of noise (—) $\rho = 0.00$, (+) $\rho = 0.01$, (○) $\rho = 0.03$, (△) $\rho = 0.05$, for the IHCP given by Example 4.5, when $(N, N_0) = (40, 40)$ and $K = 2$.

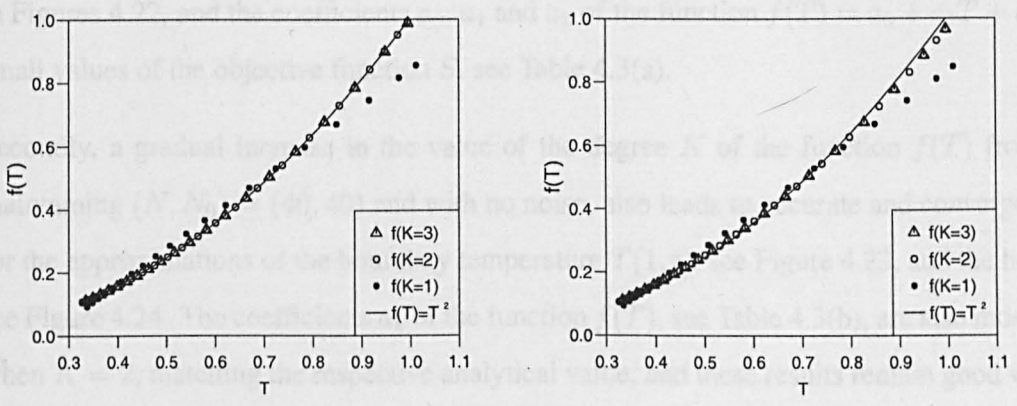

(a) (b)

Figure 4.20: The numerical approximations of the function $f(T)$, as functions of temperature T, for various $K = \{1, 2, 3\}$, for (a) $\rho = 0.00$ and (b) $\rho = 0.01$, for the IHCP given by Example 4.5, when $(N, N_0) = (40, 40)$. The analytical solution $f(T) = T^2$ is also included.

4.5.3 Inverse Problem corresponding to Example 4.3

Example 4.6 (with analytical solution)

In Example 4.6, we investigate the IHCP which corresponds to the DHCP in Example 4.3. Therefore, we consider the nonlinear IHCP in the domain $Q = (0,1) \times (0, t_f = 1]$ described by the heat equation (4.2.1) subject to the initial condition, (4.4.10) and the nonlinear boundary conditions

$$\frac{\partial T}{\partial n}(0,t) = -f\left(T(0,t)\right) + 4t^2, \qquad t \in (0,1], \tag{4.5.10}$$

$$\frac{\partial T}{\partial n}(1,t) = -f\left(T(1,t)\right) + 2 + (1+2t)^2, \qquad t \in (0,1]. \tag{4.5.11}$$

Since the IHCP in this example is derived from the DHCP given in Example 4.3, the function $f(T) = \sum_{k=0}^{K} a_k T^k$ prescribed on both the boundaries $x = 0$ and $x = 1$ has the analytical solution $f(T) = T^2$, such that analytically the only non-zero coefficient is $a_2 = 1$. As in the preceding examples, the additional measurement is the boundary temperature $T(0,t) = h(t) = 2t$, obtained from the analytical solution $T(x,t) = x^2 + 2t$.

First, when there is no noise and the number of discretisations increases from $(N, N_0) = (10, 10)$ to $(80, 80)$, and $K = 2$, the results of the approximations are rapidly convergent and accurate, as can be seen from the plots of the boundary temperature $T(1,t)$ in Figure 4.21, the heat fluxes

in Figures 4.22, and the coefficients a_0, a_1 and a_2 of the function $f(T) = a_0 + a_1 T + a_2 T^2$ with small values of the objective function S, see Table 4.3(a).

Secondly, a gradual increase in the value of the degree K of the function $f(T)$ from 1 to 4, maintaining $(N, N_0) = (40, 40)$ and with no noise, also leads to accurate and convergent results for the approximations of the boundary temperature $T(1, t)$, see Figure 4.23, and the heat fluxes, see Figure 4.24. The coefficients a_k of the function $f(T)$, see Table 4.3(b), are also most accurate when $K = 2$, matching the respective analytical value, and these results remain good when $K = 3$ and 4. However, when $K = 1$ the approximations of the boundary temperature $T(1, t)$, and the heat fluxes on both boundaries $x = 0$ and $x = 1$, significantly deviate from their respective analytical values. This is as expected since approximations when $K = 1$ become poor because a linear function cannot accurately aproximate a quadratic function.

Finally, when $K = 2$, $(N, N_0) = (40, 40)$ and the amount of noise introduced in (4.2.5) is varied from $\rho = 0.00$ to 0.05, see Figure 4.25, we obtain a gradual and proportional degradation in the results obtained with increasing ρ for the coefficients a_k, see Table 4.3 (c), the temperature $T(1, t)$, see Figure 4.26, and the heat fluxes, see Figure 4.27. Results which are also accompanied with a large value of the objective function S, see Table 4.3(c). However, the numerical solutions remain stable.

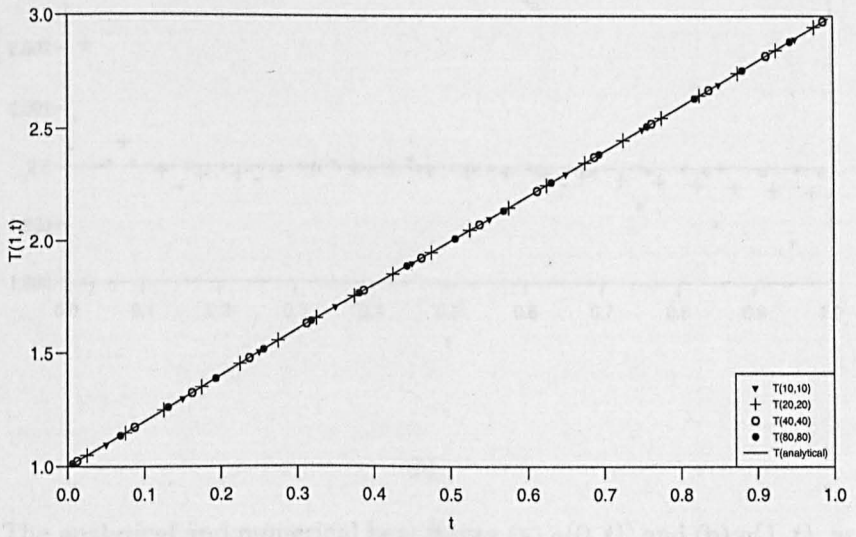

Figure 4.21: The analytical and numerical temperatures $T(1, t)$, as functions of time t, for the IHCP given by Example 4.6, for various (N, N_0), $K = 2$ and no noise.

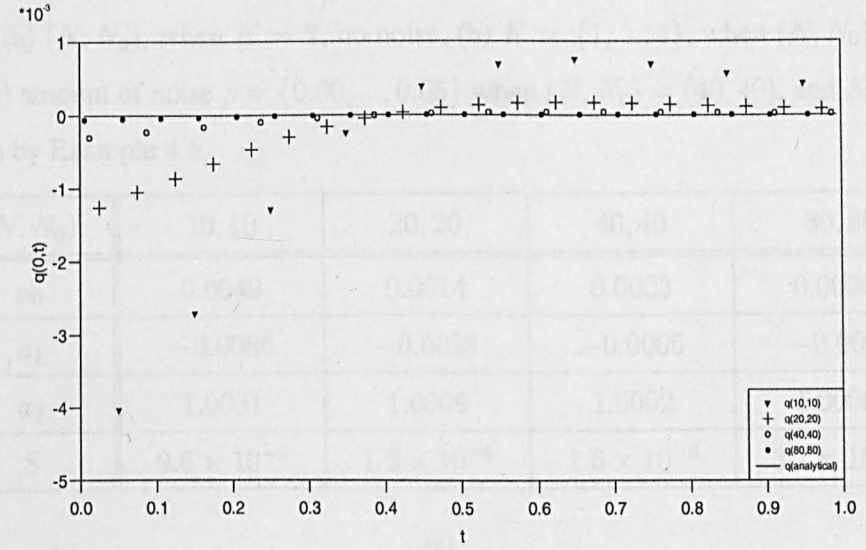

(a)

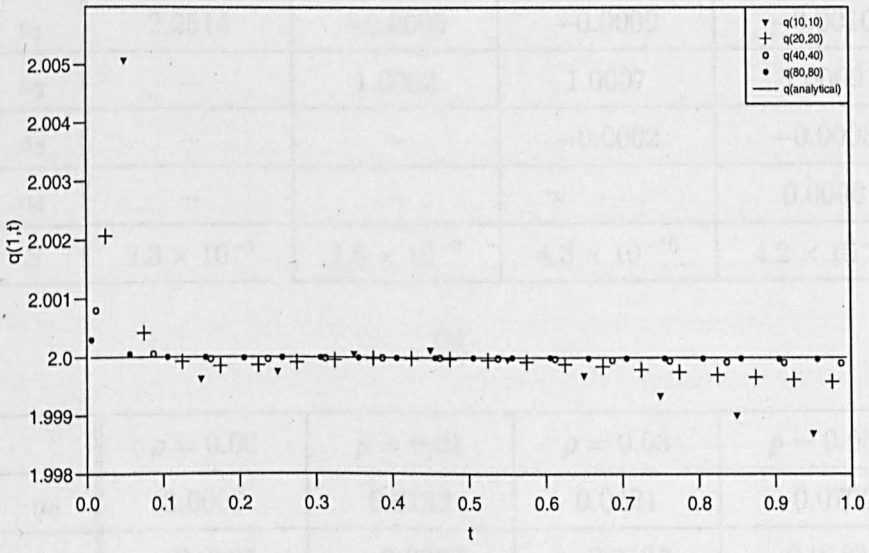

(b)

Figure 4.22: The analytical and numerical heat fluxes (a) $q(0,t)$, and (b) $q(1,t)$, as functions of time t, for the IHCP given by Example 4.6, for various (N, N_0), $K = 2$ and no noise.

Table 4.3: The coefficients a_k of the function $f(T) = \sum_{k=0}^{K} a_k T^k$ and the objective function S, for various (a) (N, N_0), when $K = 2$, no noise, (b) $K = \{1, ..., 4\}$, when $(N, N_0) = (40, 40)$, no noise, (c) amount of noise $\rho = \{0.00, ..., 0.05\}$ when $(N, N_0) = (40, 40)$, and $K = 2$, for the IHCP given by Example 4.6.

(N, N_0)	$10, 10$	$20, 20$	$40, 40$	$80, 80$
a_0	0.0049	0.0014	0.0003	0.00001
a_1	-0.0086	-0.0028	-0.0005	-0.0001
a_2	1.0031	1.0009	1.0002	1.00004
S	9.6×10^{-8}	1.2×10^{-8}	1.6×10^{-9}	3.7×10^{-10}

(a)

K	1	2	3	4
a_0	-0.9174	0.0003	0.0004	0.0004
a_1	2.2514	-0.0005	-0.0009	-0.0010
a_2	–	1.0002	1.0007	1.0009
a_3	–	–	-0.0002	-0.0003
a_4	–	–	–	0.0000
S	2.3×10^{-1}	1.6×10^{-9}	4.3×10^{-10}	4.2×10^{-10}

(b)

	$\rho = 0.00$	$\rho = 0.01$	$\rho = 0.03$	$\rho = 0.05$
a_0	0.0003	0.0143	0.0421	-0.0700
a_1	-0.0005	-0.0038	-0.0107	-0.01835
a_2	1.0002	1.0058	1.0174	1.0296
S	1.6×10^{-9}	1.8×10^{-2}	1.6×10^{-1}	4.4×10^{-1}

(c)

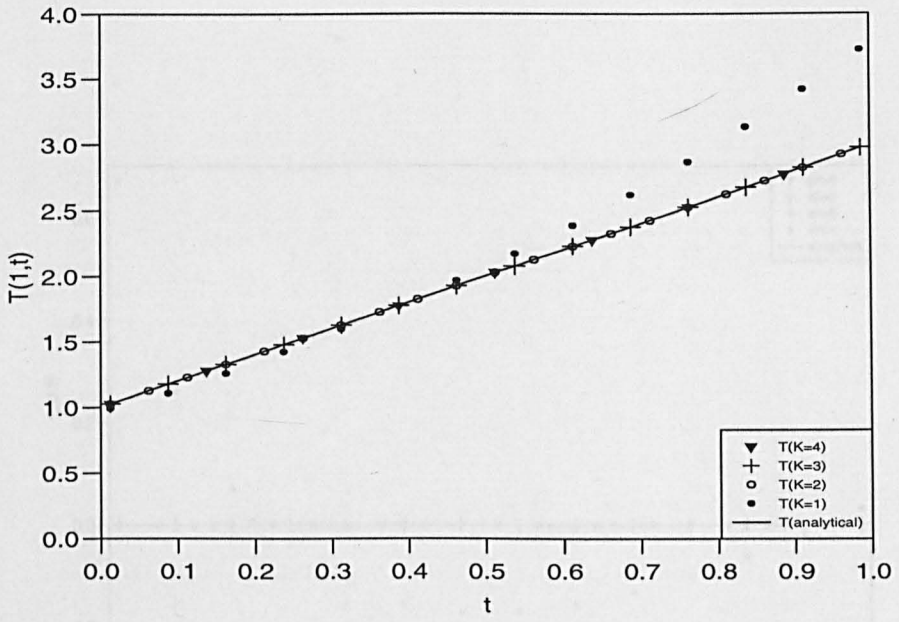

Figure 4.23: The analytical and numerical boundary temperatures $T(1,t)$, as functions of time t, for various degrees $K = \{1, ..., 4\}$, for the IHCP given by Example 4.6, when $(N, N_0) = (40, 40)$, no noise.

4.5.4 Exponential Nonlinear Inverse Problem

Example 4.7

Nonlinear boundary relationship between the heat flux and temperature in heat transfer problems can take several forms. In the preceding Examples 4.5 and 4.6 we have investigated IHCPs with quadratic boundary relationships between the heat flux and temperature. However, in many real situations the heat fluxes at the boundary can undergo an exponential decay in temperature. Therefore, in this example, we investigate a nonlinear heat transfer problem where the heat fluxes are exponential functions of the temperature. Mathematically, we solve a nonlinear IHCP in the domain $Q = (0,1) \times (0, t_f = 1]$, for the heat equation (4.2.1) subject to the initial condition, (4.2.2) given by

$$T(x,0) = g(x) = 3x^2/2 - x^3/3, \qquad x \in [0,1] \tag{4.5.12}$$

and the nonlinear boundary conditions (4.2.8) and (4.2.9) with $\alpha_0 = -1$, $\beta_0 = 1$, $\alpha_1 = -\exp(7/6)$, $\beta_1 = 3$, namely

$$\frac{\partial T}{\partial n}(0,t) = 1 - f\left(T(0,t)\right), \qquad t \in (0,1], \tag{4.5.13}$$

$$\frac{\partial T}{\partial n}(1,t) = 3 - \exp(7/6) f\left(T(1,t)\right), \qquad t \in (0,1]. \tag{4.5.14}$$

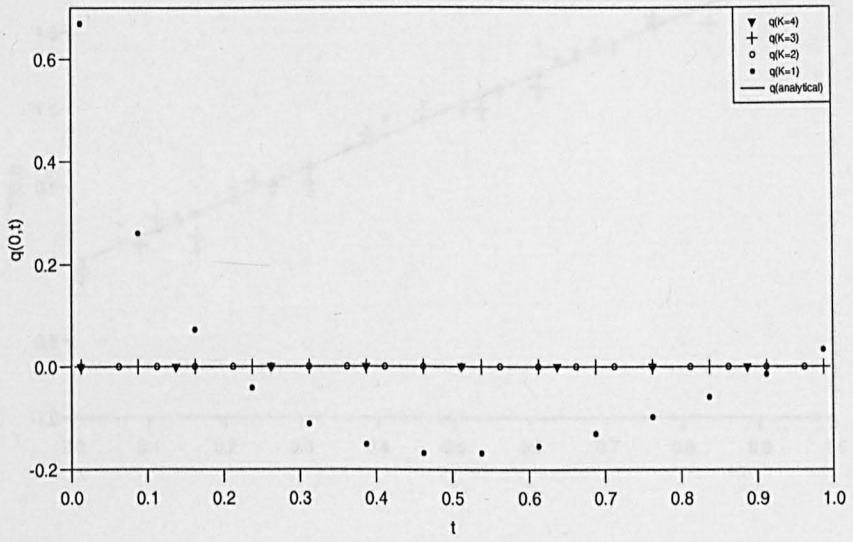

(a)

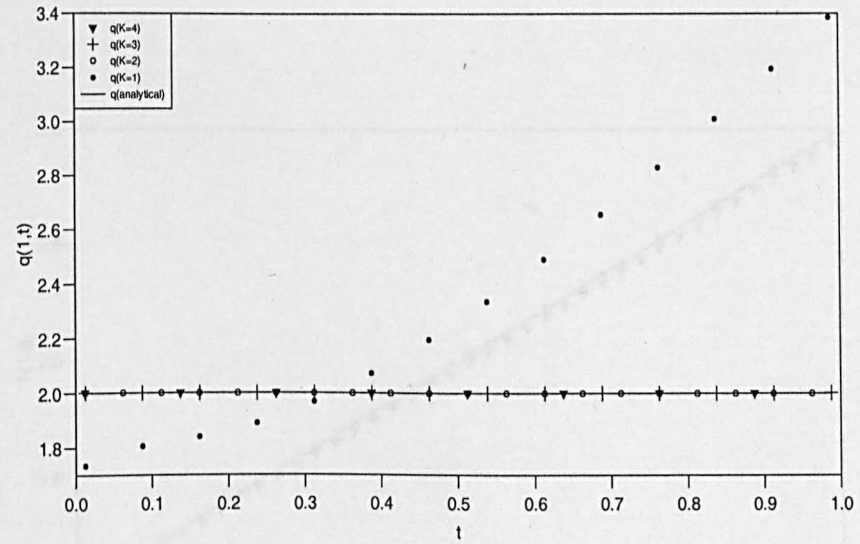

(b)

Figure 4.24: The analytical and numerical heat fluxes (b) $q(0,t)$ and, (c) $q(1,t)$, as functions of time t, for various degrees $K = \{1, ..., 4\}$, for the IHCP given by Example 4.6, when $(N, N_0) = (40, 40)$, no noise.

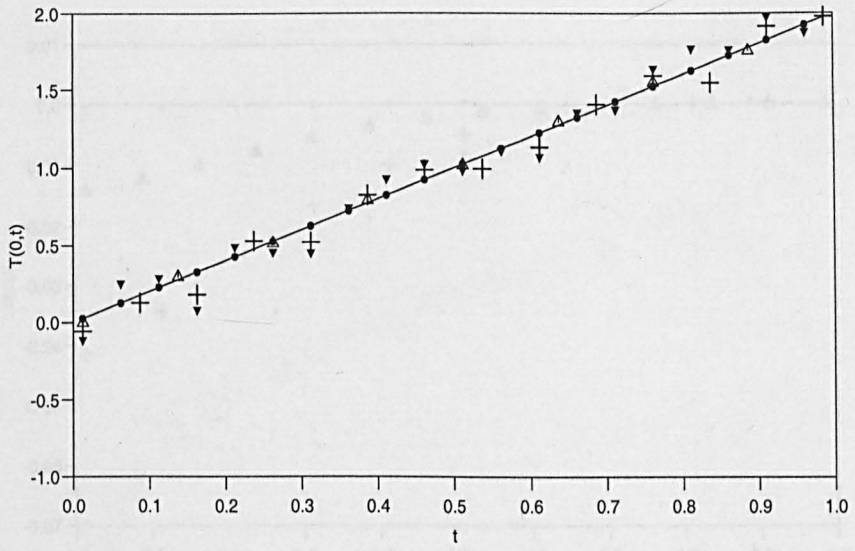

Figure 4.25: The measured boundary temperature $T(0,t)$, as a function of time t, for various amounts of noise $(-\bullet-)$ $\rho = 0.00$, $(\triangle)$ $\rho = 0.01$, $(+)$ $\rho = 0.03$ and $(\blacktriangledown)$ $\rho = 0.05$, for the IHCP given by Example 4.6, when $(N, N_0) = (40, 40)$.

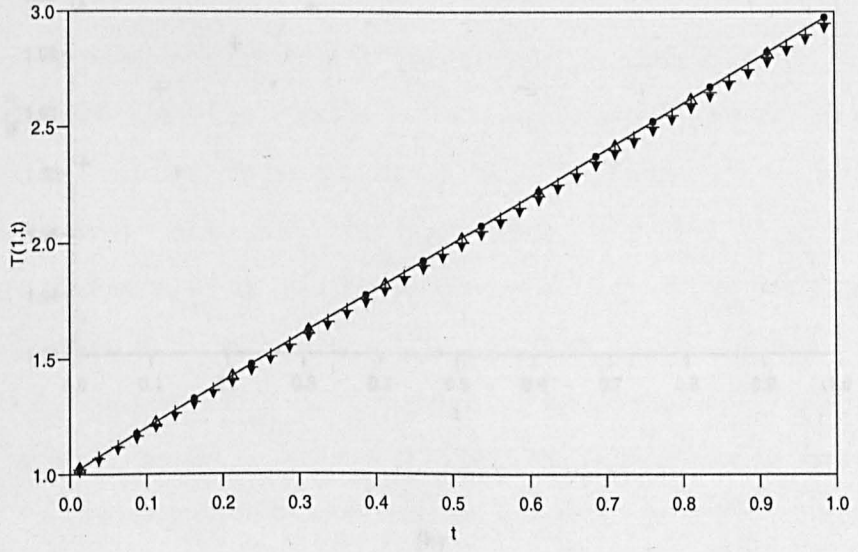

Figure 4.26: The (—) analytical and numerical boundary temperatures $T(1,t)$, as functions of time t, for various amounts of noise $(\bullet)$ $\rho = 0.00$, $(\triangle)$ $\rho = 0.01$, $(+)$ $\rho = 0.03$ and $(\blacktriangledown)$ $\rho = 0.05$, for the IHCP given by Example 4.6, when $(N, N_0) = (40, 40)$ and $K = 2$.

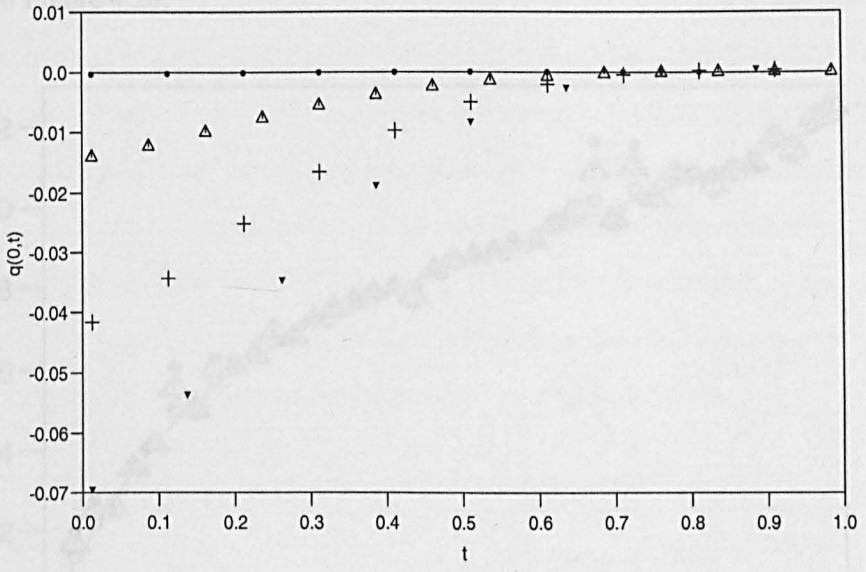

(a)

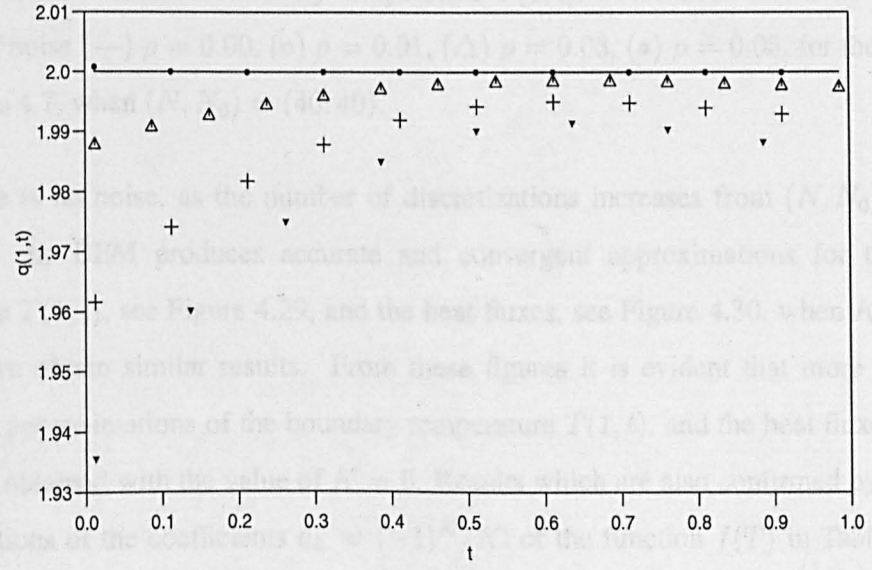

(b)

Figure 4.27: The (—) analytical and numerical heat fluxes (a) $q(0,t)$, and (b) $q(1,t)$, as functions of time t, for various amounts of noise (•) $\rho = 0.00$, (△) $\rho = 0.01$, (+) $\rho = 0.03$ and (▼) $\rho = 0.05$, for the IHCP given by Example 4.6, when $(N, N_0) = (40, 40)$ and $K = 2$.

This nonlinear IHCP has no analytical solution, such that the extra condition imposed, namely $T(0,t) = h(t)$ is obtained from the corresponding DHCP with $f(T) = \exp(-T)$, to which noise is added, see Figure 4.28.

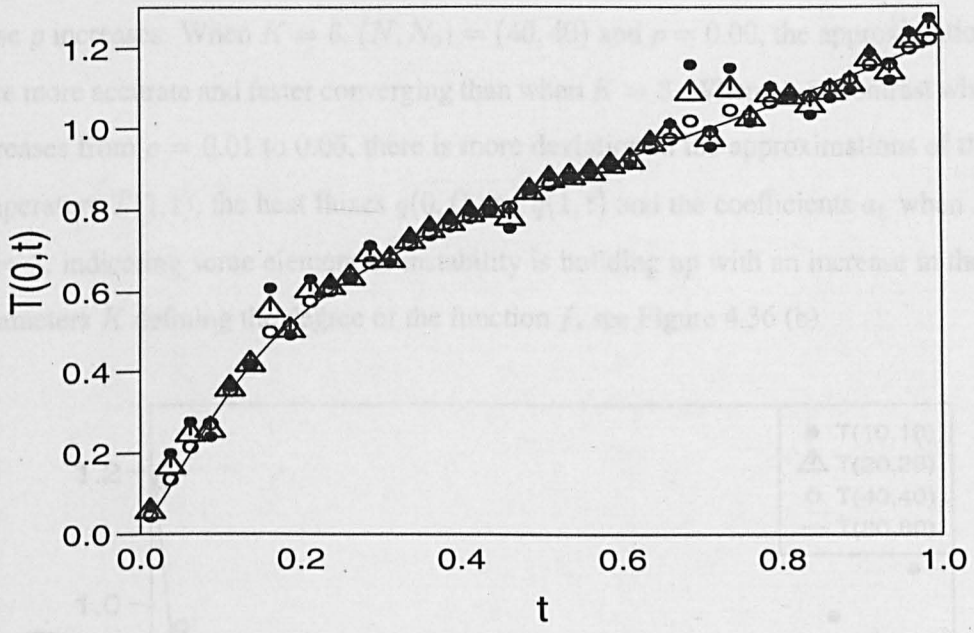

Figure 4.28: The measured boundary temperature $T(0,t)$, as a function of time t, for various amounts of noise (—) $\rho = 0.00$, (○) $\rho = 0.01$, (△) $\rho = 0.03$, (•) $\rho = 0.05$, for the IHCP given by Example 4.7, when $(N, N_0) = (40, 40)$.

When there is no noise, as the number of discretizations increases from $(N, N_0) = (10, 10)$ to (80,80), the BEM produces accurate and convergent approximations for the boundary temperature $T(1,t)$, see Figure 4.29, and the heat fluxes, see Figure 4.30, when $K = 6$. When $K = 3$, we obtain similar results. From these figures it is evident that more accurate and convergent approximations of the boundary temperature $T(1,t)$, and the heat fluxes $q(0,t)$ and $q(1,t)$, are obtained with the value of $K = 6$. Results which are also confirmed by the accurate approximations of the coefficients $a_k \approx (-1)^K/K!$ of the function $f(T)$ in Tables 4.4(a) and (b), where (a) and (b) are for $K = 3$ and 6, respectively. On plotting the approximations of the function $f(T)$, as a function of time, when $\rho = 0.00$, for both $K = 3$ and $K = 6$, we obtain results which completely overlap with the analytical solution, see Figure 4.36(a). On the other hand, as the degree K of the function $f(T)$ increases from 1 to 6, when the number of discretisations is maintained as $(N, N_0) = (40, 40)$ and there is no noise, the results obtained using the BEM for the approximations of the boundary temperature $T(1,t)$, see Figure 4.31, the heat fluxes, see Figure 4.32, the coefficients a_k, see Table 4.5, are inaccurate as expected, only

when $K = 1$, and the results improve as K increases to match the analytical values. However, when the amount of noise increases from $\rho = 0.01$ to 0.05, there is a small and gradual deviation in the approximations of the unknowns, see Figures 4.33–4.35. Further, the results presented in Table 4.6 shows that the coefficients a_k also undergo a gradual degradation, as the amount of noise ρ increases. When $K = 6$, $(N, N_0) = (40, 40)$ and $\rho = 0.00$, the approximations obtained were more accurate and faster converging than when $K = 3$. Whereas, in contrast when the noise increases from $\rho = 0.01$ to 0.05, there is more deviation in the approximations of the boundary temperature $T(1, t)$, the heat fluxes $q(0, t)$ and $q(1, t)$ and the coefficients a_k when $K = 6$ than $K = 3$, indicating some element of instability is building up with an increase in the number of parameters K defining the degree of the function f, see Figure 4.36 (b).

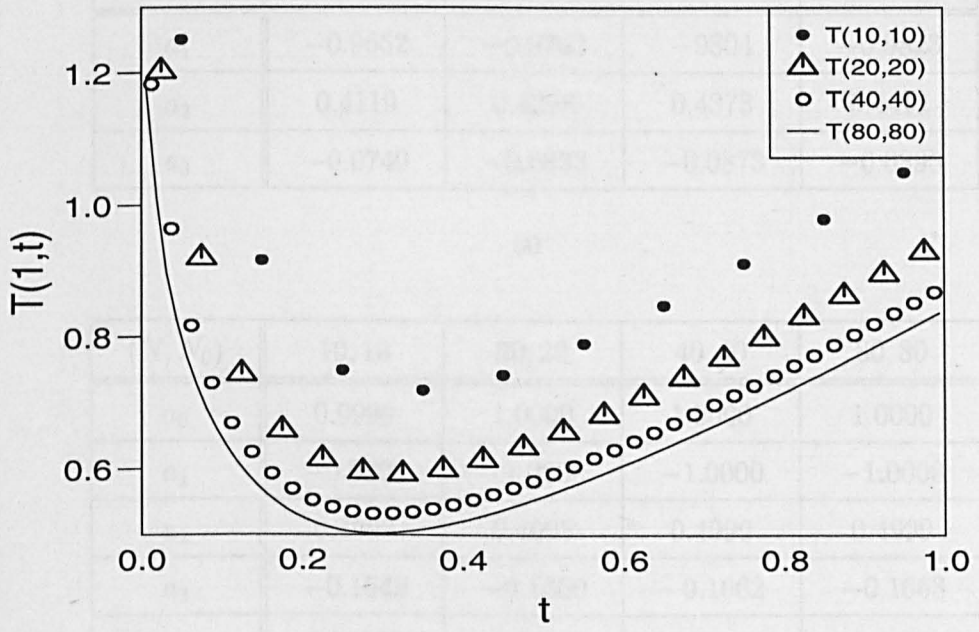

Figure 4.29: The numerical boundary temperature $T(1, t)$, as a function of time t, for various (N, N_0), when $K = 6$ and there is no noise, for the IHCP given by Example 4.7.

Table 4.4: The coefficients a_k of the function $f(T) = \sum_{k=0}^{K} a_k T^k$, (a) $K = 3$ and (b) $K = 6$, for various (N, N_0), for the IHCP given by Example 4.7, when there is no noise.

(N, N_0)	$10, 10$	$20, 20$	$40, 40$	$80, 80$
a_0	0.9959	0.9978	0.9984	0.9986
a_1	-0.9652	-0.9763	-9804	-0.9823
a_2	0.4119	0.4298	0.4373	0.4412
a_3	-0.0749	-0.0833	-0.0873	-0.0895

(a)

(N, N_0)	$10, 10$	$20, 20$	$40, 40$	$80, 80$
a_0	0.9999	1.0000	1.0000	1.0000
a_1	-0.9998	-1.0000	-1.0000	-1.0000
a_2	0.4993	0.4998	0.4999	0.4999
a_3	-0.1649	-0.1660	-0.1662	-0.1663
a_4	0.03937	0.0404	0.0407	0.0408
a_5	-0.0065	-0.0071	-0.0073	-0.0073
a_6	0.00001	0.00001	0.00005	0.000007

(b)

Table 4.5: The coefficients a_k of the function $f(T) = \sum_{k=0}^{K} a_k T^k$ and the objective function S, for various values of $K = \{1, .., 6\}$, for the IHCP given by Example 4.7, when $(N, N_0) = (40, 40)$, no noise.

K	1	2	3	4
a_0	0.8925	0.9843	0.9984	0.9858
a_1	−0.5261	−0.8813	−0.9804	−8404
a_2	–	0.2634	0.4374	0.0326
a_3	–	–	−0.0874	0.3549
a_4	–	–	–	−0.16367
a_5	–	–	–	–
a_6	–	–	–	–
S	2.9×10^{-3}	2.4×10^{-5}	9.7×10^{-8}	7.6×10^{-8}
K	–	–	5	6
a_0	–	–	0.9999	1.0000
a_1	–	–	−.9998	−1.0000
a_2	–	–	0.4987	0.4999
a_3	–	–	−0.1630	−0.1662
a_4	–	–	0.0364	0.0407
a_5	–	–	−0.0003	−0.0073
a_6	–	–	–	0.00007
R	–	–	5.4×10^{-13}	7.9×10^{-16}

Table 4.6: The coefficients a_k of the function $f(T) = \sum_{k=0}^{K} a_k T^k$ and the objective function S, for various amounts of noise $\rho = \{0.00, ..., 0.05\}$, for the IHCP given by Example 4.7, when $(N, N_0) = (40, 40)$, (a) $K = 3$, and (b) $K = 6$.

	$\rho = 0.00$	$\rho = 0.01$	$\rho = 0.03$	$\rho = 0.05$
a_0	0.9984	0.9486	0.8452	0.6930
a_1	−0.9804	−0.7602	−0.3199	0.3398
a_2	0.4373	0.1454	−0.4273	−1.2931
a_3	−0.0873	−0.0343	0.2732	0.6273
S	9.6×10^{-8}	4.2×10^{-3}	3.8×10^{-2}	1.1×10^{-1}

(a)

	$\rho = 0.00$	$\rho = 0.01$	$\rho = 0.03$	$\rho = 0.05$
a_0	1.0000	0.8648	1.0745	0.8185
a_1	−1.0000	0.4810	−0.9109	−0.02020
a_2	0.4999	−0.1992	0.9230	1.4392
a_3	−0.1662	−2.4022	−1.2291	−2.5797
a_4	0.0407	1.8392	0.8655	−1.4120
a_5	−0.0073	−0.1586	−3.6991	3.0286
a_6	0.00007	−0.1431	0.0262	−1.0250
S	7.9×10^{-16}	2.7×10^{-1}	2.8×10^{-1}	3.8×10^{-1}

(b)

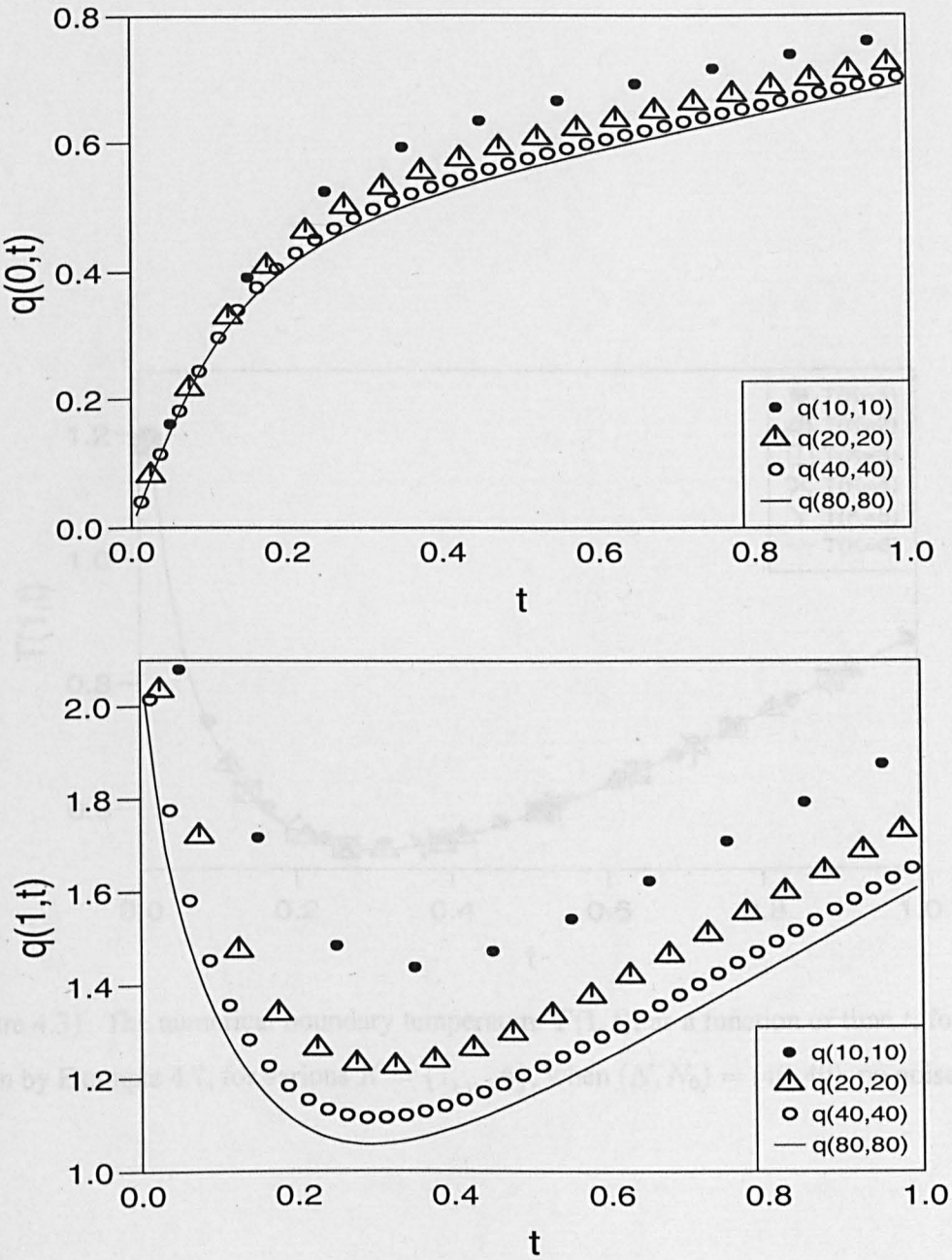

(a)

Figure 4.30: The numerical heat fluxes (a) $q(0,t)$, and (b) $q(1,t)$, as functions of time t, for various (N, N_0), when $K = 6$ and there is no noise, for the IHCP given by Example 4.7.

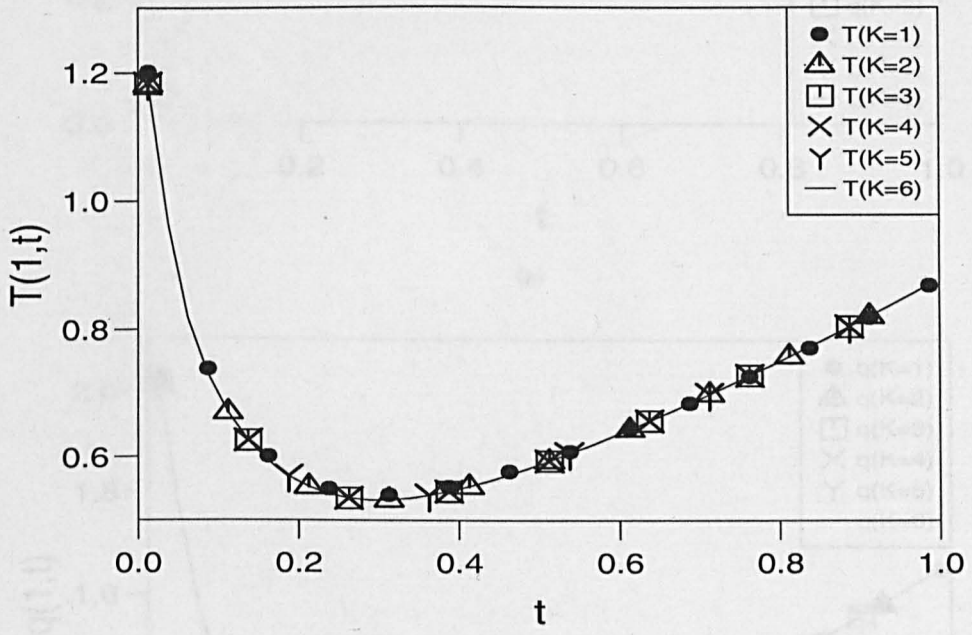

Figure 4.31: The numerical boundary temperature $T(1,t)$, as a function of time t, for the IHCP given by Example 4.7, for various $K = \{1, ..., 6\}$, when $(N, N_0) = (40, 40)$, no noise.

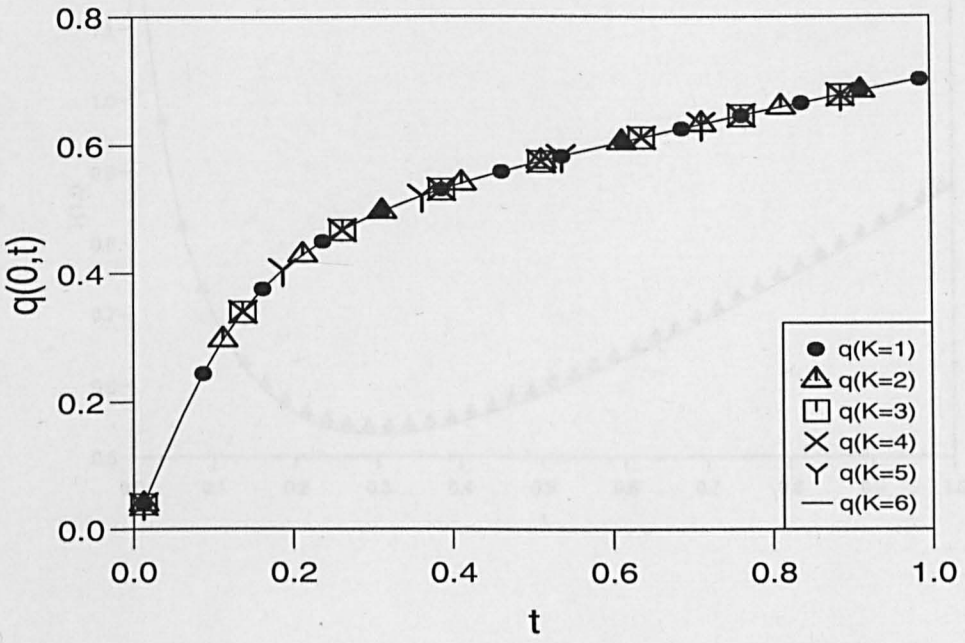

(a)

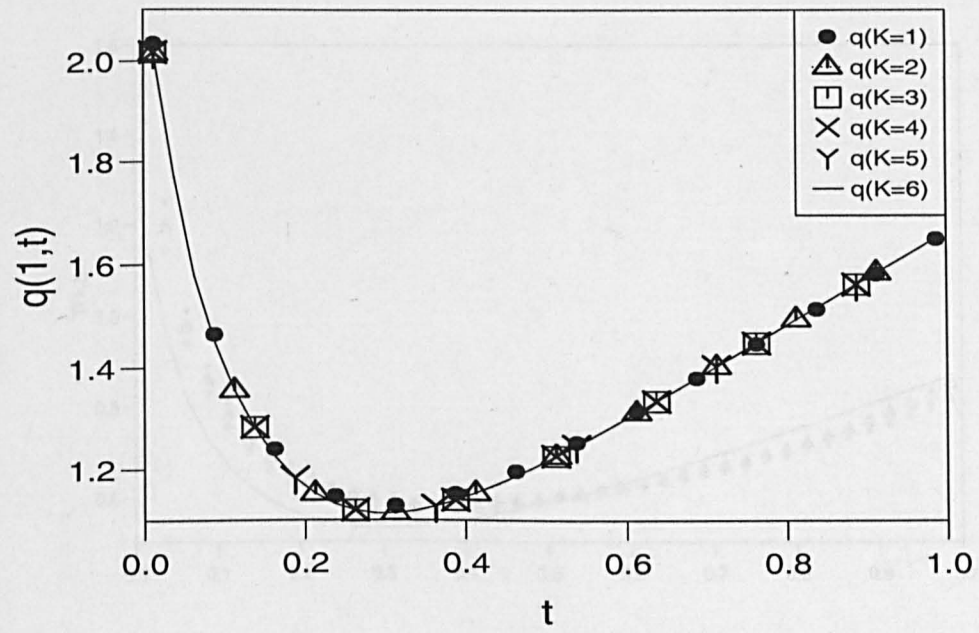

(b)

Figure 4.32: The numerical heat fluxes (a) $q(0,t)$, and (b) $q(1,t)$, as functions of time t, for the IHCP given by Example 4.7, for various $K = \{1, ..., 6\}$, when $(N, N_0) = (40, 40)$, no noise.

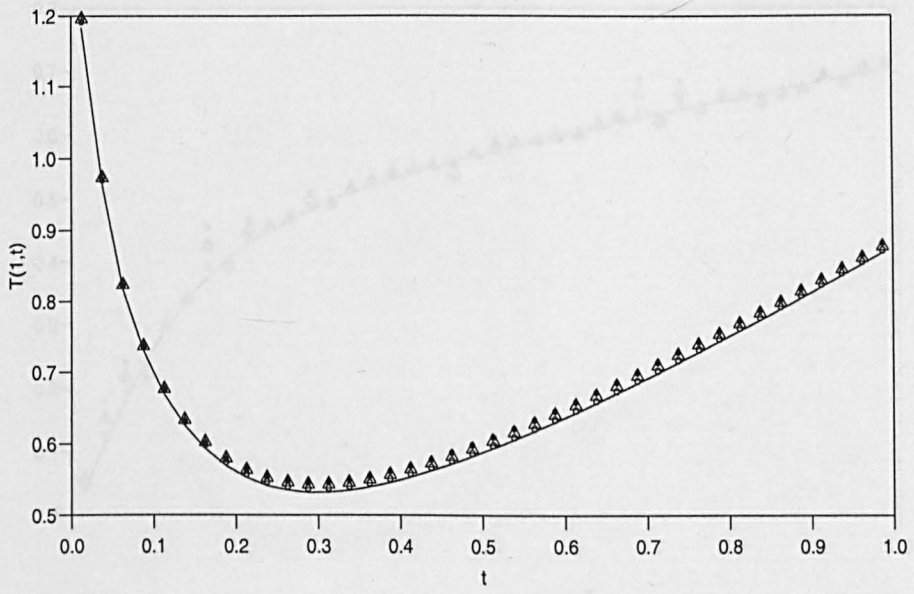

(a)

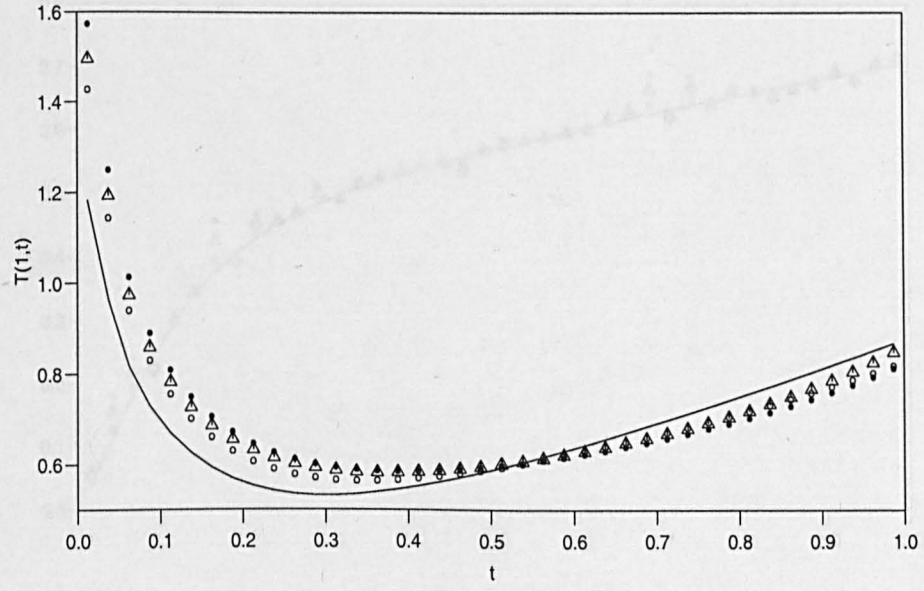

(b)

Figure 4.33: The numerical boundary temperature $T(1,t)$ as a function of time t, for various amounts of noise (—) $\rho = 0.00$, ($\circ$) $\rho = 0.01$, ($\triangle$) $\rho = 0.03$, ($\bullet$) $\rho = 0.05$, for the nonlinear IHCP given by Example 4.7, for (a) $K = 3$, and (b) $K = 6$, when $(N, N_0) = (40, 40)$.

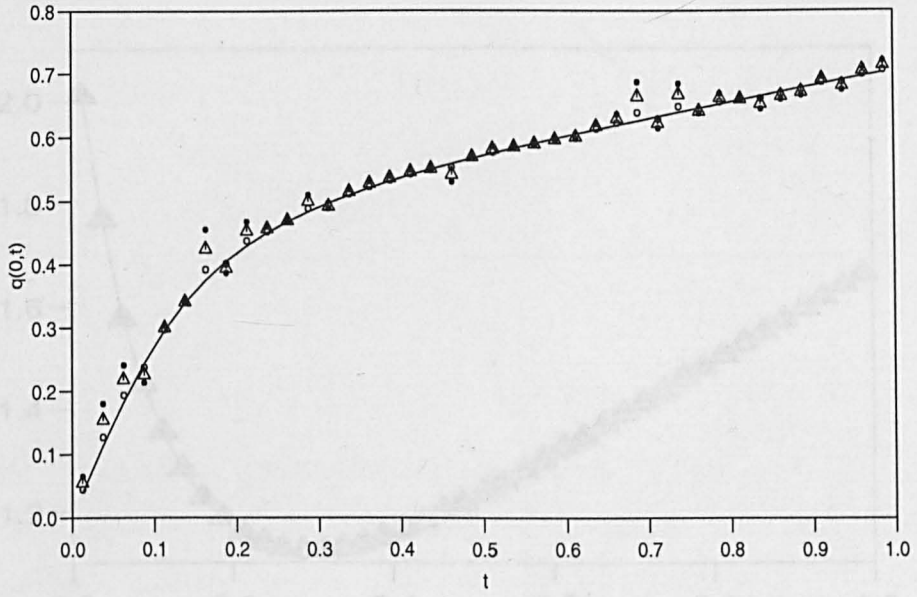

(a)

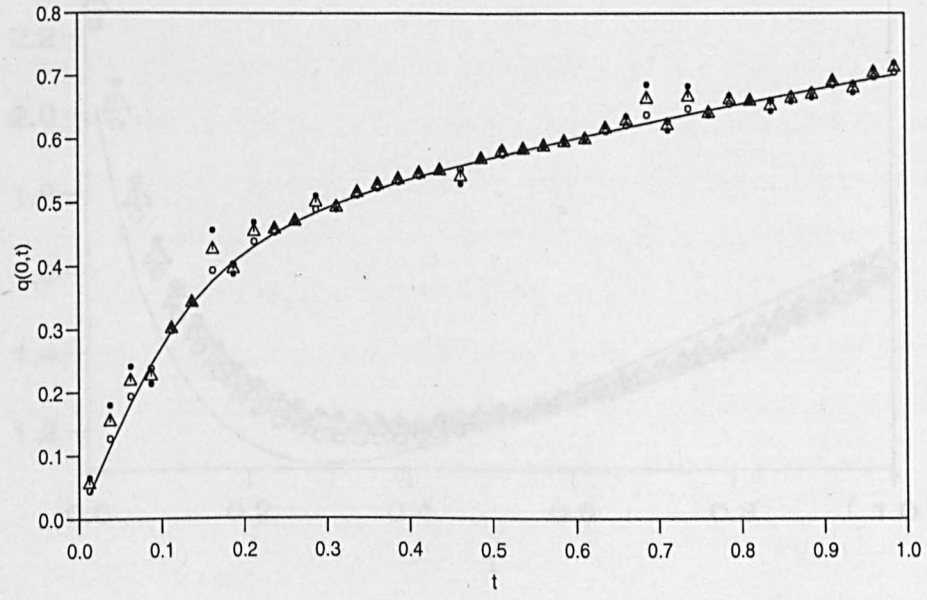

(b)

Figure 4.34: The numerical heat flux $q(0,t)$, as a function of time t, for various amounts of noise (—) $\rho = 0.00$, (○) $\rho = 0.01$, (△) $\rho = 0.03$, (•) $\rho = 0.05$, for the IHCP given by Example 4.7, for (a) $K = 3$, and (b) $K = 6$, when $(N, N_0) = (40, 40)$.

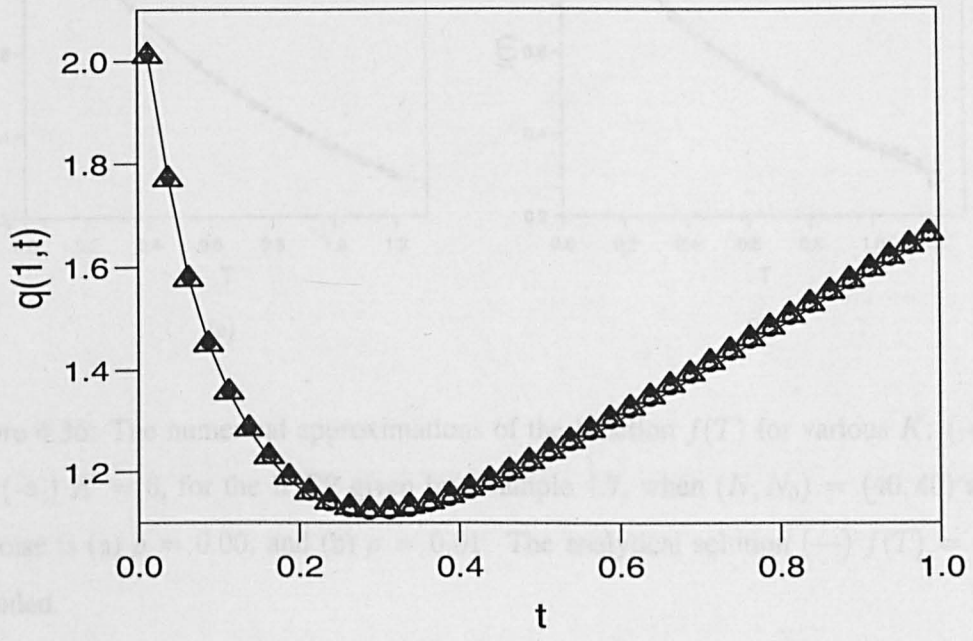

(a)

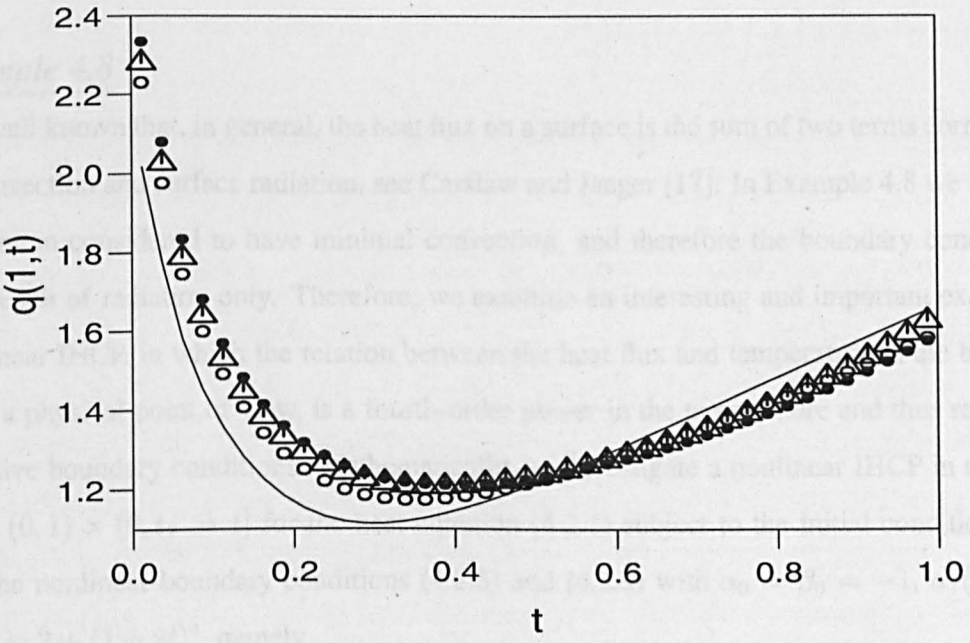

(b)

Figure 4.35: The numerical heat flux $q(1,t)$, as a function of time t, for various amounts of noise (—) $\rho = 0.00$, (○) $\rho = 0.01$, (△) $\rho = 0.03$, (•) $\rho = 0.05$, for the IHCP given by Example 4.7, for (a) $K = 3$, and (b) $K = 6$, when $(N, N_0) = (40, 40)$.

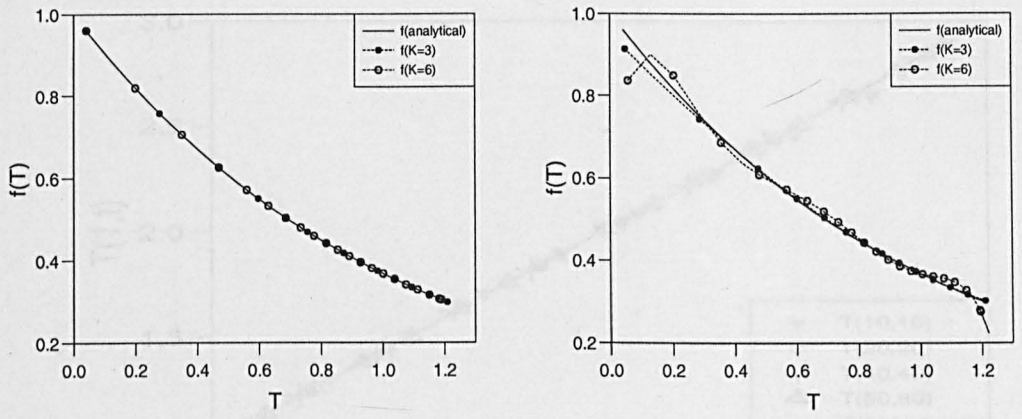

(a) (b)

Figure 4.36: The numerical approximations of the function $f(T)$ for various K: (-•-) $K = 3$, and (-o-) $K = 6$, for the IHCP given by Example 4.7, when $(N, N_0) = (40, 40)$ and amount of noise is (a) $\rho = 0.00$, and (b) $\rho = 0.01$. The analytical solution (—) $f(T) = \mathrm{e}^{-T}$ is also included.

4.5.5 Fourth-order power law nonlinear inverse problem

Example 4.8

It is well known that, in general, the heat flux on a surface is the sum of two terms corresponding to convection and surface radiation, see Carslaw and Jaeger [17]. In Example 4.8 we investigate a problem considered to have minimal convection, and therefore the boundary conditions are as a result of radiation only. Therefore, we examine an interesting and important example of a nonlinear IHCP, in which the relation between the heat flux and temperature at the boundaries, from a physical point of view, is a fourth-order power in the temperature and thus representing radiative boundary conditions. Mathematically, we investigate a nonlinear IHCP in the domain $Q = (0,1) \times (0, t_f = 1]$ for the heat equation (4.2.1) subject to the initial condition (4.4.10) and the nonlinear boundary conditions (4.2.8) and (4.2.9) with $\alpha_0 = \beta_0 = -1$, $\alpha_1(t) = 16t^4$, $\beta_1(t) = 2 + (1+2t)^4$, namely

$$\frac{\partial T}{\partial n}(0,t) = 16t^4 - f\left(T(0,t)\right), \qquad t \in (0,1], \tag{4.5.15}$$

$$\frac{\partial T}{\partial n}(1,t) = 2 + (1+2t)^4 - f\left(T(1,t)\right), \qquad t \in (0,1]. \tag{4.5.16}$$

Also the extra condition is in this case is the boundary temperature $T(0,t) = h(t) = 2t$ and this is obtained from the analytical solution $T(x,t) = x^2 + 2t$. We then seek to retrieve the radiative fourth-order power law $f(T) = T^4$.

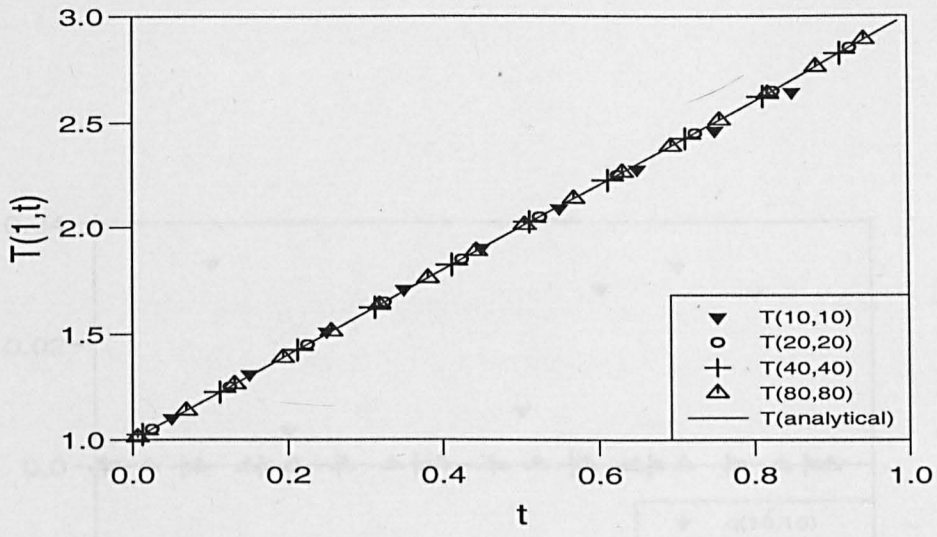

Figure 4.37: The analytical and numerical boundary temperature $T(1,t)$, as functions of time t, for the IHCP given by Example 4.8, for various (N, N_0), no noise and $K = 4$.

For no noise, $K = 4$ and the number of discretizations is increased from $(N, N_0) = (10, 10)$ to (80,80), using the BEM generates accurate and rapidly converging results for the boundary temperature $T(1,t)$, see Figure 4.37, the heat fluxes $q(0,t)$ and $q(1,t)$, see Figure 4.38, and the coefficients a_k of the function $f(T)$, see Table 4.7(a). These results compare well with the analytical values, and this indicates that the BEM can also be used with confidence to solve radiative problems with high accuracy.

Increasing K from 1 to 5, when the number of discretisations is maintained at $(N, N_0) = (40, 40)$ and there is no noise, results in approximations of the boundary temperature $T(1,t)$, see Figure 4.39, the heat fluxes $q(0,t)$ and $q(1,t)$, see Figures 4.40(a) and (b), respectively, and the coefficients a_k of the function $f(T)$ tabulated in Table 4.7(b), undergo a gradual improvement in accuracy. The best results of the approximations, which match with the analytical values, are obtained when $K = 4$. Similar findings are also evident in the approximations of the function $f(T)$, as in Figure 4.41(a) for the various degrees $K = \{3, 4, 5\}$, confirming that the BEM is a reliable method for solving the IHCP with radiative boundary conditions.

Finally, when $K = 4$, $(N, N_0) = (40, 40)$ and noise is introduced from $\rho = 0.01$ to 0.05, the results tabulated in Table 4.8 show, as expected, that the coefficients a_k, become more inaccurate as the amount of noise ρ increases. Figure 4.41(b) is a plot of the analytical and results of the approximations of the function $f(T)$ against T for various degrees $K = \{3, 4, 5\}$, when the amount of noise is $\rho = 0.01$. The results of the approximations of the function $f(T)$, are not

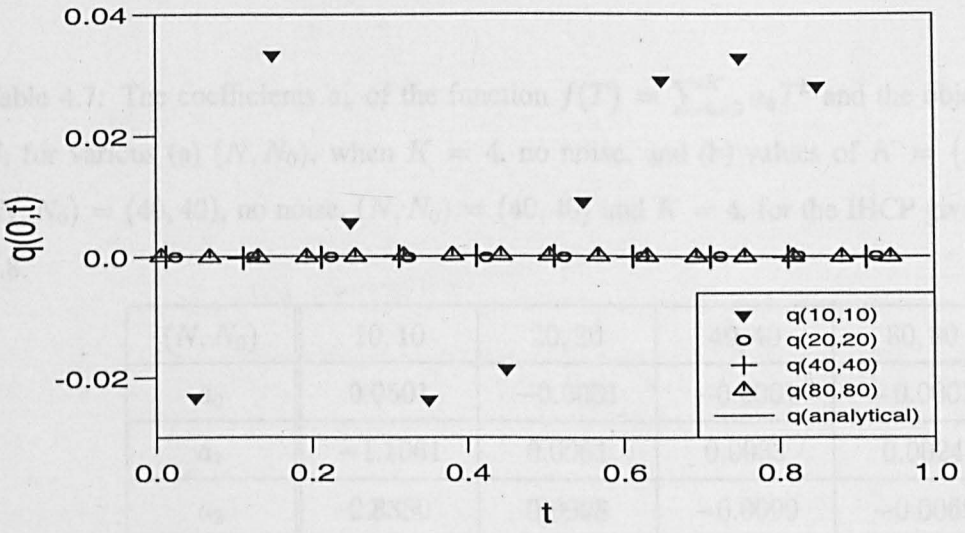

(a)

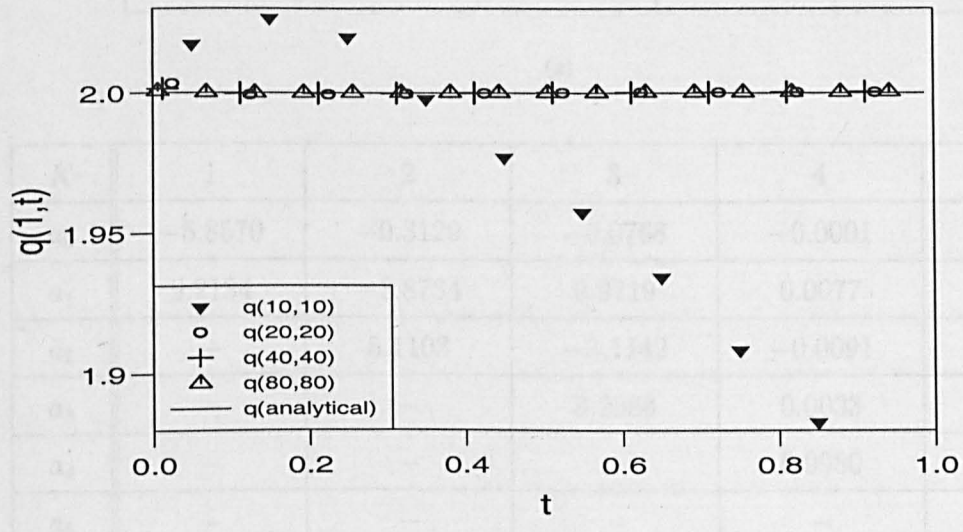

(b)

Figure 4.38: The analytical and numerical heat fluxes (a) $q(0,t)$ and (b) $q(1,t)$, as functions of time t, for the IHCP given by Example 4.8, for various (N, N_0) and $(N, N_0) = (40, 40)$, no noise and $K = 4$.

Table 4.7: The coefficients a_k of the function $f(T) = \sum_{k=0}^{K} a_k T^k$ and the objective function S, for various (a) (N, N_0), when $K = 4$, no noise, and (b) values of $K = \{1, ..., 5\}$, when $(N, N_0) = (40, 40)$, no noise, $(N, N_0) = (40, 40)$ and $K = 4$, for the IHCP given by Example 4.8.

(N, N_0)	$10, 10$	$20, 20$	$40, 40$	$80, 80$
a_0	0.0501	−0.0001	−0.0001	−0.0001
a_1	−1.1061	0.0061	0.0033	0.0024
a_2	2.8380	0.0098	−0.0090	−0.0069
a_3	−2.5262	−0.0833	0.0076	−0.0060
a_4	1.6949	0.9975	0.9980	0.9984

(a)

K	1	2	3	4	5
a_0	−5.8570	−0.3129	−0.0768	−0.0001	−0.0003
a_1	9.2134	−3.8734	0.9719	0.0077	0.0070
a_2	–	5.1103	−3.1142	−0.0091	0.0237
a_3	–	–	3.2386	0.0033	−0.0301
a_4	–	–	–	0.9980	0.9837
a_5	–	–	–	–	0.0032
S	2.3×10^{0}	2.0×10^{-1}	3.2×10^{-3}	2.7×10^{-8}	2.2×10^{-8}

(b)

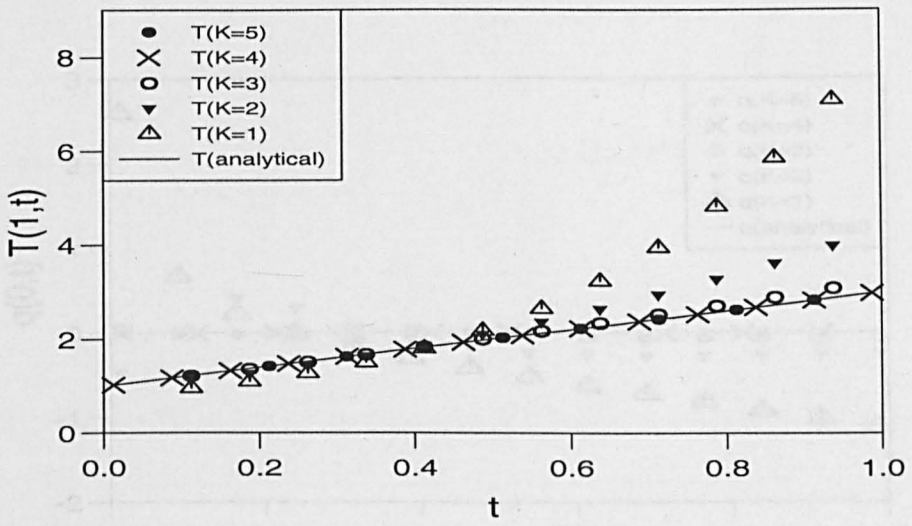

Figure 4.39: The analytical and numerical boundary temperature $T(1,t)$, as functions of time t, for the IHCP given by Example 4.8, for various $K = \{1, ..., 5\}$, when $(N, N_0) = (40, 40)$ and no noise.

Table 4.8: The coefficients a_k of the function $f(T) = \sum_{k=0}^{K} a_k T^k$ and the objective function S, for various amount of noise $\rho = \{0.00, ..., 0.05\}$, $(N, N_0) = (40, 40)$ and $K = 4$, for the IHCP given by Example 4.8.

	$\rho = 0.00$	$\rho = 0.01$	$\rho = 0.03$	$\rho = 0.05$
a_0	-0.0001	-0.0371	-0.1648	-0.0274
a_1	0.0033	-0.0300	-0.0765	-2.9659
a_2	-0.0090	-1.2438	1.4890	9.2772
a_3	0.0076	-1.7689	-1.3859	-8.1742
a_4	0.9980	1.5338	1.1496	2.9736
S	2.7×10^{-8}	1.7×10^{-2}	2.1×10^{-1}	4.8×10^{-1}

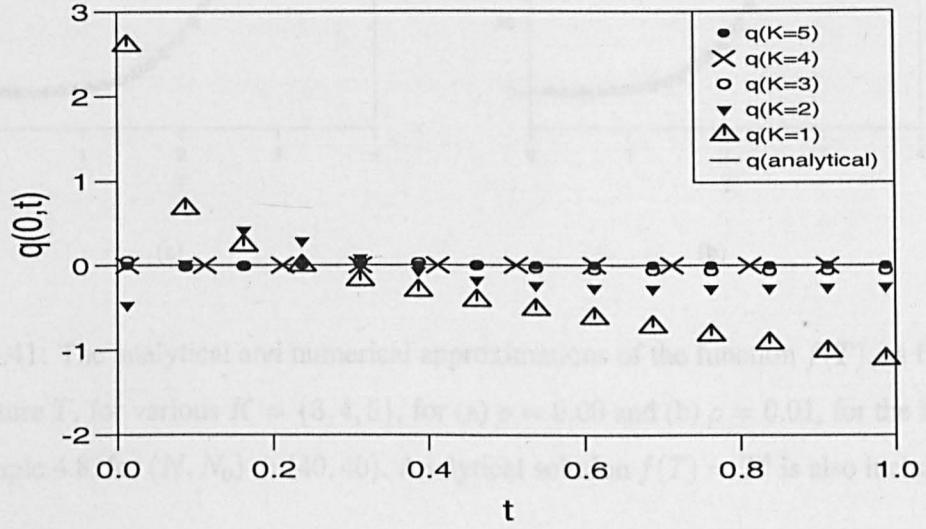

(a)

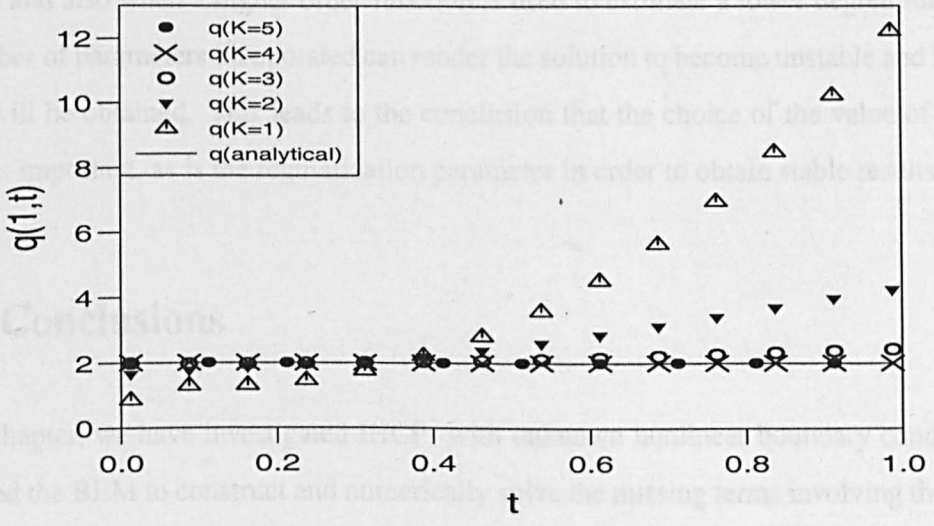

(b)

Figure 4.40: The analytical and numerical heat fluxes (a) $q(0,t)$, and (b) $q(1,t)$, as functions of time t, for the IHCP given by Example 4.8, for various $K = \{1, ..., 5\}$, when $(N, N_0) = (40, 40)$ and no noise.

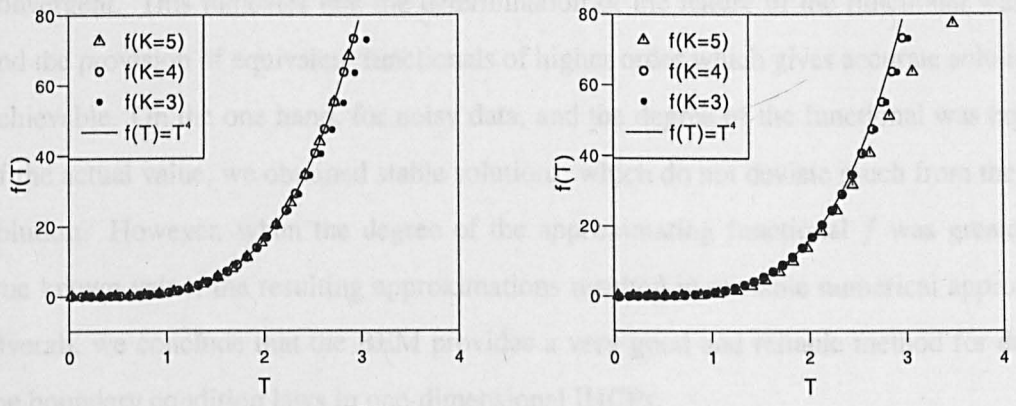

Figure 4.41: The analytical and numerical approximations of the function $f(T)$, as functions of temperature T, for various $K = \{3, 4, 5\}$, for (a) $\rho = 0.00$ and (b) $\rho = 0.01$, for the IHCP given by Example 4.8, for $(N, N_0) = (40, 40)$. Analytical solution $f(T) = T^4$ is also included.

accurate, when the degree of $f(T)$ is low, e.g. $K = 3$, or high, e.g. when $K = 5$. This confirms, that the prediction of the function with a lower degree cannot well approximate a higher order function and also when a higher order function is used to estimate a lower degree function then the number of parameters incoporated can render the solution to become unstable and hence poor results will be obtained. This leads to the conclusion that the choice of the value of the degree $K = 4$ is important, as is the regularization parameter in order to obtain stable results.

4.6 Conclusions

In this chapter, we have investigated IHCPs with unknown nonlinear boundary conditions. We have used the BEM to construct and numerically solve the missing terms involving the boundary temperature, heat flux, and coefficients of the function f relating to the boundary temperature and heat flux in the one-dimensional heat conduction. In the preliminaries, we investigated the equivalent DHCP in Examples 4.1−4.3 and found that the approximations of the numerical solutions were accurate and convergent to the analytical solutions. In the majority of this chapter we have investigated the boundary condition laws in heat conduction in inverse problems in Examples 4.4−4.8. In these examples, when the order of the estimating functional is equal to, or greater than, that of the actual known value, and no noise is introduced into the measured data, the results of the approximations using the BEM for the functional $f(T)$ are accurate, robust and

convergent. This indicates that the determination of the nature of the functional was possible, and the provision of equivalent functionals of higher order which gives accurate solutions is also achievable. On the one hand, for noisy data, and the degree of the functional was equal to that of the actual value, we obtained stable solutions, which do not deviate much from the analytical solution. However, when the degree of the approximating functional f was greater than the true known value, the resulting approximations resulted in unstable numerical approximations. Overall, we conclude that the BEM provides a very good and reliable method for determining the boundary condition laws in one-dimensional IHCPs.

Chapter 5

Reconstruction of boundary condition laws in two-dimensional steady inverse heat conduction problems

5.1 Introduction

In the previous chapters we have investigated some inverse heat conduction transient problems in one dimension. We now extend this study to the reconstruction of the boundary laws in some steady two-dimensional heat conduction problems. Recently, this research topic has attracted much interest due to its importance in many physical applications, such as in corrosion damage detection. The method used to determine the corrosion over part of a boundary involves potential and current density measurements over the uncorroded part of the boundary, see Inglese [42], Fasino and Inglese [27, 28, 29], Alessandrini *et al.* [1], Alessandrini and Sincich [2, 3].

In this chapter we consider a thermally conducting rectangular plate, whose top side is inaccessible and is in contact with a corroding liquid. We let $\Omega = (0,1)\times(0,d)$ be the rectangular domain representing the 2D transverse section of the metallic plate. The inaccessible side which is in contact with the corroding fluid is at $y = d$. Suppose that we are able to control the heat flux through the bottom side of the plate $y = 0$ of Ω. To measure the response in the temperature T, we assume that we are able, in finite time $t^* > 0$, to reach a steady temperature regime in Ω and keep this regime from time t^* onward. We also assume that t^* is small with respect to the time scale of the damage evolution. Therefore, the steady temperature T inside Ω obeys the Laplace

equation, and in the absence of corrosion at the interface $y = d$, heat exchange between the metal and fluid is described by the classical Newton cooling law, see Carslaw and Jaeger [17],

$$T_y(x, d) + \gamma(T(x, d) - T_{ext}) = 0, \tag{5.1.1}$$

where γ is the heat transfer coefficient at the interface and T_{ext} is the temperature of the fluid outside the top part of Ω. In order to simplify the notation used in equation (5.1.1), we assume $T_{ext} = 0$. Therefore, the constant γ is related to the ratio between the thermal conductivities of the fluid and the metal, and can be assumed to be non-negative for physical reasons. Further, for simplicity, the heat flux T_x through the vertical sides of Ω is assumed to be zero. Let $T(x, 0) = \psi^0(x)$ be the temperature that we observe on the bottom side of Ω when the top part is not damaged. We can then make regular readings of the temperature along the boundary $y = 0$. As soon as we observe a temperature ψ which is different from ψ^0, we are warned of damage on the surface at $y = d$.

To localize and evaluate the damage in a non-destructive framework, we first have to assume a model for the fluid-metal damage interface, namely a nonlinear boundary condition of the form

$$T_y(x, d) + \gamma f(T(x, d)) = 0, \tag{5.1.2}$$

(where T is the temperature satisfying $\nabla^2 T = 0$ in Ω, and $\gamma > 0$ is a scaling factor) to be investigated for the unknown function f, see Jones [44]. The inverse corrosion problem literature mainly deals with models based on loss of matter (LOM) or linear energy dispersion (LED) models. In LOM, the aim is to reconstruct changes occuring in the shape of the top boundary $y = d$ of Ω, subject to the boundary condition (5.1.2), see Kaup *et al.* [45], Inglese [42], Anderson and Ferris [6], etc. Time-dependent parabolic models based on LOM have also been widely studied, for example, see Bryan and Caudill [12, 13]. LED models connect corrosion with insulation breaking effects, so that we recover a positive constant coefficient γ in the Robin boundary condition analogous to (5.1.2), see Fasino and Inglese [27], Alessandrini *et al.* [1]. In these nonlinear IHCPs, we assume that the complex situation characterizing the presence of a corrosion attack on the upper surface of Ω produces a small change in the geometry, by products that precipitate on the surface and so on, and interacts with the heating in a way that can be described by a nonlinear perturbation of the boundary as:

$$T_y(x, d) + \gamma T(x, d) + \kappa h(T(x, d)) = 0. \tag{5.1.3}$$

In contrast to the linear problem described in equation (5.1.1), in equation (5.1.3) we do not

assume any knowledge of the nonlinear term $h(T(x,d))$, although γ and κ are assumed known constants.

In sections 5.4, we aim to determine the function $h(T)$ in the boundary condition (5.1.3), which models the possible presence of corrosion damage, by applying a nontrivial heat flux $T_y(x,0)$ on a suitable portion of the boundary, say $y = 0$, of the conductor and measuring the temperature $T(x,0)$ on the same portion of the boundary. Specifically, in section 5.2, we describe how the BEM is used to solve both direct and inverse problems numerically.

5.2 The Boundary Element Method (BEM)

Laplace's equation governs the physical process of steady heat conduction. The equation can be transformed into an equivalent boundary integral equation by use of the divergence theorem and approximating the integral equation numerically by a system of linear equations involving temperature and its normal derivative representing the heat flux. If either the temperature T or the heat flux $\frac{\partial T}{\partial n}$ is specified at all points on the boundary of the solution domain then the other quantity can be obtained by solving a system of linear algebraic equations. Then, using the calculated information, the temperature in the whole domain can be retrieved uniquely. This is a well-posed problem and can be solved using a direct inversion scheme, such as the Gaussian elimination method.

However, it is important to note that some physical processes are not well-posed due to the fact that it is diffficult to measure either the temperature or the heat flux on all the boundaries. In such processes, for example corrosion detection, we can assume the boundary under investigation is inaccessible and the information on it underspecified. In which case we must make measurements, or overspecify information from other accessible boundaries, e.g. on $y = 0$, to compensate. Problems of such a nature are ill-posed, and the solutions can only be obtained by means of stable approximations.

5.2.1 The discretised Laplace equation

A regular bounded domain Ω represents the region occupied by a metal conductor, which contains no heat sources, and is modelled by the Laplace equation so that the temperature T

satisfies

$$\nabla^2 T = 0 \qquad \text{in } \Omega. \tag{5.2.1}$$

The Laplace equation (5.2.1) is transformed into an equivalent integral equation through the application of the divergence theorem to the vector function $U\nabla V$ to obtain, see Jawson and Symm [43],

$$\int_{\partial\Omega} \left[T\frac{\partial G}{\partial n} - G\frac{\partial T}{\partial n} \right] dS = \eta(\underline{x})T(\underline{x}). \tag{5.2.2}$$

In two dimensions the coefficient $\eta(\underline{x})$ equals 1 if $\underline{x} \in \Omega$ and $\eta(\underline{x}) = 0.5$ if $\underline{x} \in \partial\Omega$ (smooth), and

$$G(\underline{x}, \underline{y}) = G(|\underline{x} - \underline{y}|) = \frac{1}{2\pi}\ln(r), \qquad \text{where } r = |\underline{x} - \underline{y}|, \tag{5.2.3}$$

is the fundamental solution of the two-dimensional Laplace equation (5.2.1).

In general it is not possible to solve the integral equation (5.2.2) analytically and a numerical approach becomes the only viable means. The approach involves discretising the boundary $\partial\Omega$ into a series of say N boundary elements $\partial\Omega_j$, for $j = \overline{1, N}$, such that piecewise constant variations of T and $\frac{\partial T}{\partial n}$ are assumed over the boundary $\partial\Omega$. The boundary integral equation (5.2.2) then approximates as follows:

$$\sum_{j=1}^{N} \left[T_j \int_{\partial\Omega_j} \frac{\partial G(\underline{x}, \underline{y})}{\partial n} \mathrm{d}S - T'_j \int_{\partial\Omega_j} G(\underline{x}, \underline{y}) \mathrm{d}s \right] = \eta(\underline{x})T(\underline{x}), \qquad \underline{x} \in \overline{\Omega}, \tag{5.2.4}$$

where $T_j = T(\underline{\widetilde{y}}_j)$, $T'_j = \frac{\partial T}{\partial n}(\underline{\widetilde{y}}_j)$ and $\underline{\widetilde{y}}_j$ is the centroid node (mid point) of the boundary element $\partial\Omega_j$ for $j = \overline{1, N}$. Taking $\underline{x} = \underline{\widetilde{y}}_i$ for $i = \overline{1, N}$, we obtain a system of linear algebraic equations

$$\sum_{j=1}^{N} \left[A_{ij}T_j + B_{ij}T'_j \right] = 0, \qquad i = \overline{1, N}, \tag{5.2.5}$$

where

$$A_{ij} = \int_{\partial\Omega_j} \frac{\partial G(\underline{\widetilde{y}}_i, \underline{y})}{\partial n} \mathrm{d}S - \eta(\underline{\widetilde{y}}_i)\delta_{ij}, \qquad B_{ij} = -\int_{\partial\Omega_j} G(\underline{\widetilde{y}}_i, \underline{y}) \mathrm{d}S \tag{5.2.6}$$

and δ_{ij} is the Kronecker delta symbol.

In the two-dimensional rectangular domain $\Omega \subset \mathbb{R}^2$, whose boundary is subdivided into straight-line segments $\partial\Omega_j$, the integral coefficients given in expressions (5.2.6) can be evaluated analytically, see Symm and Pitfield [81]. The discretised version of the Laplace equation (5.2.1) results in a system of N algebraic equations (5.2.5) with $2N$ unknowns. From the known boundary conditions one can prescribe N of the $2N$ unknowns. Hence, through substitution we obtain a system of N equations with N unknowns that can now be solved to obtain the remaining N boundary unknowns.

5.2.2 Discretised boundary conditions for the DHCP

In the absence of corrosion, the problem can be modelled as a linear DHCP in a rectangular transverse section of a thermally conducting material with no heat source given by

$$\nabla^2 T = 0 \quad \text{in } \Omega = (0,1) \times (0,d), \tag{5.2.7}$$

$$\frac{\partial T}{\partial n} = \varphi, \quad \text{on } \Gamma_1 = [0,1] \times \{0\}, \tag{5.2.8}$$

$$\frac{\partial T}{\partial n} = c_1 T + c_0 \quad \text{on } \Gamma_3 = (0,1) \times \{d\}, \tag{5.2.9}$$

$$\frac{\partial T}{\partial n} = 0, \quad \text{on } \Gamma_2 = \{1\} \times [0,d] \cup \Gamma_4 = \{0\} \times [0,d]. \tag{5.2.10}$$

where φ is a specified heat flux on the bottom side $y = 0$, $c_0 = \gamma T_{\text{ext}}$, $c_1 = -\gamma$, see (5.1.1), and n is the outward unit normal to the boundary.

Let N_1,...,N_4 denote the number of boundary elements on the boundaries Γ_1,...,Γ_4, respectively. For a uniform discretisation we require $N_1 = N_3$ and $N_2 = N_4 = dN_1$. Assuming that the heat flux and boundary temperature are constant over each boundary segment $\partial\Omega_j = [(x_{j-1}, y_{j-1}), (x_j, y_j)]$ then the discretised boundary conditions (5.2.8)–(5.2.10) become

$$T_i' = \varphi(\widetilde{x}_i, \widetilde{y}_i) = \varphi_i, \qquad i = \overline{1, N_1}, \tag{5.2.11}$$

$$T_i' = c_1 T(\widetilde{x}_i, \widetilde{y}_i) + c_0 = c_1 T_i + c_0, \qquad i = \overline{N_1 + N_2 + 1, N_1 + N_2 + N_3}, \tag{5.2.12}$$

$$T_i' = 0, \qquad i = \{\overline{N_1 + 1, N_1 + N_2}, \overline{N_1 + N_2 + N_3 + 1, N}\}, \tag{5.2.13}$$

where $N = N_1 + N_2 + N_3 + N_4$ and $(\widetilde{x}_i, \widetilde{y}_i)$ is the midpoint of $\partial\Omega_i$ for $i = \overline{1, N}$.

Substituting equations (5.2.11)–(5.2.13) into (5.2.5), and using elimination, $2N$ unknowns in the square system of linear N equations (5.2.5) reduces to N. This allows for a straightforward inversion of the linear system of algebraic equations for the DHCP which on rewriting becomes

$$\begin{aligned} \sum_{j=1}^{N_1+N_2} A_{ij} T_j + \sum_{j=N_1+N_2+1}^{N_1+N_2+N_3} (A_{ij} + c_1 B_{ij}) T_j + \sum_{j=N_1+N_2+N_3+1}^{N} A_{ij} T_j \\ = -\sum_{j=1}^{N_1} B_{ij} \varphi_j - c_0 \sum_{j=N_1+N_2+1}^{N_1+N_2+N_3} B_{ij}, \qquad i = \overline{1, N}. \end{aligned} \tag{5.2.14}$$

We can solve the system of linear equations (5.2.14) using the Gaussian elimination method.

In the event that corrosion occurs in the experiment, the Laplacian boundary value problem for the corrosion damage detection can then be described by equations (5.2.7), (5.2.8), (5.2.10), and

replacing equation (5.2.9) derived from equation (5.1.1) by equation (5.1.3) which is rewritten as

$$\frac{\partial T}{\partial n} + \gamma T + \kappa h(T) = 0 \quad \text{on } \Gamma_3 = (0,1) \times \{d\}. \tag{5.2.15}$$

Specifying the values of the parameters γ and κ, and the nonlinear function $h(T)$, we obtain a system of nonlinear equations for a nonlinear DHCP.

On discretisation, the boundary condition (5.2.15) becomes

$$T_i' + \gamma T_i + \kappa h(T_i) = 0 \qquad \text{for } i = \overline{N_1 + N_2 + 1, N_1 + N_2 + N_3}. \tag{5.2.16}$$

Then the equivalent system to (5.2.15) in the nonlinear situation is given by

$$\begin{aligned} \sum_{j=1}^{N_1+N_2} A_{ij} T_j + \sum_{j=N_1+N_2+1}^{N_1+N_2+N_3} \left[\left(A_{ij} - \gamma B_{ij} \right) T_j - \kappa B_{ij} h(T_j) \right] + \sum_{j=N_1+N_2+N_3+1}^{N} A_{ij} T_j \\ = - \sum_{j=1}^{N_1} B_{ij} \varphi_j, \qquad i = \overline{1, N}. \end{aligned} \tag{5.2.17}$$

We can solve the system of nonlinear equations (5.2.17) using the NAG routine C05NDF.

5.2.3 Discretised boundary conditions for the IHCP

In the IHCP, the portion Γ_1 of the boundary is accessible to both temperature and heat flux measurements, while the portion Γ_3, where the corrosion may take place, is out of reach such that no information on it is specified. Therefore, we have the Cauchy data specification on Γ_1

$$\frac{\partial T}{\partial n} = \varphi, \quad T = \psi \qquad \text{on } \Gamma_1 \tag{5.2.18}$$

and no boundary condition is specified on Γ_3. The discretisation of (5.2.18) results in

$$T_i' = \varphi_i, \quad T_i = \psi(\widetilde{x}_i, \widetilde{y}_i) = \psi_i, \quad \text{for } i = \overline{1, N_1}. \tag{5.2.19}$$

The IHCP is described by equations (5.2.7), (5.2.10) and (5.2.18).

Substituting (5.2.13) and (5.2.19) into (5.2.5) results in the following linear system of equations

$$\begin{aligned} \sum_{j=N_1+1}^{N_1+N_2} A_{ij} T_j + \sum_{j=N_1+N_2+1}^{N_1+N_2+N_3} \left(A_{ij} T_j + B_{ij} T_j' \right) + \sum_{j=N_1+N_2+N_3+1}^{N} A_{ij} T_j \\ = - \sum_{j=1}^{N_1} \left(A_{ij} \psi_j + B_{ij} \varphi_j \right), \qquad i = \overline{1, N}. \end{aligned} \tag{5.2.20}$$

This is a linear system of N equations with $N_2 + 2N_3 + N_4$ unknowns, and for a unique solution we require $N_1 \geq N_3$. However, since the Cauchy problem (5.2.7), (5.2.10) and (5.2.18) is ill-posed then this system is ill-conditioned and requires regularization, see Tikhonov and Arsenin [83]. That is, instead of the unstable inversion $\mathbf{Y} = C^{-1}\mathbf{Z}$ of the system of equations (5.2.20), generically written as $C\mathbf{Y} = \mathbf{Z}$, we employ the regularized inversion

$$\mathbf{Y}_\lambda = (C^{\mathrm{tr}}C + \lambda I)^{-1} C^{\mathrm{tr}}\mathbf{Z} \tag{5.2.21}$$

of the system $(C^{\mathrm{tr}}C + \lambda I)\,\mathbf{Y} = C^{\mathrm{tr}}\mathbf{Z}$. In (5.2.21), $\lambda > 0$ is a regularization parameter whose choice could be based on, for example, the L-curve criterion, see Hansen [35].

Once stable values of T and $\frac{\partial T}{\partial n}$ on Γ_3 have been found, then the search for the nonlinear function f can be directly constructed from (5.1.2) if $T|_{\Gamma_3}$ is monotone. Otherwise, as it occurs in Figures 5.11 (a), 5.14 (a), 5.19 (a) and 5.22 (a) for certain values of λ, if $T|_{\Gamma_3}$ is not monotone, see Figures 5.12 (a), 5.15 (a), 5.20 and 5.23, equation (5.1.2) can be regularised as described in Engl *et al.* [24].

At this stage, it is worth noting that our BEM regularised approach is different from the recent investigation of Cao *et al.* [16], compare Cao and Pereverzev [15], who used the finite element method, as well as from the BEM unregularised approach of Fasino and Inglese [28] who used instead of (5.2.21) a finite-dimensional polynomial parametrisation of the unknown corrosion law function f in (5.1.2).

5.3 Numerical Examples, Results and Discussion

Example 5.1

In order to illustrate the method employed, we consider the steady-state heat conduction problem described by the Laplace equation

$$\nabla^2 T(x,y) = 0, \qquad (x,y) \in (0,1) \times (0, d = 0.1), \tag{5.3.1}$$

and the boundary conditions

$$-\frac{\partial T}{\partial y}(x,y) = \pi\cos(\pi x), \qquad (x,y) \in \Gamma_1 = [0,1] \times \{0\}, \tag{5.3.2}$$

$$\frac{\partial T}{\partial x}(x,y) = 0, \qquad (x,y) \in \Gamma_2 = \{1\} \times [0,d] \cup \Gamma_4 = \{0\} \times [0,d], \tag{5.3.3}$$

$$\frac{\partial T}{\partial y}(x,y) = g(T(x,y)), \qquad (x,y) \in \Gamma_3 = (0,1) \times \{d\}. \tag{5.3.4}$$

Therefore, we solve a DHCP to determine the temperature T on the boundary $\partial\Omega$ and the heat flux $\frac{\partial T}{\partial y}$ on the boundary Γ_3. If $g(T) = -\pi T + \pi$, then this is a linear DHCP whose exact solution is given by

$$T(x, y) = \cos(\pi x)\exp(-\pi y) + 1. \tag{5.3.5}$$

The linear DHCP is well-posed and therefore is solvable easily by direct inversion of (5.2.14) using the Gaussian elimination method. Figures 5.1 and 5.2 illustrate the boundary temperature

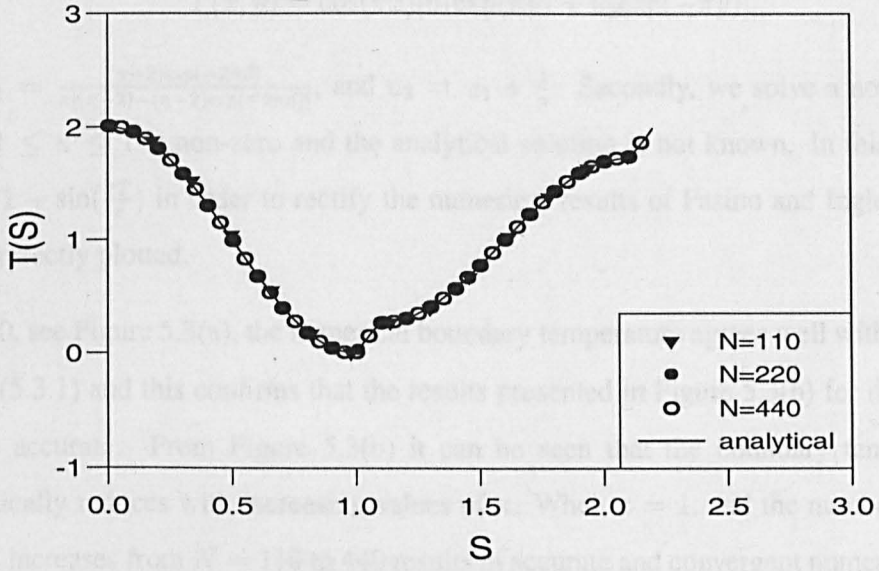

Figure 5.1: The numerical and analytical temperature T on the boundary $\partial\Omega$ for the DHCP in Example 5.1.

$T|_{\partial\Omega}$ ploted as a function of the arc-length $0 \leq S \leq 2 + 2d = 2.2$ starting from the origin, and the heat flux $\frac{\partial T}{\partial y}|_{\Gamma_3} = q$, respectively. The results are accurate in that they compare very well with the exact solution and when the number of boundary elements N increases from 110 to 440, there is a fine improvement in the numerical solutions.

Example 5.2

Now we consider the steady-state heat conduction problem described by the Laplace equation

(5.3.1) and the nonlinear boundary conditions

$$-\frac{\partial T}{\partial y}(x,y) = \cos(\pi x), \qquad (x,y) \in \Gamma_1 = [0,1] \times \{0\}, \tag{5.3.6}$$

$$\frac{\partial T}{\partial x}(x,y) = 0, \qquad (x,y) \in \Gamma_2 = \{1\} \times [0,d] \cup \Gamma_4 = \{0\} \times (0,d), \tag{5.3.7}$$

$$\frac{\partial T}{\partial y}(x,y) + \gamma T(x,y) + \kappa h(T(x,y)) = 0, \qquad (x,y) \in \Gamma_3 = (0,1) \times \{d\}. \tag{5.3.8}$$

We take $\gamma = 2$ and first we solve a linear DHCP for $\kappa = 0$ whose exact solution is given by

$$T(x,y) = \cos(\pi x)[u_1 \exp(\pi y) + u_2 \exp(-\pi y)], \tag{5.3.9}$$

where $u_1 = \frac{(\pi-2)\exp(-2\pi d)}{\pi[(\pi+2)-(\pi-2)\exp(-2\pi d)]}$, and $u_2 = u_1 + \frac{1}{\pi}$. Secondly, we solve a nonlinear DHCP when $-1 \leq \kappa \leq 1$ is non-zero and the analytical solution is not known. In this case we take $h(T) = 1 - \sin(\frac{2T}{\pi})$ in order to rectify the numerical results of Fasino and Inglese [28] which were incorrectly plotted.

For $\kappa = 0$, see Figure 5.3(a), the numerical boundary temperature agrees well with the analytical solution (5.3.1) and this confirms that the results presented in Figure 5.3(b) for different values of κ are accurate. From Figure 5.3(b) it can be seen that the boundary temperature $T|_{\Gamma_1}$ monotonically reduces with increasing values of κ. When $\kappa = 1$, and the number of boundary elements increases from $N = 110$ to 440 results in accurate and convergent numerical results for $T|_{\partial\Omega}$ and the heat flux $q|_{\Gamma_3}$, see Figures 5.4(a) and 5.4(b), respectively.

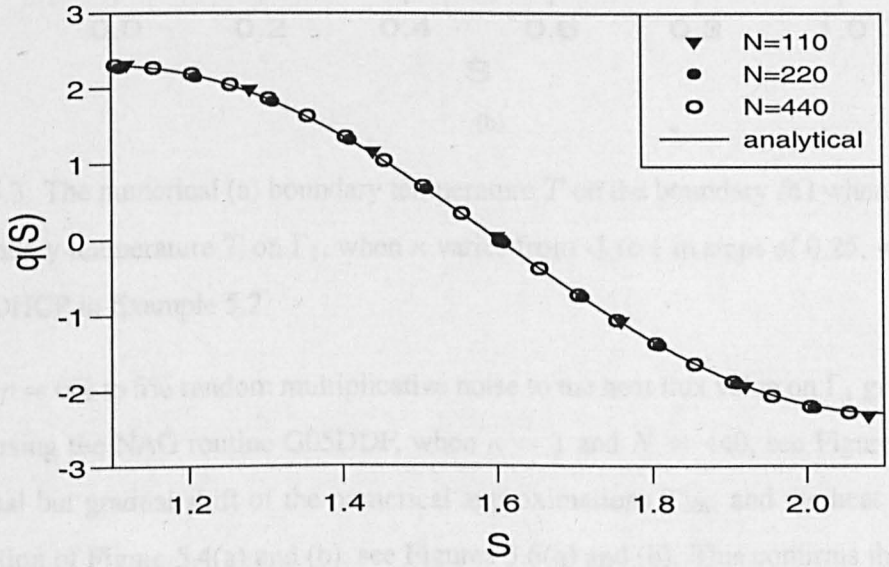

Figure 5.2: The numerical and analytical heat flux $q = \frac{\partial T}{\partial y}$ on the boundary Γ_3 for the DHCP in Example 5.1.

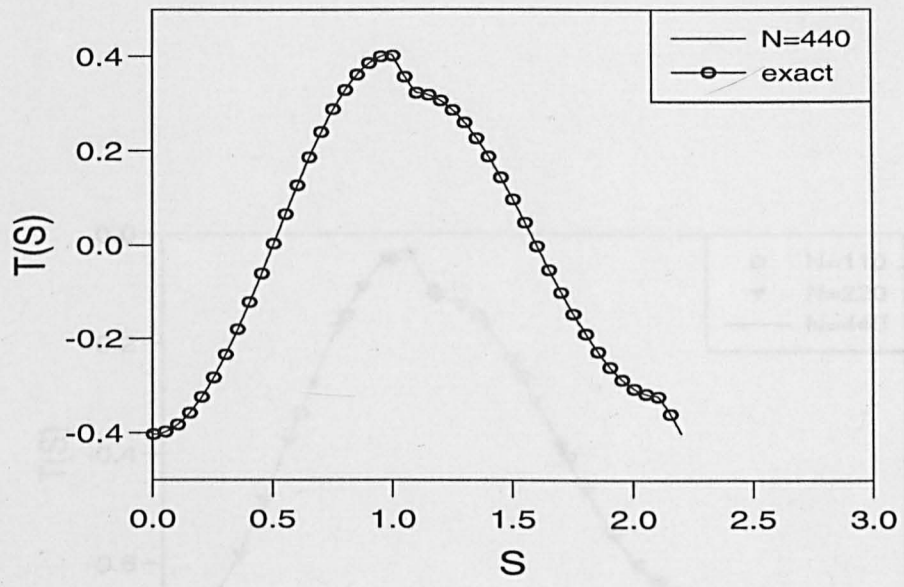

(a)

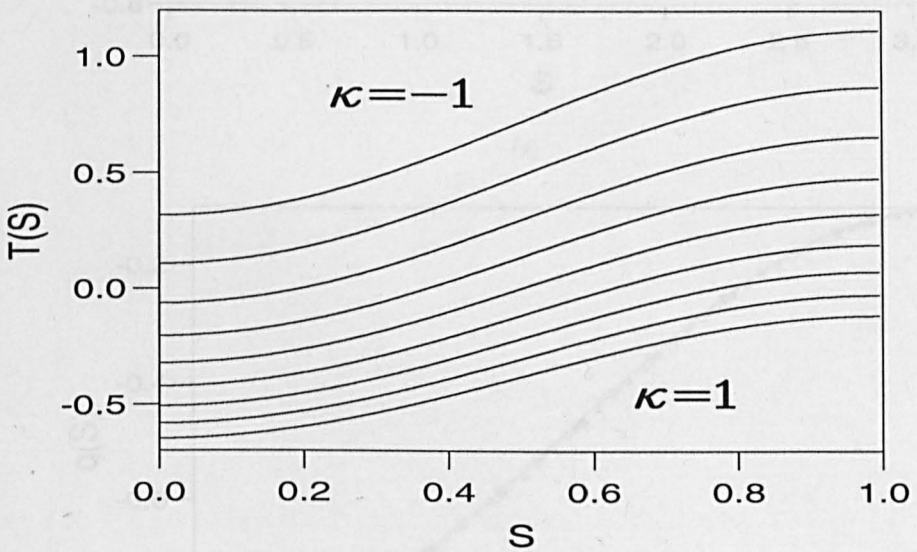

(b)

Figure 5.3: The numerical (a) boundary temperature T on the boundary $\partial\Omega$ when $\kappa = 0$, and (b) the boundary temperature T on Γ_1, when κ varies from -1 to 1 in steps of 0.25, when $N = 440$, for the DHCP in Example 5.2.

Adding $\rho = 0\%$ to 5% random multiplicative noise to the heat flux value on Γ_1 given in equation (5.3.6) using the NAG routine G05DDF, when $\kappa = 1$ and $N = 440$, see Figure 5.5, results in a minimal but gradual shift of the numerical approximations $T|_{\partial\Omega}$ and the heat flux $q|_{\Gamma_3}$, from the solution of Figure 5.4(a) and (b), see Figures 5.6(a) and (b). This confirms that the resulting numerical solutions are stable.

All the numerical results presented next are obtained for $N = 440$.

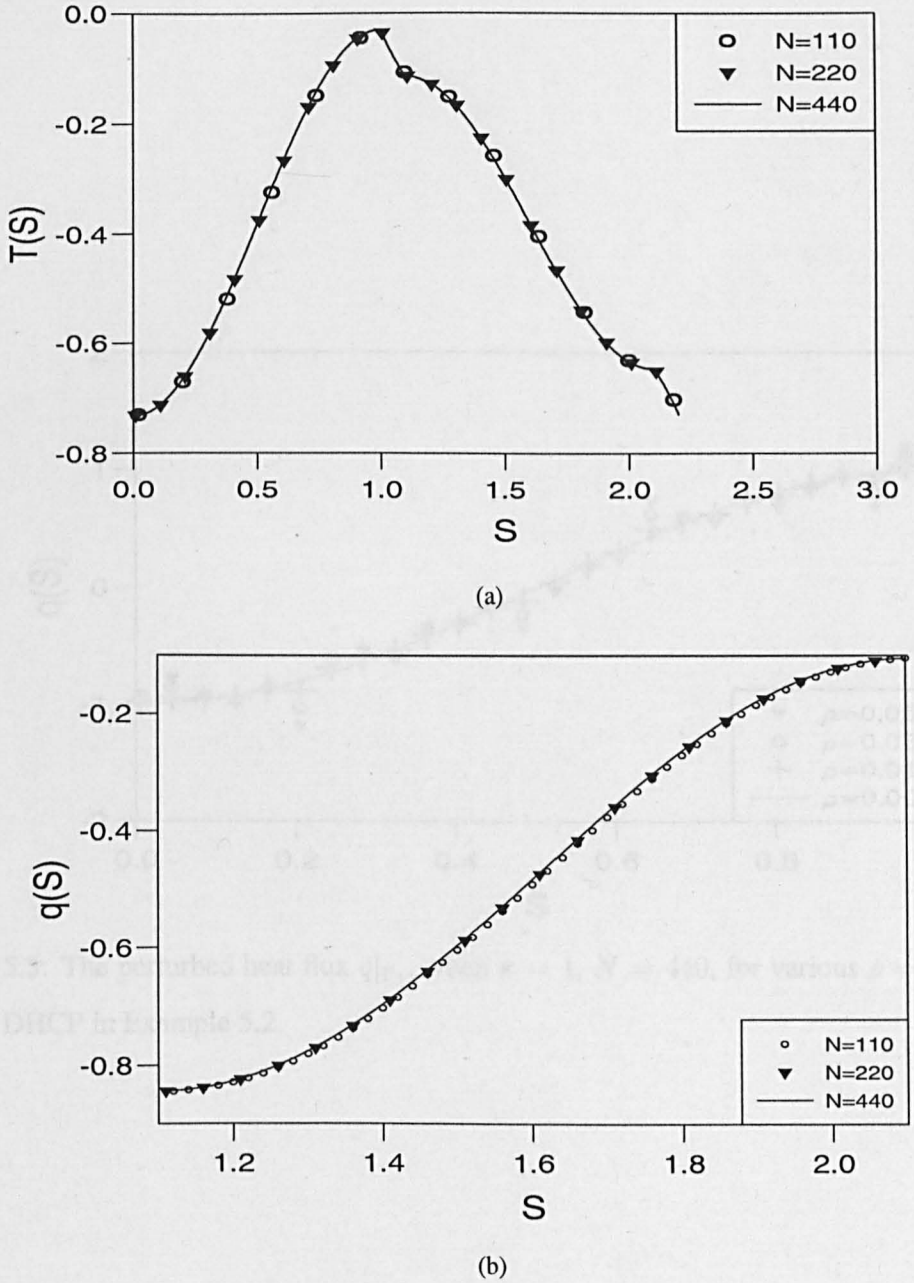

Figure 5.4: The numerical (a) boundary temperature on $\partial\Omega$, (b) heat flux q on Γ_3, for $\kappa = 1$, when N varies from 110 to 440, for the DHCP in Example 5.2.

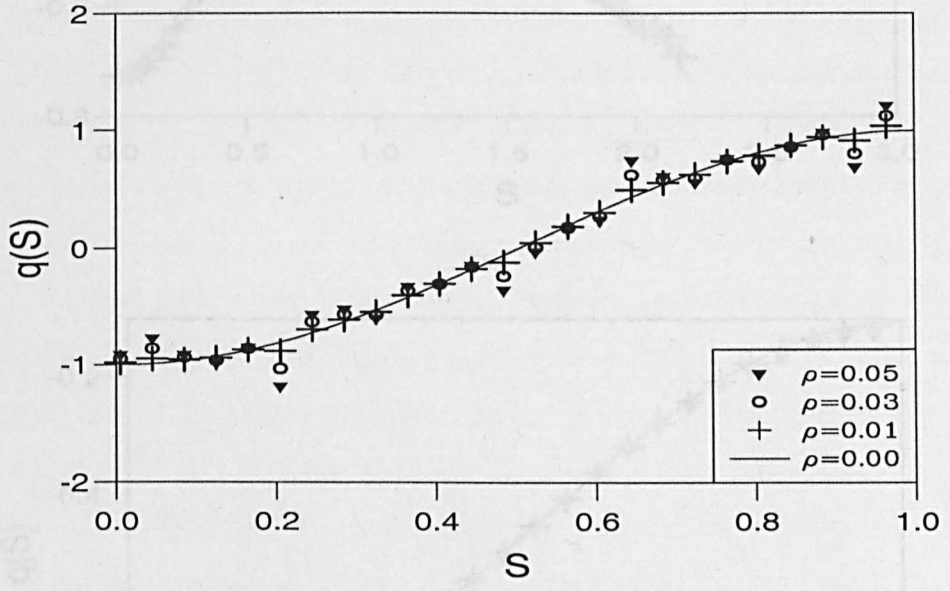

Figure 5.5: The perturbed heat flux $q|_{\Gamma_1}$, when $\kappa = 1$, $N = 440$, for various $\rho = 0.00$ to 0.05, for the DHCP in Example 5.2.

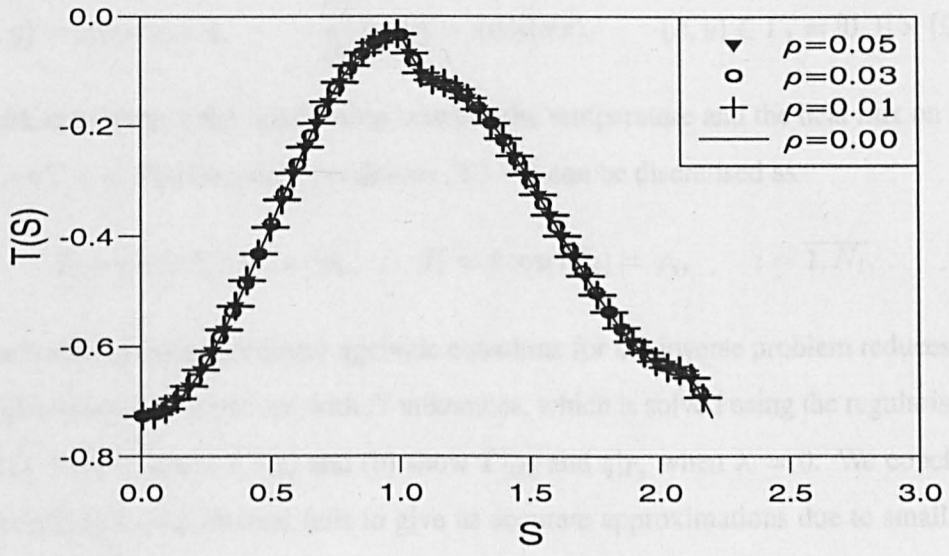

(a)

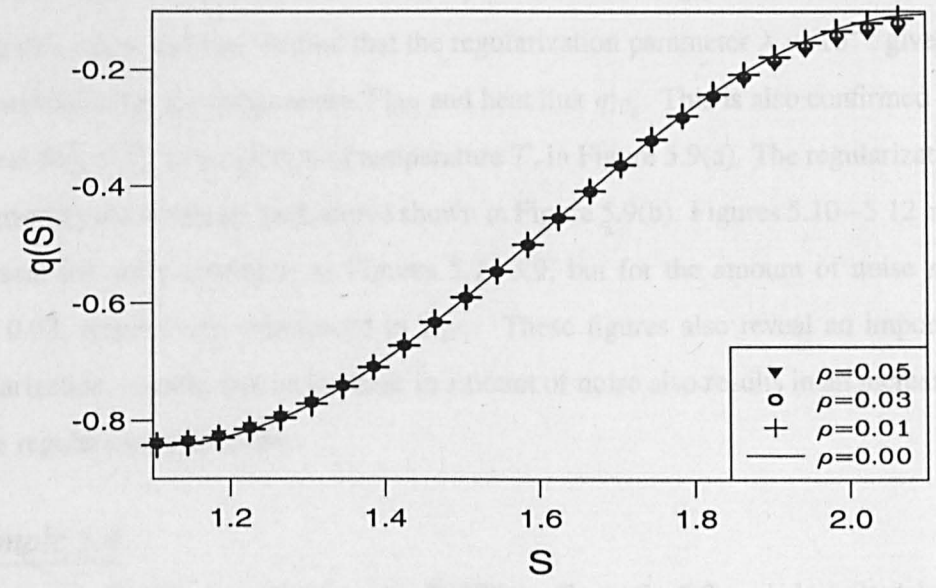

(b)

Figure 5.6: The numerical (a) boundary temperature $T|_{\partial\Omega}$, and (b) heat flux $q|_{\Gamma_3}$, when $\kappa = 1$, $N = 440$, for various $\rho = 0.00$ to 0.05, for the DHCP in Example 5.2.

Example 5.3

We consider the IHCP corresponding to the DHCP in Example 5.1 and described by the Laplace equation (5.3.1), the homogeneous Neumann boundary conditions (5.3.3) and the Cauchy boundary data on Γ_1

$$T(x,y) = \cos(\pi x) + 1, \qquad -\frac{\partial T}{\partial y}(x,y) = \pi\cos(\pi x), \qquad (x,y) \in \Gamma_1 = [0,1] \times \{0\}. \quad (5.3.10)$$

The task is to retrieve the relationship between the temperature and the heat flux on Γ_3 given by $T_y = -\pi T + \pi$. The boundary conditions (5.3.10) can be discretised as

$$T_i = cos(\pi\widetilde{x}_i) + 1 = \psi_i, \qquad T_i' = \pi\cos(\pi\widetilde{x}_i) = \varphi_i, \qquad i = \overline{1, N_1}. \quad (5.3.11)$$

The resulting system of linear agebraic equations for the inverse problem reduces to a system of N ill-conditioned equations with N unknowns, which is solved using the regularised inversion (5.2.21). First, Figures 5.7(a) and (b) show $T|_{\partial\Omega}$ and $q|_{\Gamma_3}$ when $\lambda = 0$. We conclude that the Gaussian elimination method fails to give us accurate approximations due to small errors in $\mathbf{Z}$, which are magnified on $\mathbf{Y}_0$ as a result of small, but non-zero, singular values of the matrix C. In order to stabilize the solutions we employ the Tikhonov regularisation, see equation (5.2.21). In Figures 5.8(a) and (b), we find that the regularization parameter $\lambda = 10^{-5}$ gives a very good approximation for the temperature $T|_{\partial\Omega}$ and heat flux $q|_{\Gamma_3}$. This is also confirmed by the plot of the heat flux $q(T)$, as a function of temperature T, in Figure 5.9(a). The regularization parameter λ is given by the corner of the L-curve shown in Figure 5.9(b). Figures 5.10–5.12 and 5.13–5.15 represent the same situations as Figures 5.7–5.9, but for the amount of noise $\rho = 0.01$ and $\rho = 0.03$, respectively, introduced in $T|_{\Gamma_1}$. These figures also reveal an important aspect in regularization, namely that an increase in amount of noise also results in an increase in the value of the regularising parameter.

Example 5.4

Consider the IHCP derived from the DHCP in Example 5.2 and described by the Laplace equation (5.3.1), the homogeneous Neumann boundary conditions (5.3.7) and the Cauchy boundary data on Γ_1

$$T(x,0) = \psi(x), \quad -\frac{\partial T}{\partial y} = \cos(\pi x), \qquad y = 0,\ x \in (0,1). \quad (5.3.12)$$

In (5.3.12), the Dirichlet data $\psi(x)$ is obtained by solving numerically the DHCP given by equations (5.3.1), (5.3.6)-(5.3.8) with $\kappa = 1$, $\gamma = 2$ and $h(T) = 1 - \sin(\frac{2T}{\pi})$.

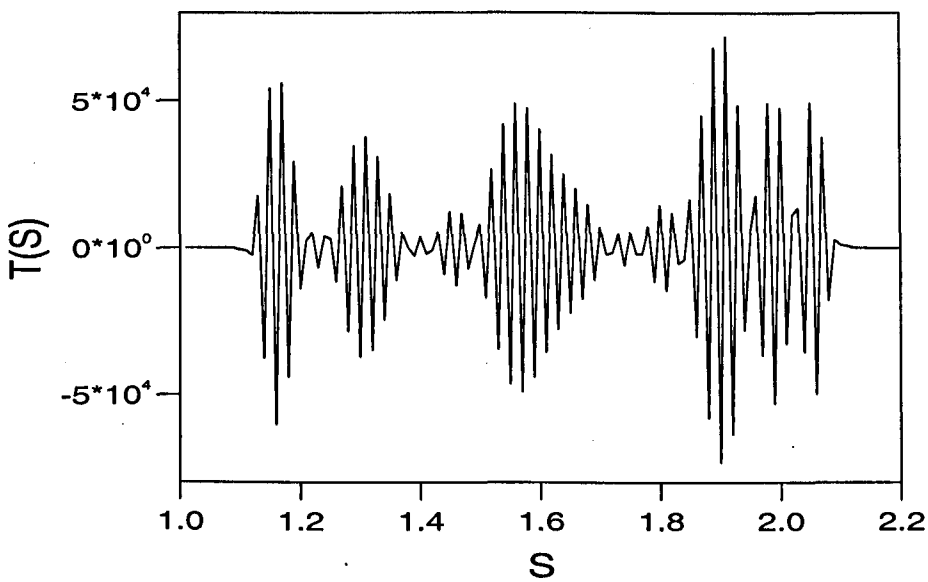

(a)

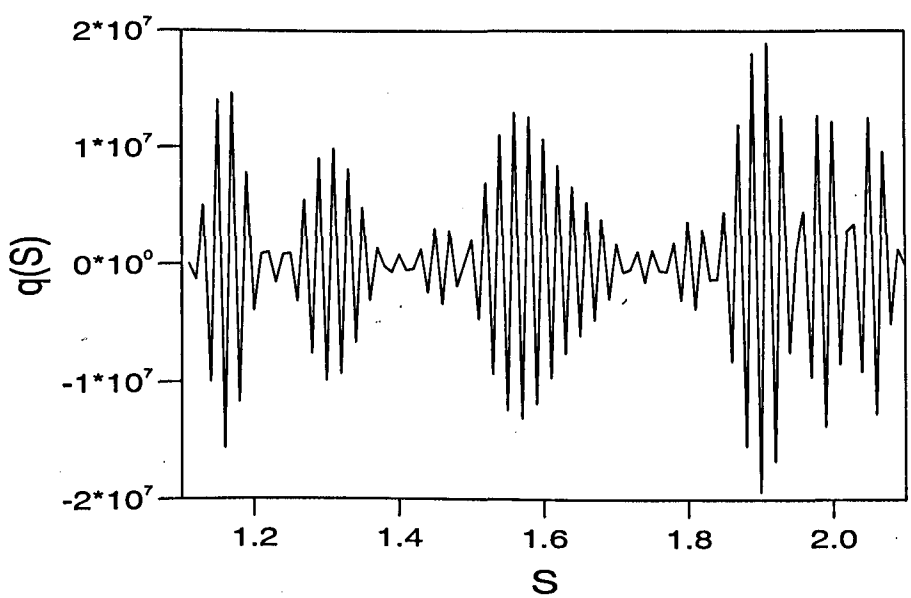

(b)

Figure 5.7: The numerical (a) boundary temperature $T|_{\partial\Omega}$ and (b) the heat flux $q|_{\Gamma_3}$, when $\lambda = 0$, when $\rho = 0.00$, for the IHCP in Example 5.3.

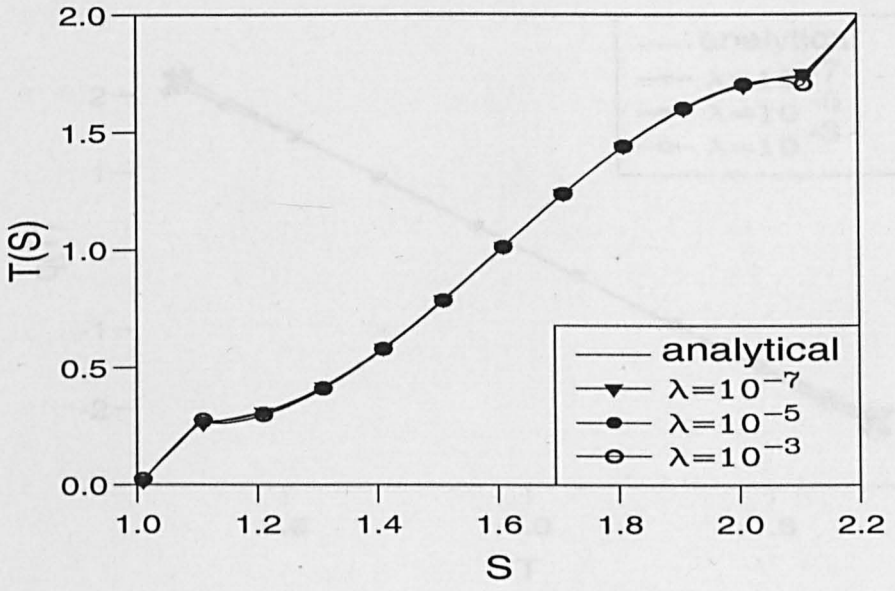

(a)

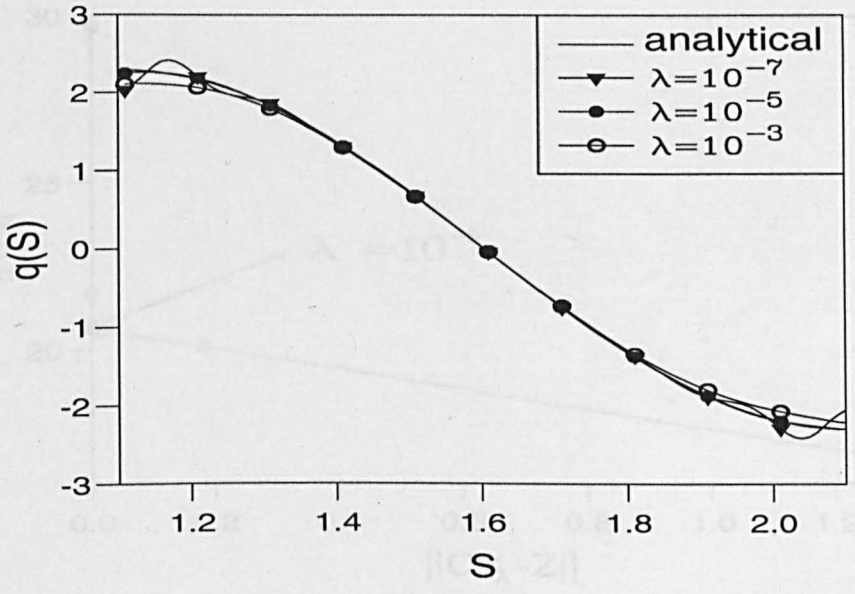

(b)

Figure 5.8: The analytical and regularised (a) boundary temperature $T|_{\partial\Omega}$, and (b) the heat flux $q|_{\Gamma_3}$, for various λ, when $\rho = 0.00$, for the IHCP in Example 5.3.

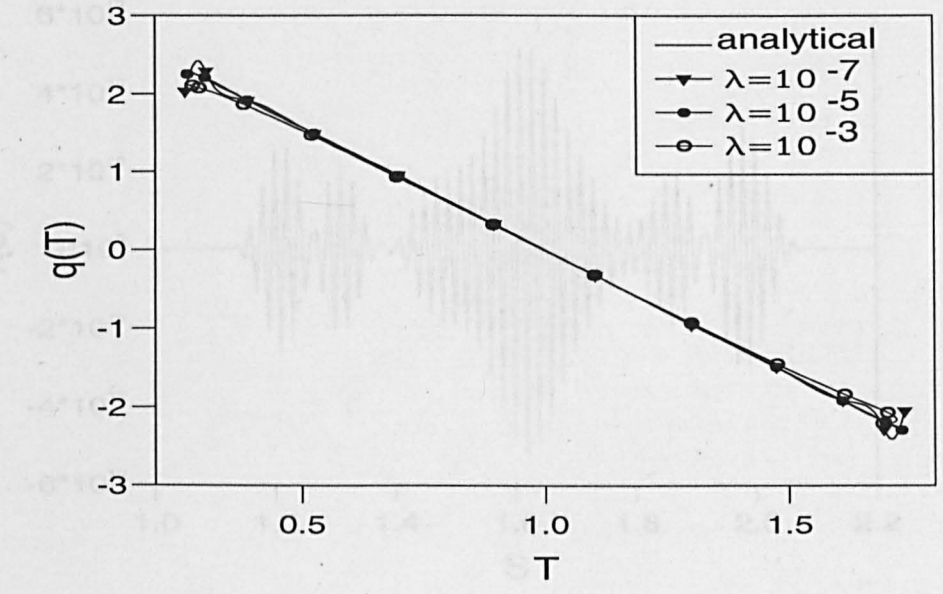

(a)

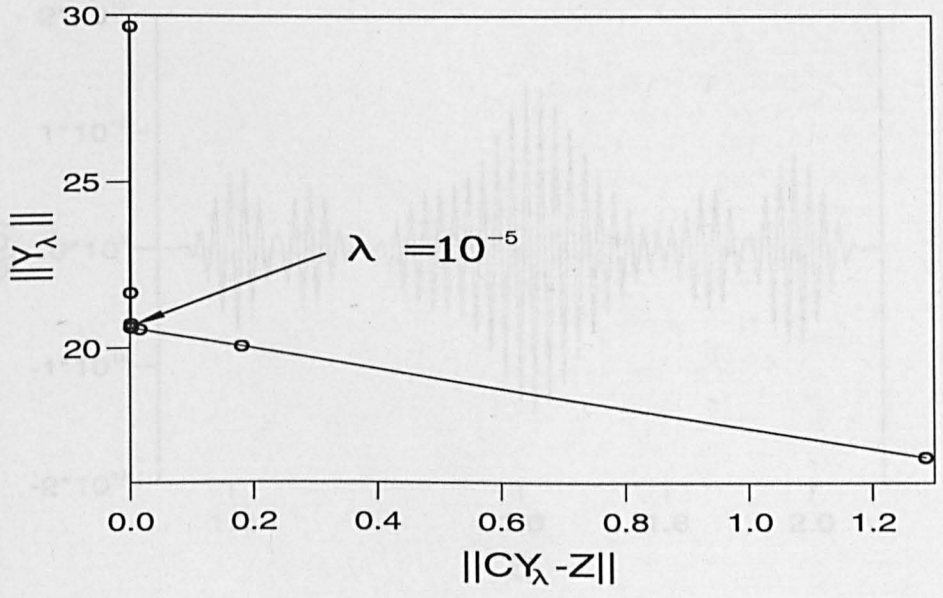

(b)

Figure 5.9: The (a) analytical and regularized heat flux $q(T)$ on Γ_3, for various λ, and (b) L-curve, when $\rho = 0.00$, for the IHCP in Example 5.3.

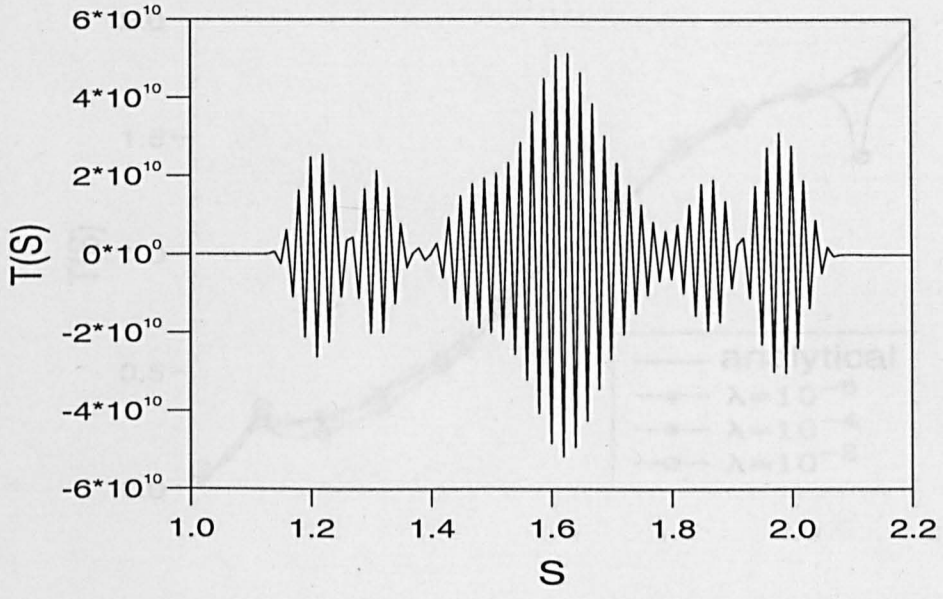

(a)

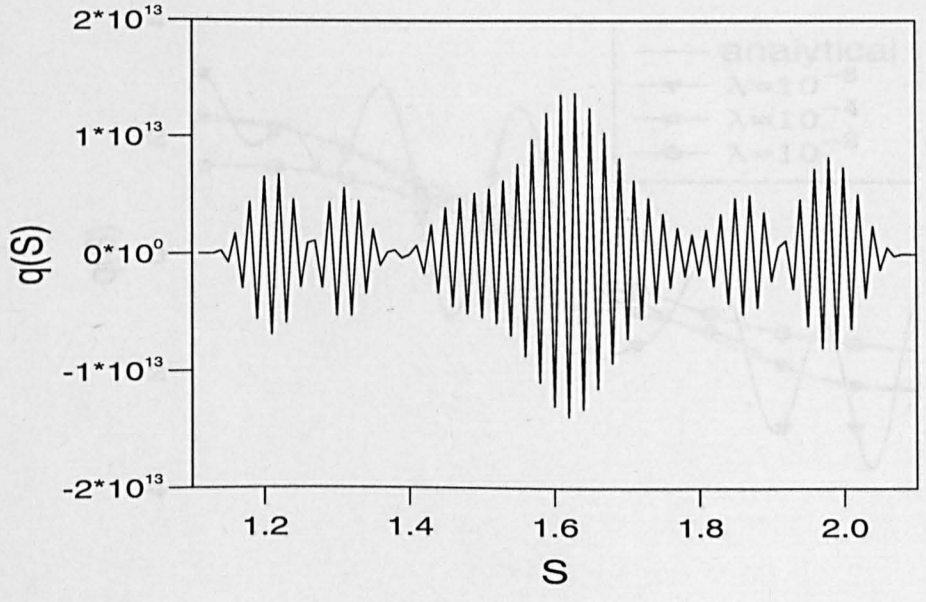

(b)

Figure 5.10: The numerical (a) boundary temperature $T|_{\partial\Omega}$, and (b) the heat flux $q|_{\Gamma_3}$, when $\lambda = 0$, when $\rho = 0.01$, for the IHCP in Example 5.3.

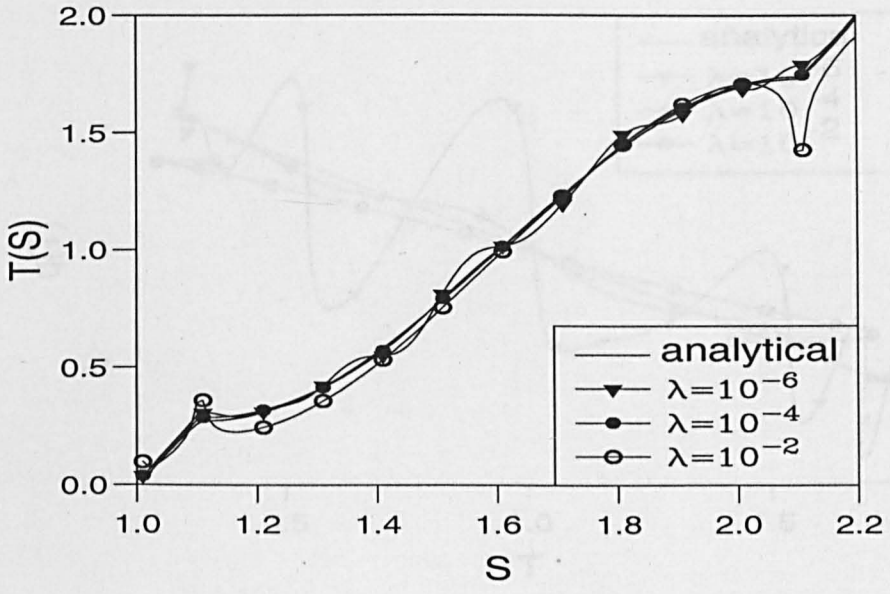

(a)

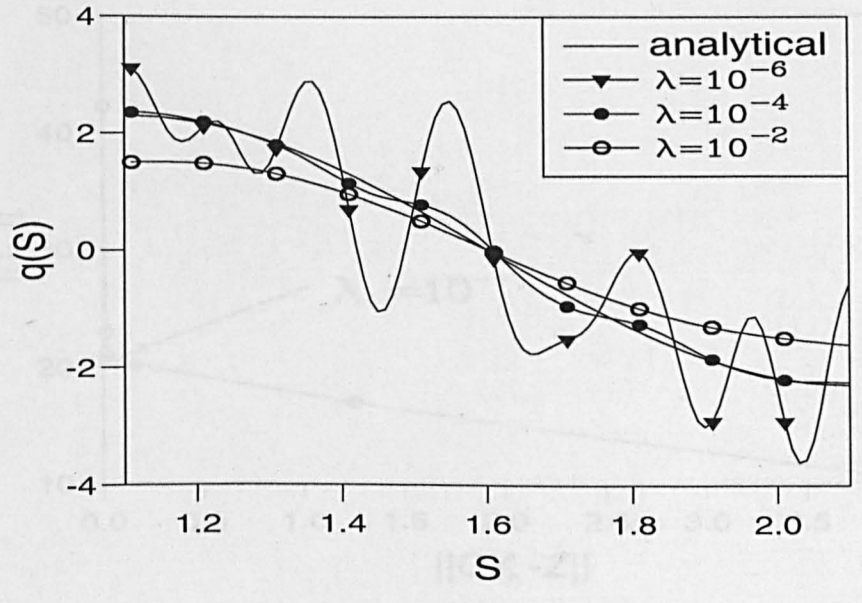

(b)

Figure 5.11: The analytical and regularised (a) boundary temperature $T|_{\partial\Omega}$, and (b) the heat flux $q|_{\Gamma_3}$, for various λ, when $\rho = 0.01$, for the IHCP in Example 5.3.

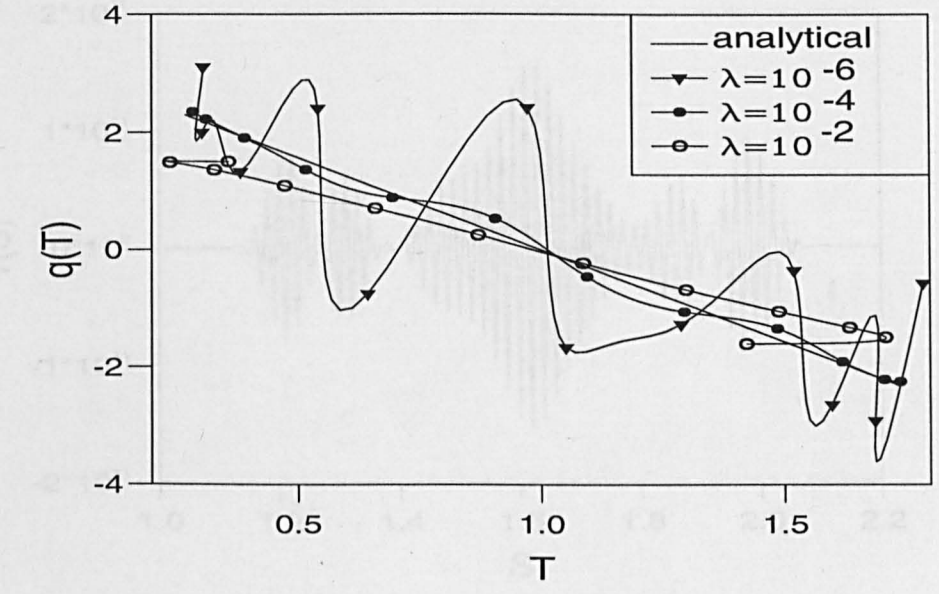

(a)

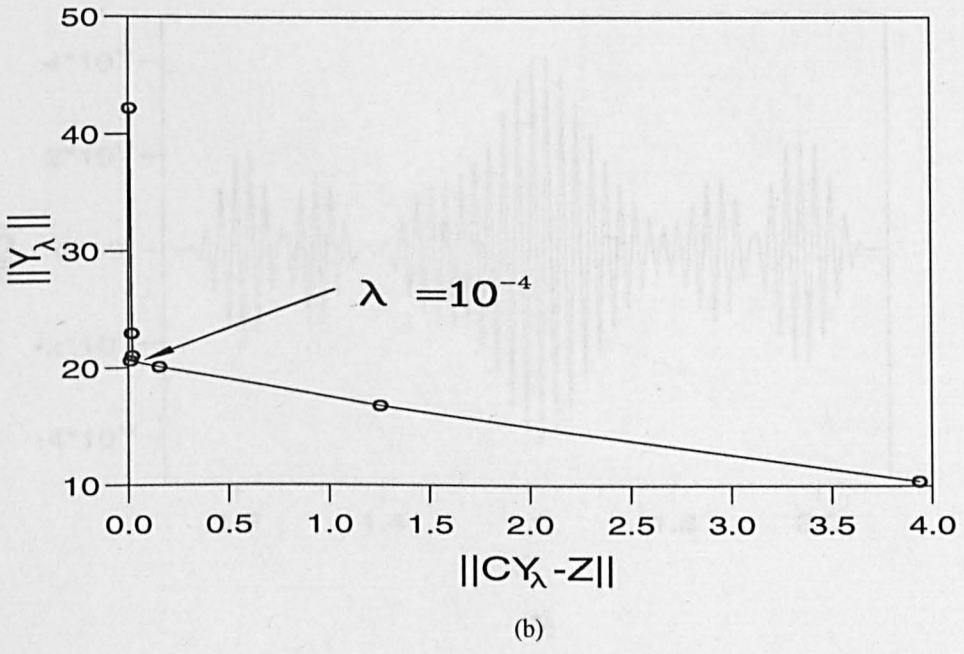

(b)

Figure 5.12: The (a) analytical and regularised heat flux $q(T)$ on Γ_3, for various λ, and (b) the L-curve, when $\rho = 0.01$, for the IHCP in Example 5.3.

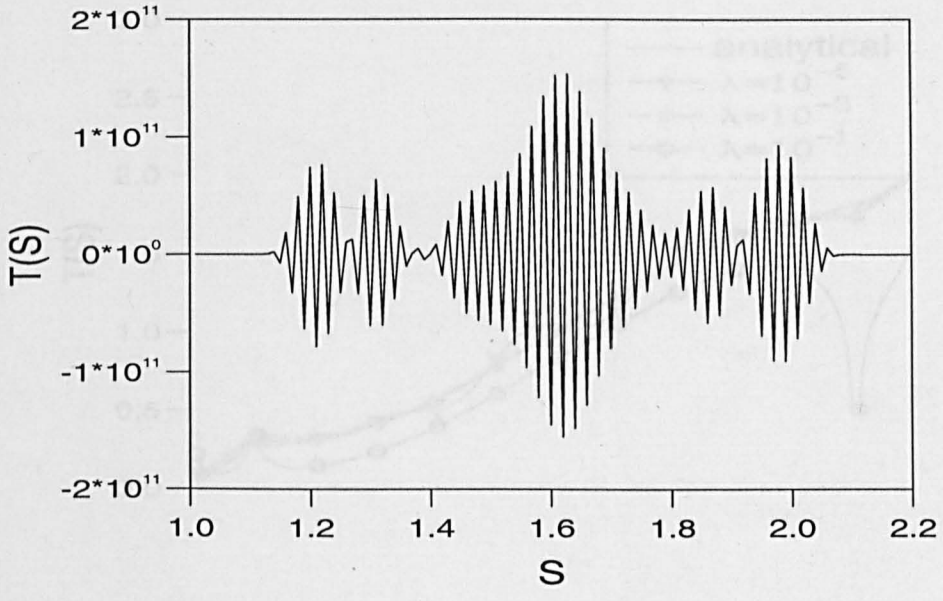

(a)

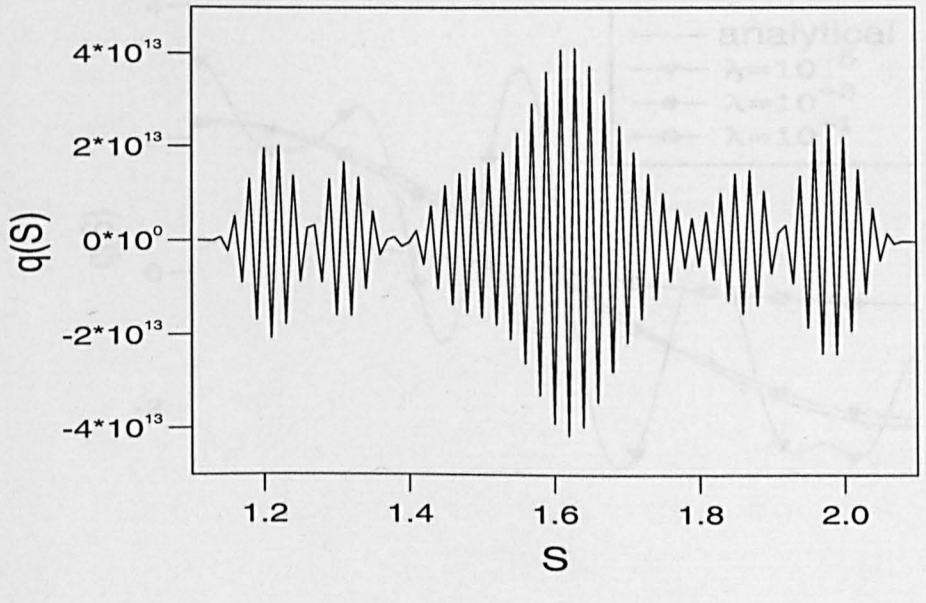

(b)

Figure 5.13: The numerical (a) boundary temperature $T|_{\partial\Omega}$, and (b) the heat flux $q|_{\Gamma_3}$, when $\lambda = 0$ and $\rho = 0.03$, for the IHCP in Example 5.3.

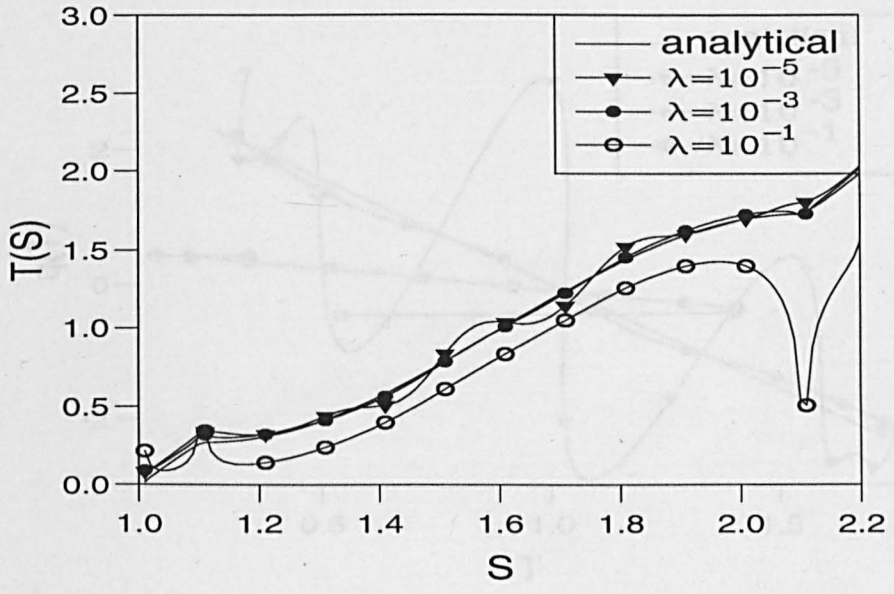

(a)

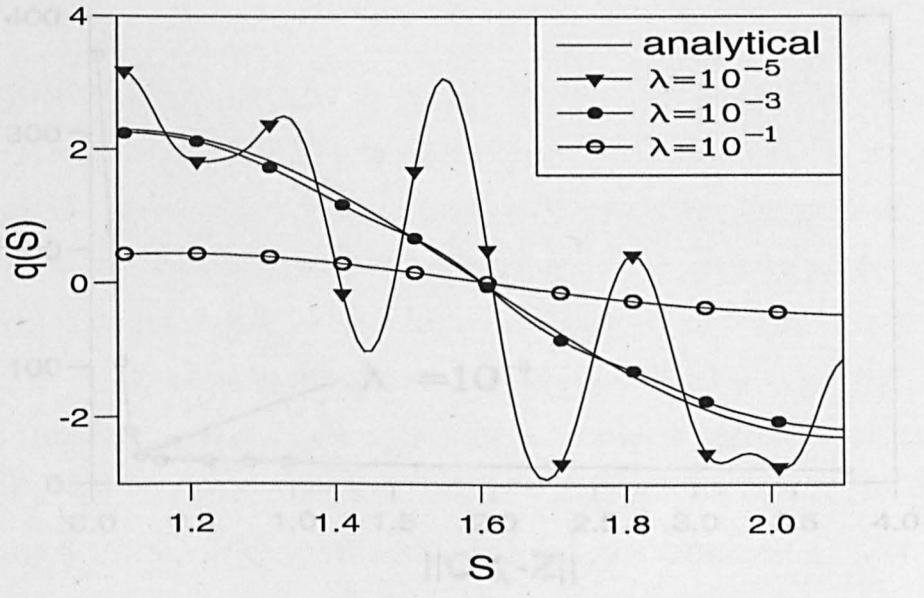

(b)

Figure 5.14: The analytical and regularised (a) boundary temperature $T|_{\partial\Omega}$, and (b) the heat flux $q|_{\Gamma_3}$, for various λ, when $\rho = 0.03$, for the IHCP in Example 5.3.

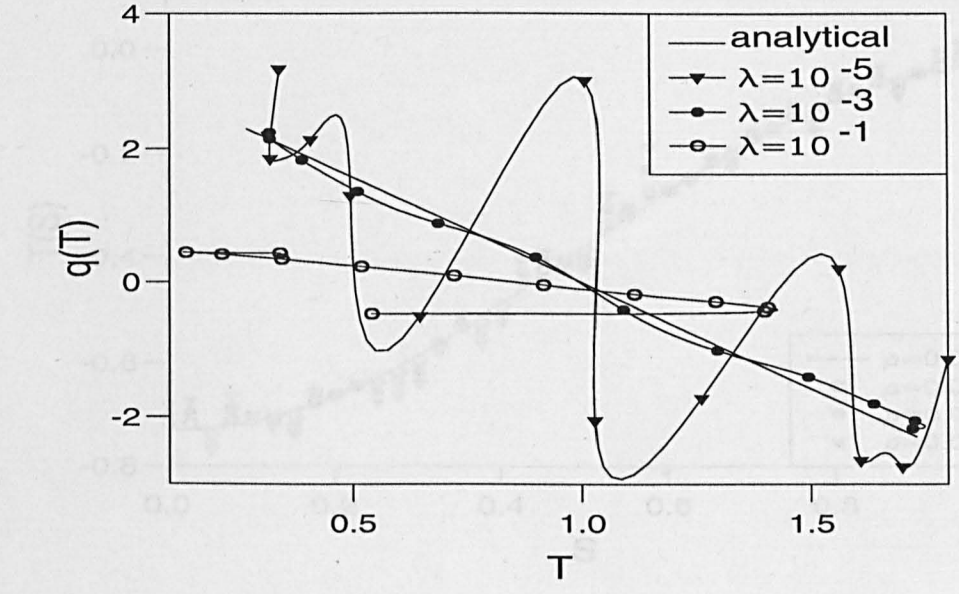

(a)

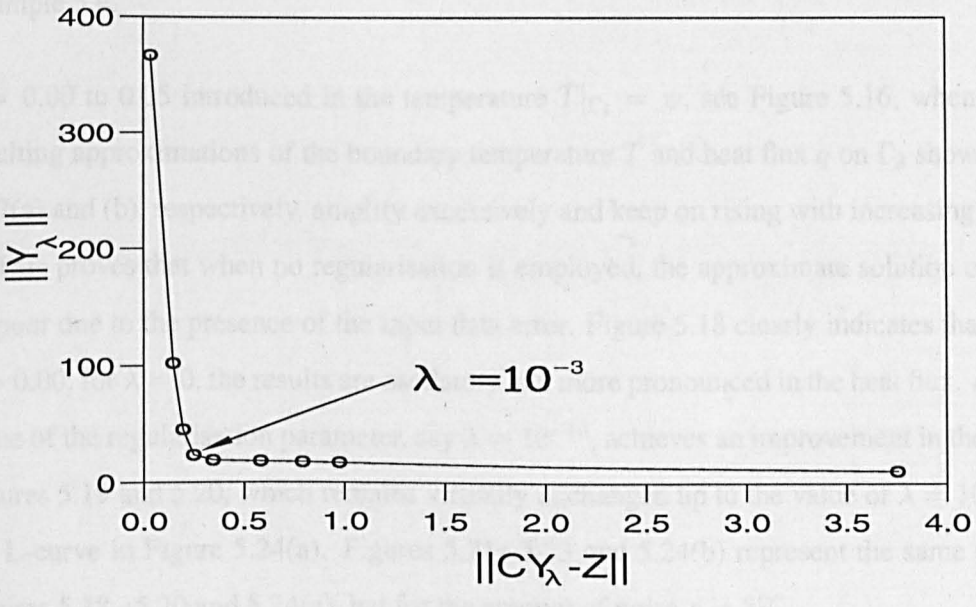

(b)

Figure 5.15: The analytical and regularised (a) heat flux $q(T)$ on Γ_3, for various λ, and (b) the L-curve, when $\rho = 0.03$, for the IHCP in Example 5.3.

In the IHCP we are concerned with the reconstruction of the nonlinear corrosion damage profile $h(T)$ from the Cauchy data (5.3.12) on the accessible portion Γ_1. This is achieved first through solving the Cauchy problem for T with Cauchy data on Γ_1. Increasing the amount of noise from

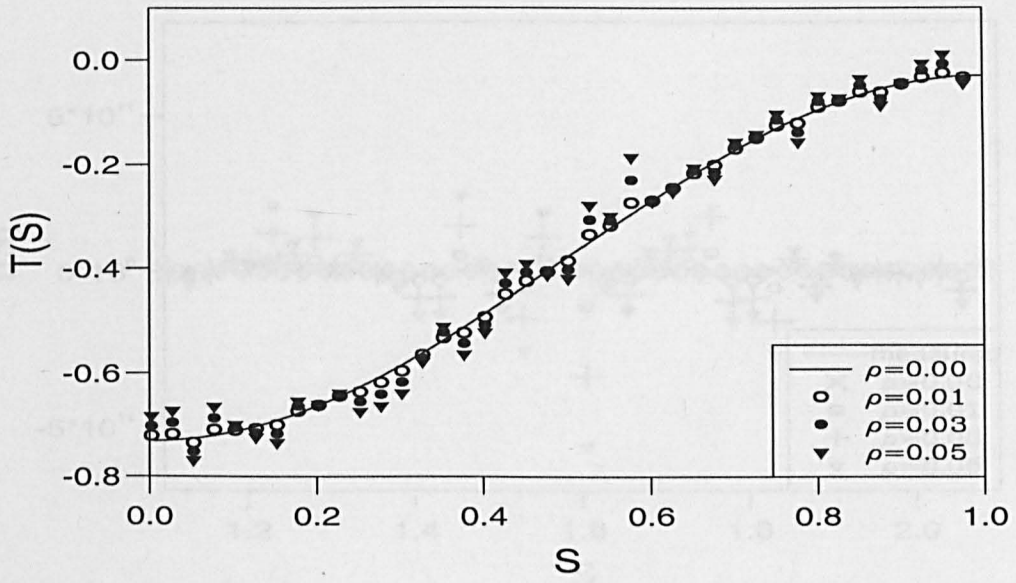

Figure 5.16: The measured temperature $T|_{\Gamma_1} = \psi$, for various $\rho = 0.00$ to 0.05, for the IHCP in Example 5.4.

$\rho = 0.00$ to 0.05 introduced in the temperature $T|_{\Gamma_1} = \psi$, see Figure 5.16, when $\lambda = 0$, the resulting approximations of the boundary temperature T and heat flux q on Γ_3 shown in Figures 5.17(a) and (b), respectively, amplify excessively and keep on rising with increasing the value of ρ. This proves that when no regularisation is employed, the approximate solution obtained will be poor due to the presence of the input data error. Figure 5.18 clearly indicates that even when $\rho = 0.00$, for $\lambda = 0$, the results are oscilatory and more pronounced in the heat flux. A very small value of the regularisation parameter, say $\lambda = 10^{-10}$, achieves an improvement in the results, see Figures 5.19 and 5.20, which remains virtually unchanged up to the value of $\lambda = 10^{-4}$, see also the L-curve in Figure 5.24(a). Figures 5.21–5.23 and 5.24(b) represent the same situations as Figures 5.18–5.20 and 5.24(a), but for the amount of noise $\rho = 3\%$.

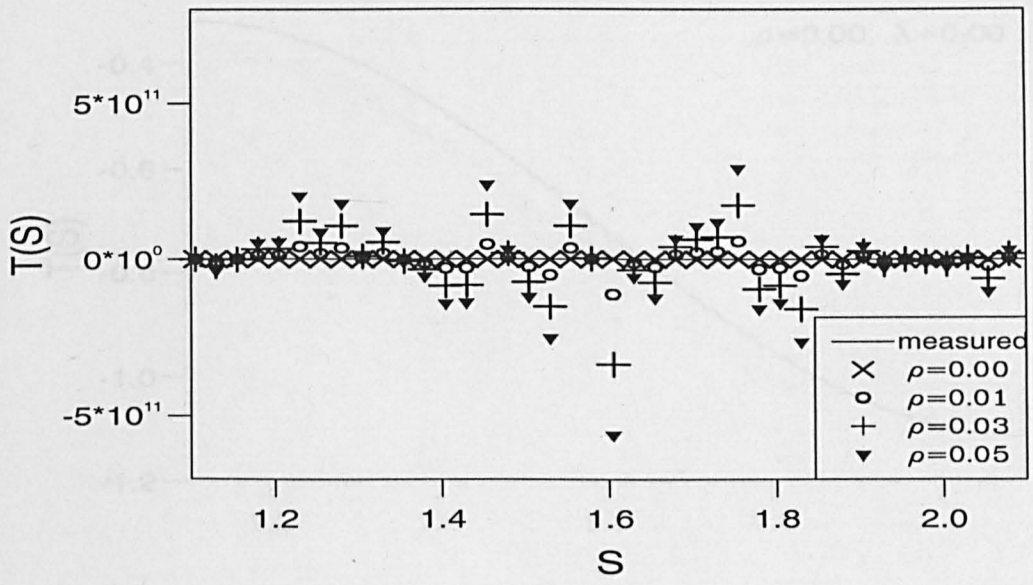

(a)

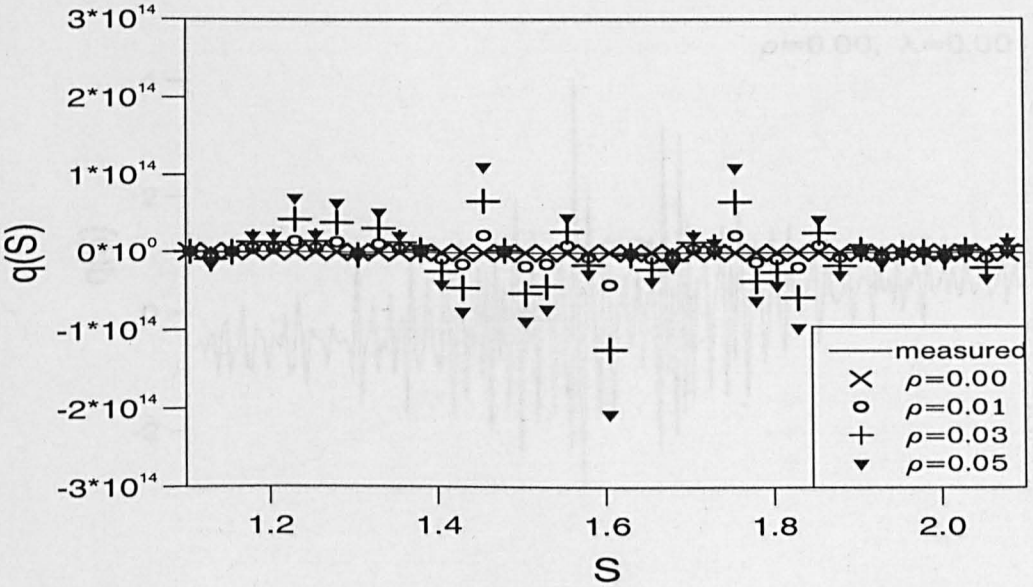

(b)

Figure 5.17: The numerical (a) boundary temperature $T|_{\Gamma_3}$, and (b) heat flux $q|_{\Gamma_3}$, for various $\rho = 0.00$ to 0.05, when $\lambda = 0$, for the IHCP in Example 5.4.

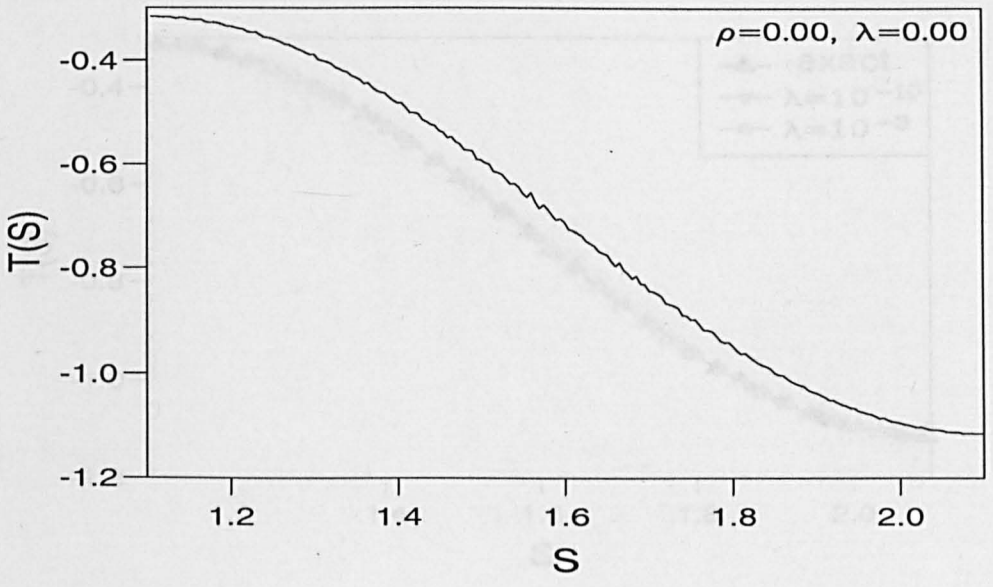

(a)

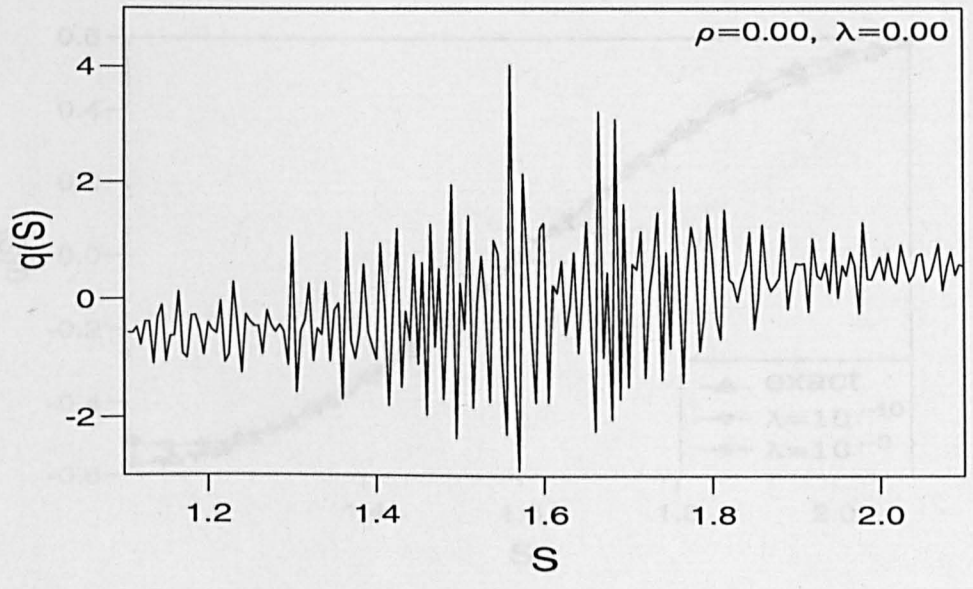

(b)

Figure 5.18: The numerical (a) boundary temperature $T|_{\Gamma_3}$, and (b) the heat flux $q|_{\Gamma_3}$, when $\lambda = 0$, when $\rho = 0.00$, for the IHCP in Example 5.4.

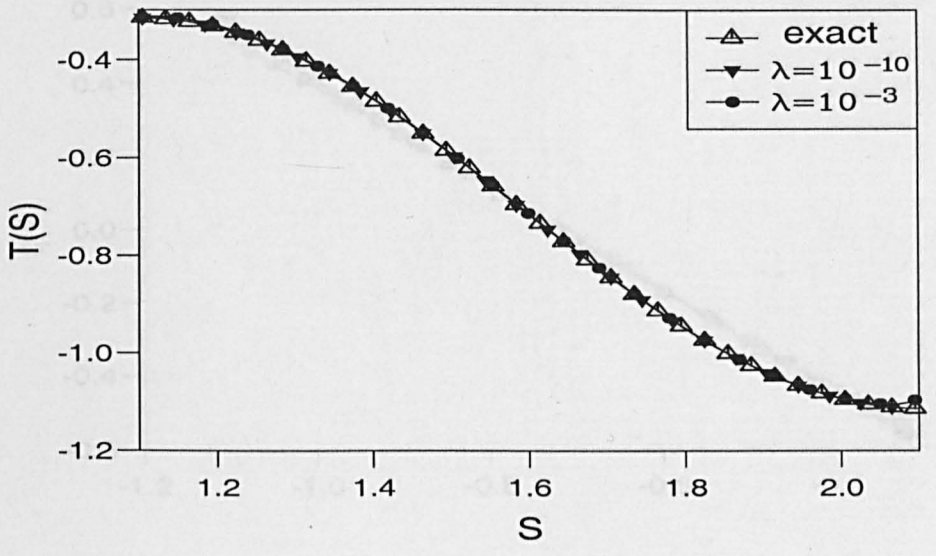

(a)

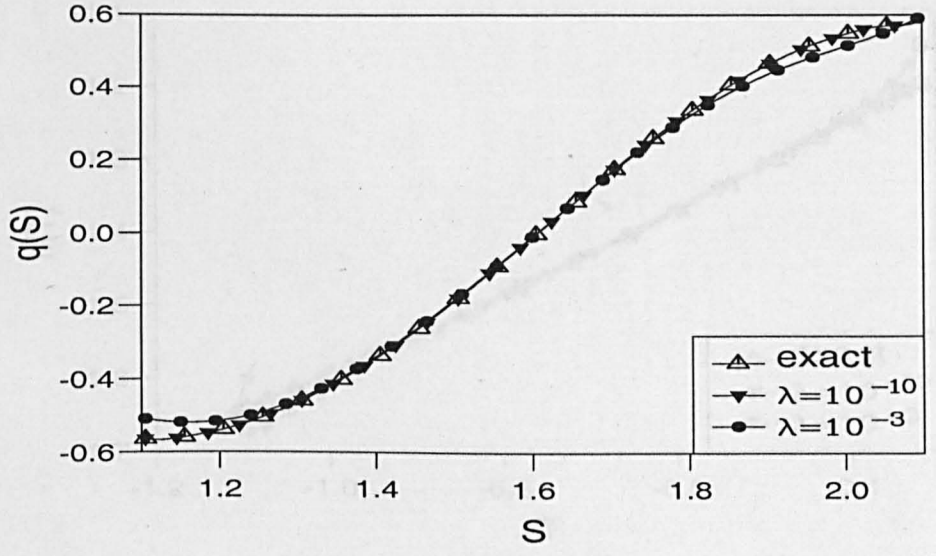

(b)

Figure 5.19: The exact and regularised (a) boundary temperature $T|_{\Gamma_3}$, and (b) heat flux $q|_{\Gamma_3}$, for various λ, when $\rho = 0.00$, for the IHCP in Example 5.4.

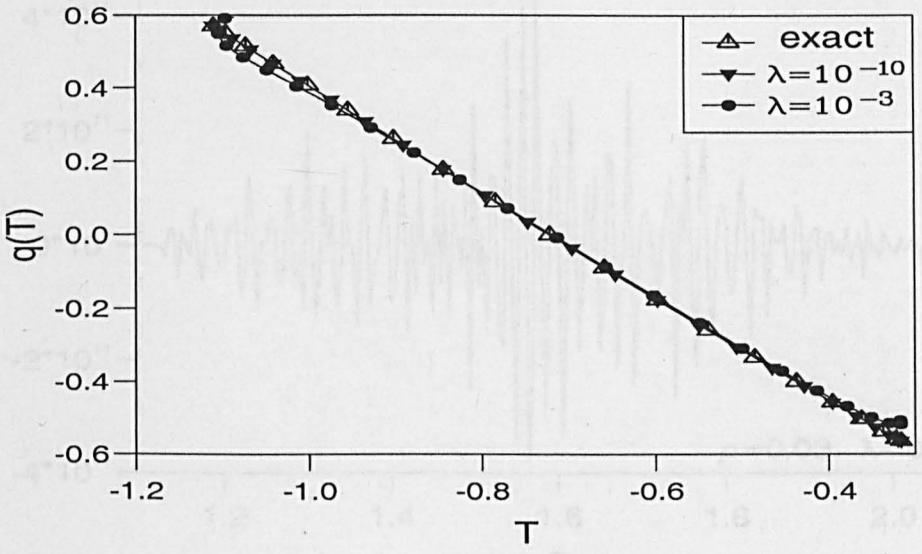

(a)

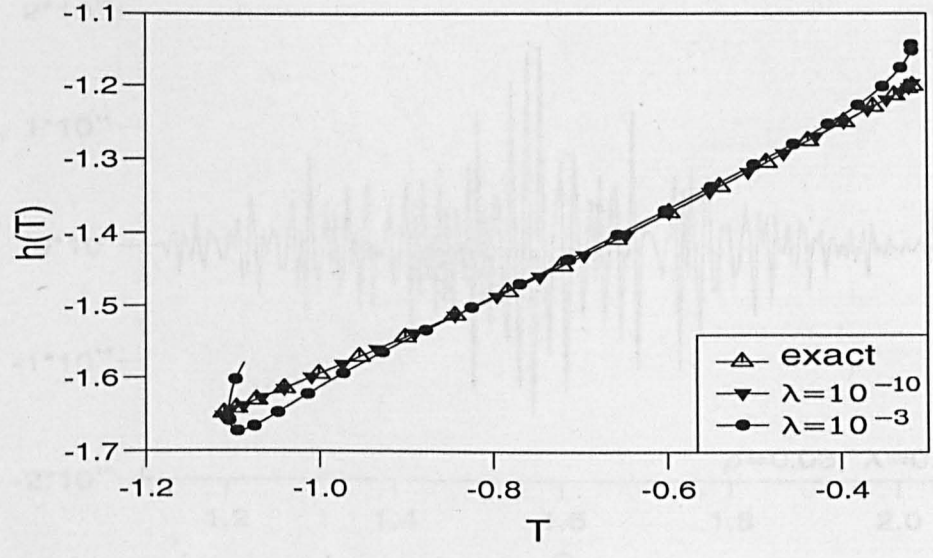

(b)

Figure 5.20: The exact and regularised (a) heat flux $q(T)$, and (b) the nonlinear function $h(T)$ for various λ, when $\rho = 0.00$, for the IHCP in Example 5.4.

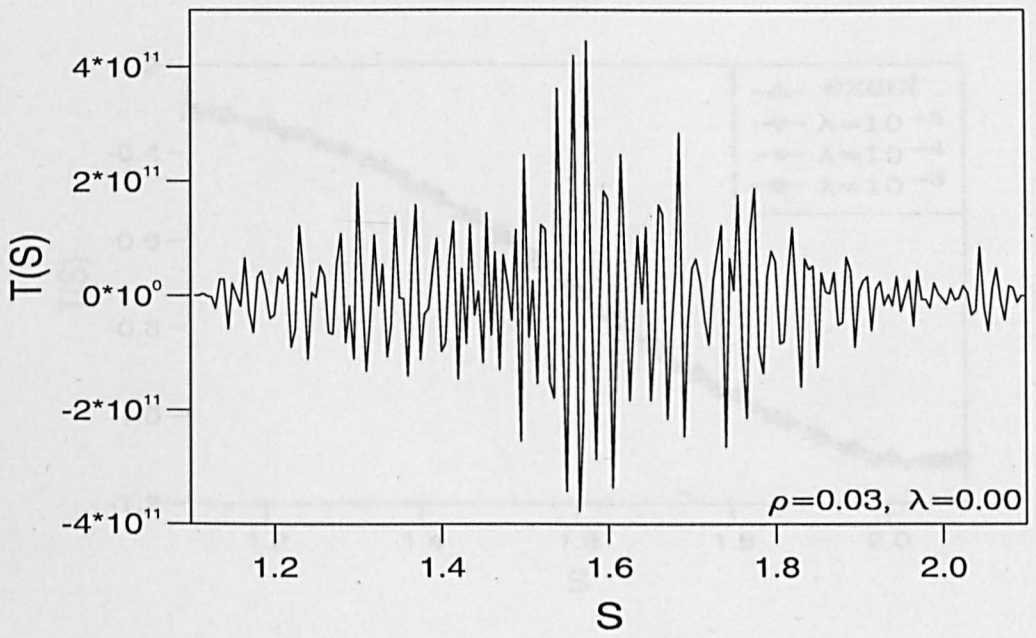

(a)

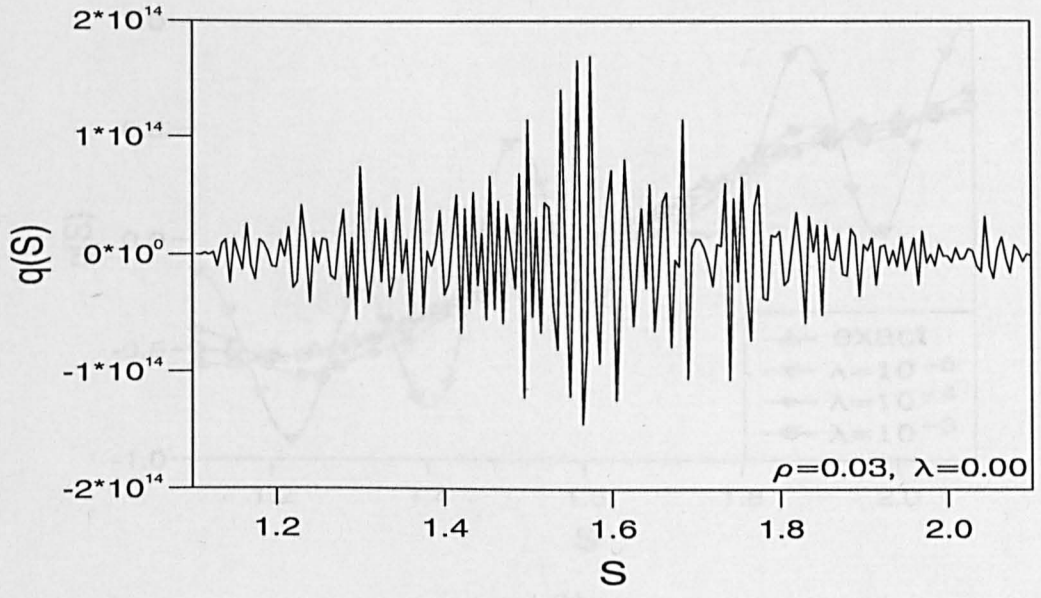

(b)

Figure 5.21: The numerical (a) boundary temperature $T|_{\Gamma_3}$, and (b) the heat flux $q|_{\Gamma_3}$, when $\lambda = 0$, $\rho = 0.03$, for the IHCP in Example 5.4.

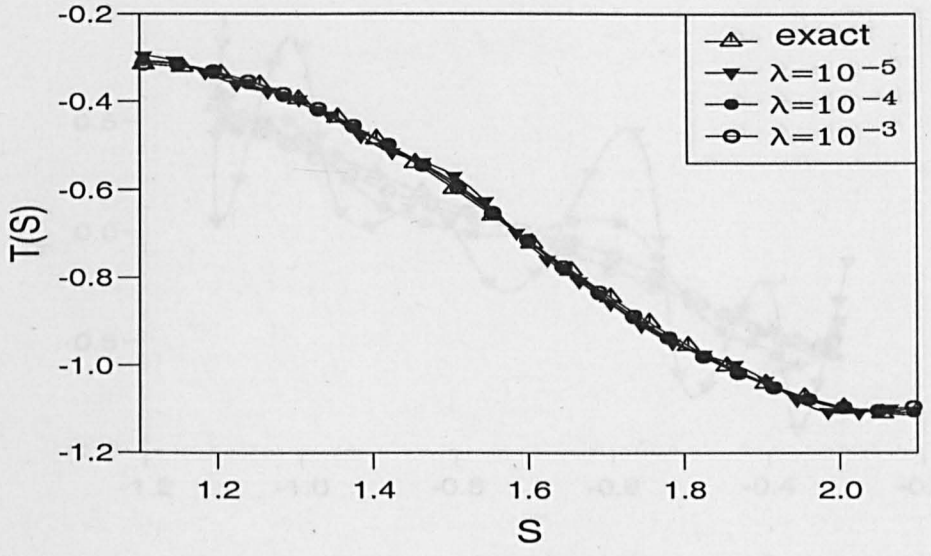

(a)

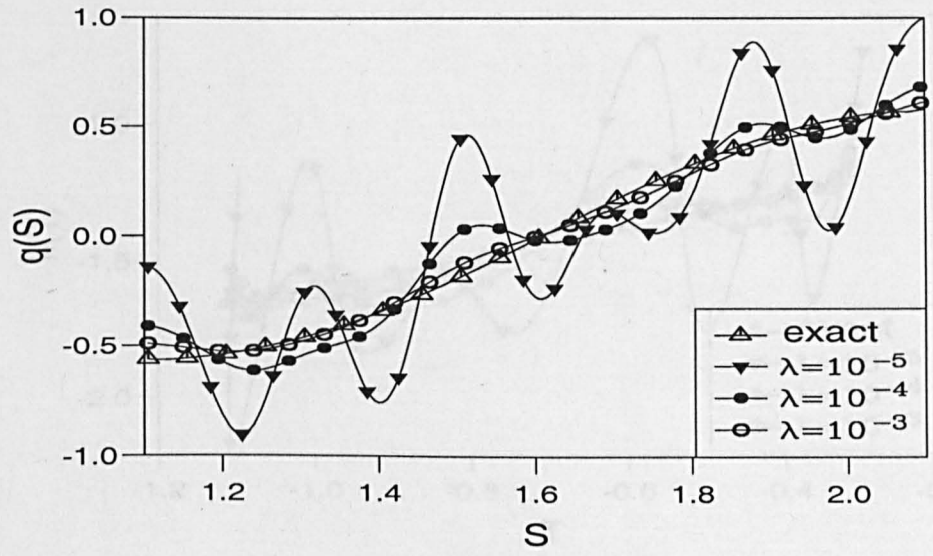

(b)

Figure 5.22: The exact and regularised (a) boundary temperature $T|_{\Gamma_3}$, (b) heat flux $q|_{\Gamma_3}$, for various λ, when $\rho = 0.03$, for the IHCP in Example 5.4.

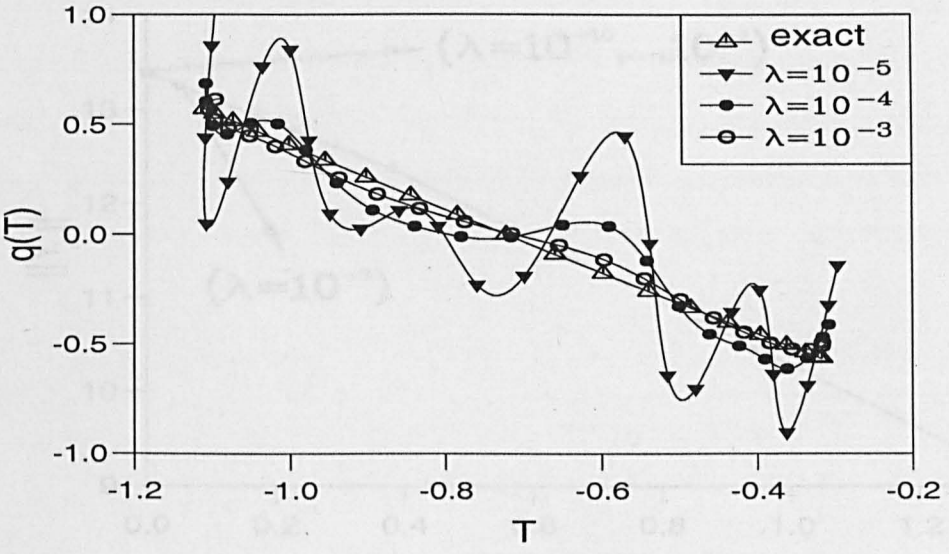

(a)

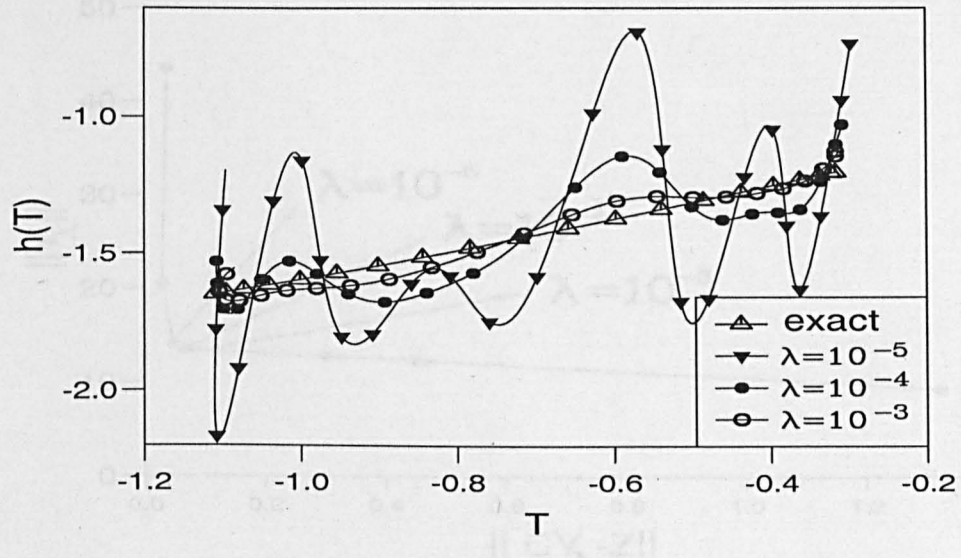

(b)

Figure 5.23: The (a) exact and regularised the heat flux $q(T)$, and (b) the nonlinear function $h(T)$ for various λ, when $\rho = 0.03$, for the IHCP in Example 5.4.

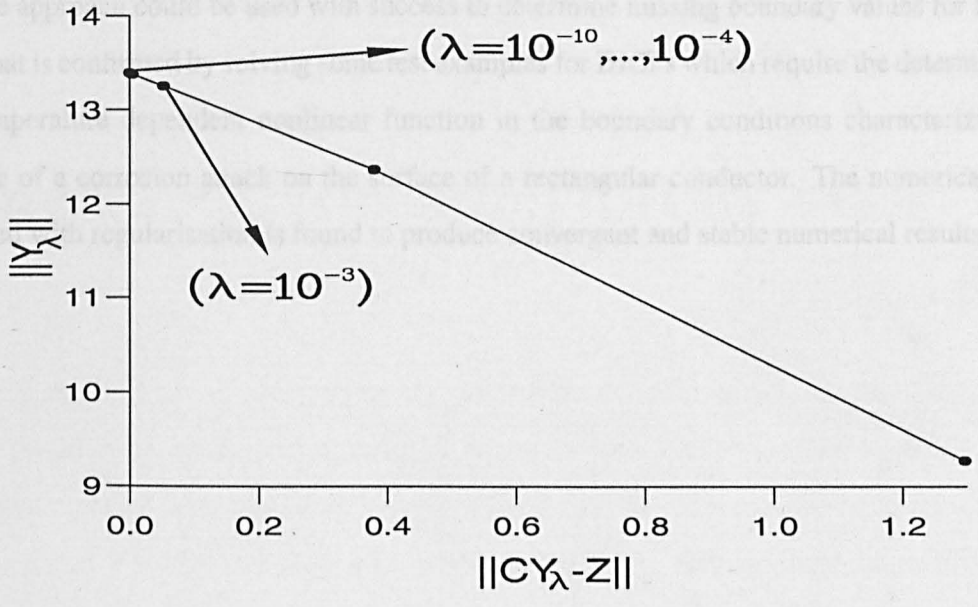

(a)

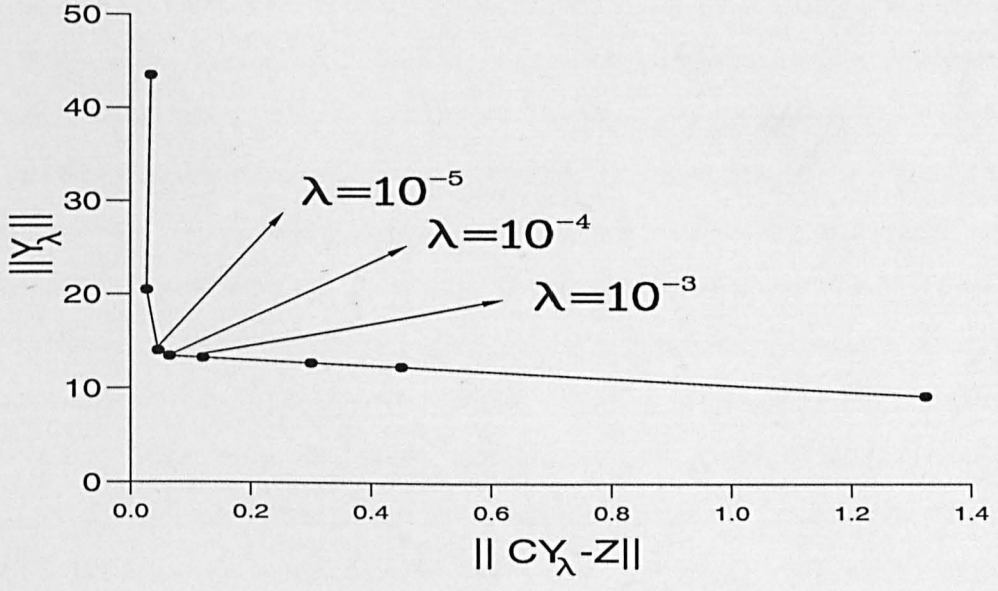

(b)

Figure 5.24: The L-curves for the IHCP in Example 5.4, when (a) $\rho = 0.00$, and (b) $\rho = 0.03$.

5.4 Conclusions

In this chapter, some two-dimensional steady-state DHCPs have been solved with high accuracy to determine unknown boundary temperatures and heat fluxes. This fact provides a backing that the same approach could be used with success to determine missing boundary values for IHCPs. A fact that is confirmed by solving some test examples for IHCPs which require the determination of a temperature dependent nonlinear function in the boundary conditions characterizing the presence of a corrosion attack on the surface of a rectangular conductor. The numerical BEM combined with regularisation is found to produce convergent and stable numerical results.

Chapter 6

General conclusions and further work

This thesis explored several applications of the BEM to solve some direct, and the corresponding inverse, boundary conditions identification problems for some heat conduction systems governed by parabolic and elliptic partial differential equations. In chapter 1 we have surveyed the development of the BEM, which is a numerical technique for solving linear partial differential equations with constant coefficients. In this technique, the heat equation is transformed into an integral form with the assistance of Green's theorem. Enforcing the boundary conditions allows one to obtain boundary integral equations with unknowns as equivalent sources or field variables along the boundary. One may then discretise the boundary into small boundary elements and assume that the boundary values are piecewise constant functions. Hence one obtains a system of linear equations. The boundary integrals were evaluated analytically, and special attention was given to the singular values of the governing matrix. The test examples in this thesis were chosen to validate the BEM and replicate some real physical problems. However, in real life no smooth data is obtainable. Hence, to investigate the suitability of using the BEM to obtain stable solutions in such situations we introduced noise into the measured additional boundary values. This thesis was mainly dedicated to solving some inverse linear or nonlinear problems using an approach based on error minimization of least-squares gap objective function to estimate the missing terms on the boundary.

Due to the ill-posedness of the inverse problems, regularization is necessary in order to stabilize the numerical results. The most known regularization technique is the Tikhonov regularization method, which is a stabilization technique that produces a smoothing factor to the output data (boundary temperature, heat flux, heat transfer coefficient, etc.).

In chapter 1, we have described how the BEM technique is used to solve direct boundary conditions identification problems using test examples with Dirichlet, Neumann and Robin boundary conditions. This has been performed in order to demonstrate the accuracy of the BEM in obtaining the uknown boundary values and temperature inside a solution domain. On increasing the number of boundary elements the numerical approximations of the solutions considerably improved in accuracy.

Recently, there has been growing interest in science, engineering and industry for numerical solutions to physical problems that require measurements of the temperature and heat transfer coefficients non-intrusively. In chapter 2, we have analysed the ability of the BEM to provide a reliable means of reconstructing one-dimensional inverse heat conduction boundary conditions identification problems. In order to achieve this we have produced the analysis in four parts. First, parts one and two aimed at the determination of the spacewise and time- dependent ambient temperatures that appear in the boundary conditions from additional, terminal, integral or point observations. Secondly, parts three and four aimed at reconstructing the spacewise and time-dependent heat transfer coefficients, using additional boundary measurements similar to those used for determining boundary temperatures and heat fluxes in the parts one and two. The BEM, employed for solving these inverse problems, has been developed. It has been shown that the BEM produced convergent and stable numerical results for both the reconstruction of a spacewise-dependent ambient temperature and of a heat transfer coefficient, see sections 2.2 and 2.3, respectively. However, the ill-conditioning of the system of linear equations decreases with an increase in the instant at which the additional boundary temperature measurements are made. Such that if it is measured in a short instant at the begining of the experiment then the system becomes highly ill-conditioned. Therefore, the problem is ill-posed, obtaining results which do not undergo substantial regularization when both the Tikhonov and singular value decomposition regularization methods were employed. Further, we conclude that in order to obtain any reasonable results in this category of inverse problems then it is important either to measure the average of the boundary measurement or the boundary measurements at the end of the experiment to represent the additional measurements. The inverse problems which require the determination of the time-dependent ambient temperature and the heat transfer coefficient have been investigated in sections 2.4 and 2.5, respectively, when either additional terminal, integral or point observations are available.

In chapter 3 we have investigated the IHCP which require determining the time-dependent

HTC from non-standard boundary measurements. A theoretical result on uniqueness of the HTC has been presented. A BEM was then derived and an in-depth numerical investigation was performed. In the numerical examples for the one-dimensional unsteady inverse heat conduction boundary conditions identification problem with linear convective boundary conditions investigated, the boundary temperature was obtained to be stable and did not significantly deviate with an increasing amount of noise. However, the heat flux and the HTC deviated considerably. To stabilize the numerical solutions, the boundary temperature obtained was used in a direct problem, which on applying the Tikhonov regularization technique and then performing direct inversion, we have obtained a substantial improvement in the prediction of the heat flux and the HTC. Research is presently in progress to extend the analysis of Chapter 3 to the determination of a timewise dependent HTC in nonlinear radiative boundary conditions.

In chapter 4, we have investigated some IHCPs with unknown nonlinear boundary conditions. We have used the BEM to construct and solve numerically the missing terms which involve the boundary temperature, heat flux, and coefficients in a polynomial function f approximating the relationship between the boundary temperature and the heat flux in some unsteady, one-dimensional direct, and the corresponding inverse, heat conduction boundary conditions identification problems. In the inverse problem, the unknown boundary function f was approximated by a polynomial of degree equal to or greater than that of the actual function f. Test examples with various boundary conditions relating the heat flux and temperature have been investigated, amongst them linear, and nonlinear quadratic, fourth-order power laws in the temperature and exponential functions f in the temperature representing some physical situations have been reconstructed. A mathematical formulation of the problem was documented and the BEM for solving this class of problems has been developed. The convergence of the numerical results has been tested by increasing the number of boundary elements, whilst the stability of the numerical solutions was investigated by perturbing with noise the additional measurements. From the examples considered, we have found that when the order of the polynomial approximating functional is equal to, or greater than, that of the actual solution then the numerical results are accurate and convergent with respect to increasing the number of boundary elements when no noise is included in the input measured boundary temperature data. Further these numerical approximations of the boundary conditions are stable when noise is introduced into the additional measured boundary temperature data if the degree of the approximating functional is relatively low, usually ≤ 5. No additional regularisation

is employed in the examples presented. This is because the engineering approach both reduces the dimensionality of the problem and brings stability to the problem (regularisation by parametrization). Hence this is a stable inverse problem with respect to noisy perturbations of the input data. For the approximating functionals with degree larger than 5, the numerical solutions of the unknown functional will deviate greatly. Hence, regularization should be employed to ensure the stability of the numerical solution. In conclusion, we conclude that the BEM provides a very good and reliable method for the determination of the boundary condition laws in one-dimensional inverse heat conduction problems. In the future it is worth exploring one-dimensional IHCP with the help of piecewise polynomial estimation rather than continuous polynomial parametrisation of the nonlinear boundary condition law.

In chapter 5 we have studied some two-dimensional, steady inverse heat conduction problems in which a functional relating the heat flux and the temperature on a portion of the boundary is unknown and has to be identified using the BEM. This task was illustrated with an inverse nonlinear test example of practical engineering interest involving the detection of the corrosion damage on the surface of a conductor in contact with a corroding fluid. We assumed that these complex situations characterize the presence of a corrosion attack on the surface of the conductor produces a small change in the geometry, by-products that precipitate on the surface and so on. This transformed interface interacts with the heating in a way that can be described by a nonlinear perturbation to the boundary. In particular, the heat flux on the corroding portion of the boundary is given in terms of an unknown nonlinear function f of the boundary temperature. Thus, in addition to the unknown boundary temperature one needs also to determine the nature of the unknown function f to help find the actual extent of the contamination due to the corrosion. The resulting inverse problem has been discretized using the BEM. The discretization yields a nonlinear system of algebraic equations for the approximation of the temperature and the unknown functional which was solved using a standard NAG minimization routine G05NDF, to minimize a defined objective function, which in this case is the least-squares error gap between the calculated and the measured boundary temperatures. The numerical results obtained through the minimization process are accurate, convergent and stable. This indicates that the BEM has been employed with great success in solving inverse boundary value identification on an underspecified portion of the boundary in some two-dimensional heat conduction problems, especially with the help of the Tikhonov regularization method. This problems requires additional boundary and heat flux measurements on another portion of the boundary and this

has been provided. This enabled us to determine the absence or presence of corrosion damage on a piece of a heat conducting material with rectangular geometry. However, it is noted that most paractical situations can occur in various geometries and in complicated shapes. Therefore, it is worth extending this study to include conductors with different geometrical shapes and those with irregular or complex shapes to test the application of the BEM in various demanding situations. Many real problems also involve time evolution, for example a corroding fluid flowing past a conducting surface can be of great interest. Therefore, in future this work is also worth extending to solving unsteady two and three-dimensional heat conduction boundary conditions identification problems. This is because we experience many problems of interest in real life involving, say corrosion damage, on an underspecified boundary or the fluid at the interface undergoing motion with time, making the problem numerically demanding but interesting and of much practical importance.

Overall, in this thesis we have obtained numerical solutions to inverse problems concerned with the estimation of surface conditions (temperature or heat flux) and heat transfer coefficients in heat conduction problems using BEMs. The main ingredients for the inverse problems investigated are additional measurements which include: (i) integral, final, average, and complete, boundary temperature measurements; (ii) heat flux; and (iii) non-standard boundary measurements. This allows us to minimize the least-squares objective function representing the residual error between the calculated and the measured values. The investigations we have conducted provide a stable, efficient and accurate BEM for determining boundary or surface conditions from the knowledge of the temperature properties at a certain chosen boundary. Although, for most mathematical quantities computed in the boundary conditions identification problems in the thesis it is also sufficient to substitute symbolic procedures with numerical ones when necessary, numerical data can be treated analytically, in a piecewise fashion, by representing them in the form of splines possesing a number of derivatives. While some errors will be inevitably introduced, and also the computations becomes expensive, the approach would remain consistent with the mathematical approaches. Hence, it is prudent for future investigations to ascertain the exactness of our functional approach. In other words, we claim that our BEM approach presented in this thesis delivers a significant amount of insight into the ability of the BEM to model, and compute efficiently and effectively, numerical approximations of solutions to the boundary phenomenon in inverse problems. The mathematical technique does not necessarily require information inside the domain. Hence, the method is highly effective

in reducing the computational time and increases the accuracy of the numerical estimations in many areas that require non-intrusive monitoring of physical situations that occur in science and engineering. It is also interesting to note that in the real physical situations modeled in the test examples there are sometimes great difficulties, especially when the boundary measurements are perturbed. In such situations the Tikhonov regularization approach has been shown to efficiently act as a supportive means for stabilization.

A sensitive analysis has been conducted to gain insight into the nature of the difficulties that can be encountered into the analysis of estimating the unknown boundary parameters associated with the inverse, unsteady one- and steady two-dimensional heat conduction problems. Some numerical test examples have been considered to verify the accuracy of the proposed methods. The stability and accuracy of the current methods have been demonstrated by several test examples, which we believe provide very strict test conditions. In the future, this analysis can be further tested by investigating unsteady two- and three-dimensional inverse heat conduction boundary conditions identification problems.

Bibliography

[1] G. Alessandrini, L. Del Piero and L. Rondi, Stable determination of corrosion by a single electrostatic boundary measurement, *Inverse Problems,* **19**, 973–84, (2003).

[2] G. Alessandrini and E. Sincich, Detecting corrosion by electrostatic measurements, *Applicable Anal.,* **85**, 107–28, (2006).

[3] G. Alessandrini and E. Sincich, Solving elliptic Cauchy problems and the identification of nonnlinear corrosion, *J. Comput. Appl. Math.*, **198**, 307–20, (2007).

[4] O.M. Alifanov, *Inverse Heat Transfer Problems*, Springer-Verlag, Berlin (1994).

[5] K.A. Ames and B. Straughan, *Non-standard and Improperly Posed Problems*, Academic Press, New York (1997).

[6] E.J. Anderson and M.C. Ferris, A direct search algorithm optimization for optimization with noisy function evaluations, *SIAM J. Optim.*, **11**, 837–57, (2000/01).

[7] J.V. Beck, B. Blackwell and C.R. St. Clair Jnr., *Inverse Heat Conduction: Ill-posed Problems,* John Wiley, New York (1985).

[8] J.V. Beck and D.A. Murio, Combined function-specification regularization procedure for solution of inverse heat conduction problem, *AIAA J.*, **24**, 180–85, (1986).

[9] R. Bialecki, E. Divo and A.J. Kassab, Reconstruction of time-dependent boundary heat flux by a BEM based inverse algorithm, *Eng. Anal. Boundary Elements*, **30**, 767–73, (2006).

[10] Bizzak, D.J. and Chyu, M.K., Use of laser-induced fluorescence thermal imaging system of local jet impingement heat transfer measurements, *Int. J. Heat Mass Transfer*, **38**, 267–74, (1995).

[11] C.A. Brebbia, J.C.F. Telles and L.C. Wrobel, *Boundary Element Techniques*, Springer-Verlag, Berlin (1984).

[12] K. Bryan and L.F. Jnr Caudill, An inverse problem in thermal imaging, *SIAM J. Appl. Math.*, **56**, 715-35, (1996).

[13] K. Bryan and L.F. Jnr Caudill, Reconstruction of an unknown boundary portion from Cauchy data in n dimensions, *Inverse Problems*, **21**, 239-55, (2005).

[14] J.R. Cannon, *The One-dimensional Heat Equation*, Addison-Wesley, Massachusetts (1984).

[15] H. Cao and S. Pereverzev, The balancing principle for the regularization of elliptic Cauchy problems, *Inverse Problems,* **23**, 1943−61, (2007).

[16] H. Cao, S. V. Pereverzev and E. Sincich, Natural linearization for corrosion identification, *J. Phys.: Conf. Ser.,* (accepted, 2008).

[17] H.S. Carslaw and J.C. Jaeger, *Conduction of Heat in Solids*, 2^{nd} edition, Clarendon Press, Oxford (1959).

[18] S. Chantasiriwan, Inverse heat conduction problem of determining time-dependent heat transfer coefficients, *Int. J. Heat Mass Transfer*, **42**, 4275−85, (1999).

[19] C. Chen and J. Zhou, *Boundary Element Methods,* Academic Press, London (1992).

[20] H.-T. Chen and X.-Y. Wu, Investigation of heat transfer coefficient in two-dimensional transient inverse heat conduction problems using the hybrid inverse scheme, *Int. J. Numer. Meth. Eng.*, **73**, 107−22, (2008).

[21] M.J. Colaco and H.R.B. Orlande, Comparison of different versions of the conjugate gradient method of function estimation, *Numer. Heat Transfer, Part A*, **36**, 229−49, (1999).

[22] E. Divo, A. Kassab, J.S. Kapat and M.K. Chyu Retrival of multidimensional heat transfer coefficient distributions using an inverse BEM-based regularized algorithm: numerical and experimental results, *Eng. Anal. Boundary Elements*, **29**, 150−60, (2005).

[23] M. Dehghan, Efficient techniques for the second-order parabolic equation subject to nonlocal specfications, *Appl. Numer. Math.*, **52**, 39−62, (2005).

[24] H. W. Engl, P. Fusek and S. V. Pereverzev, Natural linearization for the identification of nonlinear heat transfer laws, *J. Inverse Ill-Posed Problems,* **13**, 567–82, (2005).

[25] A. Farcas, L. Elliott, D.B. Ingham, D. Lesnic and N.S. Mera, A dual reciprocity boundary element method for the regularised numerical solution of the inverse source problem associated to the Poisson equation, *Inverse Problems in Engineering*, **11**, 123–39, (2003).

[26] A. Farcas and D. Lesnic, The boundary element method for the determination of a heat source dependent on one variable, *J. Eng. Math.*, **54**, 375–88, (2006).

[27] D. Fasino and G. Inglese, Discrete methods in the study of an inverse problem for Laplace's equation, *IMA J. Numer. Anal.*, **19**, 105–18, (1999).

[28] D. Fasino and G. Inglese, Recovering unknown terms in a nonlinear boundary condition for Laplace's equation, *IMA J.Appl. Math.*, **71**, 832–52, (2006).

[29] D. Fasino and G. Inglese, Recovering nonlinear terms in an inverse boundary value problem for Laplace's equation: A stability estimate, *J. Comput. Appl. Math.*, **198**, 460–70, (2007).

[30] A. Friedman, *Partial Differential Equations of Parabolic Type,* Prentice Hall, Englewood Cliffs, N.J (1964).

[31] M.G. Garroni and J.L. Menaldi, *Green's Functions for Second Order Parabolic Integro-differential Equations,* Longmann Scientific and Technical Publishers, Essex (1992).

[32] G. Golub, M. Heath and G. Wahba, Generalized cross-validation as a method for choosing a good ridge parameter, *Technometrics*, **21**, 215–33, (1979).

[33] J. Hadamard, *Lectures on the Cauchy Problem in Linear Partial Differential Equations,* Yale University Press, New Haven (1923).

[34] P.C. Hansen, Truncated singular value decomposition solutions to discrete ill-posed problems with ill-conditioned numerical rank, *SIAM J. Sci. Comput.*, **11**, 503–18, (1990).

[35] P.C. Hansen, Analysis of discrete ill-possed problems by means of the L-Curve, *SIAM Review*, **34**, 561–80, (1992).

[36] P.C. Hansen and D.P. O'Leary, The use of the L-curve in regularization of discrete ill-posed problems, *SIAM J. Sci. Comput.*, **14**, 1487–1503, (1993).

[37] D. Hinestroza and D.A. Murio, Recovery of the transient heat transfer coefficient in the nonlinear boundary value problem for the heat equation, *Comput. Math. Appl.*, **25**, 101–11, (1993).

[38] Hippensteele, S.A., Russel, L.M. and Stepka, F.S., Evaluation of a method for heat transfer measurement and visualization using a composite of a heater and liquid crystals, *ASME J. Heat Transfer*, **105**, 184–89, (1983).

[39] C.-H. Huang, D.-M. Wang and H.-M. Chen, Prediction of local thermal contact conductance in plate finned-tube heat exchangers, *Inverse Problems in Engineering*, **7**, 119–41, (1999).

[40] D.B. Ingham and Y. Yuan, *Boundary Element Method for Improperly Posed Problems*, Comput. Mech. Publ., Southampton (1994).

[41] D.B. Ingham and L.C. Wrobel (Eds.), *Boundary Integral Formulations for Inverse Analysis*, Comput. Mech. Publ., Southampton (1997).

[42] G. Inglese and F. Mariani, An inverse problem in corrosion detection, *Inverse Problems*, **13**, 977–94, (1997).

[43] M.A. Jawson and G.T. Symm, *Integral Equation Methods in Potential Theory and Elastoplastics*, Academic Press, London (1977).

[44] D.A. Jones, *Corrosion*, Prentice Hall, NY (1996).

[45] P. Kaup, F. Santosa and M. Vogelius, Method for imaging corrosion damage in thin plates from electrostatic data, *Inverse Problems*, **12**, 279–93, (1996).

[46] T. Kaiser and F. Tröltzsch, An inverse problem arising in the steel cooling process, *Wissenschaftliche Zeitung TU Karl-Marx-Stadt*, **29**, 212–18, (1987).

[47] A.B. Kostin and A.I. Prilepko, On some problems of restoration of a boundary condition for a parabolic equation, I, *Diff. Equations*, **32**, No. 1, 113–22, (1996).

[48] A.B. Kostin and A.I. Prilepko, Some problems of restoring the boundary condition for a parabolic equation, II, *Diff. Equations*, **32**, No. 11, 1515–25, (1996).

[49] K. Kurpisz and A.J. Nowak, *Inverse Thermal Problems*, Comput. Mech. Publ., Southampton (1995).

[50] D. Lesnic, L. Elliott and D.B. Ingham, Application of the boundary element method to inverse heat conduction problems, *Int. J. Heat Mass Transfer*, **39**, 1503–17, (1996).

[51] D. Lesnic, L. Elliott and D.B. Ingham, Identification of the thermal conductivity and heat capacity in unsteady nonlinear heat conduction problems using the boundary element method, *J. Comput. Phys.* **126**, 410–20, (1996).

[52] D. Lesnic, L. Elliott, D.B. Ingham, B. Clennell and R.J. Knipe, A mathematical model and numerical investigation for determining the hydraulic conductivity of rocks, *Int. J. Rock Mech. Minning Sci.*, **34**, 741–59, (1997).

[53] D. Lesnic, L. Elliott and D.B. Ingham, An alternating algorithm for solving the backward heat conduction problem using an elliptic approximation, *Inverse Problems in Engineering*, **6**, 255–79, (1998).

[54] D. Lesnic, L. Elliott and D.B. Ingham, The boundary element solution of the Laplace and biharmonic equations subjected to noisy boundary data, *Int. J. Numer. Meth. Eng.*, **43**, 479–92 (1998).

[55] D. Lesnic, L. Elliott, D.B. Ingham, B. Clennell and R.J. Knipe, The identification of piecewise homogeneous thermal conductivity of conductors subjected to a heat flow test, *Int. J. Heat Mass Transfer*, **42**, 143–52, (1999).

[56] H. Louahlia–Gualous, P.K. Panday and E.A. Artioukhine, Inverse determination of the local heat transfer coefficients for nucleate boiling on a horizontal cylinder, *J. Heat Transfer*, **125**, 1087–95, (2003).

[57] D. Maillet, A. Degiovanni and R. Pasquetti, Inverse heat conduction applied to the measurements of heat transfer coefficients on a cylinder: Comparison between an analytical and a boundary element technique, *J. Heat Transfer*, **113**, 549–57, (1991).

[58] N.S. Mera, L. Elliott, D.B. Ingham and D. Lesnic, An iterative boundary element method for solving the one dimensional backward heat conduction problem, *Int. J. Heat Mass Transfer*, **44**, 1937–46, (2001).

[59] N.S. Mera, L. Elliott, D.B. Ingham and D. Lesnic, Use of the boundary element method to determine the thermal conductivity tensor of an anisotropic medium, *Int. J. Heat Mass Transfer*, **44**, 4157–67, (2001).

[60] V.A. Morozov, On the solution of functional equations by the method of regularization, *Soviet Math. Doklady*, **7**, 414–417, (1966).

[61] V.A. Morozov, *Methods for Solving Incorrectly Posed Problems*, Springer-Verlag, New York, (1984).

[62] N.V. Muzylev, Uniqueness theorems for some converse problems of heat conduction, *U.S.S.R. Comput. Maths. Math. Phys.*, **20**, 120–34, (1980).

[63] T.T.M. Onyango, D.B. Ingham and D. Lesnic, Restoring boundary conditions in heat conduction, *J. Eng. Math.* **62**, 85–101, (2008).

[64] H.R.B. Orlande, M.J. Colaco and A.A. Malta, Estimation of the heat transfer coefficient in the spray cooling of continuously cast slabs, *National Heat Transfer Conference*, HTD-340, Vol. 2, ASME 1997, 109–16, (1997).

[65] A.M. Osman and J.V. Beck, Investigation of transient heat transfer coefficients in quenching experiments, *J. Heat Transfer*, **112**, 843–48, (1990).

[66] M.N. Özisik, *Boundary Value Problems of Heat Conduction*, Dover Publications, New York (1989).

[67] M. Pilant and W. Rundell, Undetermined coefficient problems for nonlinear elliptic and parabolic equations, *Int. Ser. Numer. Math.*, **77**, 139–54, (1986).

[68] M. Pilant and W. Rundell, An iteration method for the determination of an unknown boundary condition in a parabolic initial-boundary value problem, *Proc. Edinburgh Math. Soc.*, **32**, 59–71 (1989).

[69] M.H. Protter and H.F. Weinberger, *Maximum Principles in Differential Equations*, Prentice-Hall, Englewood Cliffs, N.J. (1967).

[70] A. Rap, L. Elliott, D.B. Ingham, D. Lesnic, and X. Wen, An inverse source problem for the convection-diffusion equation, *Int. J. Numer. Meth. Heat Fluid Flow*, **16**, 125–50, (2006).

[71] A. Rösch and F. Tröltzsch, An optimal problem arising from the identification of nonlinear heat transfer laws, *Arch. Control Sci.*, **1**, 183–95, (1992).

[72] A. Rösch, Identification of nonlinear heat transfer laws by optimal control, *Numer. Funct. Anal. Optimiz.*, **15**, 417–34, (1994).

[73] A. Rösch, Stability estimates for the identification of nonlinear heat laws, *Inverse Problems*, **12**, 743–56, (1996).

[74] A. Rösch, Fréchet differentiability of the solution of the heat equation with respect to a nonlinear boundary condition, *Z. Anal. Anw.*, **15**, 603–618, (1996).

[75] A. Rösch, Identification of nonlinear heat transfer laws by means of boundary data, *Progress in Industry*, Wiley, Teubner, 405–12, (1996).

[76] A. Rösch, A Gauss-Newton method for the identification of non-linear heat transfer laws, *Int. Ser. Numer. Math.*, **139**, 217–30, (2002).

[77] M. Slodička and R. Van Keer, Recovery of the convective transfer coefficient in parabolic problems from a nonstandard boundary condition, *Recent Advances in Applied and Theoretical Mathematics*, (ed. N.E. Mastorakis), 209–13, (2000).

[78] M. Slodička and R. Van Keer, Determination of a Robin coefficient in semilinear parabolic problems by means of boundary measurements, *Inverse Problems*, **18**, 139–52, (2002).

[79] I. Stewart, J.D. Massingham and J.J. Hagers, Heat transfer coefficient effects on spray cooling, *Iron Steel Eng.*, **63**, 17–23, (1996).

[80] J. Su and G. Hewitt, Inverse heat conduction problem of estimating time-varying heat transfer coefficient, *Numer. Heat Transfer, Part A: Applications*, **45**, 777–89, (2004).

[81] G.T. Symm and R.A. Pitfield, Solution of Laplace's equation in two dimensions. NPL Report, NAC 44, (1974).

[82] U. Tautenhanh, Error estimates for regularized solutions of non-linear ill-posed problems, *Inverse Problems*, **10**, 485–500, (1994).

[83] A.N. Tikhonov and V.Y. Arsenin, *Solution of Ill-posed Problems,* Winston-Wiley, Washington, DC., (1977).

[84] A.N. Tikhonov, A.S. Leonov and A.G. Yagola, *Nonlinear Ill-posed Problems,* Chapman & Hall, Boca Raton, Fl., (1998).

[85] A. Trombe, A. Suliman and L. Maoult, Use of an inverse method to determine natural convection heat transfer coefficients in unsteady state, *J. Heat Transfer*, **125**, 1017–26, (2003).

[86] D.H. Wolf, F.P. Incropera and R. Viskanta, Jet impingement boiling, *Adv. Heat Transfer*, **23**, 1–132, (1993).

[87] L.C. Wrobel, *The Boundary Element Method: Application in Thermo-fluids and Acoustics*, Vol.1, John Wiley and Sons Publication, U.K., (2002).

[88] P. Xu, Truncated SVD methods for discrete linear ill-posed problems, *Geophys. J.*, **135**, 505–514, (1998).